MATERIALS FOR ADAPTIVE STRUCTURAL ACOUSTIC CONTROL

Period February 1, 1996 to January 31, 1997

Final Report

VOLUME I

OFFICE OF NAVAL RESEARCH
Contract No.: N00014-92-J-1510

L. Eric Cross

PENNSTATE

1855

THE MATERIALS RESEARCH LABORATORY
UNIVERSITY PARK, PA

REPORT DOCUMENTATION PAGE

Form Approved
OMB No. 0704-0188

1. AGENCY USE ONLY (Leave blank)	2. REPORT DATE	3. REPORT TYPE AND DATES COVERED
	4/14/97	FINAL REPORT 2/1/96-1/31/97

4. TITLE AND SUBTITLE

MATERIALS FOR ADAPTIVE STRUCTURAL ACOUSTIC CONTROL

5. FUNDING NUMBERS

ONR CONTRACT NO:
N00014-92-J-1510

6. AUTHOR(S)

L. ERIC CROSS

7. PERFORMING ORGANIZATION NAME(S) AND ADDRESS(ES)

MATERIALS RESEARCH LABORATORY
THE PENNSYLVANIA STATE UNIVERSITY
UNIVERSITY PARK, PA 16802-4800

8. PERFORMING ORGANIZATION REPORT NUMBER

9. SPONSORING/MONITORING AGENCY NAME(S) AND ADDRESS(ES)

OFFICE OF NAVAL RESEARCH
CODE 1513:NRJ
800 NORTH QUINCY STREET
ARLINGTON, VA 22217-5660

GERALD T. SMITH
OFFICE OF NAVAL RESEARCH RES. REP.
536 SOUTH CLARK STREET, RM 286
CHICAGO, ILLINOIS 60606-1588

10. SPONSORING/MONITORING AGENCY REPORT NUMBER

11. SUPPLEMENTARY NOTES

12a. DISTRIBUTION/AVAILABILITY STATEMENT

12b. DISTRIBUTION CODE

13. ABSTRACT *(Maximum 200 words)*

SEE FOLLOWING TWO PAGES.

14. SUBJECT TERMS

15. NUMBER OF PAGES

16. PRICE CODE

17. SECURITY CLASSIFICATION OF REPORT	18. SECURITY CLASSIFICATION OF THIS PAGE	19. SECURITY CLASSIFICATION OF ABSTRACT	20. LIMITATION OF ABSTRACT

GENERAL INSTRUCTIONS FOR COMPLETING SF 298

The Report Documentation Page (RDP) is used in announcing and cataloging reports. It is important that this information be consistent with the rest of the report, particularly the cover and title page. Instructions for filling in each block of the form follow. It is important to *stay within the lines* to meet *optical scanning requirements*.

Block 1. Agency Use Only *(Leave blank)*.

Block 2. Report Date. Full publication date including day, month, and year, if available (e.g. 1 Jan 88). Must cite at least the year.

Block 3. Type of Report and Dates Covered. State whether report is interim, final, etc. If applicable, enter inclusive report dates (e.g. 10 Jun 87 - 30 Jun 88).

Block 4. Title and Subtitle. A title is taken from the part of the report that provides the most meaningful and complete information. When a report is prepared in more than one volume, repeat the primary title, add volume number, and include subtitle for the specific volume. On classified documents enter the title classification in parentheses.

Block 5. Funding Numbers. To include contract and grant numbers; may include program element number(s), project number(s), task number(s), and work unit number(s). Use the following labels:

C	- Contract	PR	- Project
G	- Grant	TA	- Task
PE	- Program Element	WU	- Work Unit Accession No.

Block 6. Author(s). Name(s) of person(s) responsible for writing the report, performing the research, or credited with the content of the report. If editor or compiler, this should follow the name(s).

Block 7. Performing Organization Name(s) and Address(es). Self-explanatory.

Block 8. Performing Organization Report Number. Enter the unique alphanumeric report number(s) assigned by the organization performing the report.

Block 9. Sponsoring/Monitoring Agency Name(s) and Address(es). Self-explanatory.

Block 10. Sponsoring/Monitoring Agency Report Number. *(If known)*

Block 11. Supplementary Notes. Enter information not included elsewhere such as: Prepared in cooperation with...; Trans. of...; To be published in.... When a report is revised, include a statement whether the new report supersedes or supplements the older report.

Block 12a. Distribution/Availability Statement. Denotes public availability or limitations. Cite any availability to the public. Enter additional limitations or special markings in all capitals (e.g. NOFORN, REL, ITAR).

DOD	- See DoDD 5230.24, "Distribution Statements on Technical Documents."
DOE	- See authorities.
NASA	- See Handbook NHB 2200.2.
NTIS	- Leave blank.

Block 12b. Distribution Code.

DOD	- Leave blank.
DOE	- Enter DOE distribution categories from the Standard Distribution for Unclassified Scientific and Technical Reports.
NASA	- Leave blank.
NTIS	- Leave blank.

Block 13. Abstract. Include a brief *(Maximum 200 words)* factual summary of the most significant information contained in the report.

Block 14. Subject Terms. Keywords or phrases identifying major subjects in the report.

Block 15. Number of Pages. Enter the total number of pages.

Block 16. Price Code. Enter appropriate price code *(NTIS only)*.

Blocks 17. - 19. Security Classifications. Self-explanatory. Enter U.S. Security Classification in accordance with U.S. Security Regulations (i.e., UNCLASSIFIED). If form contains classified information, stamp classification on the top and bottom of the page.

Block 20. Limitation of Abstract. This block must be completed to assign a limitation to the abstract. Enter either UL (unlimited) or SAR (same as report). An entry in this block is necessary if the abstract is to be limited. If blank, the abstract is assumed to be unlimited.

ABSTRACT

This report documents work carried out largely over the fifth and final year of the ONR sponsored University Research Initiative (URI) entitled "Materials for Adaptive Structural Acoustic Control." This program has continued to foster the successful development of new electroceramic single crystal and composite material combinations for both sensing and actuation functions in adaptive structural systems.

For the classical perovskite relaxor, dielectrics typified by lead magnesium niobate, continuing studies of properties in the temperature region above the dielectric maximum T_m have added strong additional support to the superparaelectric/spin glass model for the behavior developed earlier in the IMRL. The most exciting and important discovery of the year has been the ultra high strain capability of relaxor ferroelectric single crystal actuators. For crystal in the lead zinc niobate:lead titanate (PZN;PT) solid solution system, at compositions in the rhombohedral phase close to the morphotropic phase boundary to the tetragonal ferroelectric phase at 9 mole % PT in PZN, crystals cut and poled along the 001 cube axis exhibit massive field induced quasi linear anhysterestic strains up to 0.6%. For this poling d_{33} values up to 2,300 pC/N and coupling coefficients k_{33} of 94% have been achieved and it was the original hypothesis that these extreme numbers must be largely due to extrinsic domain wall motion. Now however it is very clear that the exact equivalence of the effect of an 001 oriented E field on the $111, \bar{1}11, 1\bar{1}1,$ and $\bar{1}\bar{1}1$ rhombohedral domains precludes this field from driving domain wall motion so that quite contrary to our earlier expectation the polarization and associated strain phenomena are purely intrinsic. At higher field levels there is an obvious step in both polarization and strain into an induced tetragonal phase which gives total reproducible induced strains up to 1.7%. Clearly the PZN:PT crystals represent a major breakthrough into a completely new regimen for piezoelectric actuation and sensing.

For antiferroelectric:ferroelectric switching compositions in the lead lanthanum zirconated titanate stannate family, new experimental studies have proven that the induced polarization P_3 and the strain x_{33} onset at different field levels. A new domain re-orientation model has been invoked to explain this startlingly unusual behavior. Both barium and strontium additives have also been explored to control hysteresis between forward and backward switching with good success. As well as being interesting for transduction we believe these compositions are sure to be important for energy storage dielectrics.

In composite sensing it is pleasing to report that the moonie flextensional patent has now been licensed to the Input:Output Corporation who have successfully fabricated and sold more than 80,000 moonie sensors. Work is continuing on the cymbal type modification of the moonie with focus now on array structures for large area panels. This topic is transitioning to a joint study between the IMRL and Penn State's ARL, on a new MURI initiative. For the very small hollow PZT spheres produced by blowing, the emphasis has been upon both poling and driving from outer surface electrodes, and exploring both by experiment and by finite element theoretical methods, the resonant mode structures which can be induced. Studies of the 2:2 composite structures confirm the very high effective hydrostatic sensitivity and are permitting closer consonance between measurement and theoretical analysis.

Actuation studies have been dominated by the initial exploration of the fantastic strain capability of the relaxor ferroelectric MPB single crystals. Obviously the induced strains are on order of magnitude larger than for conventional PZT ceramics, but the blocking force has

not yet been determined. It is expected that d_{31} will also be large and anhysteritic in these crystals, as spontaneous strain depends on Q_{44} which is a pure shear constant. The d_{15} however may be significantly more complex as an E_1 field will certainly drive domain walls in these E_3 poled crystals.

Reliability studies of conventional actuators are continuing with emphasis on using acoustic emission to explore and separate domain wall motion and crack propagation. Most earlier studies were indeterminate and difficult to interpret, recently for these strongly piezoelectric samples we have shown that electrical noise in the power supply induces very strong mechanical noise in the sample giving high spurious emission counts. New studies using a long time constant filter in the supply have permitted clear and effective separation. Over the last few years there has been a strong re-awakening of interest in bimorph type transducer amplifiers with new concepts like rainbow, cerambow and thunder appearing. Under our ONR program with Virginia Polytechnic it has been necessary to sort out the conflicting claims for these 'morph' types and these data are included for completeness. We have also begun serious study of the large electrostriction in the soft polyurethane elastomers where it has been necessary to derive new techniques to measure strain with ultra low constraint on the films.

Processing studies now involved both single crystal flux growth and a wide range of powder and ceramic processing. Current needs for integrity and better mechanical properties are driving new needs for fine grained PZT piezoceramics and new processing is permitting retention of excellent properties down to submicron grain sizes.

From the wide range of thin ferroelectric film activities in the laboratory, only those which refer to the thicker films being produced on silicon for MEMS devices are included.

MATERIALS FOR ADAPTIVE STRUCTURAL ACOUSTIC CONTROL

Period February 1, 1996 to January 31, 1997

Final Report

VOLUME I

OFFICE OF NAVAL RESEARCH
Contract No.: N00014-92-J-1510

L. Eric Cross

TABLE OF CONTENTS

APPENDICES

VOLUME I

General Summary Papers

1. Cross, L.E., "Ferroelectric Materials for Electromechanical Transducer Applications." *Mat. Chem. Phys* **43**, 108-115 (1996).

2. Cross, L.E., "Ferroelectric Ceramics: Materials and Application Issues." *Ceramic Transactions* **68**, 15-55 (1996).

3. Li. S., J.A. Eastman, Z. Li, C.M. Foster, R.E. Newnham, and L.E. Cross, " Size Effects in Ferroelectrics." *Phys. Lett. A* **212**, 341 (1996).

4. Li, Shaoping, J.A. Eastman, R.E. Newnham, and L.E. Cross, "Susceptibility of Nanostructured Ferroelectrics." *Japanese J. Appl. Physics* **35** (Part 2) [No. 4B], L502-L504 (1996).

5. Newnham, R.E., Chapter: Crystal Chemistry and Crystal Physics, in Innovative Ideas in Ceramics and Materials Curricula, edited by T. Stoebe and W. Huebner. Published by the *American Ceramic Society*, pp. 65-72 (1996).

6. Uchino, K., "New Applications of Photostriction." *Innovations in Mater. Res.* **1** (1), 11-22 (1996).

7. Aburatani, H. and K. Uchino, "Acoustic Emission (AE) Measurement Technique in Piezoelectric Ceramics." *Jpn. J. Appl. Phys.* **35** (2) [4B], L516-L518 (1996).

Materials Studies

8. Choi, S., J.M. Jung, and A.S. Bhalla, "Dielectric, Pyroelectric and Piezoelectric Properties of Calcium-Modified Lead Magnesium Tantalate-Lead Titanate Ceramics." *Ferroelectric Letters* **21**, 27-33 (1996).

9. Alberta, E. and A.S. Bhalla, "Preparation of Phase Pure Perovskite Lead Indium Niobate Ceramic." *Mater. Lett.* **29**, 127-129 (1996).

10. Zhang, Q.M., J. Zhao, T.R. Shrout, and L.E. Cross, "The Effect of Ferroelastic Coupling in Controlling the Abnormal Aging Behavior in Lead Magnesium Niobate-Lead Titanate Relaxor Ferroelectrics." *J. Mater. Res.* **12** (7), (1997).

11. Alberta, E., A.S. Bhalla, and T. Takenaka, "Piezoelectric, elastic and Dielectric Constants for Ceramics in the Solids Solution: $xPbZrO_3$ - (1-x-z)$Pb(Zn_{1/3}Nb_{2/3})\ O_3$ - $zPbTiO_3$." *Ferroelectrics* **188**, 109-124 (1996).

Materials Studies–continued

12. Zhang, Q.M. and J. Zhao, "Polarization Responses in Lead Magnesium Niobate Based Relaxor Ferroelectrics." *Applied Physics Letters* (submitted).

13. Müeller, V. and Q.M. Zhang, "Nonlinearity and Scaling Behavior in Donor Doped Lead Zirconate Titanate Piezoceramic." *Physics Review Letters* (submitted).

14. Zhang, Q.M., J. Zhao, K. Uchino, and J. Zheng, "Change of the Weak-Field Properties of $Pb(ZrTi)O_3$ Piezoceramics with Compressive Uniaxial Stresses and Its Links to the Effect of Dopants on the Stability of the Polarizations in the Materials." *J. Mat. Res.* **12**, 226 (1997).

15. Markowski, K., S.-E. Park, S. Yoshikawa, and L.E. Cross, "The Effect of Compositional Variations in the Lead Lanthanum Zirconate Stannate Titanate System on Electrical Properties." *J. Amer. Ceram.* **79** (12), 3297-3304 (1996).

16. Park, S.-E., K. Markowski, S. Yoshikawa, and L.E. Cross, "The Effect of Barium and Strontium Additions in the Lead Lanthanum Zirconate Stannate Titanate System on Electrical Properties." *J. Amer. Ceram.* **80** (2), 407-412 (1997).

VOLUME II

17. Yoshikawa, S., K. Markowski, S.-E. Park, M.-J. Pan, and L.E. Cross, "Antiferroelectric-to-Ferroelectric Phase Switching Lead Lanthanum Zirconate Stannate Titanate (PLZST) Ceramics." *SPIE Proceedings* **IV** (1997).

18. Blue, C.T., J.C. Hicks, S.-E. Park, S. Yoshikawa, and L.E. Cross, "In-situ X-ray Diffraction Study of the Antiferroelectric-Ferroelectric Phase Transition in PLSnZT." *Applied Physics Letter* **68** (21), 2942-2944 (1996).

19. Pan, M.-J., S.-E. Park, K. Markowski, and S. Yoshikawa, "Antiferroelectric-to-Ferroelectric PLZST Ceramics-II: The Effect of Pre-Stress Conditions on the Strain Behavior." Submitted *Proceedings of IEEE International Symposium on the Applications of Ferroelectrics*, Rutgers University, East Brunswick, New Jersey (August 1996).

20. M.-J. Pan, Markowski, K., S.-E. Park, S. Yoshikawa, and L.E. Cross. "Antiferroelectric-to Ferroelectric PLZSnT Ceramics-I: Structure, Compositional Modification and Electric Properties." Submitted *Proceedings of IEEE International Symposium on the Applications of Ferroelectrics*, Rutgers University, East Brunswick, New Jersey (August 1996).

Materials Studies–continued

21. Lopath, P.D., K.K. Shung, S.-E. Park, and T.R. Shrout, "Ultrasonic Transducers Using Piezoelectric Single Crystals Perovskites." Submitted *Proceedings of IEEE International Symposium on the Applications of Ferroelectrics*, Rutgers University, East Brunswick, New Jersey (August 1996).

22. Park, S.-E. and T.R. Shrout, "Characteristics of Relaxor-Based Piezoelectric Single Crystals for Ultrasonic Transducers." Proceedings of 1996 IEEE Ultrasonics Symposium, San Antonio, Texas (November 1996).

23. Park, S.-E., P.D. Lopath, K.K. Shung, and T.R. Shrout, "Relaxor-Based Single Crystal Materials for Ultrasonic Transducer Applications." Proceedings on SPIE's International Symposium on Medical Imaging, Newport Beach, California (February 1997).

24. Lopath, P.D., S.-E. Park, K.K. Shung, and T.R. Shrout, "$Pb(Zn_{1/3}Nb_{2/3})O_3/PbTiO_3$ Single Crystal Piezoelectrics for Ultrasonic Transducers." Proceedings on SPIE's International Symposium on Medical Imaging, Newport Beach, California (February 1997).

25. Park, S.-E. and T.R. Shrout, "Relaxor Based Ferroelectric Single Crystals for Electro-Mechanical Actuators." *Innovations in Materials Research* (accepted).

26. Park, S.-E. and T.R. Shrout, "Characteristics of Relaxor-Based Piezoelectric Single Crystals for Ultrasonic Transducers," *IEEE Trans. on Ultrasonics, Ferroelectric and Frequency Control Special Issue on Ultrasonic Transducers* (to be published).

27. Jin, B., R. Guo, and A.S. Bhalla, "Piezoelectric Properties and Equivalent Circuits of Ferroelectric Relaxor Single Crystals."

28. Mulvihill, M.L., K. Uchino, Z. Li, and W. Cao, "In-situ Observation of the Domain Configurations during the Phase Transitions in Barium Titanate." *Phil. Mag. B.* **74** (1), 25-36 (1996).

29. Mulvihill, M.L., L.E. Cross, and K. Uchino, "Dynamic Motion of the Domain Configuration in Relaxor Ferroelectric Single Crystals as a Function of Temperature and Electric Field." *Ferroelectrics* **186**, 325-328 (1996).

30. Sundar, V. and R.E. Newnham, "Conversion Method Measurements of Electrostriction Coefficients in Low-K Dielectrics." *Mat. Res. Bull.* **31** (5), 545-554 (1996).

31. Sundar, V., J.-F., Li, D. Viehland, and R.E. Newnham, "Interferometric Evaluation of Electrostriction Coefficients." *Mat. Res. Bull.* **31** (5), 555-563 91996).

Materials Studies–continued

32. Sundar, V., N. Kim, C. Randall, R. Yimnirun, and R.E. Newnham, "The Effect of Doping and Grain Size on Electrostriction in $PbZr_{0.52}Ti_{0.48}O_3$." Submitted *Proceedings of IEEE International Symposium on the Applications of Ferroelectrics*, Rutgers University, East Brunswick, New Jersey (August 1996).

33. Erdei, S., L. Galambos, I. Tanaka, L. Hesselik, F.W. Ainger, L.E. Cross, and R.S. Feigelson, "Segregation and Inhomogenities in Photorefractive SBN Fibers." *SPIE Proceedings V–Photorefractive Fiber and Crystal Devices: Materials, Optical Properties, and Applications II*, **2849**, 168-173 (1996).

34. Li, Shaoping, J.A. Eastman, J.M. Vertrone, R.E. Newnham, and L.E. Cross, "Coherent Coupling in Ferroelectric Superlattices." (1996).

35. Su, J., Q.M. Zhang, and R.Y. Ting, "Space Charge Enhanced Electromechanical Response in Thin Film Polyurethane Elastomers." *Applied Physics Letters* (submitted).

36. Zhang, Q.M., J. Su, and C.-H. Kim, "An Experimental Investigation of Electromechanical Responses in a Polyurethane Elastomer." *J. Appl. Phys.* **81** (6), 2770 (1997).

VOLUME III

37. Su, J., Q.M. Zhang, C.H. Kim, R.Y. Ting, and R. Capps, "Effects of Transitional Phenomena on the Electric Field Induced Strain-Electrostrictive Response of a Segmented Polyurethane Elastomer." *J. Appl. Polymer Sci.* (accepted).

Composite Sensors

38. Fernandez, J.F., A. Dogan, Q.M. Zhang, J.F. Tressler, and R.E. Newnham, "Hollow Piezoelectric Composites, Sensors and Actuators." *A: Physical* **51** (2,3), 183-192 (1996).

39. Fernandez, J.F., A. Dogan, Q.M. Zhang, and R.E. Newnham, "Piezoelectric Composites with Enclosed Hollow Spaces." Proceedings 4th Euroceramics Conference, *Electroceramics* **5**, 39-46 (1996).

40. Fernandez, J.F., A. Dogan, J.T. Fielding, K. Uchino, and R.E. Newnham, "Temperature Dependence of New Design Ceramic-Metal Piezocomposites Actuators." Proceeding 4th Euroceramics Conference, *Electroceramics* **5**, 133-138 (1996).

Composite Sensors–continued

41. Newnham, R.E., "Composite Sensors and Actuators," Disordered Materials, edited by G. Milton, K. Godlen, G. Grimmett, and P. Sen, Springer-Verlag, NY (accepted January 1997).

42. Tressler, J.F. and R.E. Newnham, "Doubly Resonant Cymbal Transducers, *IEEE Transactions of UFFC*, Special Issue on Transducers (accepted 1996).

43. Tressler, J.F., W. Cao, K. Uchino, and R.E. Newnham, "Ceramic Metal Composite Transducers for Underwater Acoustic Applications." Submitted *Proceedings of IEEE International Symposium on the Applications of Ferroelectrics*, Rutgers University, East Brunswick, New Jersey (August 1996).

44. Alkoy, S., A. Dogan, A.C. Hladky, J.K. Cochran, and R.E. Newnham, "Vibration Modes of PZT Hollow Sphere Transducers." Submitted *Proceedings of IEEE International Symposium on the Applications of Ferroelectrics*, Rutgers University, East Brunswick, New Jersey (August 1996).

45. Alkoy, S., A. Dogan, A.C. Hladky, and R.E. Newnham, "Miniature Piezoelectric Hollow Sphere Transducers (BBs)." 1996 Proceeding of IEEE International Frequency Control Symposium, pp. 586-594, Honolulu, Hawaii (1996).

46. Alkoy, S., A. Dogan, A.C. Hladky, and R.E. Newnham, "Piezoelectric Hollow Spheres." 1996 Proceeding 3rd Turkish Ceramic Society Meeting., Eds. V. Günay, H. Mandel, S. Ozgen. Istanbul, Turkey (October 1996).

47. Koc, B., A. Dogan, J.F. Fernandez, R.E. Newnham, and K. Uchino, "Accelerometer Application of the Modified Moonie (Cymbal) Transducer." *J. App. Phys.* **35**, 65-67 (1996).

VOLUME IV

48. Kumar, S., A. Bhalla, and L.E. Cross, "Underwater Acoustic Absorption by Collocated Smart Materials." *Ferroelectric Letters* **21**, 11-16 (1996).

49. Geng, X. and Q.M. Zhang, "Evaluation of Piezocomposites for Ultrasonic Transducer Applications–Influence of the Unit Cell Dimensions and the Properties of Constituents the Performance of 2-2 Piezocomposites." *IEEE Transactions of UFFC* (accepted).

50. Zhang, Q.M. and X. Geng, "Acoustic Properties of the Interface of a Uniform Medium-2-2 Piezocomposite and the Field Distributions in the Composite." *J. Appl. Phys.* (accepted).

Actuator Studies

51. Park, S.-E., and T.R. Shrout, "Ultrahigh Strain and Piezoelectric Behavior in Relaxor Based Ferroelectric Single Crystals."

52. Uchino, K. and S. Takahashi, "Multilayer Ceramic Actuators." *Current Opinion, Ceramic, Composites and Intergrowths*, p. 98-705 (1996).

53. Zheng, J., S. Takahashi, S. Yoshikawa, and K. Uchino, "Heat Generation in Multilayer Piezoelectric Actuators." *J. Amer. Ceram.* **79** (12), 3193-3198 (1996).

54. Dogan, A., J.F. Fernandez, K. Uchino, and R.E. Newnham, "New Piezoelectric Composite Actuator Designs for Displacement Amplification." *Proceeding Euroceramic Conference, Electroceramics* (5), 127-132 (1995) (in press).

VOLUME V

55. Poosanaas, P., A. Dogan., A.V. Prasadarao, S. Komarneni, and K. Uchino, "Photostriction of Sol-Gel Processed PLZT Ceramics." *J. Electroceramics* (1996) (in press).

56. Uchino, K., "Reliability of Ceramic Actuators." Submitted *Proceedings of IEEE International Symposium on the Applications of Ferroelectrics*, Rutgers University, East Brunswick, New Jersey (August 1996).

57. Uchino, K., "High Electromechanical Coupling Piezoelectrics-How High Energy Conversion Rate is Possible?-." *Proceeding MRS 1996* (1996) (in press).

58. Uchino, K., "Recent Developments in Ceramic Actuators-Comparison Among USA, Japan and Europe."

59. Xu, B., Q.M. Zhang, V.D. Kugel, Q. M. Wang, and L.E. Cross, "Optimization of Bimorph Based Double Amplifier Actuator under Quasistatic Situation." Submitted *Proceedings of IEEE International Symposium on the Applications of Ferroelectrics*, Rutgers University, East Brunswick, New Jersey (August 1996).

60. Kugel, V.D., S. Chandran, and L.E. Cross, "Caterpillar-Type Piezoelectric d_{33} Bimorph Transducer." *Appl. Phys. Lett.* **69** (14), 2021-2023 (1996).

61. Kugel, V.D., Q.M. Zhang, B. Xu, Q.-M. Wang, S. Chandran, and L.E. Cross, "Behavior of Piezoelectric Actuators under High Electric Field." Submitted *Proceedings of IEEE International Symposium on the Applications of Ferroelectrics*, Rutgers University, East Brunswick, New Jersey (August 1996).

62. Kugel, V.D., B. Xu, Q.M. Zhang, and L.E. Cross, "Bimorph-Based Piezoelectric Air Acoustic Transducer Model." *Sensors and Actuators A* (submitted 1996).

Actuator Studies–continued

63. Chandran, S., V.D. Kugel, and L.E. Cross, "CRESCENT: A Novel Piezoelectric Bending Actuator." *Proceeding SPIE's 4th Annual Symposium on Smart Structures* accepted 1997).

64. Kugel, V.D., S. Chandran, and L.E. Cross, "A Comparative Analysis of Piezoelectric Bending-Mode Actuators." Submitted *SPIE Proceedings*, Smart Structures and Materials: Smart Materials Technologies, 3040, 70-80 (1997).

65. Wang, Q.M., B. Xu, V.D. Kugel, and L.E. Cross, "Characteristics of Shear Mode Piezoelectric Actuators," Submitted *Proceedings of IEEE International Symposium on the Applications of Ferroelectrics*, Rutgers University, East Brunswick, New Jersey (August 1996).

Integration Studies

66. Elissalde, C., L.E. Cross, and C.A. Randall, "Structural-Property Relations in a Reduced and Internally Biased Oxide Wafer (RAINBOW) Actuator Material." *J. Amer. Ceram.* **79** (8), 2041-2048 (1996).

67. Xu. B., Q.M. Zhang, V.D. Kugel, Q. Wang, and L.E. Cross, "Optimization of Bimorph Based Double Amplifier Transducer under Quasistatic Conditions." Submitted *Proceedings of IEEE International Symposium on the Applications of Ferroelectrics*, Rutgers University, East Brunswick, New Jersey (August 1996).

68. Xu, B., Q. M. Zhang, V.D. Kugel, and L.E. Cross, "Piezoelectric Air Transducer for Active Noise Control." *Proceeding SPIE, Smart Structures and Integrated Systems* **271** (7), 388 (1996).

VOLUME VI

69. Chandran, S., V.D. Kugel, and L.E. Cross, "Characterization of the Linear and Non-Linear Dynamic Performance of RAINBOW Actuator." Submitted *Proceedings of IEEE International Symposium on the Applications of Ferroelectrics*, Rutgers University, East Brunswick, New Jersey (August 1996).

70. Wang, H., Q.M. Zhang, L.E. Cross, and C.M. Trottier, "Tailoring Material Properties by Structure Design–Radially Poled Piezoelectric Cylindrical Tube." *Ferroelectrics* **173**, 181-189 (1995).

Processing Studies

71. Park, S.-E., M. Mulvihill, P.D. Lopath, M. Zipparo, and T.R. Shrout, "Crystal Growth and Ferroelectric Related Properties of (1-x) Pb $(A_{1/3}Nb_{1/3})O_3$ - $xPbTiO_3$(A=Zn^{2+}, Mg^{2+})." Submitted *Proceedings of IEEE International Symposium on the Applications of Ferroelectrics*, Rutgers University, East Brunswick, New Jersey (August 1996).

72. Mulvihill, M., S.-E. Park, G. Risch, Z. Li, K. Uchino, and T.R. Shrout, "The Role of Processing Variables in the Flux Growth of PZN-PT Relaxor Ferroelectric Single Crystals." *Jpn. J. Appl. Phys.* **35** (Pt. 1; No. 7), 3984-3990 (1996).

73. Pan, M.-J., S.-E. Park, C.W. Park, K.A. Markowski, S. Yoshikawa, and C. Randall, "Superoxidation and Electrochemical Reactions during Switching in $Pb(Zr,Ti)O_3$ Ceramics." *J. Amer. Ceram.* **79** (11), 2971-2974 (1996).

74. Park, S.-E., M.L. Mulvihill, G. Risch, and T.R. Shrout, "The Effect of Growth Condition on Dielectric Properties of $Pb(Zn_{1/3}Nb_{2/3})O_3$ Crystal." *Jpn. J. Appl. Phys.* **36** (1) (1997).

75. Yoshikawa, Y. and K. Uchino, "Chemical Preparation of Lead-Containing Niobate Powders." *J. Amer. Ceram.* **79** (9), 2417-2421 (1996).

76. Ravindrathan, P., V. Srikanth, S. Komarneni, and A.S. Bhalla, "Processing of $Pb(Zn_{1/3}Nb_{2/3})O_3$: Ceramics at High Pressure." *Ferroelectrics* **188**, 135-141 (1996).

77. Ravindrathan, P., S. Komarneni, A.S. Bhalla, and R. Roy, "Low Temperature Chemical Routes to Smart Materials." *Ferroelectrics* **188**, 125-133 (1996).

78. Alberta, E.F. and A.S. Bhalla, "A Processing and Electrical Property Investigation of the Solid Solution: (x) $Pb(In_{1/2}Nb_{1/2})O_3$ - (1-x)$Pb(Sc_{1/2}Ta_{1/2})O_3$." *Ferroelectrics* **188**, 95-107 (1996).

Thin Film Ferroelectrics

79. Chen, H.D., K.R. Udayakumar, C.J. Gaskey, and L.E. Cross, "Fabrication and Electrical Properties of Lead Zirconate Titanate Thick Films." *J. Amer. Ceram.* **79** (8), 2189-2192 (1996).

80. Chen, H.D., K.K. Li, C.J. Gaskey, and L.E. Cross, "Thickness-Dependent Electrical Properties in Lanthanum-Doped PZT Thick Films." *Mat. Res. Soc. Symp. Proc.* **433**, 325-332 (1996).

81. Ravichandran, D., R. Meyer, Jr., R. Roy, R. Guo, A.S. Bhalla, and L.E. Cross, "Sol-Gel Synthesis of $Ba(Mg_{1/3}Ta_{2/3})O_3$: Phase Pure Powder and Thin Films." *Mat. Res. Bull.* **31** (7), 817-825 (1996).

82. Ravichandran, D., K. Yamakawa, R. Roy, A.S. Bhalla, S. Trolier-McKinstry, R. Guo, and L.E. Cross, "The Effect of Annealing Temperature on the Formation of $SrBi_2Ta_2O_9$ (SBT) Thin Films." Submitted *Proceedings of IEEE International Symposium on the Applications of Ferroelectrics*, Rutgers University, East Brunswick, New Jersey (August 1996).

Instrumentation

83. Su, J., P. Moses, and Q.M. Zhang, "A Bimorph Based Dilatometer for Field Induced Strain Measurement in Soft and Tin Free Standing Polymer Films." *Reviews of Scientific Instruments* (submitted).π

ABSTRACT

This report documents work carried out largely over the fifth and final year of the ONR sponsored University Research Initiative (URI) entitled "Materials for Adaptive Structural Acoustic Control." This program has continued to foster the successful development of new electroceramic single crystal and composite material combinations for both sensing and actuation functions in adaptive structural systems.

For the classical perovskite relaxor, dielectrics typified by lead magnesium niobate, continuing studies of properties in the temperature region above the dielectric maximum T_m have added strong additional support to the superparaelectric/spin glass model for the behavior developed earlier in the IMRL. The most exciting and important discovery of the year has been the ultra high strain capability of relaxor ferroelectric single crystal actuators. For crystal in the lead zinc niobate:lead titanate (PZN;PT) solid solution system, at compositions in the rhombohedral phase close to the morphotropic phase boundary to the tetragonal ferroelectric phase at 9 mole % PT in PZN, crystals cut and poled along the 001 cube axis exhibit massive field induced quasi linear anhysterestic strains up to 0.6%. For this poling d_{33} values up to 2,300 pC/N and coupling coefficients k_{33} of 94% have been achieved and it was the original hypothesis that these extreme numbers must be largely due to extrinsic domain wall motion. Now however it is very clear that the exact equivalence of the effect of an 001 oriented E field on the $111, \bar{1}11, 1\bar{1}1$, and $\bar{1}\bar{1}1$ rhombohedral domains precludes this field from driving domain wall motion so that quite contrary to our earlier expectation the polarization and associated strain phenomena are purely intrinsic. At higher field levels there is an obvious step in both polarization and strain into an induced tetragonal phase which gives total reproducible induced strains up to 1.7%. Clearly the PZN:PT crystals represent a major breakthrough into a completely new regimen for piezoelectric actuation and sensing.

For antiferroelectric:ferroelectric switching compositions in the lead lanthanum zirconated titanate stannate family, new experimental studies have proven that the induced polarization P_3 and the strain x_{33} onset at different field levels. A new domain re-orientation model has been invoked to explain this startlingly unusual behavior. Both barium and strontium additives have also been explored to control hysteresis between forward and backward switching with good success. As well as being interesting for transduction we believe these compositions are sure to be important for energy storage dielectrics.

In composite sensing it is pleasing to report that the moonie flextensional patent has now been licensed to the Input:Output Corporation who have successfully fabricated and sold more than 80,000 moonie sensors. Work is continuing on the cymbal type modification of the moonie with focus now on array structures for large area panels. This topic is transitioning to a joint study between the IMRL and Penn State's ARL, on a new MURI initiative. For the very small hollow PZT spheres produced by blowing, the emphasis has been upon both poling and driving from outer surface electrodes, and exploring both by experiment and by finite element theoretical methods, the resonant mode structures which can be induced. Studies of the 2:2 composite structures confirm the very high effective hydrostatic sensitivity and are permitting closer consonance between measurement and theoretical analysis.

Actuation studies have been dominated by the initial exploration of the fantastic strain capability of the relaxor ferroelectric MPB single crystals. Obviously the induced strains are on order of magnitude larger than for conventional PZT ceramics, but the blocking force has

not yet been determined. It is expected that d_{31} will also be large and anhysteritic in these crystals, as spontaneous strain depends on Q_{44} which is a pure shear constant. The d_{15} however may be significantly more complex as an E_1 field will certainly drive domain walls in these E_3 poled crystals.

Reliability studies of conventional actuators are continuing with emphasis on using acoustic emission to explore and separate domain wall motion and crack propagation. Most earlier studies were indeterminate and difficult to interpret, recently for these strongly piezoelectric samples we have shown that electrical noise in the power supply induces very strong mechanical noise in the sample giving high spurious emission counts. New studies using a long time constant filter in the supply have permitted clear and effective separation. Over the last few years there has been a strong re-awakening of interest in bimorph type transducer amplifiers with new concepts like rainbow, cerambow and thunder appearing. Under our ONR program with Virginia Polytechnic it has been necessary to sort out the conflicting claims for these 'morph' types and these data are included for completeness. We have also begun serious study of the large electrostriction in the soft polyurethane elastomers where it has been necessary to derive new techniques to measure strain with ultra low constraint on the films.

Processing studies now involved both single crystal flux growth and a wide range of powder and ceramic processing. Current needs for integrity and better mechanical properties are driving new needs for fine grained PZT piezoceramics and new processing is permitting retention of excellent properties down to submicron grain sizes.

From the wide range of thin ferroelectric film activities in the laboratory, only those which refer to the thicker films being produced on silicon for MEMS devices are included.

INTRODUCTION

This report summarizes work carried out in the Intercollege Materials Research Laboratory (IMRL) at Penn State in most part during the fifth and final year of the five year ONR sponsored University Research Initiative (URI) entitled "Materials for Adaptive Structural Acoustic Control." The work was carried out largely in five sections, each reporting to a senior faculty member.

These sections are:

Materials Studies	A.S. Bhalla
Composite Sensors	R.E. Newnham
Actuator Studies	K. Uchino
Integration Issues	J. Dougherty
Processing Studies	T.R. Shrout

Following the close out of the present program relevant topics will be carried forward under a new ONR sponsored MURI program, which couples the materials group much more closely to the Applied Research Laboratory (ARL) at Penn State, who are a major developer of transducer systems for US Navy use. An emphasis in this final year program has been to assure a "seamless" transition to the new program goals.

In keeping with long established precedent this report presents a very brief narrative summary of the work accomplished making reference to published papers and preprints which are attached as technical appendices.

For convenience the topics are loosely grouped under the topic headings:

(1) General Summary Papers.
(2) Materials Studies.
(3) Composite Sensors.
(4) Actuator Studies.
(5) Integration Issues.
(6) Processing Studies.
(7) Thin Film Ferroelectrics.
(8) Instrumentation.

In the General Summary Papers, the senior faculty continue to take their educational responsibilities seriously pointing up the very wide range of applicability for electroceramic ferroelectric based materials in dielectric, piezoelectric, pyroelectric and electrooptic devices, and the potential advantages of basing a core curriculum in solid state science upon the physics, chemistry, and crystallography in these practical studies. New initiatives with Argonne National labs are focused on the application of Landau theory to a nanoscale ferroelectrics. At a more practical level new applications for the phenomenon of photostriction are discussed. A key advance for the use of acoustic emission in the study of domain wall motion has been the identification and elimination of a masking piezoelectric noise source.

Relaxor ferroelectrics are certainly the major focus in materials studies with the finding of outstanding actuator capability in appropriately oriented single crystals. In other relaxor studies in the temperature region above the dielectric maximum T_m it is becoming clear from the hydrostatic electrostriction behavior that the superparelectric/spin glass model provides probably the best explanation for polarization behavior. Clearly now however the new focus must move to the induced ferroelectric phases and new phase boundary compositions. For the antiferroelectric:ferroelectric phase switching compositions, composition manipulation has yielded excellent control of switching and hysteresis, however the unusually strong influence of pre-stress suggests that in these systems capacitative energy storage may be more interesting than transduction. Fortunately the rapidly developing interest in switching power supplies suggests that such compact capacitors may be necessary components soon in piezoelectric transducer systems.

In the composite sensors (and actuators) theory and practice both show excellent progress for metal/ceramic and polymer/ceramic composites and flextensional amplifiers. It is most encouraging to see the very strong commercial interest developing in these systems. Actuation studies, as expected have been dominated by the relaxor/ferroelectric MPB single crystals which do represent a step function advance. It is interesting to see also that in the new widely publicized bimorph systems, the major advantage is in robustness under abusive treatment and not in the force/displacement performance per-se. It is pleasing also to note the expansion of interest in polymeric elastomer systems, and the start up of focused efforts to understand and exploit these interesting high strain electrostrictors.

Processing is now nicely split between addressing the needs in both single and polycrystal ceramics and it may be expected in future to expand also to new polymeric needs. It is to be expected also with the versatility of the piezoelectrics so effectively expanding there will be expanding needs for new instrumentation required on the continuing MURI program.

1.0 GENERAL SUMMARY PAPERS

In discussing ferroelectric ceramic materials Cross (Appendices 1, 2) focuses on polycrystal ceramics and thin films highlighting the essential advantages of the ferroelectric perovskites and the techniques for manipulating properties for dielectric, piezoelectric, pyroelectric and electro-optic applications. Two papers which highlight cooperation between Argonne National Lab and IMRL (Appendices 3,4) explore the application of Landau theory of finite size effects. The results highlight the correlation between thickness and coherent area at small dimensions and lead to reasonable values for critical volume. In appendix 5, Newnham makes the case for the study of physical properties of crystals as an alternative to the focus in the usual solid state physics for materials scientists. Uchino discusses his favorite photostrictive devices in appendix 6 highlighting the possibility of light driven micro-walking devices with no on-board power. Acoustic emission has been a nest of complexities for high sensitivity switching studies in ferroelectrics. Appendix 7 shows how spurious signal can easily occur in strong piezoelectrics by feedback from the power supply.

2.0 MATERIALS STUDIES

Studies in appendices 8 and 9 deal with polycrystal relaxors and relaxor solid solution, covering calcium modified lead magnesium tantalate:lead titanate and phase pure lead indium niobate in the disordered ferroelectric relaxor phase. Abnormal aging (appendix 10) in lead magnesium niobate:lead titanate is strongly influenced by elastic boundary conditions in the ceramic and can be controlled by aleovalent dopants. The peculiar antiferroelectric:ferroelectric switching under E field in $PbZrO_3$:$PbZn_{1/3}Nb_{2/3}O_3$ and in $PbTiO_3$ modified compositions in studies in appendix 11 where the low permititvity offers attractive pyroelectric response. More detailed study of the hydrostatic electrostrictive response in $PbMg_{1/3}Nb_{2/3}O_3$ (Appendix 12) offers strong additional support for the superparaelectric/spin glass model for polarization behavior in this system. Appendices 13 and 14 focus on classical PZTs, delineating properly for the first time the electric field induced nonlinearity and the elastic stress dependence of the coefficients.

The very extensive studies on the antiferroelectric phase switching compositions of the lead lanthanum zirconate titanate stannate compositions are discussed in appendices 15-20. The influence on switching fields, hysteresis and temperature stability for changing Zr:Sn and Ti:Sn rations are discussed in appendix 15, changing A site additives Ba and Sr are discussed in appendix 16, and the combined effects to maximize the range of change is covered in appendix 17. Refined x-ray studies carried out at NCCOSC/RDT&E division by J.C. Hicks and C.T. Blue confirm the expected structure change and the magnitude of the induced strain (Appendix 18). Measurement of pre-stress show that the effects are much more severs than in conventional piezoelectric PZTs (Appendix 19) however influences of higher stress levels appear to depend markedly upon composition. The sequence of studies is effectively summarized in appendix 20.

The mounting excitement of the studies of single crystal relaxor ferroelectric/ferroelectric solid solutions is clearly evident in appendices 21-25. Evidence that both the PMN:PT and PZnN:PT solid solution families have outstanding piezoelectric properties with $d_{33} > 2000$ pC/N and coupling $k_{33} > 90\%$ for crystals in the rhombohedral phase cut and poled along 001 is steadily evidenced in appendices 21-24 where the merits of such parameters are discussed in the context of high frequency medical ultrasound. The

startling actuator performance is first delineated in appendix 25 with quasi linear anhysteretic strain up to 0.6% and total reversible strain capability of order 1:7%, truly a tour de force.

The unusual piezoelectric character of the tungsten bronze structure single crystal relaxor is underscored in appendix 27 where a form of resonance is shown to persist above the temperature of the dielectric maximum T_m. CCD microscope studies of domain walls and domain dynamics in $BatiO_3$ single crystals are discussed in appendices 28 and 29, both phase and domain structure changes can be clearly followed as a function of temperature and field. The new capability, to make for the first time, precise measurements of electrostriction in simple low permittivity crystals using the new laser ultradilatometer and the ultra precise capacitance bridge systems is elegantly expounded in appendices 30 and 31. The results between direct and converse methods check precisely and give full confidence in the data, again for the first time! The system has also been used, using the converse effect, to measure electrostriction as a function of grain size in a PZT at the 52:48 composition in Appendix 32. In a second study of the tungsten bronze $(Sr_{0.6}Ba_{0.4})Nb_2O_6$ troubling radial composition gradients in the laser heated pedestal grown grown fibers are explained using the Burton-Prim-Slichter equation (appendix 33). The possibility for engineering dielectric superlattices in a $SrTiO_3$:PZT system is described in appendix 34 suggesting the possibility for very high dielectric permittivity and strongly diffuse phase transitions.

Appendices 35-37 document the increasing interest in the electromechanical characteristics of soft polyurethane elastomers. In appendix 35 thermally stimulated currents are used to document space charge in the biased polymer, explaining the dispersion and strong thickness dependence of electrostriction. More detailed characterization of the electrostrictive Q is given in appendix 36 and its relation to the "segment" motions in the polymer discussed. The proper separation of Maxwell Stress effects and true electrostriction is discussed in appendix 37, where it is shown that the Maxwell Stress effect may contribute up to 50% of measured strain.

3.0 COMPOSITE SENSORS

The major focus of composite sensor studies for underwater acoustics is upon systems which involve air as one of the phases. The reason for this focus on systems which encompass hollow spaces is admirably described in the summary papers appendices 38. 39, and 41. Systems discussed include hollow minispheres of PZT, PZT microtubes, Zig-Zag transducers, Honeycomb structures, and Moonie and Cymbal flextensionals. For the cymbal design thermally induced displacement can occur and proper design of the cover plates to obviate this problem is discussed in appendix 40. The design of a doubly resonant cymbal is given in appendix 42, and can be simply accomplished using two cover plates of dissimilar dimensions or materials. In appendix 43, finite element analysis predictions of resonance conditions and coupling coefficients for the cymbal actuator are shown to be in close agreement with experiment. More detailed analysis of the hollow PZT minisphere transducer is given in appendices 44, 45, and 46. Detailed analysis of ellipsoidal, higher circumferential and breathing modes has been carried out in a cooperative program with ISEN in France and Georgia Tech using the ATILA finite element code and experimental methods. For the tangentially poled spheres $d_h g_h \sim 135{,}000\ m^2/N$ are reported. Studies reported in appendix 47 show that the moonie (cymbal) structures can be modified to provide accelerometer capability with sensitivity more than 50 times PZT disks. In appendix 48 a simple "smart structure" sensor actuator combination is shown to provide broad band acoustic wave

absorption in water. A new more detailed and precise analysis of the 2:2 composite sensor/actuator is given in appendices 49 and 50, dealing with the optimum cell structure, reflection and matching consideration both theoretically and experimentally.

4.0 ACTUATOR STUDIES

Appendix 51 discusses the ultra high strain and piezoelectric behavior in the relaxor based single crystals. The paper gives the fullest account of measurements on the 001 oriented crystal to date and rather clear indication of the intrinsic origin of the exceptional ultra high strain behavior. Current multilayer actuator systems are described in appendix 52 which gives an excellent set of references to applications in Japan, Europe, and the USA. The problem of heat generation in high duty cycle multilayer actuators is discussed in appendix 53 where the problem is clearly traced to electric hysteresis. The displacement amplification character of the cymbal composite flextensional is highlighted in appendix 54 where cymbals have been applied to piezoelectric, electrostrive and phase switching compositions. Advantages of using the more perfect sol-gel derived PLZT compositions in photostrictive application are discussed in appendix 55. Reliability consideration for multilayer actuators are categorized in appendix 56 where the influence of compressive elastic stress upon performances is discussed. The possible major influence of domain processes in the differently oriented relaxor ferroelectric MPB single crystals is discussed in appendix 57. A roundup of recent international developments in more conventional polycrystal actuators is given in appendix 58.

Current interest in variants of the bimorph actuator/amplifier are covered in appendices 59 through 65. Doubled amplifier for potential air acoustic applications using bimorph type structures are discussed in appendix 59 and in more detail in appendix 62. A more efficient d_{33} driven Caterpillar type actuator is discussed in appendix 60. A new crescent type unimorph is introduced in appendix 63 and the performance of a very wide family of "morph" type systems is compared in appendix 64. The changes of performance of the bimorphs under high driving fields are discussed in appendix 61 and a shear mode device which does not change performance at high drive levels is described in appendix 65.

5.0 INTEGRATION STUDIES

The complex internal structure of the RAINBOW type unimorph actuator is evaluated and discussed in appendix 66 revealing both the cermet interconnected metallic lead and the modified ceramic grain boundary at the sharp interface. Optimization of the bimorph based double amplifier air acoustic actuator is discussed in appendix 67 and appendix 68 giving the sound pressures which can be generated over the frequency range 50 to 1,000 Hz. Nonlinear dynamic response has also been evaluated for the RAINBOW actuator (appendix 69) leading to distortion and higher harmonics at higher drive levels. For the 1:3 composite fabricated from transversely poled tubular ceramic elements it is shown (appendix 70) that using induced piezoelectricity in lead magnesium niobate greatly enhanced effective d_{33} can be achieved whilst still keeping d_{31} effective very close to zero.

6.0 PROCESSING STUDIES

Flux growth of single crystals in the lead zinc niobate:lead titanate (PZN:PT) and lead magnesium niobate:lead titanate (PMN:PT) families are discussed in appendices 71, 72, and 74. The influence of growth conditions in PbO and $PbO:B_2O_3$ solvents including

concentration, soak time, cooling rate, and temperature limits are evaluated by their effects on resulting crystal size, quality and electrical properties. The interesting observation of oxygen evolution from superoxidized PZTs under high electric driving fields is discussed in appendix 73 with special relevance to thin film PZT structures. Chemical preparation of lead magnesium niobate and lead zinc niobate is discussed in appendices 75, 76, and 77 significant advantage is claimed in lower temperature processing and the formation of pyrochlore free phases. Processing and electrical properties of the most interesting lead indium niobate:lead scandium tantalate (PIN:PST) solid solution are discussed in appendix 78.

7.0 THIN FILM FERROELECTRICS

There is not problem in generating thick thin PZT films on matching substrates, it is however a much more demanding problem to produce films in the range 5 to 12 μ meters thick on platinized silicon. Appendix 79 discusses the technique and appendix 80 analysis the thickness dependence of properties up to 10 μ meters in thickness. Sol-gel synthesis of barium magnesium tungsten is discussed in appendix 81 and the fabrication of strontium bismuth tantalate thin films is described in appendix 82.

8.0 INSTRUMENTATION

The need to measure d_{33} in the extremely soft polyurethane elastomer films has necessitated the design of a new type of high sensitivity low contact force ultra dilatometer described in appendix 83.

9.0 GRADUATE STUDENTS IN THE PROGRAM

Student	Section	Supervisor
Edward Alberta	Materials Studies	A.S. Bhalla
James Tressler	Composite Sensors	R.E. Newnham
Hideaki Aburatani	Actuator Studies	K. Uchino
Amod Joshi	Actuator Studies	K. Uchino
Burhanettin Koc	Actuator Studies	K. Uchino
George Risch	Processing Studies	T.R. Shrout

10.0 HONORS AND AWARDS

1. Newnham, R.E., *Honorary Doctorate of Science (Sc.D.)* of Hartwick College, New York (May 1996).

2. Newnham, R.E., *Turnbull Lecturer Award Recipient*, Materials Research Society (November 1996).

3. Uchino, K., *Outstanding Research Award from Penn State Engineering Society* (May 1996).

4. Cross, L.E., *Ultrasonics Ferroelectrics and Frequency Control 1996 Achievement Award* (November 1996).

5. Bhalla, A.S., Appointed *editor* for *Ferroelectric Reviews*, Gordon and Breach.

11.0 APPRENTICE PROGRAM

The objective of the Apprentice Program in the Center for Dielectric Studies at Penn state is to provide the opportunity for minority graduating seniors to spend time in a major University Research Laboratory over the summer break following high school graduation. It is hoped that experiencing the excitement of the ongoing research program, interacting with the eminent faculty, post doctoral fellows, graduates assistants, and the many distinguished visiting scholars in the IMRL will motivate these young people to take up careers in Science and Engineering and to start their college education with renewed vigor.

The program has been in place for some seventeen years and has now helped in the education of 45 graduating seniors. In spite of the difficulty of keeping contact with students from such diverse backgrounds we know at least two have completed graduate school (PhD), one who is a highly successful business man, and several now in Industrial Research Laboratories.

During the school year (1995-96) Debbie Laubscher who had been managing the apprentice program in the IMRL over last two years left in June to take up a position in the College of Liberal Arts at Penn State. Fortunately Peggy Klinger was able to take up directly from Debbie and we were able to run a highly successful program with the following three students.

Keith Lyons was a pre-college student in a chemical engineering program at Georgia Southern University, where he was Georgia's Hope Scholarship (which requires a minimum GPA of 3.0) to support his college studies. Working with Wenwu Cao, he helped to make composite matching layer materials and conducted literature searches using computers. He also learned how to make personal web pages. After completing his BS is considering going on to graduate school.

Irving Guzman graduated from Xavier High School (a private college prep school) in New York City, ranking 50 in a class of 209. Working with Maureen Mulvihill for Kenji Uchino, he spent the summer learning how to do computer work and how to conduct literature searches. He is enrolled at Penn State for the Fall Semester. Because he was late reaching University Park he will be working five (5) hours per week with use until the first of the year in order to bring his exposure to research up to a level comparable to the other apprentices.

Sabrina Dixon graduated from Townsend Harris High School at Queens College in Flushing, New York. She has enrolled in Penn state and plans to study electrical engineering. Working with Volkmar Müeller and Qiming Zhang, she made samples, tested electron activity and assembled the samples with circuits to prepare for testing. She also conduced literature searcher. After obtaining a baccalaureate in electrical engineering, she plans to study for a masters in business.

12.0 PAPERS PUBLISHED IN REFEREED JOURNALS

1. Cross, L.E., "Ferroelectric Materials for Electromechanical Transducer Applications." *Mat. Chem. Phys* **43**, 108-115 (1996).

2. Cross, L.E., "Ferroelectric Ceramics: Materials and Application Issues." *Ceramic Transactions* **68**, 15-55 (1996).

3. Li. S., J.A. Eastman, Z. Li, C.M. Foster, R.E. Newnham, and L.E. Cross, " Size Effects in Ferroelectrics." *Phys. Lett. A* **212**, 341 (1996).

4. Li, Shaoping, J.A. Eastman, R.E. Newnham, and L.E. Cross, "Susceptibility of Nanostructured Ferroelectrics." *Japanese J. Appl. Physics* **35** (Part 2) [No. 4B], L502-L504 (1996).

5. Uchino, K., "New Applications of Photostriction." *Innovations in Mater. Res.* **1** (1), 11-22 (1996).

6. Aburatani, H. and K. Uchino, "Acoustic Emission (AE) Measurement Technique in Piezoelectric Ceramics." *Jpn. J. Appl. Phys.* **35** (2) [4B], L5160518 (1996).

7. Alberta, E. and A.S. Bhalla, "Preparation of Phase Pure Perovskited Lead Indium Niobate Ceramic." *Mater. Lett.* **29**, 127-129 (1996).

8. Zhang, Q.M., J. Zhao, T.R. Shrout, and L.E. Cross, "The Effect of Ferroelastic Coupling in Controlling the Abnormal Aging Behavior in Lead Magnesium Niobate-Lead Titanate Relaxor Ferroelectrics." *J. Mater. Res.* **12** (7), (1997).

9. Alberta, E., A.S. Bhalla, and T. Takenaka, "Piezoelectric, elastic and Dielectric Constants for Ceramics in the Solids Solution: $xPbZrO_3$ - (1-x-z)$Pb(Zn_{1/3}Nb_{2/3}O_3$ - $zPbTiO_3$." *Ferroelectrics* **188**, 109-124 (1996).

10. Zhang, Q.M., J. Zhao, K. Uchino, and J. Zheng, "Change of the Weak-Field Properties of $Pb(ZrTi)O_3$ Piezoceramics with Compressive Uniaxial Stresses and Its Links to the Effect of Dopants on the Stability of the Polarizations in the Materials." *J. Mat. Res.* **12**, 225 (1997).

11. Markowski, K., S.-E. Park, S. Yoshikawa, and L.E. Cross, "The Effect of Compositional Variations in the Lead Lanthanum Zirconate Stannate Titanate System on Electrical Properties." *J. Amer. Ceram.* **79** (12), 3297-3304 (1996).

12. Park, S.-E., K. Markowski, S. Yoshikawa, and L.E. Cross, "Effect of Electrical Properties of Barium and Strontium Additions in the Lead Lanthanum Zirconate Stannate Titanate System on Electrical Properties." *J. Amer. Ceram.* **80** (2), 407-412 (1997).

13. Blue, C.T., J.C. Hicks, S.-E. Park, S. Yoshikawa, and L.E. Cross, "In-situ X-ray Diffraction Study of the Antiferroelectric-Ferroelectric Phase Transition in PLSnZT." *Applied Physics Letter* **68** (21), 2942-2944 (1996).

14. Mulvihill, M.L., K. Uchino, Z. Li, and W. Cao, "In-situ Observation of the Domain Configurations during the Phase Transitions in Barium Titanate." *Phil. Mag. B.* **74** (1), 25-36 (1996).

15. Mulvihill, M.L., L.E. Cross, and K. Uchino, "Dynamic Motion of the Domain Configuration in Relaxor Ferroelectric Single Crystals as a Function of Temperature and Electric Field." *Ferroelectrics* **186**, 325-328 (1996).

16. Sundar, V. and R.E. Newnham, "Conversion Method Measurements of Electrostriction Coefficients in Low-K Dielectrics." *Mat. Res. Bull.* **31** (5), 545-554 (1996).

17. Sundar, V., J.-F., Li, D. Viehland, and R.E. Newnham, "Interferometric Evaluation of Electrostriction Coefficients." *Mat. Res. Bull.* **31** (5), 555-563 91996).

18. Zhang, Q.M., J. Su, and C.-H. Kim, "An Experimental Investigation of Electromechanical Responses in a Polyurethane Elastomer." *J. Appl. Phys.* **81**, 2770 (1997).

19. Fernandez, J.F., A. Dogan, Q.M. Zhang, J.F. Tressler, and R.E. Newnham, "Hollow Piezoelectric Composites, Sensors and Actuators." *A: Physical* **51** (2,3), 183-192 (1996).

20. Fernandez, J.F., A. Dogan, Q.M. Zhang, and R.E. Newnham, "Piezoelectric Composites with Enclosed Hollow Spaces." Proceedings 4th Euroceramics Conference, *Electroceramics* **5**, 39-46 (1996).

21. Koc, B., A. Dogan, J.F. Fernanadez, R.E. Newnham, and K. Uchino, "Accelerometer Application of the Modified Moonie (Cymbal) Transducer." *J. App. Phys.* **35**, 65-67 (1996).

22. Kumar, S., A. Bhalla, and L.E. Cross, "Underwater Acoustic Absorption by Collocated Smart Materials." *Ferroelectric Letters* **21**, 11-16 (1996).

23. Zheng, J., S. Takahashi, S. Yoshikawa, and K. Uchino, "Heat Generation in Multilayer Piezoelectric Actuators." *J. Amer. Ceram.* **79** (12), 3193-3198 (1996).

24. Kugel, V.D., S. Chandran, and L.E. Cross, "Caterpillar-Type Piezoelectric d_{33} Bimorph Transducer." *Appl. Phys. Lett.* **69** (14), 2021-2023 (1996).

25. Kugel, V.D., B. Xu, Q.M. Zhang, and L.E. Cross, "Bimorph-Based Piezoelectric Air Acoustic Transducer Model." *Sensors and Actuators A* (submitted 1996).

26. Elissalde, C., L.E. Cross, and C.A. Randall, "Structural-Property Relations in a Reduced and Internally Biased Oxide Wafer (RAINBOW) Actuator Material." *J. Amer. Ceram.* **79** (8), 2041-2048 (1996).

27. Wang, H., Q.M. Zhang, L.E. Cross, and C.M. Trottier, "Tailoring Material Properties by Structure Design–Radially Poled Piezoelectric Cylindrical Tube." *Ferroelectrics* **173**, 181-189 (1995).

28. Mulvihill, M., S.-E. Park, G. Risch, Z. Li, K. Uchino, and T.R. Shrout, "The Role of Processing Variables in the Flux Growth of PZN-PT Relaxor Ferroelectric Single Crystals." *Jpn. J. Appl. Phys.* **35** (Pt. 1; No. 7), 3984-3990 (1996).

29. Pan, M.-J., S.-E. Park, C.W. Park, K.A. Markowski, S. Yoshikawa, and C. Randall, "Superoxidation and Electrochemical Reactions during Switching in $Pb(Zr,Ti)O_3$ Ceramics." *J. Amer. Ceram.* **79** (11), 2971-2974 (1996).

30. Park, S.-E., M.L. Mulvihill, G. Risch, and T.R. Shrout, "The Effect of Growth Condition on Dielectric Properties of $Pb(Zn_{1/3}Nb_{2/3})O_3$ Crystal." *Jpn. J. Appl. Phys.* **36** (1) (1997).

31. Yoshikawa, Y. and K. Uchin, "Chemical Preparation of Lead-Containing Niobate Powders." *J. Amer. Ceram.* **79** (9), 2417-2421 (1996).

32. Ravindranthan, P., V. Srikanth, S. Komarneni, and A.S. Bhalla, "Processing of $Pb(Zn_{1/3}Nb_{2/3})O_3$: Ceramics at High Pressure." *Ferroelectrics* **188**, 135-141 (1996).

33. Ravindrathan, P., S. Komarneni, A.S. Bhalla, and R. Roy, "Low Temperature Chemical Routes to Smart Materials." *Ferroelectrics* **188**, 125-133 (1996).

34. Alberta, E.F. and A.S. Bhalla, "A Processing and Electrical Property Investigation of the Solid Solution: (x) $Pb(In_{1/2}Nb_{1/2})O_3$ - (1-x)$Pb(Sc_{1/2}Ta_{1/2})O_3$." *Ferroelectrics* **188**, 95-107 (1996).

35. Chen, H.D., K.R. Udayakumar, C.J. Gaskey, and L.E. Cross, "Fabrication and Electrical Properties of Lead Zirconate Titanate Thick Films." *J. Amer. Ceram.* **79** (8), 2189-2192 (1996).

36. Ravichandran, D., R. Meyer, Jr., R. Roy, R. Guo, A.S. Bhalla, and L.E. Cross, "Sol-Gel Synthesis of $Ba(Mg_{1/3}Ta_{2/3})O_3$: Phase Pure Powder and Thin Films." *Mat. Res. Bull.* **31** (7), 817-825 (1996).

13.0 PAPERS SUBMITTED FOR PUBLICATION

1. Choi, S., J.M. Jung, and A.S. Bhalla, "Dielectric, Pyroelectric and Piezoelectric of Calcium-Modified Lead Magnesium Tantalate-Lead Titanate Ceramics." *Ferroelectric Letters* **21**, 27-33 (1996).

2. Zhang, Q.M. and J. Zhao, "Polarization Responses in Lead Magnesium Niobate Based Relaxor Ferroelectrics." *Applied Physics Letters* (submitted).

3. Müeller, V. and Q.M. Zhang, "Nonlinearity and Scaling Behavior in Donor Doped Lead Zirconate Titanate Piezoceramic." *Physics Review Letters* (submitted).

4. Park, S.-E. and T.R. Shrout, "Relaxor Based Ferroelectric Single Crystals for Electro-Mechanical Actuators." *Innovations in Materials Research* (accepted).

5. Jin, B., R. Guo, and A.S. Bhalla, "Piezoelectric Properties and Equivalent Circuits of Ferroelectric Relaxor Single Crystals."

6. Li, Shaoping, J.A. Eastman, J.M. Vertrone, R.E. Newnham, and L.E. Cross, "Coherent Coupling in Ferroelectric Superlattices." (1996).

7. Su, J., Q.M. Zhang, and R.Y. Ting, "Space Charge Enhanced Electromechanical Response in Thin Film Polyurethane Elastomers." *Applied Physics Letters* (submitted).

8. Su, J., Q.M. Zhang, C.H. Kim, R.Y. Ting, and R. Capps, "Effects of Transitional Phenomena on the Electric Field Induced Strain-Electrostrictive Response of a Segmented Polyurethane Elastomer." *J. Appl. Polymer Sci.* (accepted).

9. Newnham, R.E., "Composite Sensors and Actuators," Disordered Materials, edited by G. Milton, K. Godlen, G. Grimmett, and P. Sen, Springer-Verlag, NY (accepted January 1997).

10. Tressler, J.F. and R.E. Newnham, "Doubly Resonant Cymbal Transducers, *IEEE Transactions of UFFC*, Special Issue on Transducers (accepted 1996).

11. Zhang, Q.M. and X. Geng, "Acoustic Properties of the Interface of a Uniform Medium-2-2 Piezocomposite and the Field Distributions in the Composite." *J. Appl. Phys.* (accepted).

12. Park, S.-E., and T.R. Shrout, "Ultrahigh Strain and Piezoelectric Behavior in Relaxor Based Ferroelectric Single Crystals."

13. Su, J., P. Moses, and Q.M. Zhang, "A Bimorph Based Dilatometer for Field Induced Strain Measurement in Soft and Tin Free Standing Polymer Films." *Reviews of Scientific Instruments* (submitted).

14.0 PAPERS APPEARING IN NON REFEREED PROCEEDINGS

1. Newnham, R.E., Chapter: Crystal Chemistry and Crystal Physics, in Innovative Ideas in Ceramics and Materials Curricula, edited by T. Stoebe and W. Huebner. Published by the *American Ceramic Society*, pp. 65-72 (1996).

2. Yoshikawa, S., K. Markowski, S.-E. Park, M.-J. Pan, and L.E. Cross, "Antiferroelectric-to-Ferroelectric Phase Switching Lead Lanthanum Zirconate Stannate Titanate (PLZST) Ceramics." *SPIE Proceedings* **IV** (1997).

3. Pan, M.-J., S.-E. Park, K. Markowski, and S. Yoshikawa, "Antiferroelectric-to-Ferroelectric PLZST Ceramics-II: The Effect of Pre-Stress Conditions on the Strain Behavior." Submitted *Proceedings of IEEE International Symposium on the Applications of Ferroelectrics*, Rutgers University, East Brunswick, New Jersey (August 1996).

4. M.-J. Pan, Markowski, K., S.-E. Park, S. Yoshikawa, and L.E. Cross, "Antiferroelectric-to Ferroelectric PLZSnT Ceramics-I: Structure, Compositional Modification and Electric Properties." Submitted *Proceedings of IEEE International Symposium on the Applications of Ferroelectrics*, Rutgers University, East Brunswick, New Jersey (August 1996).

5. Lopath, P.D., K.K. Shung, S.-E. Park, and T.R. Shrout, "Ultrasonic Transducers Using Piezoelectric Single Crystals Perovskites." Submitted *Proceedings of IEEE International Symposium on the Applications of Ferroelectrics*, Rutgers University, East Brunswick, New Jersey (August 1996).

6. Park, S.-E. and T.R. Shrout, "Characteristics of Relaxor-Based Piezoelectric Single Crystals for Ultrasonic Transducers." Proceedings of 1996 IEEE Ultrasonics Symposium, San Antonio, Texas (November 1996).

7. Park, S.-E., P.D. Lopath, K.K. Shung, and T.R. Shrout, "Relaxor-Based Single Crystal Materials for Ultrasonic Transducer Applications." Proceedings on SPIE's International Symposium on Medical Imaging, Newport Beach, California (February 1997).

8. Lopath, P.D., S.-E. Park, K.K. Shung, and T.R. Shrout, "$Pb(Zn_{1/3}Nb_{2/3})O_3/PbTiO_3$ Single Crystal Piezoelectrics for Ultrasonic Transducers." Proceedings on SPIE's International Symposium on Medical Imaging, Newport Beach, California (February 1997).

9. Park, S.-E. and T.R. Shrout, "Characteristics of Relaxor-Based Piezoelectric Single Crystals for Ultrasonic Transducers," *IEEE Trans. on Ultrasonics, Ferroelectric and Frequency Control Special Issue on Ultrasonic Transducers* (to be published).

10. Sundar, V., N. Kim, C. Randall, R. Yimnirun, and R.E. Newnham, "The Effect of Doping and Grain Size on Electrostriction in $PbZr_{0.52}Ti_{0.48}O_3$." Submitted *Proceedings of IEEE International Symposium on the Applications of Ferroelectrics*, Rutgers University, East Brunswick, New Jersey (August 1996).

11. Erdei, S., L. Galambos, I. Tanaka, L. Hesselik, F.W. Ainger, L.E. Cross, and R.S. Feigelson, "Segregation and Inhomogeneities in Photorefractive SBN Fibers." *SPIE Proceedings V–Photorefractive Fiber and Crystal Devices: Materials, Optical Properties, and Applications II*, **2849**, 168-173 (1996).

12. Fernandez, J.F., A. Dogan, J.T. Fielding, K. Uchino, and R.E. Newnham, "Temperature Dependence of New Design Ceramic-Metal Piezocomposites Actuators." Proceeding 4th Euroceramics Conference, *Electroceramics* **5**, 133-138 (1996).

13. Tressler, J.F., W. Cao, K. Uchino, and R.E. Newnham, "Ceramic Metal Composite Transducers for Underwater Acoustic Applications." Submitted *Proceedings of IEEE International Symposium on the Applications of Ferroelectrics*, Rutgers University, East Brunswick, New Jersey (August 1996).

14. Alkoy, S., A. Dogan, A.C. Hladky, J.K. Cochran, and R.E. Newnham, "Vibration Modes of PZT Hollow Sphere Transducers." Submitted *Proceedings of IEEE International Symposium on the Applications of Ferroelectrics*, Rutgers University, East Brunswick, New Jersey (August 1996).

15. Alkoy, S., A. Dogan, A.C. Hladky, and R.E. Newnham, "Miniature Piezoelectric Hollow Sphere Transducers (BBs)." 1996 Proceeding of IEEE International Frequency Control Symposium, pp. 586-594, Honolulu, Hawaii (1996).

16. Alkoy, S., A. Dogan, A.C. Hladky, and R.E. Newnham, "Piezoelectric Hollow Spheres." 1996 Proceeding 3rd Turkish Ceramic Society Meeting., Eds. V. Günay, H. Mandel, S. Ozgen. Istanbul, Turkey (October 1996).

17. Geng, X. and Q.M. Zhang, "Evaluation of Piezocomposites for Ultrasonic Transducer Applications–Influence of the Unit Cell Dimensions and the Properties of Constituents the Performance of 2-2 Piezocomposites." *IEEE Transactions of UFFC* (accepted).

18. Uchino, K. and S. Takahashi, "Multilayer Ceramic Actuators." *Current Opinion, Ceramic, Composites and Intergrowths*, p. 98-705 (1996).

19. Dogan, A., J.F. Fernandez, K. Uchino, and R.E. Newnham, "New Piezoelectric Composite Actuator Designs for Displacement Amplification." *Proceeding Euroceramic Conference*, 95 (1995) (in press).

20. Poosanaas, P., A. Dogan., A.V. Prasadarao, S. Komarneni, and K. Uchino, "Photostriction of Sol-Gel Processed PLZT Ceramics." *J. Electroceramics* (1996) (in press).

21. Uchino, K., "Reliability of Ceramic Actuators." Submitted *Proceedings of IEEE International Symposium on the Applications of Ferroelectrics*, Rutgers University, East Brunswick, New Jersey (August 1996).

22. Uchino, K., "High Electromechanical Coupling Piezoelectrics-How High Energy Conversion Rate is Possible?-." *Proceeding MRS 1996* (1996) (in press).

23. Uchino, K., "Recent Developments in Ceramic Actuators-Comparison Among USA, Japan and Europe."

24. Xu, B., Q.M. Zhang, V.D. Kugel, Q. M. Wang, and L.E. Cross, "Optimization of Bimorph Based Double Amplifier Actuator under Quasistatic Situation." Submitted *Proceedings of IEEE International Symposium on the Applications of Ferroelectrics*, Rutgers University, East Brunswick, New Jersey (August 1996).

25. Kugel, V.D., Q.M. Zhang, B. Xu, Q.-M. Wang, S. Chandran, and L.E. Cross, "Behavior of Piezoelectric Actuators under High Electric Field." Submitted *Proceedings of IEEE International Symposium on the Applications of Ferroelectrics*, Rutgers University, East Brunswick, New Jersey (August 1996).

26. Chandran, S., V.D. Kugel, and L.E. Cross, "CRESCENT: A Novel Piezoelectric Bending Actuator." *Proceeding SPIE's 4th Annual Symposium on Smart Structures* accepted 1997).

27. Kugel, V.D., S. Chandran, and L.E. Cross, "A Comparative Analysis of Piezoelectric Bending-Mode Actuators." Submitted *SPIE Proceedings*, Smart Structures and Materials: Smart Materials Technologies, 3040-09 (1997).

28. Wang, Q.M., B. Xu, V.D. Kugel, and L.E. Cross, "Characteristics of Shear Mode Piezoelectric Actuators," Submitted *Proceedings of IEEE International Symposium on the Applications of Ferroelectrics*, Rutgers University, East Brunswick, New Jersey (August 1996).

29. Xu. B., Q.M. Zhang, V.D. Kugel, Q. Wang, and L.E. Cross, "Optimization of Bimorph Based Double Amplifier Transducer under Quasistatic Conditions." Submitted *Proceedings of IEEE International Symposium on the Applications of Ferroelectrics*, Rutgers University, East Brunswick, New Jersey (August 1996).

30. Xu, B., Q. M. Zhang, V.D. Kugel, and L.E. Cross, "Piezoelectric Air Transducer for Active Noise Control." *Proceeding SPIE, Smart Structures and Integrated Systems* **271** (7), 388 (1996).

31. Chandran, S., V.D. Kugel, and L.E. Cross, "Characterization of the Linear and Non-Linear Dynamic Performance of RAINBOW Actuator." Submitted *Proceedings of IEEE International Symposium on the Applications of Ferroelectrics*, Rutgers University, East Brunswick, New Jersey (August 1996).

32. Park, S.-E., M. Mulvihill, P.D. Lopath, M. Zipparo, and T.R. Shrout, "Crystal Growth and Ferroelectric Related Properties of (1-x) Pb $(A_{1/3}Nb_{1/3})O_3$ - $xPbTiO_3$(A=Zn^{2+}, Mg^{2+})." Submitted *Proceedings of IEEE International Symposium on the Applications of Ferroelectrics*, Rutgers University, East Brunswick, New Jersey (August 1996).

33. Chen, H.D., K.K. Li, C.J. Gaskey, and L.E. Cross, "Thickness-Dependent Electrical Properties in Lanthanum-Doped PZT Thick Films." *Mat. Res. Soc. Symp. Proc.* **433**, 325-332 (1996).

34. Ravichandran, D., K. Yamakawa, R. Roy, A.S. Bhalla, S. Trolier-McKinstry, R. Guo, and L.E. Cross, "The Effect of Annealing Temperature on the Formation of $SrBi_2Ta_2O_9$ (SBT) Thin Films." Submitted *Proceedings of IEEE International Symposium on the Applications of Ferroelectrics*, Rutgers University, East Brunswick, New Jersey (August 1996).

15.0 INVITED PAPERS PRESENTATIONS AT NATIONAL AND INTERNATIONAL MEETINGS

1. Cross, L.E., "Electrically Driven Phase Changes for Actuator Applications," SPIE Smart Structures and Materials, San Diego, California (February 26, 1996).

2. Cross, L.E., "Transducers Studies in MRL: Overview," 1996 ONR workshop on Transducer materials and Transducers, University Park, Pennsylvania (March 1996).

3. Cross, L.E., "Relaxor Ferroelectrics," 1996 MRS Spring Meeting, San Francisco, California (April 1996).

4. Cross, L.E., "Ferroelectric Films for Dielectric and Piezoelectric Applications," 1st Conference of Israel Materials Union (AGIL), Natonya, Israel (April 1996).

5. Cross, L.E., "Electric Field Enforced Phase Transitions," Gordon Research Conference, Session: Structural Transitions in Non-Metallic Solids, Henniker, New Hampshire (June 1996).

6. Cross, L.E., "Growth Points for Ferroelectric Research in the USA," Ninth India National Meeting on Ferroelectrics, Delhi, India (October 8, 1996).

7. Cross, L.E., "Solid State Actuators and Sensors for Smart Materials," ASME International, Atlanta, Georgia (November 17, 1996).

8. Newnham, R.E., "Composite Sensors and Actuators, SPIE Meeting, San Diego, California (February 1996).

9. Newnham, R.E., "Microwave Dielectrics," Naval Research Laboratory, Washington, DC (March 1996).

10. Alkoy, S., A. Dogan, R.E. Newnham, A.C. Hladky, and J.K. Cochran, "Vibration Modes of Tangentially Poled PZT Hollow Spheres," 1996 ONR Transducer Materials and Transducers Workshop, University Park, Pennsylvania (March 1996).

11. Newnham, R.E., "Extremely Fine-Scaled Ceramics Focused Session," Amer. Ceram. Soc. Mtg., Indianapolis, Indiana (April 1996).

12. Newnham, R.E., "Composite Sensors and Actuators," ICAT Meeting, University Park, Pennsylvania (April 1996).

13. Newnham, R.E., "Size Effects in Ferroelectrics," Center for Dielectri Studies, University Park, Pennsylvania (May 1996).

14. Newnham, R.E., "Functional Composites for Sensors and Actuators: Smart Materials," Wekstoffwoche '96, Stuttgart, Germany (May 1996).

15. Alkoy, S., A. Dogan, R.E. Newnham, A.C. Hladky, and J.K. Cochran, "Miniature Piezoelectric Hollow Sphere Transducers," Frequency Control Symposium, IEEE-UFFC 50th Anniversary Meeting, Honolulu, Hawaii (June 1996).

16. Newnham, R.E., "Sensor and Actuators: Smart Crystals," Congress and General Assembly of the International Union of Crystallography, Seattle, Washington (August 13-16, 1996).

17. Fernandex, J.F., A. Dogan, K. Uchino, J.T. Fielding, J. Tressler, and R.E. Newnham, "Frequency and Size Effects in Metal-Ceramic Piezocomposites," International Conference on Electronic Ceramics and Applications, University of Aveiro, Portugal (September 2-4, 1996).

18. Villegas, M., J.F. Fernandez, C. Moure, P. Duran, V. Sundar, and R.E. Newnham, "Properties of $Pb(Zn_{0.33}Nb_{0.67})O_3$-Based Electrostrictive Ceramics," International Conference on Electronic Ceramics and Applications, University of Aveiro, Portugal (September 2-4, 1996).

19. Newnham, R.E., "Size Effects in Ferroic Oxides," International Symposium on Applications on Ferroelectric Thin Films, CURREAC, Hamamatsu, Shizuoka, Japan (September 24-26, 1996).

20. Newnham, R.E., "Size Effects in Ferroics," Toyama Prefectural University, Department of Electronics, Japan (September 27, 1996).

21. Newnham, R.E., "Smart Ceramics," Science and Art of Ceramics, The Royal Institution, London, England (October 21-23, 1996).

22. Newnham, R.E., "Molecular Mechanisms in Smart Materials," Turnbull Lecture, Materials Research Society, Boston, Massachusetts (December 2-6, 1996).

23. Fernandez, J.F., A. Dogan, J. Tressler, K. Uchino, and R.E. Newnham, "Tailoring Performance of Cymbal Actuators," Fifth International Conference on new Actuators, Bremen Germany (June 1996).

24. Fernandez, J.F., A. Dogan, J. Tressler, K. Uchino, and R.E. Newnham, "Properties of Piezoelectric Based Actuators," Fifth International Conference on New Actuators, Bremen, Germany (June 1996).

25. Newnham R.E., "Molecular Mechanisms in Smart Materials," Materials Science and Engineering Department, Penn State, University Park, Pennsylvania (September 1996).

26. Uchino, K., "Reliability of Ceramic Actuators," Amer. Ceram. Soc. Annual Mtg., Indianapolis, Indiana (April 1996).

27. Uchino, K., "High Electromechanical Coupling Piezoelectrics-How High Energy Conversion Rate is Possible?-," MRS 1996 (1996).

28. Uchino, K., "Recent Developments in Ceramic Actuators," SPIE's Symp. Smart Mater. Structures, MEMS (1996).

16.0 INVITED PAPERS PRESENTED AT UNIVERSITY, INDUSTRY, AND GOVERNMENT LABORATORIES

1. Cross, L.E., "Piezoelectric and Electrostrictive Ceramic Sensors and Actuators," United Technologies Research Center (March 11, 1996).

2. Cross, L.E., "University/Government Interaction," CDS Penn State Roadmap for Dielectrics Workshop (May 1, 1996).

3. Cross, L.E., "Relaxor Ferroelectric Self Assembling Self Limiting Nano-Composites," Ohio State Univesity, Materials Seminar (October 15, 1996).

4. Cross, L.E., "Ferroelectric Materials for Developing Application Needs," AMP Global Expert Professional Leadership Program, 1st International Lecture (October 22, 1996).

5. Cross, L.E., "Ferroelectric Films for Dielectric and Piezoelectric Applictaion," University of West Virginia, Physics Colloquium (November 21, 1996).

6. Newnham, R.E., "Microwave Dielectrics," Naval Research Laboratory, Washington, DC (March 22, 1996).

7. Tressler, J.F., W. Cao, K. Uchino, and R.E. Newnham, "Ceramic-Metal Composite Transducers for Underwater Acoustic Applications," 1996 ONR Transducer Materials and Transducers Workshop, University Park, Pennsylvania (March 25-27, 1996).

8. Dogan, A., J.F. Fernandez, K. Uchino, and R.E. Newnham, "The 'Moonie' and 'Cymbal' Electromechanical Actuators," 1996 ONR Transducer Materials and Transducers Workshop, University Park, Pennsylvania (March 25-27, 1996).

9. Sundar, V., R. Yimnirun, and R.E. Newnham, "The Role of Polarization Mechanisms in Electrostrictive Effects for Low Permittivity Glasses and Ceramics," 1996 ONR Transducer Materials and Transducers Workshop, University Park, Pennsylvania (March 25-27, 1996).

10. Alkoy, S., A. Dogan, R.E. Newnham, A.C. Hladky, and J.K. Cochran, "Vibration Modes of Tangentially Poled PZT Hollow Spheres," 1996 ONR Transducer Materials and Transducers Workshop, University Park, Pennsylvania (March 25-27, 1996).

11. Newnham, R.E., "Size Effects in Ferroelectrics," Center for Dielectric Studies, Penn State University, University Park, Pennsylvania (May 1, 1996).

12. Newnham, R.E., "Molecular Mechanism in Smart Materials," Materials Science and Engineering Department, Penn State University, University Park, Pennsylvania (September 5, 1996).

13. Newnham, R.E., "Electronic Ceramics," Ceramic Arts Department, College of Arts and Architecture, Penn State University, University Park, Pennsylvania (October 3, 1996).

14. Newnham, R.E., "Molecular Mechanisms in Smart Materials," Mathematics Workshop for Materials Studies and Industrial Applications, Penn State University, University Park, Pennsylvania (October 24-26, 1996).

15. Newnham, R.E., "Ceramic Engineering in the 21st Century," Corning Research Laboratory, Corning, New York (October 31, 1996).

16. Newnham, R.E., "Smart Ceramics," Seminar at Berks Campus of the Pennsylvania State University, Reading, Pennsylvania (November 11, 1996).

17. Uchino, K., "Recent Development of Piezoelectric Acuators," Kyocera, Kagoshima, Japan (June 1996).

18. Uchino, K., "Domain Contribution to Piezoelectricity," NEC, Kawasaki, Japan (June 1996).

19. Uchino, K., "High k Single Crystals," Toshiba, Kawasaki, Japan (June 1996).

20. Uchino, K., "Novel Ceramic Actuators," OMRON, Sakura, Japan (July 1996).

21. Uchino, K., "Recent Development of Ceramic Actuators," NGK Insulators, Nagoya, Japan (July 1996).

22. Uchino, K., "Reliability of Ceramic Actuators," Chichibu-Onoda Cement (July 1996).

23. Uchino, K., "Ceramic Actuators," Allied Signal, NJ (August 1996).

24. Uchino, K., "Ceramic Actuators," Japan Energy, Saitama, Japan (September 1996).

25. Uchino, K., "Recent Development of Ceramic Actuators," Taiyo Yuden, Takasaki, Japan (September 1996).

26. Uchino, K., "High Power Ultrasonic Applications," Mitsui Petrochemical, Chiba, Japan (September 1996).

27. Uchino, K., "Recent Development of Ceramic Actuators," TDK, Chiba, Japan (September 1996).

28. Uchino, K., "Ceramic Actuators," Goddard Space Flight Center, MD (September 1996).

29. Uchino, K., "Piezoelectric Actuator/Sensor Materials," Kasei Optonics, Odawara, Japan (October 1996).

30. Uchino, K., "High Power Piezoelectric Measurements," Chichibu-Onoda Cement, Sakura, Japan (October 1996).

31. Uchino, K., "Piezoelectric Actuators and Ultrasonic Motors," MTEC, Bangkok, Thailand (October 29- Nov.1, 1996).

32. Uchino, K., "Piezoelectric Actuators," National University of Singapore, Singapore (November 1996).

33. Uchino, K., "Piezoelectric Actuators," Mitsubishi Materials, Omiya, Japan (November 1996).

34. Uchino, K., "Relaxor Ferroelectric Single Crystals," Foster-Miller Inc., Boston, MA (December 1996).

35. Uchino, K., "Piezoelectric Actuators and Ultrasonic Motors," National Univ. of Singapore, Singapore (December 1996).

36. Uchino, K., "Piezoelectric Actuators," Hitachi Metal, Saitama, Japan (December 1996).

37. Uchino, K., "High Power Ultrasonic Devices," Tokin, Sendai, Japan (December 1996).

17.0 CONTRIBUTED PAPERS AT NATIONAL AND INTERNATIONAL MEETINGS

1. Mulvihill, M. L., L.E. Cross, K. Uchino, and W. Cao, "Domain Related Phase Transitions in Lead Zinc Niobate Relaxor Ferroelectric Single Crystals," 1996 ONR Transducer Materials and Transducers Workshop, State College, Pennsylvania (March 1996).

2. Tressler, W. Cao, K. Uchino, and R. E. Newnham, "Capped Ceramic Electroacoustic Transducers," 1996 ONR Transducer Materials and Transducers Workshop, University Park, PA (March 1996).

3. Dogan, A., J. F. Tressler, J. F. Fernandez, K. Uchino, and R. E. Newnham, "Electroactive Roto-Flextensional Actuators," Amer. Ceram. Soc. Annual Mtg., Indianapolis, IN (April 1996).

4. Joshi, A., S. J. Yoon, and K. Uchino, "Evaluation of PYW-PZT Composition for High Power Applications," Amer. Ceram. Soc. Annual Mtg., Indianapolis, IN (April 1996).

5. Witham, J. P. and K. Uchino, "Optical Study of Domains in PLZT Ceramics," Amer. Ceram. Soc. Annual Mtg., Indianapolis, IN (April 1996).

6. Tressler, J. F., J. F. Fernandez, K. Uchino, and R. E. Newnham, "Capped Ceramic Pressure Sensors," Amer. Ceram. Soc. Annual Mtg., Indianapolis, IN (April 1996).

7. Aburatani, H. and K. Uchino, "Stress and Fatigue Estimation in Multilayer Ceramic Actuators Using An Internal Strain Gauge," Amer. Ceram. Soc. Annual Mtg., Indianapolis, IN (April 1996).

8. Chen, Y. H. and K. Uchino, "Monomorph Characteristics in Zinc Borate Doped PZT," Amer. Ceram. Soc. Annual Mtg., Indianapolis, IN (April 1996).

9. Poosanaas, P., A. Dogan, A. V. Prasadarao, S. Komarneni, and K. Uchino, "Effect of Ceramic Processing Method on the Photostrictive Properties of WO_3 and Nb_2O_5 Doped PLZT," Amer. Ceram. Soc. Annual Mtg., Indianapolis, IN (April 1996).

10. Zheng, Z. and K. Uchino, "Critical Uniaxial Stress in Piezoelectric Ceramics," Amer. Ceram. Soc. Annual Mtg., Indianapolis, IN (April 1996).

11. Joshi, A., S. J. Yoon and K. Uchino, "Compact Ultrasonic Motor," Amer. Ceram. Soc. Annual Mtg., Indianapolis, IN (April 1996).

12. Koc, B., A. Dogan, R. E. Newnham, and K. Uchino, "Characterization of the Modified Cymbal Transducers," Amer. Ceram. Soc. Annual Mtg., Indianapolis, IN (April 1996).

13. Witham, J. P. and K. Uchino, "Optical Study of Domains in PLZT Ceramics," 17th Smart Actuator Symp., University Park, PA (April 1996).

14. Chen, Y. H. and K. Uchino, "Semiconductive Characteristics in Zinc Borate Doped PZT," 17th Smart Actuator Symp., University Park, PA, April (1996).

15. Poosanaas, P., A. Dogan, A. V. Prasda Rao, S. Komarneni, and K. Uchino, "Photostrictive Properties of PLZT Ceramics Derived from A Sol-Gel Processing," 17th Smart Actuator Symp., University Park, PA, (April 1996).

16. Belegundu, U., S. E. Park, M. Mulvihill, T. Shrout, K. Uchino, and L. E. Cross, "Dielectric and Piezoelectric Properties of).90PZN-0.10PT Single Crystals," 17th Smart Actuator Symp., University Park, PA (April 1996).

17. Dogan, A., P. Poosanaas, A. V. Prasda Rao, S. Komarneni, and K. Uchino, "Photostrictive Properties of PLZT Ceramics," Turkish Ceram. Soc. III. Ceram. Congress, Istanbul, Turkey (1996).

18. Poosanaas, P., A. Dogan, A. V. Prasda Rao, S. Komarneni, and K. Uchino, "Photostrictive Properties of PLZT Ceramics Derived from A Sol-Gel Process," Proc. 6th Annual Workshop on Sci. and Tech. Exchange between Thai Professionals in North America and Thailand, Edmonton, Alberta, Canada (1996).

19. Tressler, J. F., W. Cao, K. Uchino and R. E. Newnham, "Ceramic-Metal Composite Transducers for Underwater Acoustic Applications," Proc. 10th Int'l Symp. Appl. Ferroelectrics, East Brunswick, NJ (August 1996).

20. Mulvihill, M. L., L. E. Cross, K. Uchino and W. Cao, "Domain Related Phase Transitions in Lead Zinc Niobate Relaxor Ferroelectric Single Crystals," Proc. 10th Int'l Symp. Appl. Ferroelectrics, P2-51, East Brunswick, NJ (August 1996).

21. Aburatani, H., K. Uchino, "Acoustic Emission (AE) Measurement in Piezoelectric Ceramics," Proc. 10th Int'l Symp. Appl. Ferroelectrics, East Brunswick, NJ (August 1996).

22. Park, S. E., M.L. Mulvihill, G. Risch and T.R. Shrout: "The Effect of Growth Conditions on Dielectric Properties of $Pb(Zn_{1/3}Nb_{2/3})O_3$ Crystals," Proc. 10th Int'l Symp. Appl. Ferroelectrics, East Brunswick, NJ (August 1996).

23. Mulvihill, M. L., "Domain Related Phase Transitions in Lead Zinc Niobate Relaxor Ferroelectric Single Crystals," 17th Smart Actuator Symp., State College, Pennsylvania (April 1996).

24. Alkoy, S., A. Dogan, A.C. Hladky, J.K. Cochran, and R.E. Newnham, "Vibration Modes of PZT Hollow Sphere Transducers," 10th Int'l Symp. on Applications of Ferroelectrics, East Brunswick, NJ (August 1996).

25. Dogan, A., J.F. Fernandez, K. Uchino, and R.E. Newnham, "The Cymbal Electromechanical Actuator," 10th Int'l Symp. on Applications of Ferroelectrics, East Brunswick, NJ (August 1996).

26. McNeal, M.P. S.J. Jang, and R.E. Newnham, "Particle Size Dependent High Frequency Dielectric Properties of $BaTiO_3$," 10th Int'l Symp. on Applications of Ferroelectrics, East Brunswick, NJ (August 1996).

27. Sundar, V., N.C. Kim, R. Yimnirun, C.A. Randall, and R.E. Newnham, The Effect of Doping and Grain Size on Electrostriction in $PbZr_{0.52}Ti_{0.48}O_3$," 10th Int'l Symp. on Applications of Ferroelectrics, East Brunswick, NJ (August 1996).

28. Tressler, J.F., W. Cao, K. Uchino, and R.E. Newnham, "Ceramic-Metal Composite Transducers for Underwater Acoustic Applications," 10th Int'l Symp. on Applications of Ferroelectrics, East Brunswick, NJ (August 1996).

29. Newnham, R.E., "Size Effects in Ferroic Oxides," Amer. Ceram. Soc. Mtg., Indianapolis, IN (April 1996).

30. Newnham, R.E. and G.R. Ruschau, "Composites Sensors and Actuators," Amer. Ceram. Soc. Mtg., Indianapolis, IN (April 1996).

31. Koc, B., A. Dogan, R.E. Newnham, and K. Uchino, "Characterization of the Modified Cymbal Transducers," Amer. Ceram. Soc. Mtg., Indianapolis, IN (April 1996).

32. Bowen, C.P., T.R. Shrout, R.E. Newnham, and C.A. Randall, "Effects of Processing Conditions on Electrically Generated Composite Materials," Amer. Ceram. Soc. Mtg., Indianapolis, IN (April 1996).

33. Alkoy, S., A. Dogan, and R.E. Newnham, "Piezoelectric Hollow Sphere Transducers," Amer. Ceram. Soc. Mtg., Indianapolis, IN (April 1996).

34. Tressler, J.F., J.F. Fernandez, K. Uchino, and R.E. Newnham, "Capped Ceramic Pressure Sensors," Amer. Ceram. Soc. Mtg., Indianapolis, IN (April 1996).

35. Sundar, V., T.R. Shrout, C.A. Randall, and R.E. Newnham, "Electrostrictive and Dielectric Property Variations with Grain Size in Undoped PZT 52/48," Amer. Ceram. Soc. Mtg., Indianapolis, IN (April 1996).

36. Fernandez, J.F., A. Dogan, K. Uchino, J.T. Fielding, J. Tressler, and R.E. Newnham, "Frequency and Size Effects in Metal-Ceramic Piezocomposites," International Conference on Electronic Ceramics and Applications, University of Aveiro, Portugal (September 1996).

37. Villegas, M., J.F. Fernandez, C. Moure, P. Duran, V. Sundar, and R.E. Newnham, "Properties of $Pb(Zn_{0.33}Nb_{0.67})0_3$-Based Electrostrictive Ceramics," International Conference on Electronic Ceramics and Applications, University of Aveiro, Portugal (September 1996).

38. Tressler, J.F., W. Cao, K. Uchino, and R.E. Newnham, "Ceramic-Metal Composite Transducers for Underwater Acoustic Applications," 1996 ONR Transducer Materials and Transducers Workshop, University Park, PA (March 1996).

39. Dogan, A., J.F. Fernandez, K. Uchino, and R.E. Newnham, "The 'Moonie' and 'Cymbal' Electromechanical Actuators," 1996 ONR Transducer Materials and Transducers Workshop, University Park, PA (March 1996).

40. Sundar, V., R. Yimnirun, and R.E. Newnham, "The Role of Polarization Mechanisms in Electrostrictive Effects for Low Permittivity Glasses and Ceramics," 1996 ONR Transducer Materials and Transducers Workshop, University Park, PA (March 1996).

41. Venkataramani, V.S., "Particle Engineering of Intelligent Processing of Piezoelectric Ceramics," Amer. Ceram. Soc. Mtg., Indianapolis, IN (April 1996).

42. Meyer, R.J., J. Witham, S. Yoshikawa, and T.R. Shrout, "Fabrication of Perovskite Fibers Using Sol-Gel Technology," Amer. Ceram. Soc. Mtg, Indianapolis, IN (April 1996).

43. Bowen, C.P., T.R. Shrout, R.E. Newnham, C.A. Randall, "Effects of Processing Conditions on Electrically Generated Composite Materials, Amer. Ceram. Soc. Mtg., Indianapolis, IN (April 1996).

44. Zhao, J., Q.M. Zhang, and T.R., "Aging Characteristics of Relaxor Ferroelectrics of PMN-PT Under Constant Bias Electric Field," Amer. Ceram. Soc. Mtg., Indianapolis, IN (April 1996).

45. Park, S.E., M.J. Pan, K. Markowski, S. Yoshikawa, T.R. Shrout, and L.E. Cross, "E-Field Induced Phase Transition of Antiferroelectric Lead Lanthanum Zirconate Titanate Stannate (PLZTs) Ceramics, Amer. Ceram. Soc. Mtg., Indianapolis, IN (April 1996).

46. Meyer, R., Jr., J. Witham, S. Yoshikawa, and T.R. Shrout, "Fabrication of Perovskite Ceramic Fibers Using Sol-Gel Technology, MRS Meeting, San Francisco, CA (April 1996)

47. Alberta, E.F. and A.S. Bhalla, "Dielectric Piezoelectric and Pyroelectric Constants for Lead Indium Niobate Based Ceramics," 10th Int'l Symp. on Applications of Ferroelectrics, East Brunswick, NJ (August 1996).

48. Alberta, E.F. and A.S. Bhalla, "Preparation of Phase Pure Perovskite Lead Indium Niobate Ceramics," 10th Int'l Symp. on Applications of Ferroelectrics, East Brunswick, NJ (August 1996).

49. Ravichandran, D., E.K. Yamakawa, R. Roy, A.S. Bhalla, S. Trolier-McKinstry, R. Guo, and L.E. Cross, "The Effect of Annealing Temperature on the Formation of $SrBi_2Ta_2O_9$ Thin Films," 10th Int'l Symp. on Applications of Ferroelectrics, East Brunswick, NJ (August 1996).

50. Ravichandran, D., R. Roy, A.S. Bhalla, R. Guo, and L.E. Cross, "Alkoxide Derived $SrBi_2Nb_2O_9$ Phase Pure Powders and Thin Films," MRS Fall Meeting (1996).

51. Uchino, K., "Reliability of Ceramic Actuators," proc. 10th Intenational Symposium on Applications of Ferroelectrics, P2-79, East Brunswick, New Jersey (August 1996).

52. Aburatani, H. and K. Uchino, "Acoustic Emission (AE) Measurement in Piezoelectric Ceramics," Proc. 10th International Symposium on Applications of Ferroelectrics, P3-40, East Brunswick, New Jersey (August 1996).

53. Poosanaas, P., K. Uchino, K. Tonooka, and S. Thakoor, "Influence of Dopants and Surface roughness on Photovoltaic Properties in PLZT Ceramics," 19th Smart Actuator Symposiurm, Univesity Park, Pennsylvania (September 1996).

54. Chen, Y.H. and K. Uchino, "High-Power Characteristicsin Zinc Borate Doped PZT," 19th Smart Actuator Symposium, University Park, Pennsylvania (September 1996).

55. Belegundu, U. and K. Uchino, "In situ Observation of Domain Reorientation in 0.90PZN-0.10PT Single Crystals Under the Application of Electric Field and Temperature," Mater. Res. Soc., Fall Meeting, Boston, Massachusetts (December 1996).

18.0 BOOKS (AND SECTIONS THERE OF

1. Uchino, K., Piezoelectric Actuators and Ultrasonic Motors, Kluwer Academic Publishers, Norwell, Massachusetts (1996).

2. Randall, C.A. and J.P. Dougherty, "Integrated Ceramic Packaging," The Era of Materials, to be published by The Pennsylvania Academy of Science.

3. Cross, L.E. and S. Trolier-McKinstry, "Ferroelectrics," The Era of Materials, to be published by The Pennsylvania Academy of Sciences.

4. Cross, L.E. and S. Trolier-McKinstry, "Thin Film Integrated Ferroelectrics," Encyclopedia of Applied Physics, VCH Publishers.

GENERAL SUMMARY PAPERS

APPENDIX 1

ELSEVIER

Materials Chemistry and Physics 43 (1996) 108–115

MATERIALS CHEMISTRY AND PHYSICS

Review

Ferroelectric materials for electromechanical transducer applications[1]

Leslie Eric Cross

Intercollege Materials Research Laboratory, The Pennsylvania State University, University Park, PA 16802-4800, USA

Received 10 January 1995; accepted 15 February 1995

Abstract

This paper explores the special characteristics of ferroelectric materials which make them highly suitable for application as both sensors and actuators in electromechanical (smart) systems. The domain structure which gives the possibility to impart a polar axis in a randomly axed polycrystal ceramic is essential for piezoelectricity, but all electromechanical behavior may be traced ultimately to the electrostrictive coupling between polarization and strain fields. Topics to be discussed will include: (1) the special advantages of materials in the lead zirconate:lead titanate solid solution systems for both sensing and actuation; (2) domain and phase switching contributions to electrical, mechanical and coupled responses; (3) scaling effects in ferroics and the origins of the relaxor ferroelectric behavior of electrostrictive ceramics: (4) composite polymer:ceramic systems and the maneuverability engendered by phase connectivity control.

Keywords: Sensors; Actuators; Piezoelectric; Ferroelectric; Electrostrictive: Ceramic composites

1. Introduction

Interest in electromechanical transduction has recently increased markedly with the realization of the possibility of using electro-active sensors and actuators, coupled through sophisticated solid state electronics, to modify and control the mechanical behavior of complex materials and structures. The phenomenon of piezoelectricity is exciting in this context, as the converse effect gives direct conversion of the electric field into elastic strain (shape change) for the actuation function and the direct effect permits conversion of elastic stress into electrical polarization (electric field) for the sensing function. For a randomly axed ceramic polycrystal the spherical texture symmetry forbids piezoelectricity irrespective of the symmetry of the ceramic grain; however, in some ferroelectric ceramics, the reorientable domain structure permits the induction of a macroscopic polar axis, reducing the symmetry to conical and producing a very strong piezoelectric response.

This review will explore the many advantages of ferroelectric compositions in the lead zirconate:lead titanate (PZT) solid solutions for both sensing and actuation. The state of understanding of both intrinsic single domain and extrinsic domain wall and phase boundary contributions to response will be examined, and the composition manipulations used to modify the extrinsic responses explored. In lead magnesium niobate (PMN) based solid solutions a nanometer scale ordering of Mg:Nb cations breaks up the conventional ferroelectric coupling, leading to glass-like relaxor ferroelectric response.

The absence of stable macrodomains in certain composition:temperature regions leads to highly reproducible electrostriction properties. The performance will be compared and contrasted to the more conventional PZTs.

For large area transducers, the density and rigidity of PZT gives problems, and the manner in which this may be addressed and at the same time properties markedly improved in piezoceramic:polymer composites will be briefly explored.

[1] ICEM invited paper.

Elsevier Science S.A.
SSDI 0254-0584(95)01617-4

2. Material considerations

For an insulating crystal the piezoelectric and electrostrictive responses may be completely defined by a simple tensor equation

$$x_{ij} = s_{ijkl}X_{kl} + d_{mij}E_m + M_{mnij}E_mE_n \quad (1)$$

where x_{ij} and X_{kl} are components of elastic strain and elastic stress, respectively; E_mE_n are components of electric field; s_{ijkl} the conventional elastic compliances in infinitesimal strain; d_{mij} the piezoelectric tensor components; and M_{mnij} the electrostriction tensor components.

In Eq. (1) the Einstein summation convention is assumed so that as *ijklmn* run from 1 to 3 a set of nine equations for the components of x_{ij} is generated.

If the crystal symmetry is such that third rank polar tensor components are permitted, the crystal is piezoelectric, so that when all components of stress are zeros

$$x_{ij} = d_{mij}E_m \quad (2)$$

describes the actuating function; again *mij* run from 1 to 3. Frequently Eq. (2) is constructed in matrix form, $x_o = d_{mo}E_m(3)$, where now o runs from 1 to 6, and m from 1 to 3. From energy considerations one may derive a complementary equation

$$P_m = d_{mij}X_{ij} \quad (3)$$

which delineates the sensing function.

For higher crystal symmetries (such as centric) where all $d_{mij} \equiv 0$, the strain then depends on the higher order effect

$$x_{ij} = M_{mnij}E_mE_n \quad \text{for all } X_{nkl} \equiv 0 \quad (4)$$

which defines electrostriction and dielectric susceptibility

$$\eta_{mn} = M_{mnij}X_{ij} \quad (5)$$

defines the converse effect, which is the elastic stress dependence of dielectric permittivity. In a single crystal such as quartz, the nonzero d_{mij} depend on the symmetry and are well determined material constants.

For a randomly axed polycrystal ceramic, the spherical texture symmetry (Curie group $\infty\infty$) forbids piezoelectricity; however, in a ferroelectric ceramic domain switching permits the induction of a polar axis which remains after the field is removed, lowering the symmetry to Curie group ∞mm, which permits nonzero piezoelectric d_{33}, $d_{31} = d_{32}$, $d_{24} = d_{15}$ constants (Fig. 1(a)). The need to pole the electroceramic leads to many important consequences.

(1) For effective poling in a randomly axed structure there is a need for many possible domain orientations so that P_s may thread through, making only small angles

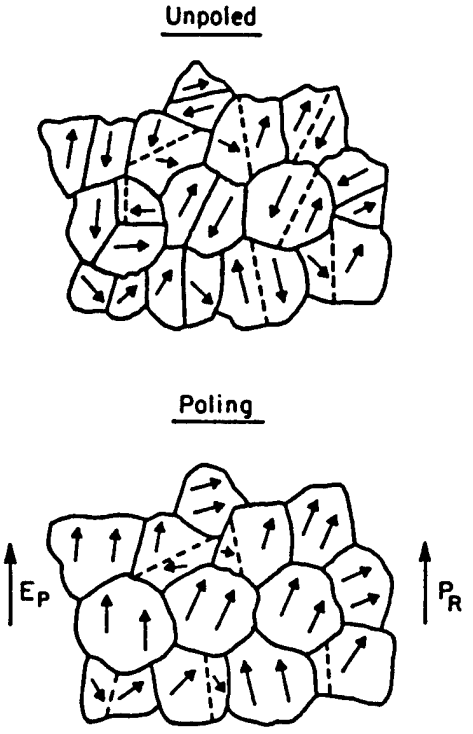

Fig. 1(a). The importance of domain structure in the ferrolectric ceramic to permit poling to a piezoelectrically active state. (Unpoled) The symmetry is $\infty\infty$, which is centric and forbids piezoelectricity. (Poling) The symmetry is ∞mm, which is noncentric (polar) and permits piezoelectricity.

with the poling E field. Such a requirement favors ferroelectric states from a high symmetry paraelectric prototype—hence the popularity of the simple cubic mixed oxide perovskite structure ferroelectrics.

(2) Unlike ferromagnets, the ordering in a ferroelectric domain is 'soft' so that the P vector may be sensibly changed in both magnitude and direction by quite realizable E fields. This intrinsic softening becomes strongly enhanced near ferroelectric phase transitions and close to the transition can contribute in a major way to both dielectric and piezoelectric activity.

(3) After poling the ferroelectric ceramic can settle into any one of the very large family of metastable complex domain configurations. Thus the measured property constants $\bar{\varepsilon}_{11}$, $\bar{\varepsilon}_{33}$, $\bar{d}_{33}$, $\bar{d}_{31}$, $\bar{d}_{15}$, $\bar{s}_{11}$, $\bar{s}_{12}$, ... are in fact orientational averages which depend in a complex manner on fabrication, grain size, poling conditions, etc.

(4) Since the domain structure must be changeable at high electric fields to permit the poling, it is sensible to expect that there may be ancillary (extrinsic) shape change due to reversible domain wall motion and that these extrinsic effects may contribute strongly to dielectric and piezoelectric performance.

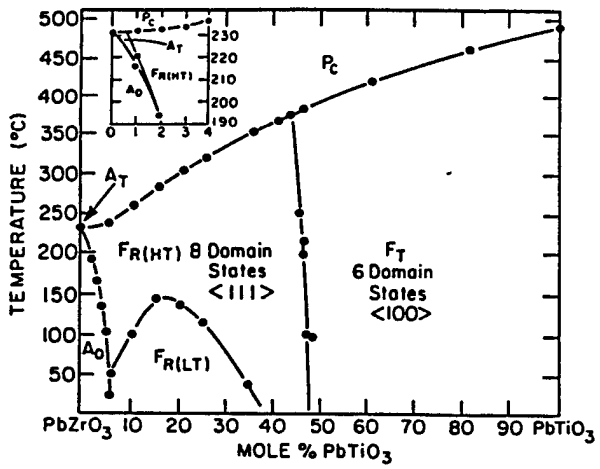

Fig. 1(b). The PZT solid solution phase diagram.

3. Advantages of the $PbZrO_3$:$PbTiO_3$ (PZT) system

From the phase diagram of the PZT solid solution system, several advantages for this system are immediately evident (Fig. 1(b)).

(1) Above the Curie temperatures the symmetry is cubic, the structure is perovskite [1].

(2) The high Curie temperatures across the whole diagram lead to stable ferroelectric states over wide usable temperature ranges.

(3) The morphotropic phase boundary (MPB) [2] separating rhombohedral (8 domain states) and tetragonal (6 domain states) ferroelectric forms is first order, so there is necessarily a two-phase region near this 52/48 Zr/Ti composition.

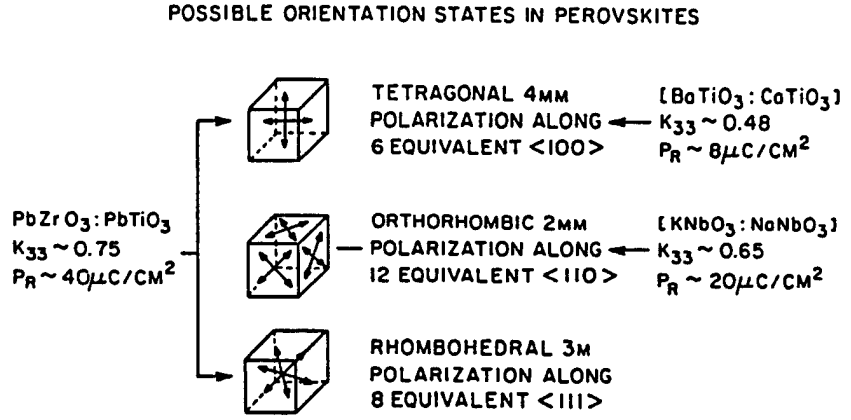

Fig. 1(c). The value of the mixed phase region at the MPB in poling of PZT vs. other perovskite ferroelectrics.

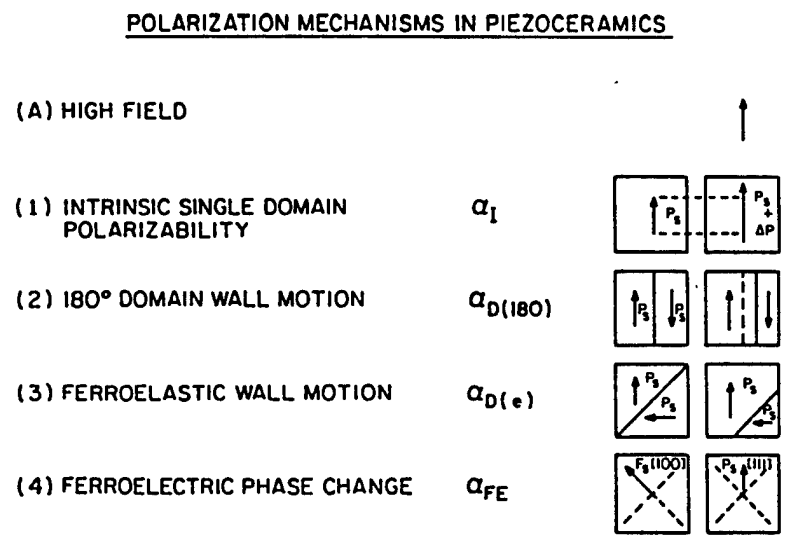

Fig. 2. Possible contributors to the dielectric polarizability in an MPB composition of PZT.

(4) In the two-phase region the poling field may draw upon 14 orientation states leading to exceptional ceramic polability (Fig. 1c).

(5) As the MPB is near vertical on the phase diagram, intrinsic property enhancement for compositions chosen near to the boundary persists over a wide temperature range.

PZT compositions have been studied for more than 40 years, and a huge library of empirical data involving a vast range of PZTs and additive and substitutional compositions is available; however, some facets of the basic understanding are very fragile. Looking just at the possible polarization changes under electric field (Fig. 2), polarization in the domain itself may be changed (Fig. 2.1), 180° domain walls may move (Fig. 2.2), non 180° walls which must also be shape changing may move (Fig. 2.3) and for MPB compositions, the balance of phases may be changed (Fig. 2.4), also leading to shape change.

The intrinsic polarizability and associated piezoelectric responses have been difficult to evaluate, as there are no good single crystals of the appropriate compositions. However, intensive studies by Haun et al. [3–9] have developed a framework of Landau–Ginsburg–Devonshire theory that provides a function which fits well with all aspects of the phase diagram (Fig. 3) and permits evaluation of the intrinsic component of response at any composition or temperature within the phase field.

$$
\begin{aligned}
\Delta G = {} & \alpha_1[P_1^2 + P_2^2 + P_3^2] + \alpha_{11}[P_1^4 + P_2^4 + P_3^4] \\
& + \alpha_{12}[P_1^2P_2^2 + P_2^2P_3^2 + P_3^2P_1^2] + \alpha_{111}[P_1^6 + P_2^6 + P_3^6] \\
& + \alpha_{112}[P_1^4(P_2^2 + P_3^2) + P_2^4(P_1^2 + P_3^2) + P_3^4(P_1^2 + P_2^2)] \\
& + \alpha_{123}P_1^2P_2^2P_3^2 + \sigma_1[p_1^2 + p_2^2 + p_3^2] + \sigma_{11}[p_1^4 + p_2^4 + p_3^4] \\
& + \sigma_{12}[p_1^2p_2^2 + p_2^2p_3^2 + p_3^2p_1^2] + \sigma_{111}[p_1^6 + p_2^6 + p_3^6] \\
& + \sigma_{112}[p_1^4(p_2^2 + p_3^2) + p_2^4(p_1^2 + p_3^2) + p_3^4(p_1^2 + p_2^2)] \\
& + \sigma_{123}p_1^2p_2^2p_3^2 + \mu_{11}[P_1^2p_1^2 + P_2^2p_2^2 + P_3^2p_3^2] \\
& + \mu_{12}[P_1^2(p_2^2 + p_3^2) + P_2^2(p_1^2 + p_3^2) + P_3^2(p_1^2 + p_2^2)] \\
& + \mu_{44}[P_1P_2p_1p + P_2P_3p_2p_3 + P_3P_1p_3p_1] + \beta_1[\theta_1^2 + \theta_2^2 + \theta_3^2] \\
& + \beta_{11}[\theta_1^4 + \theta_2^4 + \theta_3^4] + \gamma_{11}[P_1^2\theta_1^2 + P_2^2\theta_2^2 + P_3^2\theta_3^2] \\
& + \gamma_{12}[P_1^2(\theta_1^2 + \theta_2^2) + P_2^2(\theta_1^2 + \theta_3^2) + P_3^2(\theta_1^2 + \theta_2^2)] \\
& + \gamma_{44}[P_1P_2\theta_1\theta_2 + P_2P_3\theta_2\theta_3 + P_3P_1\theta_3\theta_1] \\
& - \tfrac{1}{2}S_{11}[X_1^2 + X_2^2 + X_3^2] - S_{12}[X_1X_2 + X_2X_3 + X_3X_1] \\
& - \tfrac{1}{2}S_{44}[X_4^2 + X_5^2 + X_6^2] - Q_{11}[X_1P_1^2 + X_2P_2^2 + X_3P_3^2] \\
& - Q_{12}[X_1(P_2^2 + P_3^2) + X_2(P_1^2 + P_3^2) + X_3(P_1^2 + P_2^2)] \\
& - Q_{44}[X_4P_2P_3 + X_5P_1P_3 + X_6P_1P_2] - Z_{11}[X_1^2p_1 + X_2^2p_2 + X_3^2p_3] \\
& - Z_{12}[X_1(p_2^2 + p_3^2) + X_2(p_1^2 + p_3^2) + X_3(p_1^2 + p_2^2)] \\
& - Z_{44}[X_4p_2p_3 + X_5p_1p_3 + X_6p_1p_2] - R_{11}[X_1\theta_1^2 + X_2\theta_2^2 + X_3\theta_3^2] \\
& - R_{12}[X_1(\theta_2^2 + \theta_3^2) + X_2(\theta_1^2 + \theta_3^2) + X_3(\theta_1^2 + \theta_2^2)] \\
& - R_{44}[X_4\theta_2\theta_3 + X_5\theta_1\theta_3 + X_6\theta_1\theta_2]
\end{aligned}
$$

Fig. 3(a). Thermodynamic function.

During the course of many years of empirical development a wide range of low level additives (0–5 mol%) have been found to have a marked influence upon the extrinsic contributions to dielectric and piezoelectric response [10]. In general, the aliovalent oxides fall into two distinct groups: electron donors where the charge on the cation is larger than that which it replaces, and electron acceptor additives where the charge on the cation is smaller than that which it replaces. The donor additions enhance both dielectric and piezoelectric response at room temperature and under high fields show symmetric unbiased hysteresis loops with good squareness and lower coercivity (hence the name soft PZTs) [11,12]. The acceptor additives in general reduce both dielectric and piezoelectric response, give rise to highly asymmetric hysteresis, larger electrical coercivity (hence the name hard PZTs) and much higher mechanical Q. That the dopants largely effect the extrinsic properties may be judged from low temperature measurement of the response for different dopants in the same Zr/Ti ratio (PZT) (Fig. 4). The weak field permittivity has a very large difference at room temperature ($3000 \Rightarrow \approx 750$) which is completely absent at helium temperature, where domain and phase boundary contributions are lost, and the level agrees well with the calculated intrinsic response.

In the acceptor modified compositions there are very good explanations of how the domain (not the domain wall) is stabilized [13,14]. Essentially, the charged acceptor associates with an oxygen vacancy to produce a slowly moving defect dipole pair, which orients in the field of the domain, slowly stabilizing the existing vari-

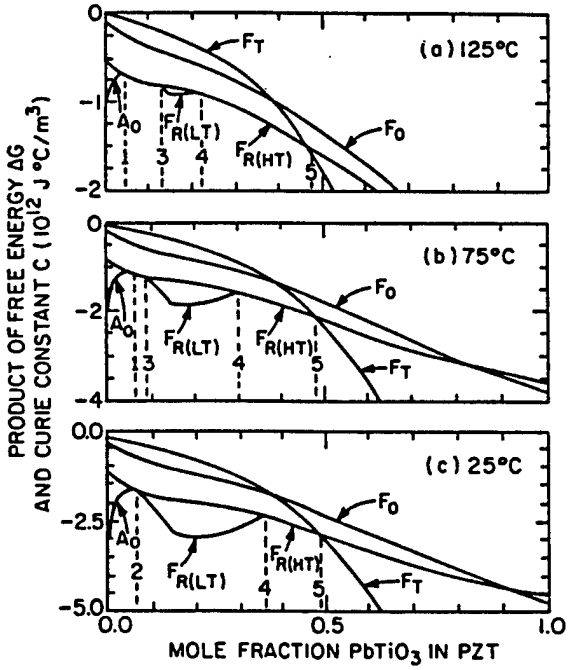

Fig. 3(b). Free energy as a function of composition and temperature.

	Mole Fraction $PbTiO_3$ in PZT										
	0.0	0.1	0.2	0.3	0.4	0.5	0.6	0.7	0.8	0.9	1.0
T_c (°C)	231.5	256.5	300.6	334.4	364.3	392.6	418.4	440.2	459.1	477.1	492.1
$C(10^5$ °C)	2.027	2.050	2.083	2.153	2.424	4.247	2.664	1.881	1.642	1.547	1.500
$Q_{11}(10^{-2}$ m^4/C^2)	4.620	5.080	5.574	6.175	7.260	9.660	8.116	7.887	8.142	8.504	8.900
$Q_{12}(10^{-2}$ m^4/C^2)	-1.391	-1.540	-1.720	-1.997	-2.708	-4.600	-2.950	-2.480	-2.446	-2.507	-2.600
$Q_{44}(10^{-2}$ m^4/C^2)	4.664	4.900	5.165	5.522	6.293	9.190	6.710	6.356	6.417	6.569	6.750
α_1 (10^7 m/F) at 25 °C	-4.582	-6.376	-7.470	-8.116	-7.904	-4.887	-8.340	-12.47	-14.84	-16.17	-17.05
α_{11} (10^7 m^5/C^{2}F)	62.35	41.25	31.29	22.30	13.62	4.764	3.614	0.6458	-3.050	-5.845	-7.253
α_{12} (10^8 m^5/C^{2}F)	-16.71	-4.222	-0.0345	1.688	2.391	1.735	3.233	5.109	6.320	7.063	7.500
$\zeta(10^8$ m^5/C^{2}F)	-34.42	-0.2897	9.284	11.75	11.26	6.634	10.78	15.52	18.05	19.44	20.32
α_{111} (10^8 m^9/C^{4}F)	5.932	5.068	4.288	3.560	2.713	1.336	1.859	2.348	2.475	2.518	2.606
α_{112} (10^8 m^9/C^{4}F)	311.2	34.45	18.14	15.27	12.13	6.128	8.503	10.25	9.684	8.099	6.100
α_{123} (10^9 m^9/C^{4}F)	-104.1	-8.797	-7.545	-7.052	-5.690	-2.894	-4.063	-5.003	-4.901	-4.359	-3.660
$\zeta(10^9$ m^9/C^{4}F)	84.41	13.39	4.627	3.176	2.402	1.183	1.596	1.851	1.652	1.256	0.7818

Fig. 3(c). Values of coefficients to fit the properties of PZTs.

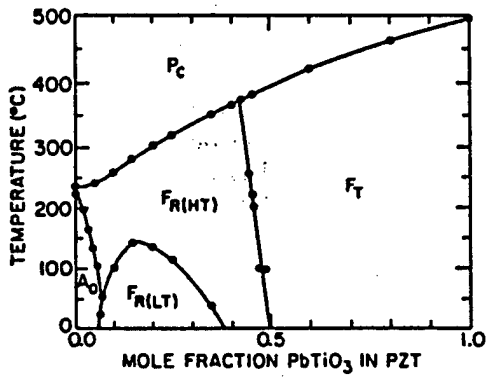

Fig. 3(d). Comparison of observed and calculated phase diagram from PZT.

ant over other possible domain states. Bias phenomena in both poled and unpoled samples are logically explained, as are facets of the aging behavior and the time dependence of mechanical Q. For donor doped samples there are only 'hand waving' arguments as to why the domain walls should become more mobile at weak fields, and much work needs to be done to determine the physics of the softening in these materials. An

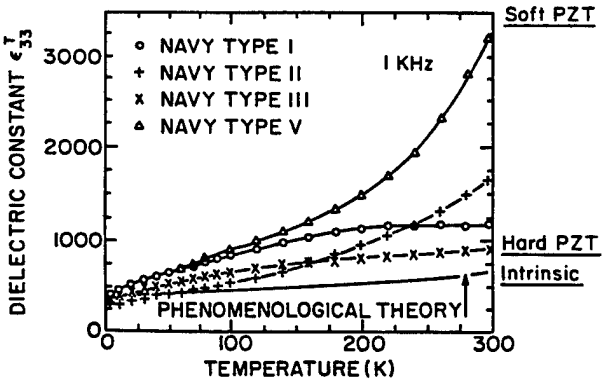

Fig. 4(a). Freeze out of extrinsic contributions to dielectric response in several PZTs at the 52:48 Zr/Ti ratio.

alternative approach to formulating ultra soft compositions has been the combination of PZT with a relaxor ferroelectric in a three component solid solution. A very wide range of compositions with complex chemistry on the B site of the ABO_3 perovskite have been explored. In general, the effect is to lower the Curie point T_c, raise ε, raise d_{33} and d_{31}, K_t and K_p.

4. Electrostrictive relaxor ferroelectrics

In the $Pb(B_1B_2)O_3$ perovskites for which $PbMg_{1/3}Nb_{2/3}O_3$ (PMN) is a useful prototype, it is clear from the dielectric response [15] (Fig. 5(a)), that a new type of dispersive high permittivity response occurs. At low temperatures PMN is a ferroelectric, as evidenced by pronounced dielectric hysteresis (Fig. 5(b)); however, for zero field cooled samples there is no evidence of a noncubic structure, nor is there any optical birefringence in the single crystal (Fig. 5(c)). The origin of this unusual behavior has been traced by careful transmission electron microscopy (TEM) studies to an unusual self-limiting nanoscale ordering of the B site cations. In PMN contrary to expectation the Mg:Nb order is 1:1 rather than 1:2, leading to strong short range chemical inhomogeneity [16]. Presumably the local charge unbalance limits the scale of ordering to $\approx$5 nm, and it cannot be changed even by very long thermal annealing. On cooling the wide difference in Curie temperature between ordered and disordered regions gives rise to local polar regions in a paraelectric matrix, which are on a scale where the electrocrystalline anisotropy energy is comparable to thermal energy [17]. At higher temperature this gives rise to super paraelectric-like behavior, but on cooling the polar fluctuations freeze out in a glass-like Vogel–Fulcher freezing in the dielectric response (Fig. 6) [18,19].

The very high polarizability over a wide temperature range gives rise to massive electrostriction in PMN based compositions (Fig. 7), and the absence of a stable

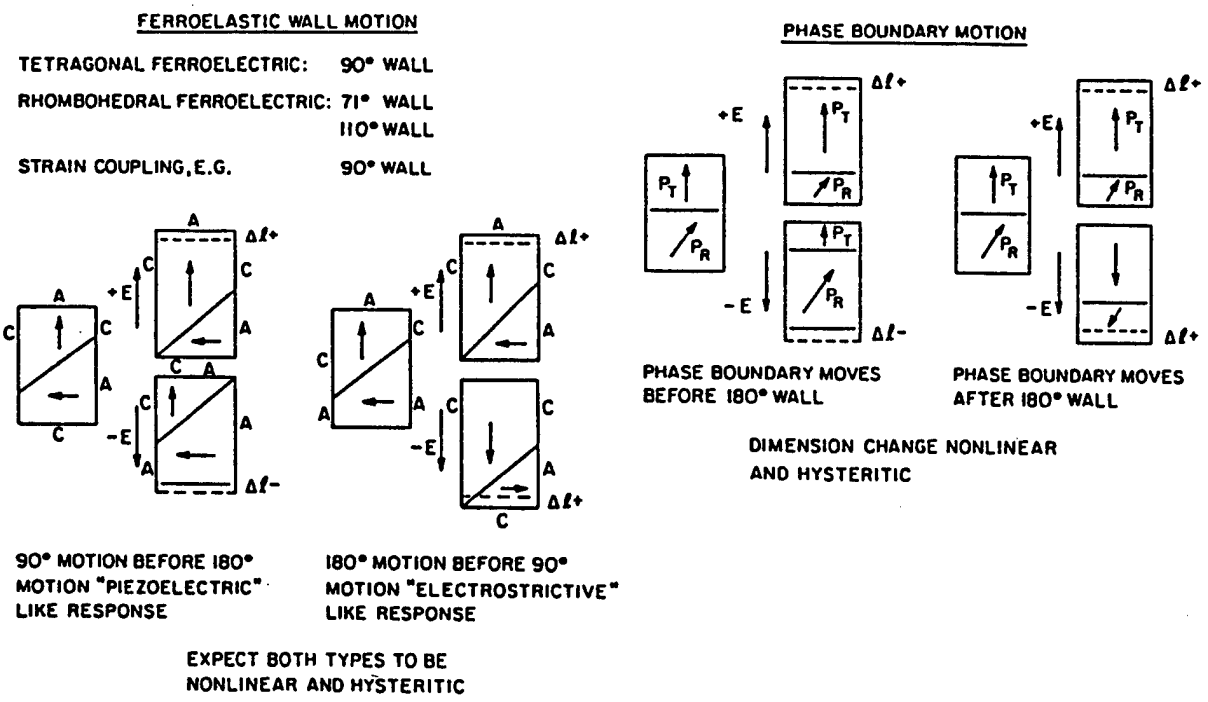

Fig. 4(b). Mechanisms which can contribute to the extrinsic response in PZT ceramic piezoelectrics.

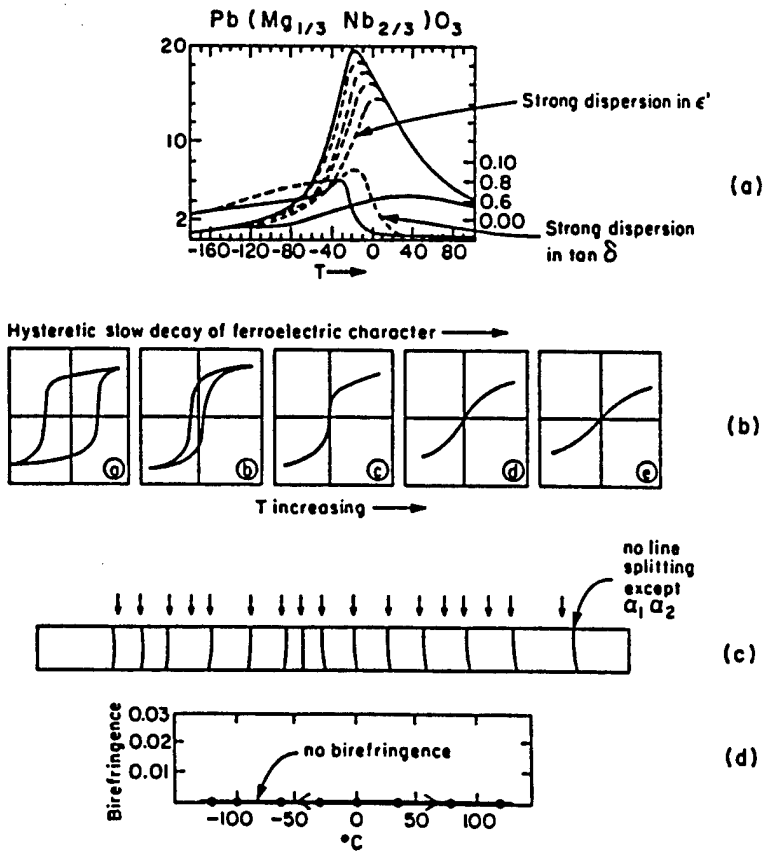

Fig. 5. Special features of relaxor ferroelectrics. (a) Weak field dielectric permittivity vs. T. (b) High field hysteritic behavior vs. T. (c) Low temperature X-ray and single crystal optics showing 'cubic' macro properties down to below −100 °C.

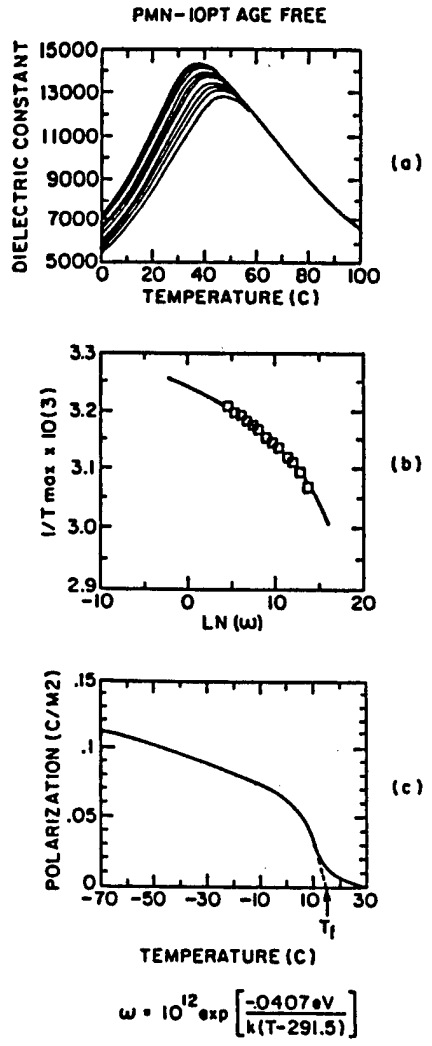

Fig. 6. Vogel–Fulcher type freezing of dielectric response in PMN:10% PT. (a) Dielectric response as function of frequency and temperature. (b) Plot of $1/T_{max}$ vs. frequency; square dots are experimental. (c) Decay of polarization on heating showing the thawing temperature $T_f = 291$ K.

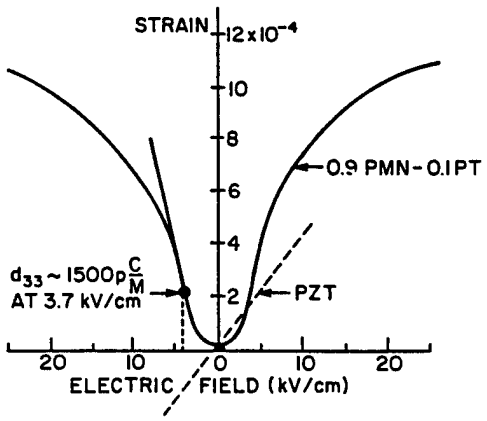

Fig. 7. Electrostrictive deformation x_3 for field applied along E_3 in lead magnesium niobate:10% lead titanate ceramics.

domain structure leads to highly reproducible anhysteritic strain behavior. Under bias fields the PMNs can be induced into very strong piezoelectric response, giving a family of potential agile transducers.

5. Piezoceramic composites

As was evident in Eq. (1), dielectric, piezoelectric and elastic properties of the poled piezoceramic are tensor quantities and for many types of application it is possible to spell out a figure of merit which often requires the enhancement of some components of the tensor and the diminution of others.

A typical example is the Navy requirement for sensing very weak hydrostatic pressure waves in water. For hydrostatic pressure the stress $X_{11} = X_{22} = X_{33} = -p$, where p is the pressure; thus the change of polarization ΔP from Eq. (3) is $\Delta P = d_{33}(-p) + d_{31}(-p) + d_{31}(-p) = (d_{33} + 2d_{31})(-p) = d_h(-p)$, where d_h is the hydrostatic d coefficient.

The voltage generated by the hydrophone is

$$\frac{(-p)g_h = (d_{33} + 2d_{31})(-p)}{\varepsilon_{33}}$$

where g_h is the hydrostatic voltage coefficient.

Often the figure of merit $d_h g_h$ (roughly a power figure) is used, i.e.,

$$\frac{d_h g_h = (d_{33} + 2d_{31})^2}{\varepsilon_{33}}$$

Unfortunately, for PZT, even though both d_{33} and d_{31} are large, $d_{33} \simeq -2d_{31}$, so that d_h is small and ε_{33} is large—just the wrong combination for a hydrophone.

In exploring composites for hydrophone applications it would be advantageous from density and flexibility

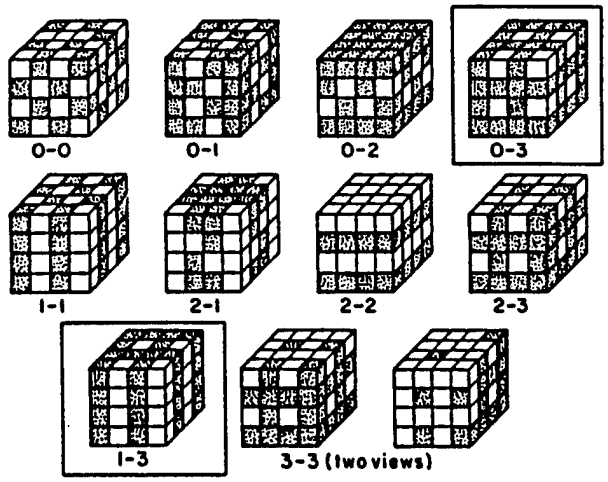

Fig. 8. Parameter considerations in polymer:piezoceramic composites and the simple cubes model illustrating phase self-connectivity concepts.

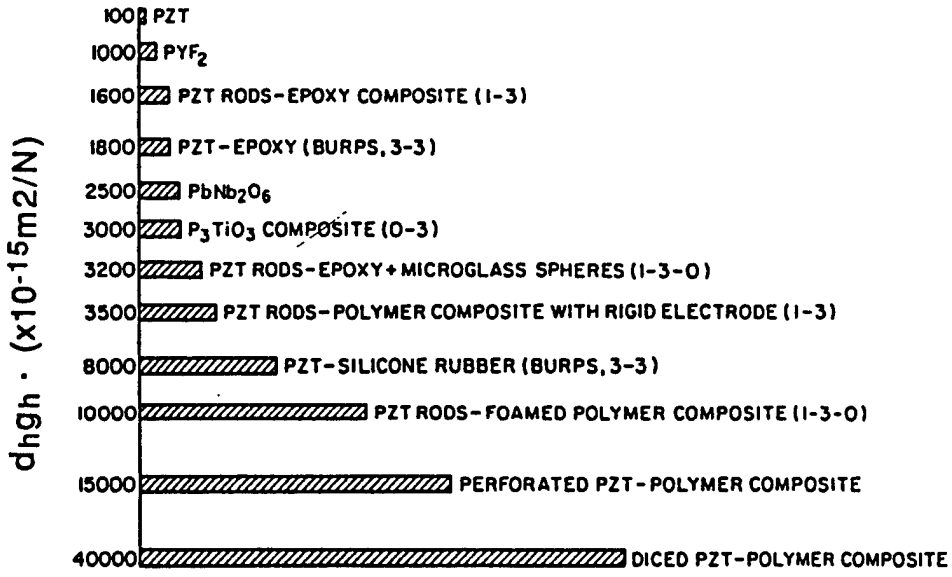

Fig. 9. Improvement in figure of merit for hydrophone ($d_h g_h$) in composites of different connectivities.

considerations to combine the ceramic with a dielectric polymer. Comparing dielectric and elastic properties for these two systems a fascinating juxtaposition is evident: PZT is very soft dielectrically ($\varepsilon \approx 3000$) whilst the average polymer is very stiff ($\varepsilon \approx 10$). Conversely the polymer is very soft elastically ($s_{11} \approx 30.10^{-11}$ m^2 N^{-1}), but the ceramic is very stiff ($s_{11} \approx 2.10^{-11}$ m^2 N^{-1}). Thus by careful control of the mode in which each phase is self-connected in the composite it is possible to 'steer' the fluxes and fields to enhance wanted coefficients and diminish unwanted responses [20].

The important concepts are summarized in Fig. 8 together with the simple cubes model for connectivity [21], which is such an aid in thinking and which has given rise to the now internationally accepted notation for the designation of phase self-connection in three dimensions.

Comparisons of the $d_h g_h$ product for some early composites to single phase materials are given in Fig. 9.

A significant advantage for the use of fine scale 1:3 composites produced by a 'dice and fill' method [22] from bulk PZT is illustrated in Fig. 8, which shows the strong enhancement of K_t and the lowering of acoustic impedance, both of which carry important gains for electromedical tomography systems.

New ceramic injection molding methods are now being applied to the fabrication of both large area and fine scale 1:3 transducers and promise a revolution in the economics of fabricating these most useful electromechanical elements [23,24].

References

[1] F.S. Galasso, *Structure, Properties and Preparation of Perovskite Type Compounds*, Pergamon, Oxford, 1969.
[2] B. Jaffe, W.R. Cooke, Jr., and H. Jaffe, *Piezoelectric Ceramics*, Academic Press, London, 1971.
[3] M.J. Haun, E. Furman, H.A. McKinstry and L.E. Cross, *Ferroelectrics, 99* (1989) 27.
[4] M.J. Haun, E. Furman, S.J. Jang and L.E. Cross, *Ferroelectrics, 99* (1989) 13.
[5] M.J. Haun, E. Furman, S.J. Jang and L.E. Cross, *Ferroelectrics, 99* (1989) 55.
[6] M.J. Haun, E. Furman, T.R. Halemane and L.E. Cross, *Ferroelectrics, 99* (1989) 74.
[7] M.J. Haun, Q. Zhang, E. Furman, S.J. Jang and L.E. Cross, *Ferroelectrics, 99* (1989) 45.
[8] M.J. Haun, T.R. Halemane, R.E. Newnham and L.E. Cross, *Jpn. J. Appl. Phys., 24* (1985) 209.
[9] M.J. Haun, E. Furman, S.J. Jang and L.E. Cross, *IEEE Trans. UFFC, 36* (1989) 393.
[10] J. Herbert, *Ferroelectric Transducers and Sensors Electrocomponent Monograph*, Vol. 3, Gordon & Breach, London.
[11] R. Greson and H. Jaffe, *J. Phys. Chem. Solids, 24* (1963) 979.
[12] R. Gerson, *J. Appl. Phys., 31* (1960) 188.
[13] K. Carl and K.H. Hardtl, *Ferroelectrics, 17* (1978) 472.
[14] D. Dederichs and G. Arlt, *Ferroelectrics, 68* (1986) 281.
[15] G.A. Smolensky, V.A. Isupov, A.I. Agranovskaya and S.N. Popov, *Sov. Phys. Solid State, 2* (1960) 2906.
[16] C. Randall, D. Barker, R. Whatmore and P. Groves, *Ferroelectrics, 76* (1987) 277.
[17] L.E. Cross, *Ferroelectrics, 76* (1987) 241.
[18] D. Viehland, The glassy polar behavior of relaxor ferroelectrics, *Ph.D. Thesis*, Penn State University, 1991.
[19] D. Viehland, S.J. Jang, L.E. Cross and M. Wuttig, *J. Appl. Phys., 68* (1991) 2916.
[20] R.E. Newnham, D.P. Skinner and L.E. Cross, *Mater. Res. Bull., 13* (1978) 525.
[21] D.P. Skinner, R.E. Newnham and L.E. Cross, *Mater. Res. Bull., 13* (1978) 599.
[22] W.A. Smith, *Proc. ISAF 1986*, Lehigh University (1986).
[23] L.J. Bowen and K. French, *Proc. Int. Symp. Appl. Ferroelectrics, 10* (1993) 160.
[24] L.J. Bowen, R.L. Gentleman, H.T. Phan, D.F. Fiore and K. French, *Proc. IEEE Ultrasonics Symp., 1993*, p. 499.

APPENDIX 2

FERROELECTRIC CERAMICS: MATERIALS AND APPLICATION ISSUES

L. Eric Cross
Evan Pugh Professor of Electrical Engineering
Materials Research Laboratory
The Pennsylvania State University
University Park, PA 16802

ABSTRACT

The unusual properties of the perovskite structure ferroelectric ceramics which makes them attractive for several different fields of application include:

- The very high dielectric permittivity for capacitor dielectrics, still the largest market segment.
- The polability to high remanent polarization inducing very strong direct and converse piezoelectric effects for electromechanical transduction in sensors and actuators.
- Large pyroelectric effects in the poled structures with interesting application in bolometric infra-red detection and imaging.
- The transparency of the high band gap structure combined with very strong electro-optic effects beginning to yield new possibilities for photorefractive high density optical information storage and phase matchable broad band optical second harmonic generation.

New developments in each of these areas will be highlighted focusing primarily upon the materials issues. With our enhanced capability to deposit well controlled thin films of many of the most interesting composition families the new possibilities which these afford will be briefly reviewed.

The film structures provide new capability to generate exceedingly fine controlled microstructure which raises new concerns as to the influence of scale upon the cooperative phenomena which give rise to both ferroelectric and antiferroelectric phases. Experience with the self assembling self limiting nanostructures which appear in relaxor ferroelectrics and their influence on properties will be briefly reviewed.

INTRODUCTION

In considering the full family of applications for ferroelectric ceramics in dielectric, piezoelectric, pyroelectric, and electro-optic systems it is evident that the properties exploited are softness, thus unlike structural ceramics where it is the elastic stiffness which is of most interest, in functional ceramics it is the control and exploitation of compliance which is important [1].

In conventional dielectric systems the multilayer ceramic capacitor (MLC) is the most widely used component with a market approaching 100 billion units worldwide per year [2]. Tape casting is widely used for assembly and the dielectrics are mostly barium titanate based. It will be shown that the higher permittivity units draw upon the very high intrinsic polarizability near the phase transitions. Newer lead based relaxor ferroelectric systems will be examined to highlight the rather different spin glass like response. However, even though these composition can be co-fired with both silver and copper metallurgy they are not yet a major segment of the MLC market. As the voltage of semiconductor electronics decreases, dielectric layers must get thinner, exploration of recent techniques for forming submicron thin films of the lead based ferroelectrics suggest that these may offer interesting new capacitance structures for high density semiconductor packaging.

Piezoelectric ferroelectrics for sensor and actuator functions in mechanical systems are a rapidly developing market, where the lead zirconate:titanate (PZT) compositions are very widely used. The behavior in these poled ceramic elements is very complex and even after more than 40 years of use, the balance of contributions to response, particularly in the 'soft' high sensitivity compositions is still not fully understood. For sensing, composite systems give the possibility to 'tune' the tensor response and offer new possibilities in both large area and high frequency acoustic systems. Piezoceramic actuators can supply immense mechanical force, but only over minute throw. Simple mechanical amplification as

in flextensional, moonie and rainbow structures are of increasing interest. Energy density consideration in thin film systems suggest that ferroelectric piezoelectric films must be important new players in micro-electro mechanical systems (MEMS). Piezoelectric diaphragm type micro motors give high torque at low speeds with reliability now up to 10,000 hours of continuous operation.

Pyroelectric point detectors are extensively used for thermal sensing in a wide range of industrial and consumer applications. Current research focus is upon long wavelength IR imaging where both hybrid and thin films compete. Very low thermal mass with high thermal isolation of the pixel plane is essential for high sensitivity, and again thin films are of special interest in new air bridge isolated imagers.

Optical applications of ferroelectrics mostly draw on the high electro-optic and non-linear optic characteristics of ferroelectrics. Guided wave structures on single crystal lithium niobate are a mature technology using indiffusion to modify the index. Recently stress optic modification has been demonstrated in strontium barium niobate which may permit more complex structures with lower attenuation. In harmonic generation quasi phase matching using domain divided crystals promises high intensity blue light from laser diodes. Perhaps the area which shows most promise is that exploiting the strong photo-refractive effects in $BaTiO_3$, $KNbO_3$, and $Sr_{0.6}Ba_{0.4}Nb_2O_6$. Optical amplification, frequency conversion, information storage, pattern recognition and optical soliton generation have all been observed.

In the following article, the general principles controlling properties of interest will be briefly reviewed, the wide range of information available will be referenced and the focus will be upon new developments. For each area, the impact of the growing availability of high quality ferroelectric thin films will be assessed.

GENERAL CONSIDERATIONS

Ferroelectric crystals are named for the analogy of their dielectric properties to the magnetic properties of ferromagnets, however a number of important qualitative and quantitative differences strongly impact the properties and the manner in which they can be exploited in devices.

1. Unlike magnetism, electric monopoles (carriers of charge) are common in all systems. The resulting charge transport properties strongly influence the static and low frequency dynamic dielectric, piezoelectric, pyroelectric, and electro-optic properties. There is always a decay of depolarizing fields and a strong influence on the electrical boundary conditions in ceramics.
2. Electrical ordering is soft so that although many systems follow Curie Weiss behavior in the para form i.e., The susceptibility η is given by

$$\eta = C/CT - \theta) \qquad (1)$$

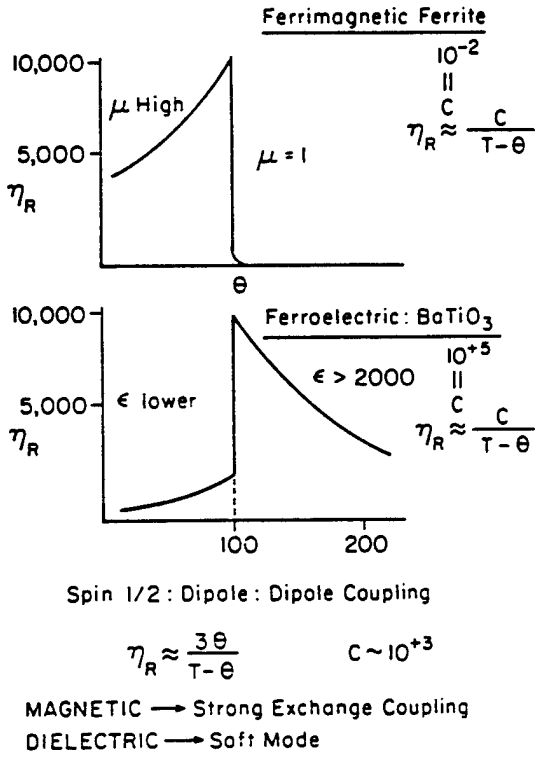

Figure 1 Comparing Curie Weiss behavior in a $BaTiO_3$ type ferroelectric with the Curie Weiss behavior of a typical ferrimagnetic ferrite.

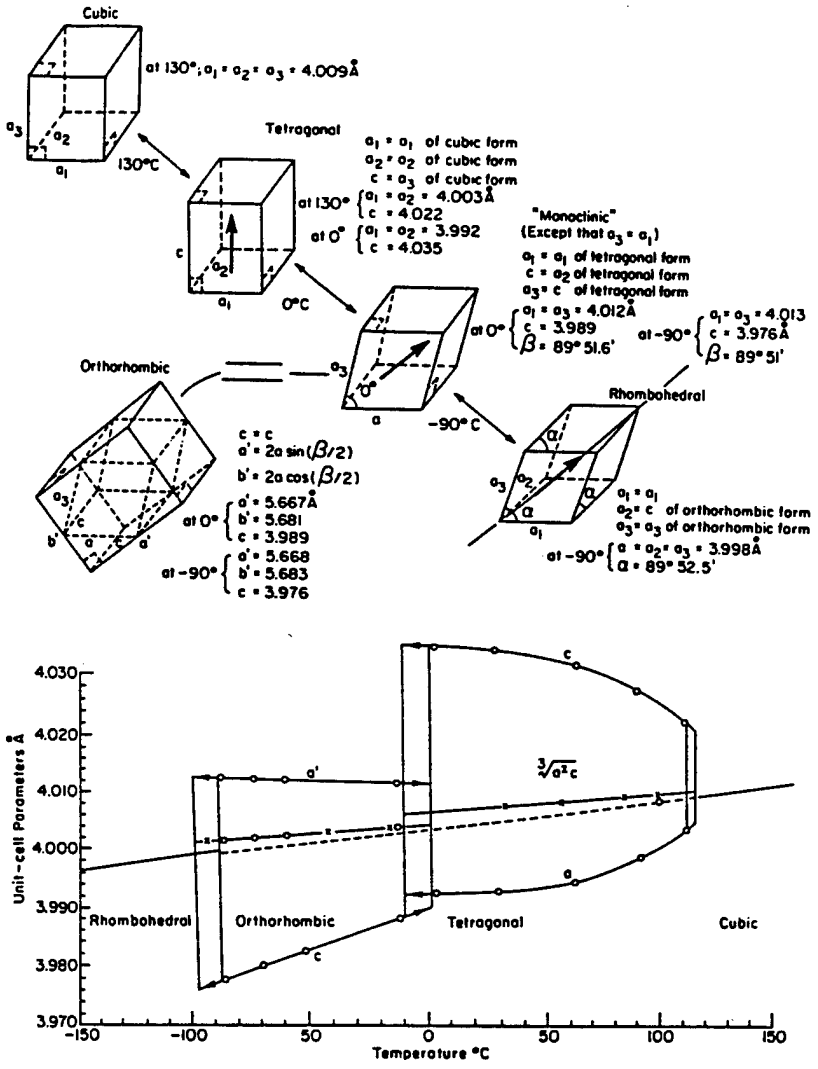

Figure 2 Strains associated with the spontaneous polarization in the ferroelectric phases of $BaTiO_3$.

where C is the Curie Constant and θ the Curie Weiss temperature. The ferroelectric C ~ 10^{+5}K compared to the magnetic C ~ 10^{-2}, very high dielectric permittivity persists in the paraelectric phase of the ferroelectric for a wide range of temperatures above θ (fig. 1) and even in the ferroelectric phase the state of ordering can be quite markedly affected by rather modest field levels.

3. Since the polarization in the oxide ferroelectrics is mostly generated by the displacive relative motions of ions in the structure it is not surprising that the coupling of polarization to the lattice is much stronger in the ferroelectric. Spontaneous deformations on polarizing are often of a few % (fig. 2) and elastic energy is a strong contributor to the nature of the Curie point transition. The high induced strain suppresses fluctuations in polarization and leads to whole families of useful electrostrictive devices.
4. The oxide ferroelectric of interest are high band gap insulators with good optical transparency in visible light and large electro-optic and non linear optic constants. Both these families of properties involve electric field induced optical anisotropy, are difficult to exploit in transparent polycrystal ceramics and need high quality single crystals. To tune properties however as in the other property areas it is necessary to modify and control the lattice by suitable solid solution. Solid solutions are however by definition incongruently melting and both difficult and expensive to grow in large optically perfect crystals. Thus it is perhaps not surprising that in spite of many very promising device concept this area is the last to achieve full commercialization.

   It does however appear probably that with the developing new techniques for growing excellent quality epitaxial oxide films for high T_c superconductors now being applied to ferroelectrics it may soon be possible to achieve quality oriented films of any solid solution composition, making possible the exploitation of many of the earlier concepts in much better optimized materials.

DIELECTRIC SYSTEMS

In randomly axed polycrystal ceramics, ferroelectrics derived from high symmetry prototypic (paraelectric) phases are essential both to avoid anisotropy above T_c and to provide many orientations for the polarization below T_c. Compositions in the perovskite structure are universally applied (fig. 3) with modified barium titanate $BaTiO_3$ much the most widely used. For very high permittivity (Z5U, Y5V)

characteristics the high dielectric peak at the Curie temperature is maneuvered by solid solution into the room temperature region, and broadened by deliberately induced heterogeneity (fig. 4). Some typical formulations are given in Table 1 and characteristics of permittivity versus Temperature in figure 5 [2,3,4].

For the lower flatter (X7R) characteristics also shown in figure 4, higher purity $BaTiO_3$ is used but grain growth is inhibited. In the fine grain ceramic the inability to form a twin (domain) structure leads to a high internal stress which raises the intrinsic polarizability near the 0°C tetragonal:orthorhombic ferroelectric transition. The grain growth inhibitor can be chosen to "pad" the Curie point peak leading to a broad flatter but lower permittivity response.

TABLE I. Typical Practical $BaTiO_3$ Based Dielectric Formulation from Herbert.

Item	K_{max}	Temp. range for K_{max} -20%	AO/BO_2	Ba	Sr	Ca	Mg	Ti	Zr	Sn
				Composition in cation%						
A	2280	-20 to+100	0.98	48.5	0.73	–	–	49.5	–	0.73
B	3260	0 to 120	1.03	45.3	–	4.8	1.08	44.0	4.8	–
C	3450	-10 to 72	1.01	44.2	–	5.7	0.75	42.9	6.4	–
D	5000	12 to 75	1.02	47.6	2.5	–	0.45	45.3	0.45	3.38
E	8200	42 to 70	1.005	35.5	12.5	1.8	0.8	46.9	2.6	–

An alternative approach for very high K Z5U type dielectrics is to use the lead based relaxor ferroelectric compositions based on $PbMg_{1/3}Nb_{2/3}O_3$ (PMN). In PMN limited 1:1 ordering of Mg:Nb cations on the B site of the ABO_3 structure leads to nanoscale compositional heterogeneity [5,6] and the appearance of small micropolar regions at temperatures well above the dielectric maximum [7]. In the relaxor, electrocrystalline anisotropy is inadequate to stabilize the micropolar P_s vectors and a new large fluctuating component is added to the polarizability [8]. The dielectric maximum is due to a freezing out of the fluctuating component with the expected strong dielectric dispersion [9].

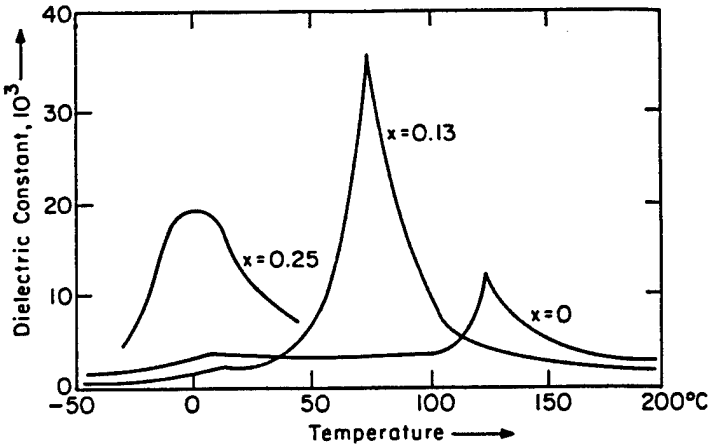

Figure 3 Permittivity temperature curves for solid solution in the $BaTiO_3$:$BaZrO_3$ composition system.

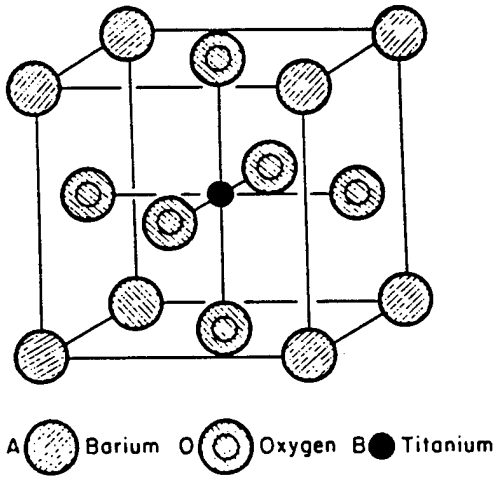

Figure 4 The unit cell for a cubic perovskite ($P_{n1}3_m$ symmetry) $BaTiO_3$ at a temperature above T_c.

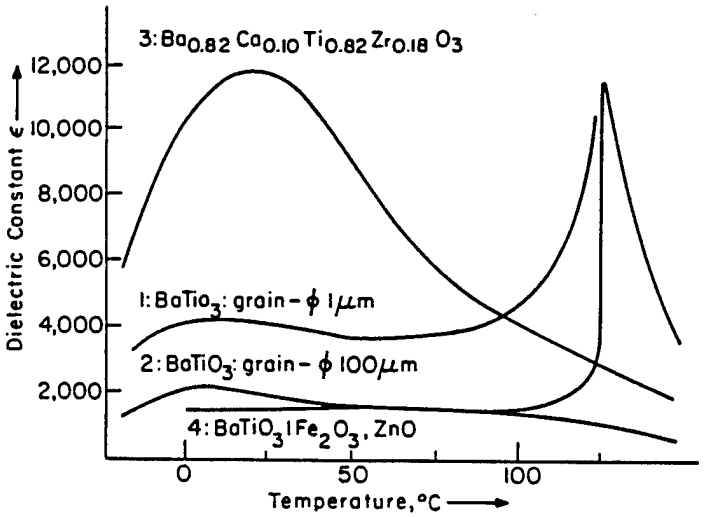

Figure 5 Typical compositions for Curie point dhifted Z5U type composition and a grain size controlled $BaTiO_3$ with broad flat temperture characteristic.

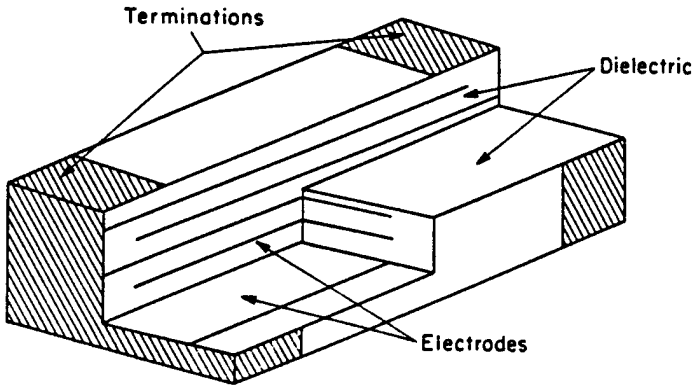

Figure 6 Construction of a Typical Ceramic MLC.

The temperature of the dielectric maximum may be manipulated as in other ferroelectric solid solution[10], but the rounded broader nature of the dielectric maximum is intrinsic to the nanocomposite nature induced by local ordering[11]. Also, since the scale of this heterogeneity is of order 5-10 nm properties are not strongly influenced by grain size in properly prepared ceramics and are largely preserved in thin films down to sub micron thicknesses [12].

In all MLC development, a frequent objective has been to provide maximum capacitance in minimum volume (fig. 6). Since volumetric efficiency C/v is given by $\varepsilon_o\varepsilon/t^2$ where ε is the useable permittivity and t the dielectric thickness. Obviously there is a strong need to optimize ε but an even strongly urge to reduce the dielectric thickness t. A minimum t is set by dielectric breakdown and

$$V_{working} << E_B t \qquad (2)$$

where $V_{working}$ is the device working voltage, E_B the dielectric breakdown field and t the dielectric thickness. Breakdown in all dielectrics is a complex process. In ceramics it is certainly extrinsic, and there is much empirical evidence that E_B increases markedly with decreasing thickness (fig. 7)[13]. In digital 1C circuits, current working voltages are in the range 3 to 5 volts and are going steadily down with time towards 1 volt. From figure 7, even at 1 μm thickness the working field is only 30 Kv/cm which gives ample margin of safety. Currently most manufacturers of high capacitance MLCs can tape case to a fired thickness ~7 μm so there is a strong urge to go thinner. At the research and pilot level, using automated lay-up, thicknesses of 2 μm have been achieved in 100 layer capacitors and there is evidence of work at 1 μm with 1/2 μm thick electrode layers.

As dimensions become sub micron, thin film techniques must become important. To develop new dielectrics to this regimen where applied fields will reach to above 30 Kv/cm it will be essential to give more careful consideration to the non linearity in polarizability which is an essential feature of all ferroic systems. Typical high field curves for a proper ferroelectric, relaxor ferroelectric and antiferroelectric compositions are given in figure 8.

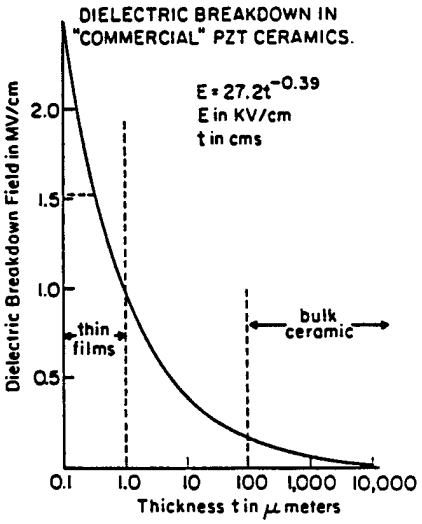

Figure 7 Breakdown field E_B as a function of ceramic dielectric thickness from the empirical equation of Gerson and Marshal [13].

For the ferroelectric dielectric only the slope permittivity of the saturation arm of the hysteresis loop is useful for a capacitor which works under DC bias as in guarding the power plane of an 1C package. Even so the permittivity is more than 500 ε_o and persists to above 15 Ghz [14,15]. Relaxor ferroelectrics have no remanent P_s but under bias the permittivity falls from ~6000 ε_o to 1200 ε_o a good advantage over the conventional ferroelectric [16]. The system of most interest is the antiferroelectric based on lead zirconate which switches to ferroelectric at high field. This is the only system in which effective ε increases markedly with field. If the full P_s can be used, volumetric efficiency ~ I Farad/cc is possible and single sheets could give capacitance of order 35 $\mu f/cm^2$ [17,18].

TYPICAL RESPONSES OF DIELECTRIC MATERIALS UNDER EVALUATION FOR USE AS AN INTEGRAL DECOUPLING CAPACITOR IN MULTICHIP MODULES

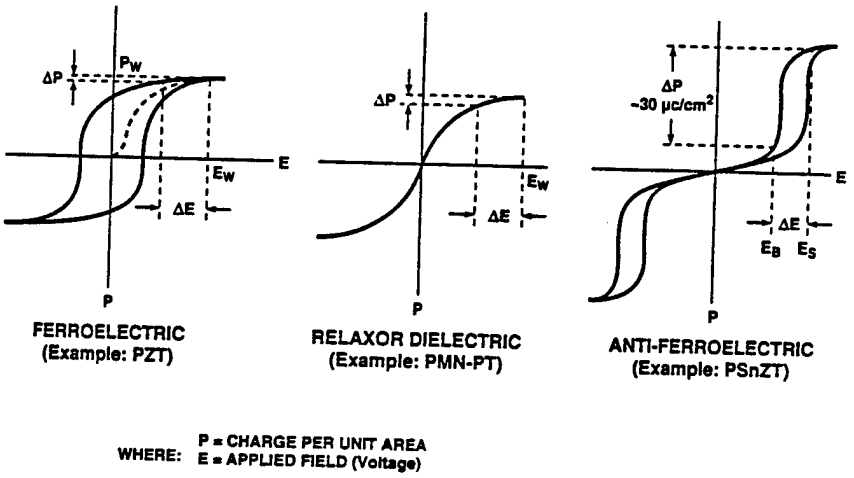

Figure 8 High E field response in typical ferroelectric, relaxor ferroelectric and antiferroelectric phase switching compositions.

PIEZOELECTRIC CERAMICS

For high coupling piezoceramic systems the perovskite structure lead zirconate titanate solid solutions have been the materials of choice [19]. The reasons are straightforward.

(a) The system embraces a wide range of high Curie temperature ferroelectric phases, giving a wide working temperature range in the ferroelectric phase[20].

(b) At compositions near the 52:48 Zr/Ti ratio there is an unusual morphotropic phase boundary (MPB) separating tetragonal and rhombohedral symmetry phases which have domain polarizations along <001> and <111> families of directions[21].

(c) Near the first order MPB compositions there is a range of two phase coexistence so that the six tetragonal and eight rhombohedral domain states can be poled to thread a very large remanent polarization through the

randomly axed ceramic inducing conical symmetry and strong non zero piezo coefficients d_{31}, d_{33}, and d_{15}[22].

(d) In compositions close to the MPB which is near vertical on the temperature/composition diagram one may stay close to the instability of the phase transition over a very wide temperature range, with correspondingly high values of the intrinsic polarizability and deformability.

(e) One must be in the ferroelectric state with a mobile domain structure at high fields to be able to induce the symmetry breaking remanent polar state essential to induce piezoelectricty. However, as a consequence the use state is a metastable poled domain ensemble (fig. 9). It is clear from the + - symmetry of the total figure 9b that the basic deformation mechanism is electrostrictive, however for a limited range of fields about the poled working point the deformation (fig. 9b) is clearly piezoelectric.

(f) To control the piezoelectric response it is important to control the electrical coercivity. i.e. the width of the hysteresis loops. For very low drive fields low coercivity is desirable as the saturation arm becomes steeper yielding higher piezoelectric constant. In high drive systems, a very high coercivity is desirable so that the larger driving field does not induce depoling and consequent hysteresis loss and heating, but the levels of $d_{31}d_{33}$ will be lower due to the flatter saturation arm.

Even at very low drive fields we may expect the response to be complex with possible contributions to both polarization and elastic strain from intrinsic polarization change in the domain, reversible domain wall motion in both tetragonal and rhombohedral domain structures, possible reversible motion of the phase boundary separating polar tetragonal and polar rhombohedral regions in the same grain.

Intrinsic single domain response has been addressed in a series of papers applying Landau Ginsburgh Devonshire (LGD) phenomenological theory [23,24,25,26,27]. For practical application a very large range of substituents have been tried to control the extrinsic domain wall component of response. Lower level additives (fig. 10) can be divided into donor like, i.e. substituents which carry more electron charge than the ions for which they substitute in the lattice (fig. 10a) and acceptor like, i.e. substitutent which carry less charge than the ion being substituted (fig. 10b). The acceptor ions appear to pair with oxygen vacancies in the lattice to provide a slowly changing defect dipole which orients in the domain field stabilizing the

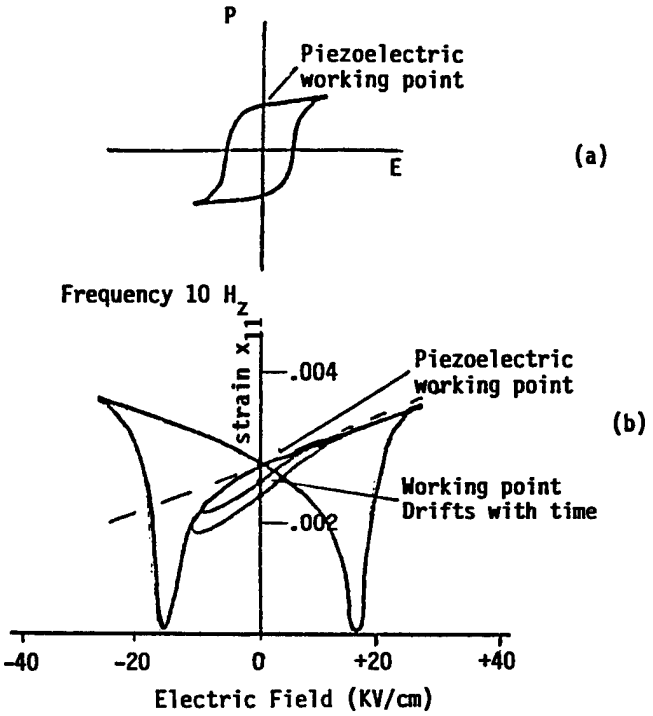

Figure 9 (a) Polarization vs. Field in a PZT ceramic.
(b) Piezoelectric/Electrostrictive strain vs. field large strain electro.

MODIFIERS OF THE EXTRINSIC RESPONSE

DONOR ADDITIVES		ACCEPTOR ADDITIVES
Nb_2O_5	$PbNb_2O_6$	Fe_2O_3
Ta_2O_5	$PbTa_2O_6$	Al_2O_3
WO_3		Cr_2O_3
Bi_2O_3		MnO_2
Sb_2O_3		MgO
La_2O_3		NiO
Wall Motion Promoters		Wall Motion Inhibitors

Figure 10 Common lower level (>5 mole%) donor dopants an acceptor dopants use in 'soft' and 'hard' PZT formulations.

existing variant at the expense of others and thus indirectly stabilizing the wall structure [28,29]. Donor dopants lower the coercivity and strongly enhance both dielectric and piezoelectric responses [30,31]. Although a number of "hand waving" arguments have been advanced there is still no clear understanding of the mechanisms involved in the donor modified systems.

Based on PZT very many third valence compensated components have been added to form three component solid solutions, all of which soften behavior, reduce the Curie temperature. Figure 11 lists just a few of the very many compositions which have been used.

The importance of the extrinsic components to the PZT response may be adduced from the fact that even in the hardest compositions at room temperature some 25% of piezoelectric response is extrinsic, whilst in the very soft donor doped compositions more than 75% of total response is extrinsic.

ELECTROSTRICTIVE CERAMICS

In section 2, the very high permittivity which is achieved in the nano-composite relaxor ferroelectrics was briefly reviewed. It was shown that these ceramics in the PMN system may be taken to large values of polarization under high electric field, but that they do not retain a remanent polar state. Since in all perovskite ferroelectrics the basic coupling to the lattice is electrostrictive it is natural to ask whether the high polarizability may be directly exploited to produce high strain by the relation

$$x_{kl} = Q_{ijkl} P_i P_j \qquad (3)$$

where x_{kl} is the induced strain.
$P_i P_j$ are components of the polarization.
Q_{ijkl} is the electrostriction constant in polarization notation.

Electrostrictive strains x_{33} and x_{11} as a function E_3 are shown for PMN and a PMN 10% PT in figure 12ab, and the quadratic nature of the strain confirmed in figure 13 [32]. In fact for PMN and PMN:PT the electrostriction constants Q_{11} and Q_{12} are essentially independent of temperature (fig. 14) [33].

For valence compensated additions the systems studied have included:

$Pb(Ni_{1/3}Nb_{2/3})O_3$:$PbTiO_3$:$PbZrO_3$
$Pb(Co_{1/3}Nb_{2/3})O_3$:$PbTiO_3$:$PbZrO_3$
$Pb(Mn_{1/3}Nb_{2/3})O_3$:$PbTiO_3$:$PbZrO_3$
$Pb(Cu_{1/3}Nb_{2/3})O_3$:$PbTiO_3$:$PbZrO_3$
$Pb(Mn_{1/3}Ta_{2/3})O_3$:$PbTiO_3$:$PbZrO_3$
$Pb(Zn_{1/3}Nb_{2/3})O_3$:$PbTiO_3$:$PbZrO_3$
$Pb(Ni_{1/3}Fe_{1/3}Nb_{1/3})O_3$:$PbTiO_3$:$PbZrO_3$

$Pb(Cu_{1/3}Nb_{2/3})O_3$:$PbTiO_3$
$Pb(Cd_{1/3}Nb_{2/3})O_3$:$PbTiO_3$
$Pb(Zn_{1/2}Te_{1/2})O_3$:$PbTiO_3$
$Pb(Mg_{1/2}Te_{1/2})O_3$:$PbTiO_3$

$Pb(Sb_{1/2}Nb_{1/2})O_3$:$PbTiO_3$:$PbZrO_3$
$Pb(Sn_{1/2}Nb_{1/2})O_3$:$PbTiO_3$:$PbZrO_3$
$Pb(Sb_{1/2}Nb_{1/2})O_3$:$PbTiO_3$
$Pb(Sn_{1/2}Nb_{1/2})O_3$:$PbTiO_3$

$Pb(Mg_{1/2}V_{1/2})O_3$:$PbTiO_3$:$PbZrO_3$
$Pb(Mn_{1/3}Sb_{2/3})O_3$:$PbTiO_3$:$PbZrO_3$
$Ph(Li_{1/4}Nb_{3/4})O_3$:$PbTiO_3$:$PbZrO_3$
$Pb(Sb_{1/2}Nb_{1/2})O_3$:$PbTiO_3$:$PbZrO_3$
$Pb(Fe_{1/2}Sb_{1/2})O_3$:$PbTiO_3$:$PbZrO_3$
$Ph(In_{1/2}Nb_{1/2})O_3$:$PbTiO_3$:$PbZrO_3$
$Pb(In_{1/2}Nb_{1/2})O_3$:$PbZrO_3$:$PbSnO_3$:$PbTiO_3$
$Pb(Mg_{1/2}V_{1/2})O_3$:$PbTiO_3$:$PbZrO_3$

$(Ag_{1/2}Bi_{1/2})TiO_3$:$PbZrO_3$:$PbTiO_3$
$(Ag_{1/2}Bi_{1/2})ZrO_3$:$PbTiO_3$:$PbZrO_3$

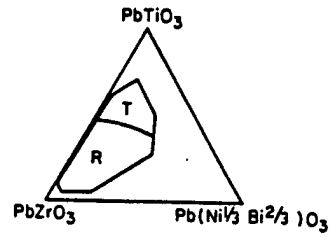

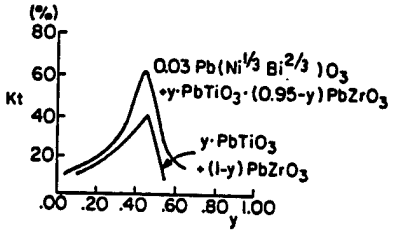

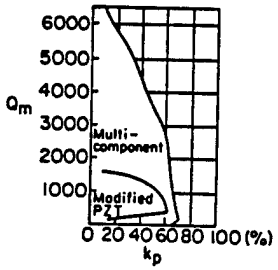

Figure 11 Valence compensated relaxor ferroelectric additives in three component PZT based systems.

An unexpected bonus for the relaxor, is that the steady accretion of polarization for temperatures above T_m leads to an expansion term in dilatation of the form

$$\Delta v \alpha (Q_{11} + 2Q_{12}) P_{<111>}^2 \quad (4)$$

which compensates for thermal contraction. Thus for a range of temperatures near 20°C it is possible to mate PMN with ULE glass diaphragms to control surface deformable mirror [34].

Because of the reproducible zero strain state in PMN, due to the absence of a stable domain structure it has found wide application in optics. Perhaps the most important recent application has been in control of the alignment tilt mirrors in the wide field and planetary camera replacement in the Hubble Space Telescope. These four small tilt mirrors permit perfect alignment of the compensators of the original mirror with a massive improvement in performance (fig. 15).

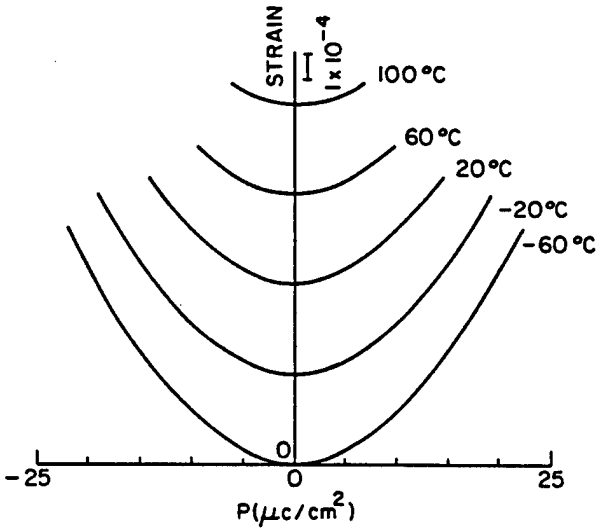

Figure 12 Typical polarization vs. strain curves in a PMN electrostrictive actuator as a function of temperature.

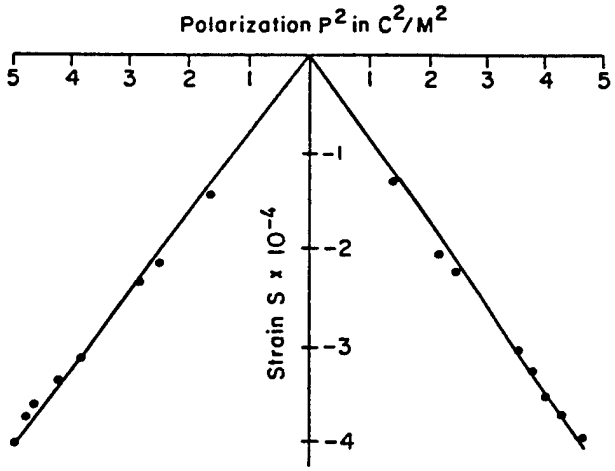

Figure 13 Quadratic electrostrictive transverse response in a PMN:10% PT actuator composition.

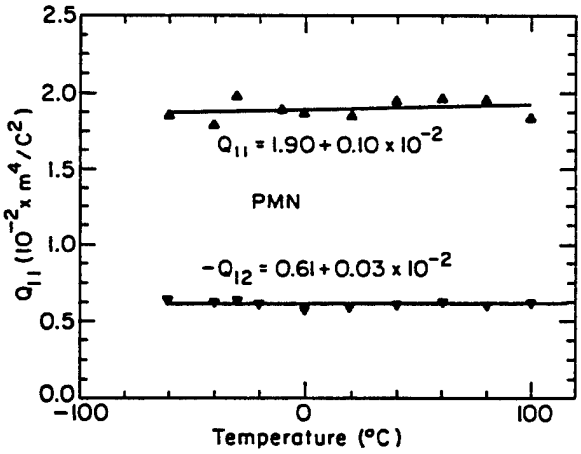

Figure 14 Electrostriction constants Q_{11} and Q_{12} as a function of temperature in a PMN:10%PT relaxor ferroelectric.

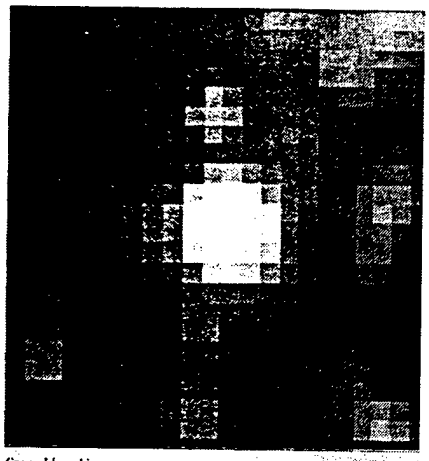

Ground-based image.

Image from Wide Field and Planetary Camera I.

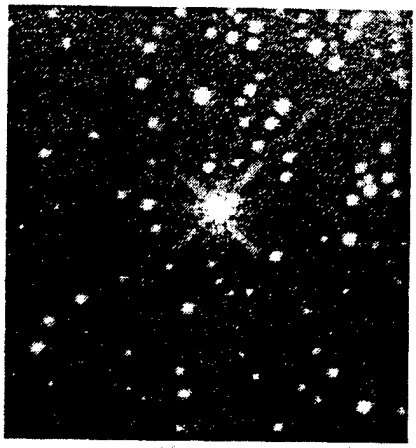

Image from Wide Field and Planetary Camera II.

Figure 15 Example of the improvement of the image from the Hubble Space Telescope of the Star Melnick 34 using the new wide field and planetary camera II incorporating tilt mirrors controlled by multilayer PMN:PT actuators.

PIEZOELECTRIC COMPOSITES

Dielectric, piezoelectric and elastic properties of poled piezoelectric ceramics are tensor quantities and for many types of application it is possible to spell out a figure of merit for the material which often requires the enhancement of some of these tensor coefficients and the diminution of others.

A typical example is the requirement for sensing of very weak hydrostatic pressure waves using large area sensors as in many Navy hydrophone needs (fig. 16). For hydrostatic pressure (fig.17) the stress $X_{11} = X_{22} + X_{33} = -p$, so that the polarization change P_3 is given by

$$\begin{aligned} P_3 &= d_{33}(-p) + d_{31}(-p) + d_{31}(-p) \\ &= (d_{33} + 2d_{31})(-p) \\ &= d_h(-p) \end{aligned}$$

where d_h is called the hydrostatic piezoelectric charge coefficient.

The voltage generated by the hydrophone, working into a very high impedance load will be given by

$$g_h = \frac{(d_3 + 2d_{31})}{\varepsilon_{33}} \tag{5}$$

and a figure of merit often used for hydrophone materials is the product $d_h g_h$

$$d_h \; g_h = \frac{(d_{33} + 2d_{31})^2}{\varepsilon_{33}} \tag{6}$$

For high sensitivity PZTs, there is an unfortunate near cancellation such that

$$d_{33} \cong -2d_{31} \tag{7}$$

so that $d_h << d_{33}$ or d_{31}, and PZT alone is not a good hydrophone material.

In exploring composites for hydrophone applications it would be advantageous from the point of view of density and of flexibility to combine the ceramic with a dielectric polymer. Comparing the dielectric and elastic properties between two such phases, a fascinating juxtaposition is evident

Dielectrically PZT is ultra soft ($k \sim 3{,}000$) whilst the polymer is quite stiff ($k \sim 10$) but in the elastic response, just the converse is true. The polymer is ultra soft ($s_{11} \sim 30.10^{-11} M^2/N$) but the ceramic is very stiff ($s_{11} \sim 2.10^{-11} M^2/N$) thus by careful control of the mode in which each phase is self-connected in the composite one can "steer" the fluxes and fields so as to enhance wanted coefficients and diminish unwanted coefficients so as to vastly improve the figure of merit.

Over some twelve years of intensive effort to design effective composites three important basic principles have emerged.

- Connectivity. The mode of self interconnection of the phases controls the fluxes and fields in the system enabling a tailoring of the tensor coefficients.

- Symmetry. Both the symmetry of the individual component phases and the macro symmetry of their arrangement in the composite can be used for additional control.

- Scale. The model of averaging for the property coefficients depends upon the scale of the composite phases in relation to the wavelength of excitation. Unusual resonances can occur when λ and d are comparable.

A major aid in thinking about the design of connectivity was the simple cubes model [35] (fig.18) and the associated notation, now internationally accepted which describes the dimensionality of the connectivity for active and passive phases.

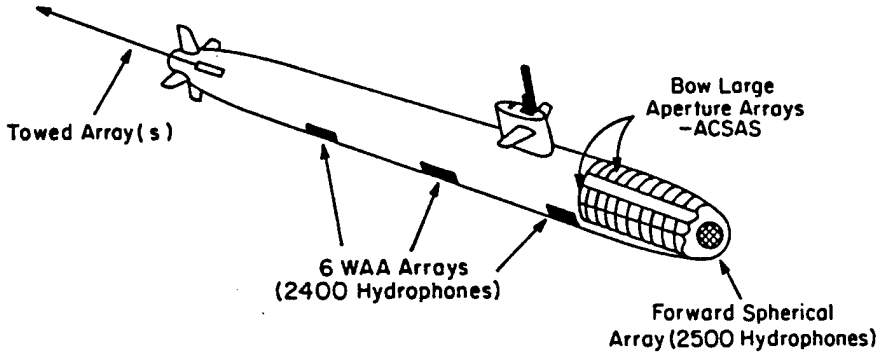

Figure 16 Examples of the need for large area hydrophone sensors in modern submarine acoustics.

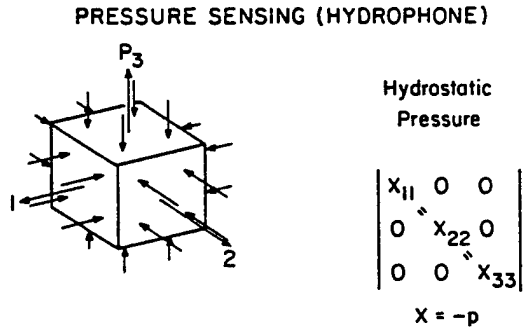

Figure 17 Stress System seen by the material under hydrostatic conditions in the hydrophone.

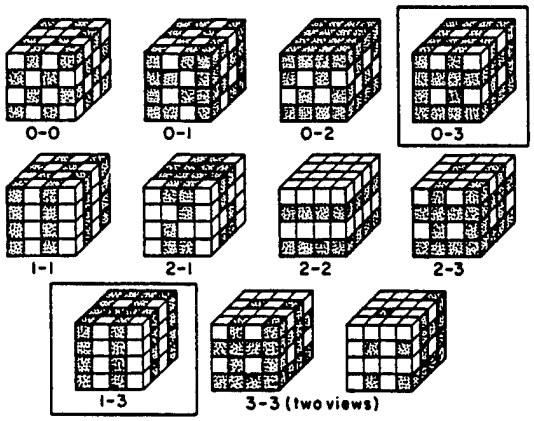

Figure 18 The simple 'cubes model for connectivity patterns possible in simple two phase piezoceramic:polymer composites.

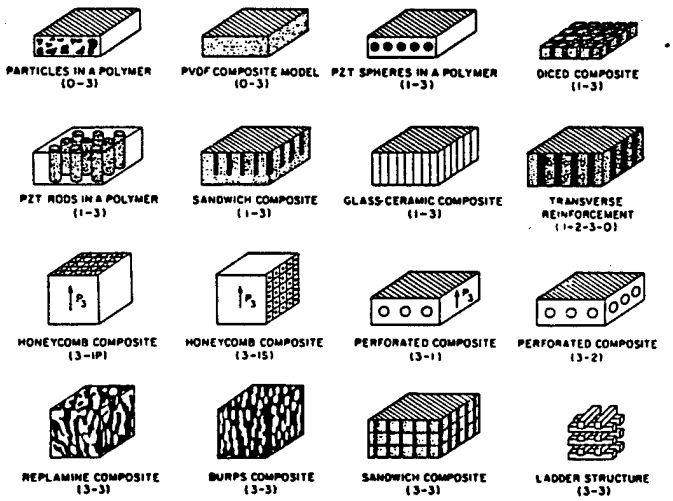

Figure 19 Examples of composite piezoceramic:polymer composites with different phase connectivities.

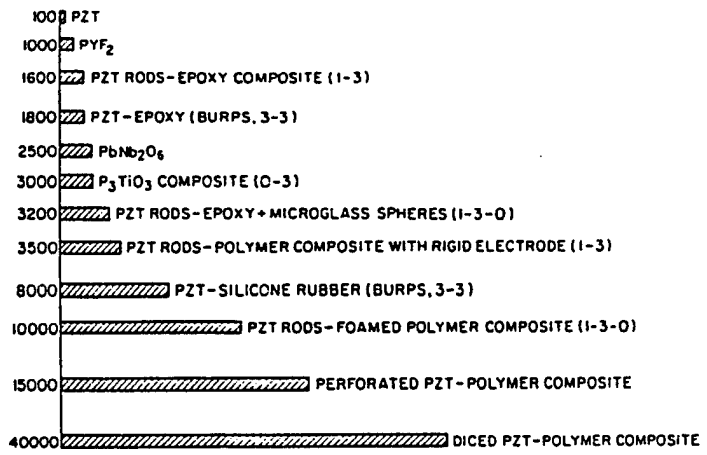

Figure 20 Hydrostatic figures of merit achieved using several different connectivities.

An indication of the many types of connectivities which have been used at Penn State for piezoceramic:polymer composites is shown in figure 19 and a measure of the improvement in hydrophone figure of merit over pure PZT for some of these systems is shown in figure 20.

The special case of the 1:2:3:0 composite which uses PZT rods in a foamed polymer matrix with transverse glass reinforcement is given in figure 21.

For the 1:3 type composites a major impediment to evolution for large scale structures has been the problem of assembly. Recently Fiber Materials of Biddeford, Maine have applied their ultraloom technology originally evolved for thick section carbon:carbon composites to this problem. Using the ultraloom they are able to stitch PZT posts into a template structure which contains the transverse glass fiber reinforcement and make sections up to four feet in width and of almost any length.

TENSOR ENGINEERING IN ACTIVE COMPOSITES

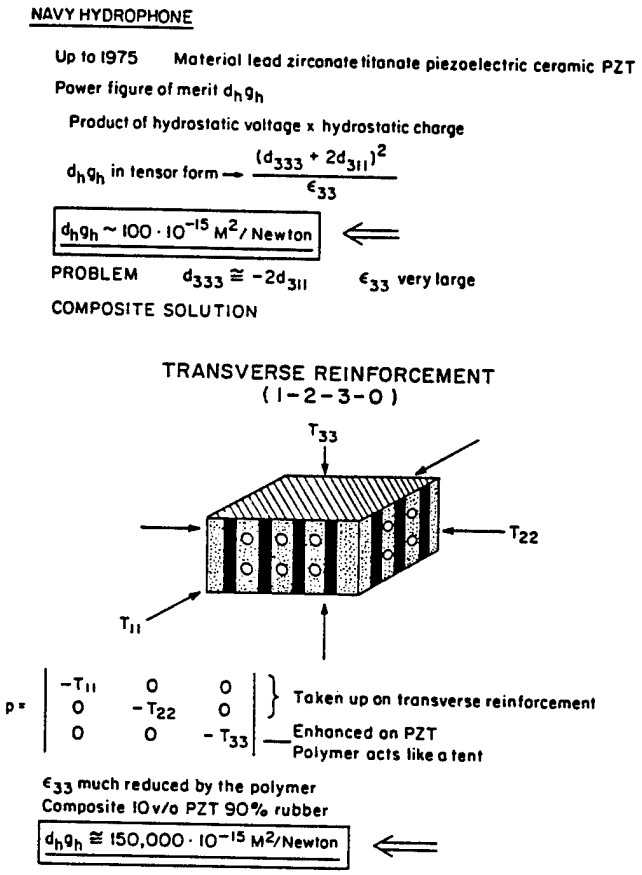

Figure 21 Figure of merit for a 1:2:3:0 transverse reinforced foamed polymer composite vs. performance of solid PZT.

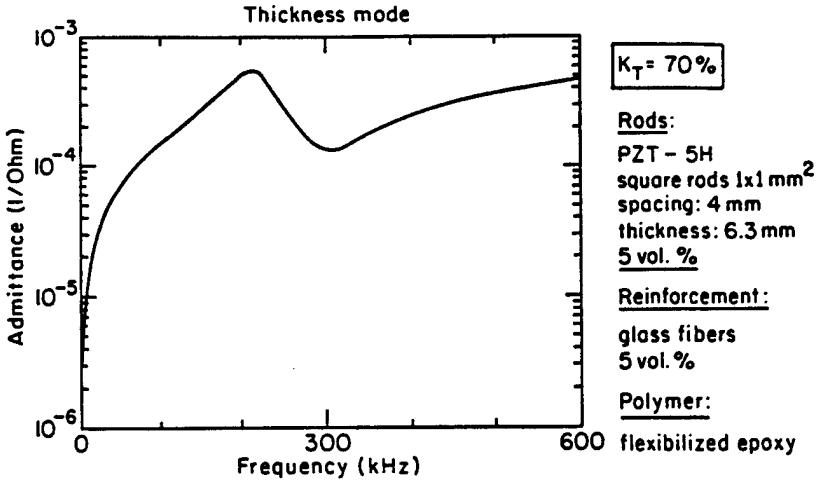

Figure 22 Thickness resonance curve for a Fiber Materials Inc. 1:3 composite containing 5 volume% PZT rods.

The FMI composites are not only interesting for very large area hydrophones, but can also be used in an actuator mode. It is interesting to note that with only 5 vol% PZT and a resultant density of 2.2 gm/cm^3 the transverse coupling coefficient k_t at 0.70 is larger than that of solid PZT (fig. 22).

The 1:3 type concept has also been applied to transducers for medical ultrasonics [36,37]. Here the required frequencies are much higher ~10Mhz so that the scale is very much smaller and the rod structure can be cut from solid PZT (fig.23). Beam characteristics, pulse shape and coupling factor are much improved over solid PZT transducers.

PYROELECTRICS

Thermal detection can be used for any wavelength of electromagnetic radiation, provided there is a convenient absorber which will convert the radiation into heat. For most parts of the electromagnetic spectrum there are other more convenient receptors, however in the long wavelength infra red for wavelength of 7 to

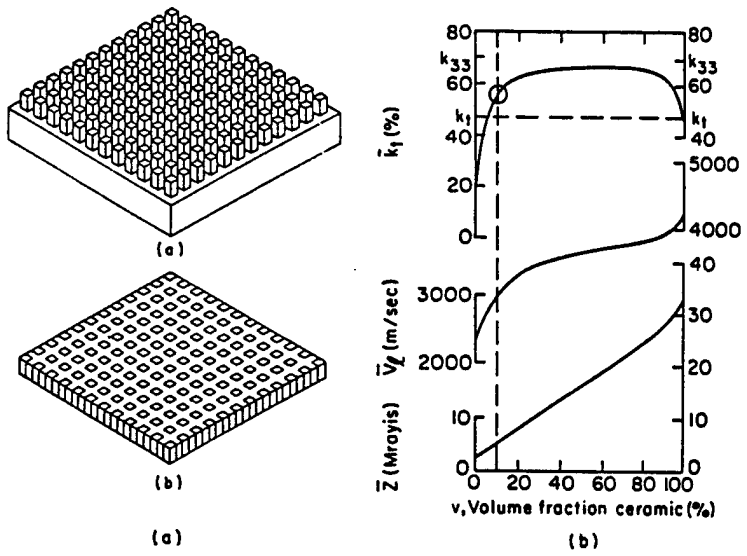

Figure 23 Piezoelectric ceramic: Polymer composites applied to electromedical transduction.
(a) The die and fill method of construction.
(b) Transverse couplinge composite as a function of volume fraction PZT.
After Smith [37].

13 μ meters photon detectors have to be cooled to helium temperatures and though highly sensitive become cumbersome and expensive. It is just in this wavelength region that detection and particularly imaging by thermal detectors becomes most interesting.

In the pyroelectric and other thermal detectors the objective is to obtain very high responsivity to longwave IR radiation so that low signals from warm bodies may be

observed over background noise. In all thermal detectors the overall responsibility is the product of two terms:

(a) The induced temperature change in the detecting element per unit of incident IR irradiation.
(b) The thermometric sensitivity of the detecting element.

RESPONSIBILITY	=	Induced temperature change ΔT in the detecting element	×	Thermometric sensitivity of the detector element.

Considering first the optimization of (a). Most values of ΔT for high sensitivity detectors and imagers are very small compared to the temperature drift even in a highly temperature stabilized environment so it is customary to chop the incident IR at a low frequency (10 -30 Hz) and examine only the AC component of ΔT.

For a solid state detecting element, a compact expression for (a) may be written in the form

$$\Delta T = \frac{I_o}{\left(g^2 + \omega^2 c^2 d^2\right)^{\frac{1}{2}}} \qquad (8)$$

Where I_o is the absorbed intensity
g the effective thermal conduction to the environment.
ω the chopping frequency.
c the volume specific heat
d the element thickness.

Clearly from equation 1 for high sensitivity the numerator I_o should be as large as possible and systems have been designed using radiation concentrators, thermal collectors and antenna structures. Very effective highly absorbing blacks of exceedingly low thermal mass have also been designed.

To further improve responsivity the denominator must be kept very small. Thermal isolation (g), thermal mass (cd) and chopping frequency must be simultaneously

addressed. Contrary to intuition excellent thermal isolation (very low g) is an absolute pre-requisite to permit ultra low thermal mass (very small detector thickness) and a reasonable chopping frequency, together with high sensitivity.

In isolated single (point) detectors, thermal isolation is easy as the element may be mounted on a polymer film drum head and connected by thin evaporated metal leads. For imaging systems isolation of the individual pixels is much more difficult and a major problem in most current hybrid systems.

(b) Many material systems change their properties rapidly with temperature and can be used as thermometric elements. Gases, as in the golay cell, one of the earliest high sensitivity thermal sensors, thermistors primarily simple NTC compositions [38], but high Tc superconductors have recently been applied [39], optical refractive index as in recent pyrooptic studies, but of most relevance to this paper pyroelectric and dielectric properties.

In the simple pyroelectric sensor, it is the differential change of remanent polarization with temperature $\partial P/\partial T$ which provides a current source

$$i = \frac{\partial P}{\partial T} \cdot \frac{\partial T}{\partial t} \qquad (9)$$

where $\partial T/\partial t$ is the rate of change of temperature. $\partial P/\partial T$ is called the pyroelectric coefficient p.

To achieve a voltage output the pyroelectric must charge its self capacitance

$$\Delta V = \frac{\Delta Q}{C} = p_1 \; A\Delta T/C \qquad (10)$$

for thin sheet detector polarized normal to the plane

$$C = \varepsilon A/t \qquad (11)$$

$$\frac{\partial V}{\partial T} = \frac{p_1 \; t}{\varepsilon} \qquad (12)$$

If the dielectric permittivity is a strong function of temperature as in ferroelectrics near the Curie transition additional response may be achieved by operating the material under bias and inducing an additional pyroelectric p_2 where

$$p_2 = \left(\frac{\partial \varepsilon}{\partial T}\right) E_b \qquad (13)$$

and

$$\frac{\partial V}{\partial T} = \frac{(P_1 + P_t)\; t}{\varepsilon} = \left(\frac{\partial \varepsilon}{\partial T} \cdot V + t \frac{\partial P}{\partial T}\right) \varepsilon^{-1} \qquad (14)$$

It has become conventional to develop material figures of merit for pyroelectric and dielectric systems.

For current mode operation $F_i = P_T/\varepsilon C^1$ where C^1 is volume specific heat.

For voltage made operation $F_V = P_T/\varepsilon C^1$ and for high signal to noise.

$$F_d = Pt/C^1(\varepsilon \tan \delta)^{1/2} \qquad (15)$$

recognizing that the loss tangent δ is an effective noise source endemic to the dielectric.

An excellent summary of the figures of merit for a very wide range of pyroelectric and biased dielectric materials has been tabulated by Kulwicki et. al. [40] and is reproduced here as Tables II and III.

Point detectors are a mature technology used in a very wide range of consumer products, intruder alarms, proximity detectors, level sensors, etc. Frequently used materials include $LiTaO_3$, lead germanate (PGO) PLZT and the polymer PVDF. For very high sensitivity units such as horizon sensors in spacecraft the water soluble TGS family is still used and detectors which have sensitivities approaching within a factor of three of ultimate thermal noise limited performance have been produced.

In current imaging systems hybrid technology is used with the sensing plane reticulated into pixel elements that are solder bump bonded to the silicon MOS image processing electronics. Materials competition is between barium strontium titanate and lead scandium tantalate polished to thickness between 10 and 25 μ meters. Noise equivalent temperatures of 0.07°C in the object plane have been achieved with F1 optics. It is perhaps an interesting comment on the current social scene that the major commercial market for imagers in USA is in law enforcement, whilst in England it is to fire brigades for seeing victims in smoke filled rooms [41]!

Markets for current imagers are limited by the difficulty and high cost of the hybrid approach. With the advent of ferroelectric thin films there has been a strong drive to lower cost by using integrated approaches and depositing films on an air bridge thermal isolation system fabricated by MEMS technology. Initial results look most promising and it may be that by this approach thermal imaging may supplement night vision in automobiles and contribute to collision avoidance in fog.

TABLE II. Normal Pyroelectric ($T < T_c$)

Material	Bias kV/cm	T_c °C	c′ J/cm³K	p μC/cm²K	ε_r	tan δ	F_v cm²/C	F_d (cm³/J)$^{1/2}$	Reference
Single crystals									
TGS	0	49	2.3	0.028	38	0.01	3620	0.066	Herbert [16]
DTGS	0	60	2.4	0.055	43	0.02	6020	0.083	Whatmore (Felix) [25]
ATGSAs	0	51	2.5	0.07	32	0.008	9900	0.19	Bhalla [38]
$LiTaO_3$	0	665	3.2	0.18	43	0.003	1440	0.051	Byer [35]
$LiNbO_3$	0	1210	3.0	0.083	28	0.005	1140	0.025	Byer [35]
SBN 46/54	0	132	2.1	0.043	380	0.003	610	0.065	Byer [35]
PGO:Ba	0	70	2.0	0.032	81	0.001	2200	0.19	Whatmore (Watton) [39]
Ceramics									
PLZT 7/65/35	0	150	2.6	0.13	1900	0.015	300	0.032	Liu [41]
PLZT 8/65/35	0	105	2.6	0.18	4000	0.003	190	0.066	Deb [42]
PZNFTU	0	230	2.7	0.039	290	0.0031	570	0.052	Osbond [23]
PSZNFTU	0	170	2.7	0.049	400	0.0028	520	0.058	Osbond [23]
PGO	0	178	2.6	0.002	25	0.003	350	0.009	Kanduser [43]
Polymerics									
PVDF	0	none	2.4	0.0027	12	0.015	1040	0.009	Whatmore [39]
Thin films									
$PbTiO_3$ sol-gel	0	490	2.9	0.095	200	0.02	1870	0.056	Polla [28]
PLT 90/10 sputtered	0	330	3.2	0.065	200	0.006	1150	0.062	Takayama [44]
PCT 70/30 sputtered	0	270	3.3	0.05	390	0.015	440	0.021	Yamaka [45]
PZT 54/46 sol-gel	0	380	3.1	0.07	950	0.016	260	0.019	Ye [28]

Table III. Phase Transition Materials ($T \cong T_{t(c)}$)

Material	Bias kV/cm	T_t °C	c′ J/cm³K	p'_{max} μC/cm²K	ε_r	tan δ	F_v cm²/C	F_d (cm³/J)$^{1/2}$	Reference
Single crystals									
DTGFB	0	74	2.0	1.4	2400	0.02	3300	0.34	Dougherty [36]
KTN 67/33	2.5	4	3.7	8.0	25000	0.002	1000	0.46	Stafsudd [46]
BST 65/35	5	5	2.5	0.3	20000	0.007	170	0.034	Whatmore [39]
Ceramics									
BST 67/33	1	21	3.2	23.0	31000	0.028	2700	0.84	This work
BST 67/33	2	22	3.2	6.3	33000	0.021	670	0.25	This work
BST 67/33	6	24	3.2	0.70	8800	0.004	280	0.12	This work
BST 65/35	40	29	2.5	0.10	1200	0.0013	380	0.11	Whatmore [39]
PMN:La	90	40	3.0	0.085	1200	0.0008	800	0.10	Whatmore [39]
PScT	53	40	2.7	0.38	2900	0.0027	550	0.17	Shorrocks [47]
PZT 94/6*	0	50	2.6	0.37	300	0.02	5300	0.19	Lian [48]
PZNT 90/8/2*	0	30	2.6	0.185	290	0.019	2800	0.10	Takenaka [49]
PCT 70/30:PCoW 96/4	0	106	3.3	3.0	7400	0.037	1380	0.18	Deb [52]
PLZT 8/60/40 (*sic*)	0	142	3.7	3.2	16200	0.062	600	0.092	Deb [50]
PZN/BT/PT 80/10/10**	0	12	2.7	5.93	4670	0.01	5310	1.08	Deb [51]
PZN/BT/PT 80/10/10	0	85	2.7	2.9	18300	0.018	660	0.20	Deb [51]
Thin films									
PScT sputtered	40	40	2.7	0.52	6000	0.012	360	0.076	Watton [24]
PScT sol-gel	--	40	2.7	0.30	7000	0.002	180	0.10	Shorrocks [20]
PScT MOCVD	20	40	2.7	0.08	1000	0.002	330	0.07	Ainger [53]
KTN metalorganic	30	40	3.7	20.0	1200	0.01	50000	5.0	Schubring [54] "pumped"

* rhombohedral-rhombohedral phase transition
** rhombohedral-tetragonal phase transition

ELECTRO-OPTICS

In paraelectric and ferroelectric crystals the high intrinsic dielectric softness means that large internal (cooperative) ion motions can be induced by quite modest electric fields. Changes of mutual separation of the ions lead to strong distortions of the electronic charge distribution and hence strong changes in the optical refractive index and correspondingly large electrooptic effects. It is interesting to note that in these systems it is the electric field related constants which are exceptionally large and the polarization related constants quite normal.

For a single crystal the optical refraction behavior is defined by the optical indicatrix

$$\frac{x_1^2}{n_1^2} + \frac{x_2^2}{n_2^2} + \frac{x_3^2}{n_3^2} = 1 \qquad (16)$$

where $n_1 n_2 n_3$ are the principle refracture indices. If the optical impermeability is defined by

$$B_{11} = \frac{1}{n_1^2} \qquad B_{22} = \frac{1}{n_2^2} \qquad B_{33} = \frac{1}{n_3^2} \qquad (17)$$

Then the relationship may be expressed simply in tensor form

$$B_{ij} x_i x_j = 1 \qquad (18)$$

The perturbation to the impermeability ΔB_{ij} by electric field components $E_k E_l$ then takes the form

$$\Delta B_{ij} = f^X_{ijk} E_k + L^X_{ijkl} E_k E_l \qquad (19)$$

The f_{ijk} are the linear electrooptic tensor coefficients measured at constant stress (superscript X) and the $L^{\wedge}_{ijkl}$ are the quadratic electrooptic tensor coefficients measured again at constant stress.

For non zero f constants the crystal must be in a non centric piezoelectric group, and the f carry the same symmetry constraints as the piezoelectric d constants. The quadratic L constants have the same constraints as the electrostriction tensor and all transparent crystal have non zero quadratic constants.

Since the electric field produces elastic distortion, the f constant encompasses a stress/strain optic component in the form

$$\Delta B_{ikj} = e^{x}_{ijk} E_k + P^{E}_{ikjl} x_{kl} \qquad (20)$$

where p_{ikjl} are the stress optic tensor coefficients and x_{kl} the piezoelectrically induced strain components.

Awareness of the stress optic effects are of major importance as for a crystal under AC field at low frequency the system is free to deform and measurement give the constant (zero) stress f constant. However, as the crystal passes through elastic resonances it becomes successively more inertia clamped and the measurement drops back to the e constants. Because of the very high piezoelectric and electrostriction constants in ferroelectrics the change from f to e can be substantial.

As the dielectric constant goes through orders of magnitude changes with temperature in paraelectric and ferroelectric phases the constants f and M are similarly temperature dependent. In terms of the polarization components (equation 19) may be rewritten

$$\Delta B_{ij} = r_{ijk} P_k + M_{ijkl} P_k P_l \qquad (21)$$

The r and M constants are now similar to those in normal non ferroelectric oxides and only change slowly the temperature. For perovskite oxides, these constants are continuous through the ferroelectric phase transitions and optical changes between para and ferro phases can be calculated by simply inserting the appropriate non zero components of spontantous polarization $P_k P_l$ into the equation for the prototypic form.

Polycrystal ceramic oxides are usually opaque to visible light due to strong scattering at grain boundaries and pores. In the lead lanthanum zirconate titanate (PLZT) ferroelectric and relaxor ferroelectric compositions it was found to be possible to hot press to near theoretical density and produce highly transparent ceramics [42]. With increasing lanthanum concentration the Curie range goes to lower temperature so that in a 65:35 Zr/Ti composition at 9 mole% La_2O_3 the system will not support a remanent polarization and the electrooptic effects are quadratic [43]. Between crossed polarizers thin sheet PZT is opaque, but can be biased under moderate field to highly transmitting. The switching speed is fast enough to provide protection against flash blindness and these materials are the basis for the Airforce Nuclear flash blindness helmets supplied to nuclear bomber pilots [44]. In commercial application however, the halfwave (transmitting) voltage is a little too high and the material too expensive to compete with ferroelectric liquid crystal systems.

For single crystals applications in simple electro-optics it is necessary to be able to grow large single crystals. Potassium dilhydrogen phosphate (KDP) has been widely used in its paraelectric phase above Tc for large area modulators. In guided wave structures lithium niobate is the crystal of choice. For the niobate crystals the refractive index may be enhanced by indiffusion of titanium so that guided wave structures can be fabricated on the crystal surface and a wide range of modulators, switches and other components are currently fabricated by this means.

In the tungsten bronze structure $Ba_{0.4}Sr_{0.6}Nb_2O_6$ (SBN) large optically perfect single crystals have now been grown. An advantage for SBN is that its stress optic coefficients are sufficiently large that guiding structures may be fabricated by local stress generated by capping films, preserving the high optical quality of the guiding path [45].

For lithium niobate, $BaTiO_3KNbO_3$ and SBN, high intensity laser light can promote carriers from traps in the band gap leading to a photo current. Because of the spontaneous polarization in the ferroelectric state the current flow is not symmetrical and re-trapping leads to an internal field which modulates the refractive index through the high electro-optic coefficients. A very wide range of research are presently exploring potential application for the strong photo refractive effects in these crystals [46].

Optical phase conjugation [47], holographic interferometry [48], image amplification at low light levels [49], optical beam fanning [50], moving object correlation [51], spacial soliton self trapping [52], and dynamic tuneable ferroelectric domain gratings for quasi phase matched harmonic generation [53] have all been generated at the research level.

For thin film systems optical applications have so far proved difficult as the quality and homogeneity of most present ferroelectric films is far from ideal. With the new capabilities which are being developed using Chemical Vapor Deposition (CVD) to produce truly epitaxial single crystal films it should be possible in future to exploit the capability that this will afford to produce excellent quality crystals with compositionally 'tuned' properties most suitable for specific optical applications.

REFERENCES

1. L.E. Cross, "Ferroelectric Ceramics: Tailoring Properties for Specific Applications," Ferroelectric Ceramics, Monte Verita, Edited by N. Setter, E. Colla, Birkhausen, Verlad, Basel (1993).

2. A.J. Bell, Multilayer Ceramic Processing, Ibid.

3. L.E. Cross and K.H. Hardtl, "Ferroelectrics," Kirk Othner Encyclopedia of Chemical Technology, John Wiley and Sons (1980).

4. K. Kinoshita and A. Yamaji, "Grain Size Effects on the Dielectric Properties in Barium Titanate Ceramics," J. Appl. Phys. **47**, 371 (1976).

5. L.E. Cross, "Relaxor Ferroelectrics," Ferroelectrics **76**, 241 (1987).

6. C. Randall, D. Barker, R. Whatmore, and P. Groves, "Short Range Order Phenomena in Lead Based Perovskites," Ferroelectrics **76**, 277 (1987).

7. P. Asadipour, "Polarization Mechanisms in Relaxor Ferroelectrics," MS Thesis, The Pennsylvania State University (May 1986).

8. D. Viehland, S.J. Jang, L.E. Cross, and M. Wuttig, "Freezing of the Polar Fluctuations in Lead Magnesium Niobate Relaxors," J. Appl. Phys. **68**, 2916 (1990).

9. D. Viehland, S.J. Jang, L.E. Cross, and M. Wuttig, "Local Polar Configurations in Lead Magnesium Niobate Relaxors, "J. Appl. Phys. **69**, 414 (1991).

10. S.W. Choi, T.R. Shrout, S.J. Jang, and A.S. Bhalla, "Dielectric and Pyroelectric Properties in the $Pb(Mg_{1/3}Nb_{2/3})O_3$:$PbTiO_3$ System," Ferroelectrics **100**, 29, 1989.

11. D. Viehland, M. Wuttig, and L.E. Cross, "The Glassy Behavior of Relaxor Ferroelectrics," Ferroelectrics **120**, 71 (1991).

12. J. Chen, "Electrical and Electromechanical Properties of Ferroelectric Thin Films for MEMS Applications," PhD Thesis, The Pennsylvania State University (August 1993).

13. R. Gerson and T.C. Marshall, "Dielectric Breakdown in Porous Ceramics," J. Appl. Phys. **30**, 1650 (1959).

14. W. Williams, III, "Investigation of Thin Film Ferroelectric Materials for Application in High Frequency Decoupling Capacitors," ISIF 1995, Colorado Springs, CO (March 20, 1995).

15. V. Chivukula, "Dielectric Properties of Ferroelectric Thin Films in the Frequency Range Hz to Ghz," ISIF 1995, Colorado Springs, CO (March 20, 1995).

16. L.E. Cross, "Dielectric Design in Ferroelectric Thin Films," Proceedings Electroceramics IV, Aachen Germany (September 5, 1994).

17. K.G. Brooks, J. Chen, K.R.Udayakumar, and L.E. Cross, " Electric Field Forced Switching in la Modified Lead Zirconate Stannate Titanate," J. Appl. Phys. **75** (3), 1699 (1994).

18. L.E. Cross, "Induced Strain Response in Ferroelectric Relaxor Ferroelectric on Phase Switching Films," Nato Advanced Research Workshop, Villa del Mar, Italy (June 20, 1994).

19. B. Jaffe, W.R. Cooke, Jr., and H. Jaffe, "Piezoelectric Ceramics," Academic Press, NY (1971)

20. E. Sawaguchi, "Ferroelectricity versus Antiferroelectricity in Solid Solutions of $PbZrO_3$ and $PbTiO_3$," J. Phys. Soc. Japan **8**, 515 (1953).

21. B. Jaffe, R.S. Roth, and S. Marzullo, "Properties of Piezoelectric Ceramics in the Solid Solution Lead Titanate - Lead Zirconate Lead Oxide Tinoxide and Lead Titanate Lead Hafnate," J. Res. National Bureau of Standards 55,2626 (1955).

22. W. Cao and L.E. Cross, "Distribution Function of Coexisting Phases in Complete Solid Solution System," J. Appl. Phys. **73**, 3250 (1993).

23. M.J. Haun, E. Furman, S.J. Jang, and L.E. Cross, "Thermodynamic Theory of the Lead Zirconate-Titanate Solid Solution System, Part 1: Phenomenology," Ferroelectrics **99**, 13 (1989).

24. M.J. Haun, E. Furman, H.A. McKinstry, and L.E. Cross, "Thermodynamic theory of the Lead Zirconate-Lead Titanate Solid Solution System: Part II-Tricritical Behavior," Ferroelectrics **99**, 27 (1989).

25. M.J. Haun, Z.Q. Zhuang, E. Furman, S.J. Jang, and L.E. Cross, "Thermodynamic Theory of the Lead Zirconate-Lead Titanate Solid Solution System: Part III- Curie Constant and Sixth Order Polarization Interaction Dielectric Stiffness Coefficients," Ferroelectrics **99**, 45 (1989).

26. M.J. Haun, E. Furman, T.R. Halemane, and L.E. Cross, "Thermodynamic Theory of the Lead Zirconate-Lead Titanate Solid Solution System: Part IV- Tilting of the Oxygen Octahedra," Ferroelectric **99**, 55 (1989).

27. M.J. Haun, E. Furman, S.J. Jang, and L.E. Cross, "Thermodynamic Theory of the Lead Zirconate-Lead Titanate Solid Solution System: Part V- Theoretical Calculations," Ferroelectrics **99**, 63 (1989).

28. K. Carl and K.H. Hardtl, "Stabilization of Domain in Acceptor Doped PZT Ceramics," Ferroelectrics **17**, 472 (1978).

29. D. Dederichs and G. Arlt, "Isothermal Aging in Iron Modified Lead Zirconate Titanate Ceramics," Ferroelectric **68**, 281 (1986).

30. R. Gerson and H. Jaffe, "Domain Processes in Lead Titanate Zirconate Ceramics," J. Phys. Chem. Solids **24**, 979 (1963).

31. R. Gerson, "Donor Doped Lead Zirconate:Titanate Ceramics," J. Appl. Phys. **31**, 188 (1960).

32. L.E. Cross, S.J. Jang, R.E. Newnham, S. Nomura, and K. Uchino, "Large Electrostriction Effects in Relaxor Ferroelectrics," Ferroelectrics **23**, 187 (1980).

33. Q. Zhang, W. Pan, A. Bhalla, and L.E. Cross, "Electrostrictive and Dielectric Response in Lead Magnesium Niobate Lead Titanate (PMN 0.1PT) and Lead Lanthanum Zirconate Titanate (PLZT 9.5/65/35) Under Variation of Temperature and Electric Field," J. Am. Ceram. Soc. **72**, 599 (1989).

34. R. Aldrich, ITEK Optics Division, Private Communication.

35. R.E. Newnham, D.P. Skinner, and L.E. Cross, "Connectivity and Piezoelectric/Pyroelectric Composites," Mat. Res. Bull. **13** (5), 525 (1978).

36. A.A. Shaulov, M.E. Rosar, W.A. Smith, and B.M. Singer, "Composite Ultrasonic Transducers" Proc. ISAF86, pp. 231, Lehigh University (1986).

37. W.A. Smith, "Composite Piezoelectric Materials for Medical Ultrasonic Imaging Transducers. A Review," Proc. ISAF86, pp. 249, Lehigh University (1986).

38. K.C. Liddiard, "Thin Film Resistance Bolometer IR Detectors," Infrared Physics **24**, 57 (1984).

39. M.C. Foote, B.R. Johnson, and B.D. Hunt, "Transition Edge $YB_2Cu_3O_7$ Microbolometers for Infrared Staring Arrays," Proc. SPIE (January 1994).

40. B.M. Kulwicki, A. Amin, H. Beratan, and C.M. Hanson, "Pyroelectric Imaging," Proc. ISAF92, Greenville, South Carolina (August 30, 1992).

41. R. Watton, "Ferroelectric Materials and IR Bolometric Arrays: From Hybrid Array Towards Integration," Proc. ISIF5, Colorado Springs, Colorado (April 1993).

42. G.H. Haertling, "Improved Hot-Pressed Electro-Optic Ceramics in the $(PbLa)(ZrTi)O_3$ System," J. Am. Ceram. Soc. **54**, 303 (1971).

43. J.T. Cutchen, J.O. Harris, and G.R. Laguna, "Electro-optic Devices Using Quadratic PLZTs," Sandia Lab Technical Report SLA-73-0777 (1973).

44. J.T. Cutchen, "PLZT Thermal/Flash Goggles Concepts and Constraints," Ferroelectrics **27**, 173 (1980).

45. H. Taylor, Texas A&M, Private Communication.

46. A.M. Glass, "Optical Materials," Science **235**, 1003 (1987).

47. G. Salamo, M.J. Miller, W.W. Clark, G.L. Wood, and E.J. Sharp, "Strontium Barium Niobate as a Self-Pumped Phase Conjugator," Optical Comm. **39**, 417 (1986).

48. N. Kukhtarev, Bo Su Chen, P. Venkateswarlu, G. Salamo, and M. Klein, "Reflection Holographic Gratings in [111] Cut $Bi_{12}TiO_{20}$ Crystal for Real Time Interferometry," Optical Comm. **104**, 23 (1993).

49. R.R. Neurgaonkar, W.K. Cory, J.R. Oliver, E.J. Sharp, G.L. Wood, and G.J. Salamo, "Growth and Optical Properties of Ferroelectric Tungsten Bronze Crystals," Ferroelectrics **142**, 167 (1993).

50. S.R. Montgomery, M.P. Gallagher, G.J. Salamo, E.J. Sharp, G.L. Wood, and R.R. Neurgaonkar, "Cooperative Photorefractive Beam Fanning in $BaSrKNaNb_5O_{15}$," J. Opt. Soc. Am. B **11**, 1694 (1994).

51. E.J. Sharp, G.L. Wood, G.J. Salamo, R.J. Anderson, Jan M. Yarrison-Rice, and R.R. Neurgaonkar, "Photorefractive Image Processing Using Mutually Pumped Phase Conjugators," SPIE Optical Pattern Recognition **2237**, 347 (1994).

52. M. Segev, B. Crosignani, A. Yariv, and B. Fischer, " Spatial Solitons in Photorefractive Media," Phys. Rev. Letters **68**, 923 (1992).

53. A.S. Kerwitsch, M. Segev, A.Yariv, G. Salamo, T.W. Towe, E.J. Sharp, and R.R. Neurgaonkar, "Tuneable Quasi Phase Matching Using Dynamic Ferroelectric Domain Gratings Induced by Photorefractive Space Change Fields," J. Appl. Phys. Letters **64**, 3068 (1994).

APPENDIX 3

8 April 1996

PHYSICS LETTERS A

ELSEVIER

Physics Letters A 212 (1996) 341–346

Size effects in nanostructured ferroelectrics

Shaoping Li [a], J.A. Eastman [a], Z. Li [a], C.M. Foster [a], R.E. Newnham [b], L.E. Cross [b]

[a] *Materials Science Division, Argonne National Laboratory, 9700 South Cass Ave, Argonne, IL 60439, USA*
[b] *Materials Research Laboratory, Pennsylvania State University, University Park, PA 16802, USA*

Received 7 November 1995; revised manuscript received 18 January 1996; accepted for publication 22 January 1996
Communicated by L.J. Sham

Abstract

The finite size effect in ferroelectrics results in structural instability, imposing a limitation of physical sizes and dimensions of materials in which electric dipoles can be sustained. To evaluate the ultimate limitation of physical sizes for a stable polar phase, the characteristic sizes, i.e., *anisotropic correlation lengths* of electric dipoles, in a ferroelectric have been examined by considering the surface effect. The size dependence on the Curie temperature in particular is calculated with consideration of crystallographic anisotropy. The mean-field theory shows that the limitation of transverse critical sizes is strongly dependent upon the thickness. In turn, the limitation of the critical thickness is also closely associated with the transverse critical sizes.

The great fascination of nanostructured materials is that their properties are different from, and often superior to, those of conventional materials that have phase or grain structures on a coarse size scale. However, phase stability is an important aspect of materials with reduced spatial dimensions in the nanometer size regime. The reduction in physical sizes of ferroelectrics from the macroscopic down to the mesoscopic regimes usually results in a change of stability of the polarization [1–4]. Experimentally it is well known that the polarization can be inhibited [1,2] or even enhanced [3] in nanostructured materials, i.e., zero-dimensionality (0-D) atom clusters and cluster assemblies, or thin films (two-dimensional layers). The anomalies induced by the finite size effects in ferroelectrics can be understood within several scenarios [4]. First, for example, many size effects in ferroelectrics are explained by the occurrence of a monodomain configuration, which is energetically favorable in systems with small size. However, this effect is unrelated to a change in the structural instability of a polar phase as the physical dimensions or sizes are reduced. Second, some size effects in polar systems can be attributed to a depolarizing field influence [5]. Nevertheless, experimentally the depolarizing field effect seems to be much weaker than expected [4]. In addition, the depolarization field effect cannot explain why sometimes ferroelectric stability can be even enhanced in some types of thin films or nanometer-sized materials [3]. A third source of strong finite size effects on polarization stability is a surface effect [3] (for review articles, see Ref. [6]), or more generally, an interface effect. The main physical consequences of surface effects are two-fold. (1) Close to the surface of a system the original translational invariance of the

PII S0375-9601(96)00077-1

system tends to be broken as compared to the bulk interior. As a result, changes in the local symmetry and features of soft modes occur such that the polarization characteristic (dipole–dipole interactions) at the surface differs from that within the interior [4]. Accordingly, the total energy of the system is altered by the surface effect, *which is represented by a surface energy or a surface tension* [4] *and is proportional to the total surface area.* (2) As the physical sizes of a confined system reach a mesoscopic level (100 nm or less), the fraction of atoms located in (or near) surfaces increases substantially. They are structurally associated with surface or interfacial environments, thus surface effects can play a vital role in controlling the properties of nanostructured materials.

In recent years, interest has focused on a variety of ferroelectric nanostructured materials. In addition, the use of capacitors constructed from ferroelectric thin films has stimulated interest in developing ferroelectric non-volatile memory devices [7]. Since the basic properties of ferroelectric materials and devices are based upon the existence of spontaneous polarization, the physical sizes of materials, within which electric dipole can be sustained, impose a limit on the performance of nanostructured materials. Thus, there is a pressing need to determine the characteristic sizes of the confined ferroelectric systems. The characteristic (or critical) sizes of a ferroelectric are defined as the minimum physical sizes below which the ferroelectricity in the material disappears.

In this Letter we address a particular aspect of the finite size effect on ferroelectric instability: *the polarization suppression caused by the surface effect in a confined system.* More specifically, we employ a mean-field theory to examine ferroelectric phase instability in a ferroelectric with the smallest possible dimensions. Various theoretical approaches, such as Landau–Ginzburg (LG) theory [3,6,8], the Ising model in a transverse field [9] and the scaling theory [10], have been exploited to discuss the ferroelectric instability in terms of reduction of thicknesses in films by consideration of the surface effect. More recently, attempts have also been made to evaluate the critical sizes of a confined system [11] or in nanometer sized particles [12]. However, the oversimplifications in recent theoretical analyses resulted in some inaccuracies in quantitative assessment of dipole correlation ranges. The main insufficiency in previous theoretical calculations [11,12] arises from ignoring the anisotropy of correlation forces. The correlation forces of dipoles in ferroelectrics are highly anisotropic in nature. More precisely the parallel alignment of dipoles along the polar c-axis is due primarily to a relatively strong long-range dipole interaction, resulting in intercell correlation and the formation of long dipole chains with a transverse optic phonon character. In directions normal to the polar axis, however, the "force" which tends to produce parallel alignment of dipoles is much weaker and short-ranged [13]. Normally, the transverse correlation lengths are believed to be an order of magnitude less than the longitudinal correlation range [13].

In order to estimate the characteristic sizes for a ferroelectric cell, we consider a rectangular ferroelectric cell with the perovskite structure and volume $a_0 \times b_0 \times c_0$. a_0 and b_0 are the width and length of the cell along the x-axis and y-axis, respectively, and c_0 is the thickness of the cell in the direction of the z-axis. The order parameter for describing the O_h–C_{4v} proper ferroelectric phase transition is the polarization vector $\boldsymbol{P}$, which is oriented along the z-axis, i.e., $\boldsymbol{P} = (0, 0, P(x, y, z))$. Choosing the coordinate origin at the center of the cell, we write the free energy of the cell as [6,8]

$$\begin{aligned}\Phi = \int_v \Big[& \tfrac{1}{2}AP^2 + \tfrac{1}{4}BP^4 + \tfrac{1}{6}CP^6 \\ & + \tfrac{1}{2}D_{11}(\nabla_z P)^2 + \tfrac{1}{2}D_{44}(\nabla_x P)^2 + \tfrac{1}{2}D_{44}(\nabla_y P)^2 \Big] \\ & + \int_{s_1} \tfrac{1}{2}D_{11}\delta_3^{-1}P^2 \, \mathrm{d}x \, \mathrm{d}y \\ & + \int_{s_2} \tfrac{1}{2}D_{44}\delta_1^{-1}P^2 \, \mathrm{d}z \, \mathrm{d}y \\ & + \int_{s_3} \tfrac{1}{2}D_{44}\delta_1^{-1}P^2 \, \mathrm{d}z \, \mathrm{d}x, \end{aligned} \tag{1}$$

where $A = A_0(T - T_{c0})$ and T_{c0} is the normalized Curie temperature of the bulk crystal, below which the bulk material exhibits a ferroelectric phase. A_0, B and C are normalized coefficients of Landau free

energy expression, in which the elastic strain coefficients and relevant coupling parameters are tacitly included [14]. Likewise, D_{11} and D_{44} represent the normalized coefficients of the gradient terms along different crystallographic directions [15]. Physically this comes about because for electric dipole forces the parallel alignment is more energetically favorable for an isolated pair of c-axis dipoles than for an isolated pair of dipoles normal to the polar axis. δ_i is defined as the extrapolation length [6] and measures the strength of the surface effect. S represents a closed surface of the cell of volume V, which consists of six surface planes S_1, S_2 and S_3. Moreover, the volume and surface integrals are associated with the free energy of the interior cell and "bare" surfaces of the cell, respectively. The depolarizing field is neglected here since in practice electrodes typically cover both top and bottom surfaces of a ferroelectric cell. Basically, the homogeneous volume energy in Eq. (1) is negative when $T < T_{c0}$. δ_i is considered as a positive value ($\delta_i > 0$) in this work. In other words, the surface energies are positive in our case. Accordingly, at the critical sizes, a balance among the volume, surface and gradient energies determines a characteristic temperature point temperature ($T_c < T_{c0}$) [6], i.e., a new phase transition point, instead of the original bulk Curie point T_{c0}. Beyond this transition temperature point T_{c0}, the polar (low symmetry) phase will be suppressed in the cell with the dimensions less than the critical sizes. This process is analogous to the classical homogeneous nucleation process in that condensed phase nuclei are not stable unless the radii of the condensed phase nuclei are larger than a specific critical size.

By varying the total free energy of Eq. (1) with respect to P, Eq. (1) yields

$$\begin{aligned}\hat{\delta}\Phi = \int_v \Big[& AP\hat{\delta}P + BP^3\hat{\delta}P + CP^5\hat{\delta}P \\ & + D_{44}\nabla_x P\hat{\delta}(\nabla_x P) + D_{44}\nabla_y P\hat{\delta}(\nabla_y P) \\ & + D_{11}\nabla_z P\big(\hat{\delta}\nabla_z P\big)\Big]\,\mathrm{d}V \\ & + \int_{s_1} D_{11}\delta_3^{-1}P\hat{\delta}P\,\mathrm{d}S_1 + \int_{s_2} D_{44}\delta_1^{-1}P\hat{\delta}P\,\mathrm{d}S_2 \\ & + \int_{s_3} D_{44}\delta_1^{-1}P\hat{\delta}P\,\mathrm{d}S_3. \end{aligned} \tag{2}$$

With the help of both following integral equations,

$$\int_v D_{44}\nabla_x P\hat{\delta}(\nabla_x P)\,\mathrm{d}v = \int_v \left(\frac{\partial}{\partial x}\big(D_{44}\nabla_x P\hat{\delta}P\big) - \big(D_{44}\nabla_x^2 P\big)\hat{\delta}P\right)\mathrm{d}v, \tag{3a}$$

$$\int_v D_{44}\nabla_y P\hat{\delta}(\nabla_y P)\,\mathrm{d}v = \int_v \left(\frac{\partial}{\partial y}\big(D_{44}\nabla_y P\hat{\delta}P\big) - \big(D_{44}\nabla_y^2 P\big)\hat{\delta}P\right)\mathrm{d}v, \tag{3b}$$

$$\int_v D_{11}\nabla_z P\hat{\delta}(\nabla_z P)\,\mathrm{d}v = \int_v \left(\frac{\partial}{\partial z}\big(D_{11}\nabla_z P\hat{\delta}P\big) - \big(D_{11}\nabla_z^2 P\big)\hat{\delta}P\right)\mathrm{d}v, \tag{3c}$$

and the divergence theorem,

$$\int_v \frac{\partial}{\partial x}\big(D_{44}\nabla_x P\hat{\delta}P\big)\,\mathrm{d}v = \int_{s_3}\big(D_{44}\boldsymbol{n}\cdot\nabla_x P\hat{\delta}P\big)\,\mathrm{d}S_3, \tag{4a}$$

$$\int_v \frac{\partial}{\partial y}\big(D_{44}\nabla_y P\hat{\delta}P\big)\,\mathrm{d}v = \int_{s_2}\big(D_{44}\boldsymbol{n}\cdot\nabla_y P\hat{\delta}P\big)\,\mathrm{d}S_2, \tag{4b}$$

$$\int_v \frac{\partial}{\partial z}\big(D_{11}\nabla_z P\hat{\delta}P\big)\,\mathrm{d}v = \int_{s_1}\big(D_{11}\boldsymbol{n}\cdot\nabla_z P\hat{\delta}P\big)\,\mathrm{d}S_1, \tag{4c}$$

the following variation equation can be easily obtained from Eq. (2),

$$\begin{aligned}\hat{\delta}\Phi = \int_v \Big[& A(T-T_{c\infty})P + BP^3 + CP^5 \\ & - D_{44}\big(\nabla_x^2+\nabla_y^2\big)P - D_{11}\nabla_z^2 P\Big]\hat{\delta}P\,\mathrm{d}v \\ & + \int_{s_1} D_{11}\big(\nabla_z + \delta_3^{-1}\big)P\hat{\delta}P\,\mathrm{d}x\,\mathrm{d}y \\ & + \int_{s_2} D_{44}\big(\nabla_y + \delta_1^{-1}\big)P\hat{\delta}P\,\mathrm{d}x\,\mathrm{d}z \\ & + \int_{s_3} D_{44}\big(\nabla_x + \delta_1^{-1}\big)P\hat{\delta}P\,\mathrm{d}z\,\mathrm{d}y. \end{aligned} \tag{5}$$

Therefore, from Eq. (5), the condition of free energy equilibrium can be written as

$$D_{44}\left(\nabla_x^2+\nabla_y^2\right)P+D_{11}\nabla_z^2P=AP+BP^3+CP^5, \tag{6}$$

with the corresponding boundary conditions

$$\left(\nabla_i\pm\delta_i^{-1}\right)P\,|_{x_i=\pm a_i/2}=0 \quad (i=1,2,3). \tag{7}$$

Here $x_i=x$, y, z, and $a_i=a_0$, b_0, c_0. Eq. (6) is a three-dimensional equation. The exact kink solution of similar equations has only been discussed previously in a one-dimensional case [16]. An analytical solution of Eq. (6) can be obtained by the integral method with additional symmetric boundary conditions and will be discussed in a follow-up paper. For brevity, when the physical sizes of the cell become small enough, in the vicinity of the size-driven transition point, an approximate solution of Eq. (6) can be found from the ansatz

$$D_{44}\left(\nabla_x^2+\nabla_y^2\right)P+D_{11}\nabla_z^2P-\left(A+BP_0^2+CP_0^4\right)P\approx 0, \tag{8}$$

where P_0 is the polarization $P(0, 0, 0)$ at the coordinate origin in the finite system. Eq. (8) yields

$$P=P_0\cos(k_xx)\cos(k_yy)\cos(k_zz), \tag{9}$$

with

$$D_{44}\left(k_x^2+k_y^2\right)+D_{11}k_z^2=A+BP_0^2+CP_0^4. \tag{10}$$

Note that if the sizes of the system become large, Eq. (10) will degenerate into an ordinary Devonshire equation. Substitution of Eq. (9) into Eq. (7) leads to the following results,

$$k_i^1\tan\left(\tfrac{1}{2}k_i^1a_i\right)=1/\delta_i \quad \left(k_i^1=k_x^1,\ k_y^1,\ k_z^1\right). \tag{11}$$

In the present study we are mainly interested in the critical sizes of the cell at ambient temperatures, i.e., $T_c\ll T_{c0}$. By expanding $\tan(\frac{1}{2}k_i^1a_i)$ in Eq. (11) as a Taylor series and neglecting higher order terms of $k_i^1a_i$, the solution of Eq. (10) can be written as

$$P_0=\pm\left[-\frac{B}{2C}\left(1-\sqrt{1-\frac{4A_0C}{B^2}(T-T_c)}\right)\right]^{1/2}$$

(for the second order transition), (12a)

$$P_0=\pm\left[-\frac{B}{2C}\left(1+\sqrt{1-\frac{4A_0C}{B^2}(T-T_c)}\right)\right]^{1/2}$$

(for the first order transition), (12b)

where

$$T_c=T_{c0}-\left[\frac{2D_{44}}{A_0\delta_1}\left(\frac{1}{a_0}+\frac{1}{b_0}\right)+\frac{2D_{11}}{A_0c_0\delta_3}\right]. \tag{13}$$

Eq. (13) determines the critical temperature of a size-driven phase transition in the case of a second order phase transition. For the situation of the first order phase transition, the critical temperature of the size-driven phase transition can be approximately written as

$$T_c^*=T_{c0}+\frac{3B^2}{16A_0C}-\left[\frac{2D_{44}}{A_0\delta_1}\left(\frac{1}{a_0}+\frac{1}{b_0}\right)+\frac{2D_{11}}{A_0c_0\delta_3}\right]. \tag{14}$$

Eqs. (13) and (14) present a restriction which can determine characteristic sizes of the cell. Fig. 1 shows the Curie temperature dependence of lateral critical size corresponding to different thicknesses. For convenience, here we take $\delta=\delta_i$ and $a_0=b_0$. It can be seen that the lateral critical size a_0 decreases with an increase in the thicknesses. Obviously, a physically sensible indication here is that the lateral size effect is cooperatively associated with the thickness of the system. Fig. 2 exhibits an overall profile between the size driven transition temperature and the cell's spatial dimensions and sizes. The interesting aspect in Fig. 2 is that a decrease in the thickness of the cell causes an increase in the critical size of

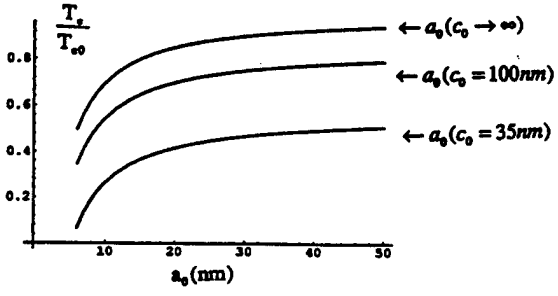

Fig. 1. T_c dependence of lateral sizes for several different thicknesses.

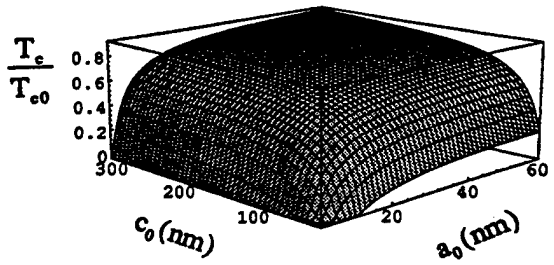

Fig. 2. Transverse sizes and thickness as a function of the normalized transition point.

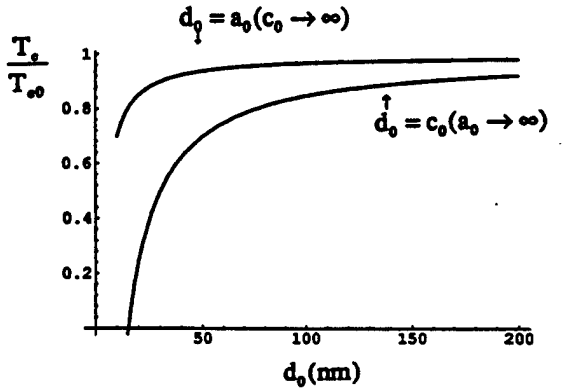

Fig. 3. T_c versus the minimum critical thickness and width.

the lateral dimensions, *and vice versa*. Clearly, the lateral dimension has a minimum critical size as the thickness of the cell becomes very large. Below such a minimum critical size, the confined system becomes a one-dimensional (1-D) system, corresponding to an ultra-thin ferroelectric fiber in reality. Similarly, in another extreme case, when the lateral dimensions become quite large, the critical thickness also approaches its minimum value. It is important to mention that when the thickness of the confined system reaches its minimum critical value, the critical sizes in the transverse dimensions must become infinitely large. In such a case, the system is believed to be a true two-dimensional (2-D) layer in the sense that the crossover of ferroelectric condensation reached is associated with a reduction in its thickness. In some sense, this situation is quite similar to the asymptotic case described by the Kosterlitz–Thouless theory [17]. The minimum values of critical sizes along different orientations can be estimated by the following. By letting $a_0 \to \infty$ in Eq. (14), the critical thickness of c_0 is obtained in a range of 10–15 nm at the room temperature. Whereas by setting $c_0 \to \infty$, the critical value of a_0 will be close to a range of 2–3 nm. Evidently, the characteristic sizes of the cell are anisotropic in character. The anisotropic characteristics of minimum critical sizes are plotted in Fig. 3. The case of $c_0 \to \infty$ in Fig. 3 describes the critical size a_0 changing as a function of T_c in a 3-D to 1-D phase transition. The behaviour of c_0 in the system with $a_0 \to \infty$ illustrates the features in a 3-D to 2-D phase transition. All the free energy coefficients of $BaTiO_3$ used for the numerical calculation are listed in Table 1.

Next, let us discuss a 3-D to 0-D phase transition to assess the sizes of a ferroelectric cell with ultra-small area and thickness. In this situation, both c_0 and a_0 are finite and are always larger than their minimum critical sizes as discussed above. Quantitatively, if the thickness of c_0 is taken as 40 nm, from Eq. (14), the critical value of a_0 will be on the scale of 5–6 nm. This result agrees well with recent experimental results [20]. In addition, the estimation offered also provides a verification that ferroelectrics have a potential as high density memories ($>$ Gbits/in^2) as well.

Essentially, the fundamental reason for this physical effect resides in that the characteristic sizes in different crystallographic orientations are uniquely determined by the interfacial environment as a whole. Several points should be emphasized here: (1) In a 3-D to 0-D transition, the characteristic sizes are constrained by one another, resulting in a critical

Table 1
Parameters of the free energy expression for $BaTiO_3$ at room temperature (c.g.s units unless specified)

A_0	B	C	D_{11} (cm)^2	D_{44} (cm)^2	δ (cm)
5.6×10^{-4} [a] [18]	-1.7×10^{-13} [19]	3.8×10^{-23} [19]	5×10^{-15}	5×10^{-16} [18]	1×10^{-7}

[a] In fact, the elastic and electrostriction contributions to the coefficients A and B become quite large when $T_c \ll T_{c0}$ and the corresponding corrections have to be considered [14,15,18,21].

volume over which dipoles can be strongly correlated. Such a minimum critical volume V_0 can be approximately obtained from Eq. (14) with the help of $V_0 = c_0 a_0^2$, giving rise to a correlation volume on the order of magnitude of 1000 nm^3. Note that the estimation of dipole correlation volume offered is roughly an order of magnitude larger than the expected correlation volume of electric dipole fluctuation in an infinite medium near the Curie range [13]. This can be understood by considering the possibility of a large surface effect (2). One way to quantify the validity of Eq. (14) is to compare with experimental results. It is encouraging to find that the size dependence of the transition temperature T_c in Eq. (10) agrees reasonably well with the empirical relations obtained by Ishikawa et al. [1].

As a final remark, it should be mentioned that both the gradient coefficients D_{jj} and the extrapolation length δ_i are crucial for determining the critical sizes of a confined system. The gradient coefficients D_{jj} are a measure of the delocalized coupling strength of the dipoles, which is estimated to be about 10^{-15} to 10^{-16} cm^2 [21–23]. An accurate determination of D_{jj} can be carried out by experimental measurements [24]. On the other hand, δ_i is estimated to be about 1–10 (nm) for perovskite oxides [12]. In principle, the value of δ_i can be either positive or negative, depending upon the nature of the surface effect. When δ_i is positive, the polarization can be even enhanced as physical sizes of the system are reduced [3]. As a matter of fact, the phenomenological argument of surface effects discussed is similar to the one used to find critical fields of type II superconductors in the LG theory [8].

In conclusion, we have performed a mean-field study of the finite size effect on structural instability in a ferroelectric cell within the context of an anisotropic 3-D Landau–Ginzburg–Devonshire ϕ^6-model. We have for the first time evaluated the anisotropic critical sizes for a confined ferroelectric system, describing their implications for physical dimensionality of ferroelectrics.

We acknowledge Drs. D. Wolf, S. Phillpot, K. Merkle and C. Youngdahl for their encouragement and Dr. K.-S. Chan for useful discussions. S.L., J.A.E, Z.L. and C.M.F. thank for the financial support from the U.S. Department of Energy, Basic Energy Science-Division of Materials Science, under contract No. W-31-109-ENG-38. R.E. Newnham and L.E. Cross gratefully acknowledge the National Science Foundation which funded this study through a Materials Research Grant, Contract DMR 9223847.

References

[1] K. Ishikawa, K. Yoshokawa and N. Okada, Phys. Rev. B 37 (1988) 5852.
[2] R.E. Newnham and S.T. McKinstry, in: Ceramic transaction Vol. 32 (Am. Ceram. Soc., 1993).
[3] J.F. Scott et al., Physica B 150 (1988) 160.
[4] H. Ikawa, in: Ceramic transaction, Vol. 32 (Am. Ceram. Soc., 1993).
[5] I.P. Bartra, P. Wurfel and B.D. Silverman, Phys. Rev. Lett. 30 (1973) 384;
R. Kretschmer and K. Binder, Phys. Rev. B 20 (1979) 1065.
[6] D.R. Tilley, in: Ferroelectric ceramics, eds. N. Setter and E.L. Colla (Birkhäuser, Basel, 1993) p. 163;
D.L. Mills, Phys Rev. B 3 (1971) 3887;
K. Binder and P.C. Hohenberg, Phys. Rev. B 6 (1972) 3461.
[7] J.F. Scott, Phys. World 8 (1995) 46.
[8] D.R. Tilley and B. Zeks, Solid State Commun. 49 (1984) 823;
W. Zhong et al., Phys. Rev. B 50 (1994) 12375.
[9] M.G. Cottam, D.R. Tilley and B. Zeks, J. Phys. C 17 (1984) 1793;
B. Qu, W. Zhong and P. Zhong, Phys. Rev. B 52 (1995) 766.
[10] K. Binder, Ferroelectrics 35 (1981) 99.
[11] Y.G. Wang, W.L. Zhong and P.L. Zhang, Phys. Rev. B 51 (1995) 17235.
[12] W.L. Zhong et al., Phys. Rev. B 50 (1994) 689.
[13] S.H. Wemple, Phys. Rev. B 2 (1970) 2679; Phys. Rev. 180 (1969) 547.
[14] A.F. Devonshire, Philos. Mag. 40 (1949) 1040; 42 (1951) 1065.
[15] W. Cao and L.E. Cross, Phys. Rev. B 44 (1991) 5.
[16] F. Falk, Z. Phys. B 51 (1983) 177;
T.C. Lubensky and M.H. Rubin, Phys. Rev. B 3 (1975) 3885;
M.I. Kaganov and A.N. Omelyanchouk, Sov. Phys. JETP 34 (1972) 895.
[17] A. Chowdhury, B.J. Ackerson and N.A. Clark, Phys. Rev. Lett. 55 (1985) 833.
[18] V.A. Zhirnov, Sov. Phys. JETP 35 (1959) 822.
[19] W.J. Merz, Phys. Rev. 91 (1953) 513.
[20] S. Schlag and H.-F. Ericke, Solid State Commun. 91 (1994) 883.
[21] D.G. Sannikov, Sov. Phys. JETP 14 (1962) 98;
J.F. Scott and B. Pouligny, J. Appl. Phys. 63 (1988) 1547.
[22] V.L. Ginzburg, Sov. Phys. Solid State 2 (1961) 1824.
[23] T. Mitsui and J. Furuich, Phys. Rev. 90 (1953) 193.
[24] P. Hong and G.B. Olson, Solid State Commun. 85 (1993) 681.

APPENDIX 4

Jpn. J. Appl. Phys. Vol. 35 (1996) pp. L 502–L 504
Part 2, No. 4B, 15 April 1996

Susceptibility of Nanostructured Ferroelectrics

Shaoping LI, J. A. EASTMAN, R. E. NEWNHAM[1] and L. E. CROSS[1]

Materials Science Division, Argonne National Laboratory, 9700 South Cass Ave, Argonne, IL 60439, U.S.A
[1]*Materials Research Laboratory, Pennsylvania State University, University Park, PA16802, U.S.A*

(Received February 29, 1996; accepted for publication March 18, 1996)

The onset of long-range order in the size-driven ferroelectric phase transition has been discussed extensively by use of mean field theory in the literature. In order to prevent erroneous analysis of the dielectric permitivity of nanometric sized ferroelectrics, we present a pertinent description of the dielectric susceptibility of nanostructured ferroelectrics within the context of Landau-Ginzburg theory. Consequently, we also discuss the influence of size on the dielectric permittivity of thin films and relevant implications.

KEYWORDS: dielectric permittivity, ferroelectric phase transition, thin films

The technological advances in materials synthesizing process have led to the realization of ferroelectric systems confined in reduced dimensional structures. These nanostructured systems, by virtue of their high dielectric permittivity and reduced physical dimensions, have important implication for many advanced applications. In recent years a number of studies on nanostructured ferroelectrics have been carried out extensively. Theoretically, the mean field theory has been widely employed to study the size effect on nanostructred ferroelectrics.[1–20] However, there exist some insufficiencies in the recent theoretical analysis of nanostructured ferroelectrics.

In this letter, starting from a simple but clean model, we discuss the dielectric susceptibility of ferroelectric thin films in detail. Following the expression of the free energy from Tilley and Zeks,[1] we now consider a $O_h - C_{4v}$ proper ferroelectric phase transition in a thin film case. The free energy of a ferroelectric thin film with the thickness L can be written as,

$$F = S\int_{-\frac{L}{2}}^{\frac{L}{2}} \left\{ \Phi_0 + \frac{1}{2}AP^2 + \frac{1}{4}BP^4 + \frac{1}{6}CP^6 + \frac{D_{11}}{2}\left(\frac{\mathrm{d}P}{\mathrm{d}z}\right)^2 \right\} \mathrm{d}z + \int \frac{D_{11}}{2d} P^2 \mathrm{d}S \tag{1'}$$

or

$$\Phi = \frac{F}{S} = \int_{-\frac{L}{2}}^{\frac{L}{2}} \left\{ \Phi_0 + \frac{1}{2}AP^2 + \frac{1}{4}BP^4 + \frac{1}{6}CP^6 + \frac{D_{11}}{2}\left(\frac{\mathrm{d}P}{\mathrm{d}z}\right)^2 + \frac{D_{11}P^2}{2d}\delta\left(z \pm \frac{L}{2}\right) \right\} \mathrm{d}z \tag{1''}$$

where S is the surface area of the film with plane surface at $z = \pm L/2$; $\delta(z)$ is the delta function; and d is the extrapolation length and measures the strength of the surface effect.[1] $A = A_0(T - T_c)$, B, and C are normalized free energy coefficients, in which elastic coefficients and other relevent coupling parameters are tacitly included. T_c is the bulk Curie tempreature. D_{11} is the gradient term, describing the polarization inhomogeneity. The order parameter is the polarization P, which is oriented along the z-axis, i.e., $P = \{0, 0, P(x, y, z)\}$. If considering an external electric field E_{ext}, according to Lubensky and Rubin,[21,22] eq. (1) becomes,

$$\Phi = \int_{-\frac{L}{2}}^{\frac{L}{2}} \left\{ \Phi_0 + \frac{1}{2}AP^2 + \frac{1}{4}BP^4 + \frac{1}{6}CP^6 + \frac{D_{11}}{2}\left(\frac{\mathrm{d}P}{\mathrm{d}z}\right)^2 + \frac{D_{11}P^2}{2d}\delta\left(z \pm \frac{L}{2}\right) - E_{ext}P - E'_{ext}P\delta\left(z \pm \frac{L}{2}\right) \right\} \mathrm{d}z. \tag{2}$$

Varying total free energy of eq. (2) with respect to P, we can obtain a variation equation,

$$\hat{\delta}\Phi = \int_{-\frac{L}{2}}^{\frac{L}{2}} \left\{ \left(AP + BP^3 + CP^5 + \frac{D_{11}P}{d}\delta\left(z \pm \frac{L}{2}\right) - E_{ext} - E'_{ext}\delta\left[z \pm \frac{L}{2}\right] \right) \hat{\delta}P + D_{11}\left(\frac{\mathrm{d}P}{\mathrm{d}z}\right)\hat{\delta}\left(\frac{\mathrm{d}P}{\mathrm{d}z}\right) \right\} \mathrm{d}z. \tag{3}$$

With the help of the integral formula,

$$\int_{-\frac{L}{2}}^{\frac{L}{2}} \left\{ D_{11}\left(\frac{\mathrm{d}P}{\mathrm{d}z}\right)\hat{\delta}\left(\frac{\mathrm{d}P}{\mathrm{d}z}\right) \right\} \mathrm{d}z = D_{11}\left(\frac{\mathrm{d}P}{\mathrm{d}z}\right)\hat{\delta}P\Big|_{-\frac{L}{2}}^{\frac{L}{2}} - \int_{-\frac{L}{2}}^{\frac{L}{2}} \left\{ D_{11}\left(\frac{\mathrm{d}^2P}{\mathrm{d}z^2}\right)\hat{\delta}P \right\} \mathrm{d}z, \tag{4}$$

eq. (3) gives

$$\hat{\delta}\Phi = \int_{-\frac{L}{2}}^{\frac{L}{2}} \left\{ -D_{11}\left(\frac{\mathrm{d}^2P}{\mathrm{d}z^2}\right) AP + BP^3 + CP^5 - E_{ext} \right\} \hat{\delta}P\mathrm{d}z + \int_{-\frac{L}{2}}^{\frac{L}{2}} \left\{ \pm D_{11}\left(\frac{\mathrm{d}P}{\mathrm{d}z}\right) + \frac{D_{11}P}{d} - E'_{ext} \right\} \delta\left(z \pm \frac{L}{2}\right)\hat{\delta}P\mathrm{d}z. \tag{5}$$

By assuming $E_{ext}(x) = E_{ext}$ to be uniform, the Euler-Lagrange equation resulting from eq. (3) has a form,

$$D_{11}\frac{\mathrm{d}^2P}{\mathrm{d}z^2} = AP + BP^3 + CP^5 - E_{ext} \tag{6}$$

with the corresponding boundary conditions

$$\left[\pm D_{11}\frac{\partial P}{\partial z}+\left(D_{11}\frac{P}{d}\right)\right]\Big|_{z=\pm\frac{L}{2}}=E'_{\rm ext}. \tag{7}$$

Strictly speaking, the susceptibility of ferroelectrics is defined as the ratio between the polarization and external field in the case of very small measurement signal, i.e.,

$$\chi=\left.\frac{\partial P}{\partial E_{\rm ext}}\right|_{E_{\rm ext}\to 0}. \tag{8}$$

Therefore, for a small signal case, the average inverse susceptibility of a nanometric thin film should be written as

$$\langle\chi^{-1}\rangle=\frac{1}{L}\frac{\partial^2\Phi}{\partial P^2}=\frac{1}{L}\int_{-\frac{L}{2}}^{\frac{L}{2}}\left\{A+BP^3+CP^5+\left(\frac{D_{11}}{d}\right)\delta\left(z\pm\frac{L}{2}\right)\right\}{\rm d}z. \tag{9}$$

The identity equation

$$\int\left\{D_{11}\partial^2\left(\frac{{\rm d}P}{{\rm d}z}\right)^2\Big/\partial P^2\right\}{\rm d}z\equiv 0 \tag{10}$$

is used for derivation of eq. (9). In fact, the average inverse susceptibility of $\langle\chi^{-1}\rangle$ in eq. (9) represents

$$\langle\chi^{-1}\rangle=\frac{1}{L}\int_{-\frac{L}{2}}^{\frac{L}{2}}\left(\frac{1}{\chi}+\frac{1}{\chi'}\delta\left(z\pm\frac{L}{2}\right)\right)\Big|_{E_{\rm ext}\to 0}{\rm d}z. \tag{11}$$

Equation (11) is a generalization of the bulk and surface susceptibilities introduced by Binder[17,23] and Lubensky.[21] According to the definition of eq. (8), the small signal case describes the case in which external field approaches zero, *e.g.*, $E_{\rm ext}\to 0$. Thus eqs. (6) and (7) yield,

$$D_{11}\frac{{\rm d}^2P}{{\rm d}z^2}=AP+BP^3+CP^5 \tag{12'}$$

and

$$\left.\pm\frac{\partial P}{\partial z}\right|_{z=\pm\frac{L}{2}}+\frac{P}{d}=0. \tag{12''}$$

An analytical kink solution of eq. (12) can be obtained exactly,[24] it is, however, quite cumbersome. For simplicity, an approximate solution of eq. (12) can be found from the Ansatz,

$$D_{11}\frac{{\rm d}^2P}{{\rm d}z^2}\approx(A+BP_0^2+CP_0^4)P \tag{13'}$$

$$\left.\pm\frac{\partial P}{\partial z}\right|_{z=\pm\frac{L}{2}}+\frac{P}{d}=0. \tag{13''}$$

where P_0 is the polarization $P(0, 0, 0)$ at the coordinate origin. Equations (13) give,

$$P=P_0\cos(kz) \tag{14}$$

where

$$P_0=\pm\left\{-\frac{B}{2C}\left[1-\sqrt{1-\frac{4A_0C}{B^2}(T-T^*)}\right]\right\}^{1/2} \quad \text{(for the second order transition)} \tag{15}$$

$$P_0=\pm\left\{-\frac{B}{2C}\left[1+\sqrt{1-\frac{4A_0C}{B^2}(T-T^*)}\right]\right\}^{1/2} \quad \text{(for the first order transition)} \tag{16}$$

$$T^*=T_{\rm c}-\frac{D_{11}}{A_0dL} \tag{17}$$

and

$$k\tan\left[\frac{kL}{2}\right]=\frac{1}{d}. \tag{18}$$

Note that the validity of the approximation and solution of eqs. (13) can be verified by directly integrating eqs. (12) with additional symmetric boundary conditions ${\rm d}P/{\rm d}z\to 0$ and $P\to P_0$ at $z\to 0$. Consequently, the shift of the Curie point can be expressed as,

$$T_1^*=T_{\rm c}+\frac{3B^2}{16A_0C}-\frac{D_{11}}{A_0dL} \quad \text{(for the first order phase transition)} \tag{19'}$$

and

$$T_2^*=T_{\rm c}-\frac{D_{11}}{A_0dL}. \quad \text{(for the second order phase transition)} \tag{19''}$$

When temperature is close to the range of size-driven phase transition, for the case of the second order phase transition, from eqs. (9) and (14), the average susceptibility of thin films can be written as,

$$\langle\chi^{-1}\rangle=A_0[T-T_2^*] \qquad T>T_2^*; \tag{20'}$$

$$\langle\chi^{-1}\rangle=-2A_0[T-T_2^*] \qquad T<T_2^*. \tag{20''}$$

Equations (20) represent the dielectric susceptibility of ferroelectric thin films within the scheme of Landau-

Ginzburg model. When the thickness of films L become very large, eqs. (20) degenerate into the expressions for describing the dielectric susceptibility of normal ferroelectrics.[25] It should be pointed out here that recently Wang and Smith have discussed the susceptibility of nanostructured ferroelectrics.[3] The susceptibility derived from eq. (5) in ref. 3 is a result of the specific solution (not a general solution[26]) of eq. (2) in ref. 3. This solution is not suitable for describing a small signal case. More concretely, the polarization and susceptibility derived from a specific solution of eq. (2) in ref. 3 is closely associated with an external field. They do not represent the polarization and susceptibility in the case of $E_{ext} \to 0$. In fact, in this solution, the polarization P would become zero as the external field is null. Thus the dielectric permittivity obtained there is not pertinent for describing a small signal case.

Several aspects should be addressed here. (i) Within the context of Landau-Ginzburg continuum model, the phase transition in thin films still shows Ising character. Although near the critical point of a ferroelectric, the dielectric susceptibility obtained from Landau theory could be modified by a logarithmic correction factor,[17] the significantly diffuse or smeared phase transition in thin films, which has been experimentally observed, should have some other physical implications. We believe that the broad phase transition character in thin films might be mainly attributed to the interactions at surfaces or interfaces of thin films. A possible explanation for this effect has been discussed recently by Li and Newnham.[27] (ii) The shift of the Curie point in eqs. (19) strongly enhance the influence of elastic and electrostriction on the size-driven phase transition. In the Devonshire theory, the Curie constant for normal perovsike oxides, such as $BaTiO_3$, is in the range of 10^5 K, giving rise to a large dielectric peak near the original phase transition point. However, from eqs. (19), it can be seen that there is a significant shift of the Curie point when the thickness of thin films is small. In most of intrinsic perovskite ferroelectrics, as a matter of fact, the thermodynamic parameters are largely related to the elastic and electrostrictive interaction. Since the elastic coefficients are associated with temperature, hence, the shift of the Curie temperature will change the magnitude of A_0 drastically. By considering the elastic interactions, according to the Devonshire theory, the Curie constant in eqs. (20) can be lowered in a range of 10^3–10^4 K when temperature is far away from the original Curie point.[28] Clearly, this effect explains the reason why near the transition temperature the experimentally obtained susceptibility of nanostructured ferroelectrics is much lower than that of bulk materials. (iii) In this paper we have only discussed the situation for thin films. For the case of nanometeric sized ferroelectric particles, the anisotropic polarization correlation has to be considered. Essentially ferroelectrics are anisotropic media. The correlation forces of polarization in ferroelectrics are anisotropic in nature. We have discussed the finite size effect on ferroelectrics using a three dimensional Landau-Ginzburg ϕ^6-model in a separate paper.[8]

S. Li and J. A. Eastman thank the financial support from the U.S. Department of Energy, Basic Energy Science-Materials Science, under contract No. W-31-109-ENG-38. R. E. Newnham and L. E. Cross gratefully acknowledge the National Science Foundation which funded this study through a Materials Research Grant, Contract DMR 9223847.

1) D. R. Tilley and B. Zeks: Solid State Commun. **49** (1984) 823.
2) D. R. Tilley: *Ferroelectric Ceramics*, eds. N. Setter and E. L. Colla (Birkhaus, Basel, 1993) p. 163.
3) C. L. Wang and S. R. Smith: J. Phys. Condens. Matter **7** (1995) 7163.
4) W. L. Zhong, Y. G. Wang, P. L. Zhang: Phys. Lett. **189A** (1994) 121.
5) Y. G. Wang, W. L. Zhong and P. L. Zhang: Phys. Rev. B. **51** (1995) 17235.
6) Y. G. Wang, W. L. Zhong and P. L. Zhang: Solid State Commun. **92** (1994) 519.
7) W. L. Zhong, Y. G. Wang, P. L. Zhang and B. D. Qu: Phys. Rev. B **50** (1994) 689.
8) S. Li, *et al.*: to be published Physics Lett. A (1996).
9) C. L. Wang, W. L. Zhong and P. L. Zhang: J. Phys. Cond. Matt. **3** (1992) 4743; B. Qu, W. Zhong, P. Zhang: Phys. Rev. B **52** (1995) 766.
10) B. Qu, W. Zhong and P. Zhang: Jpn. J. Appl. Phys. **34** (1995) 4114.
11) C. L. Wang, S. Smith and D. R. Tilley: J. Phys. Condens. Matter **6** (1994) 9633.
12) D. Schwenk, F. Fishman and F. Schwabl: J. Phys. Condens. Matter **2** (1990) 5400; Ferroelectrics **104** (1990) 349, and Phys. Rev. B **38** (1988) 11618.
13) J. F. Scott, *et al.*: Physica B **150** (1988) 160.
14) F. Agnilera-Granja and J. L. Moran Lopez: Solid State Commun. **74** (1990) 155.
15) I. P. Bartra, P. Wurfel and B. D. Silverman: Phys. Rev. Lett. **30** (1973) 384; Phys. Rev. B **8** (1973) 3257, and P. Wurtel and I. P. Batra: Ferroelectrics **12** (1976) 55.
16) K. Binder: Ferroelectrics **35** (1981) 99; Ferroelectrics **73** (1987) 43.
17) R. Kretschmer and K. Binder: Phys. Rev. B **20** (1979) 1065.
18) M. G. Cottam, D. R. Tilley and B. Zeks: J. Phys. C **17** (1984) 1793.
19) H. K. Sy: J. Phys. Condens. Matter **5** (1993) 1213.
20) D. R. Tilley: Solid State Commun. **65** (1988) 657.
21) T. C. Lubensky and M. H. Rubin: Phys. Rev. B **12** (1975) 3885.
22) D. L. Mills: Phys. Rev. B **3** (1971) 3887; and R. Wang and D. L. Mills: Phys. Rev. B **18** (1992) 11681.
23) K. Binder and P. C. Hohenberg: Phys. Rev. B **6** (1972) 3461; **9** (1974) 2194.
24) F. Falk: Z. Phys. B **51** (1983) 177.
25) T. Mitsui, I. Tatsuzaki and E. Nakamura: *An Introduction to the Physics of Ferroelectrics* (Gordon & Breach New York, 1976).
26) Under the influence of an external field, a general solution of the polarization and relevant susceptibility in ferroelectric films have been discussed in detail in ref. 17.
27) S. Li and R. E. Newnham: to be published.
28) V. A. Zhirnov: Sov. Phys. JETP **35** (1959) 822.

APPENDIX 5

CRYSTAL CHEMISTRY AND CRYSTAL PHYSICS

R. E. Newnham
Intercollege Materials Research Laboratory
The Pennsylvania State University
University Park, PA 16802, USA

ABSTRACT

In relating physical properties to crystal structure, microstructure, and composite design, courses in crystal chemistry and crystal physics provide an interesting alternative to the usual solid state physics and materials science courses. Large-scale crystal models constructed by the students offer an intuitive understanding of phenomena as diverse as cleavage, corrosion, elasticity, and thermal conductivity, making it possible to establish correlations with bondlengths, bond strengths, polyhedral connectivities, and surface structures. The tensor and matrix methods introduced in crystal physics provide a mathematical formalism applicable to nearly all anisotropic properties, and help in visualizing the variation in tensor coefficients with direction. The usual 32 crystallographic point groups used in applying Neumann's Principle can be augmented with planar groups for surface properties, continuous groups for liquid crystals and textured solids, color groups for composite media, and black-and-white groups for magnetic materials.

INTRODUCTION

As a teenager, I read the Mr. Tompkins books written by physicist George Gamow. Mr. Tompkins was a magic man who could change size in accordance with his thoughts. When thinking about the universe, he grew to immense size so that he could examine the planets and stars at close range, and when he took up the study of fundamental particles, he shrank to nuclear dimensions. In the book on human anatomy, Mr. Tompkins recorded his observations when riding around the body on a red blood corpuscle.

These thoughts often return to me when I teach our introductory courses on crystal chemistry and crystal physics. Having thought about crystals, ceramics and their properties, for many years, I often look at the structure models in my office and dream about being 1 Å tall. I walk around inside the crystals, hop across grain boundaries and domain walls, and push on the atomic bonds. These thought processes and emotional feelings I try to transmit to my students, along with some scientific ideas and technological goals. Some of my students fall in love with materials, just as I have.

The modus operandi of materials research and development programs is to seek fundamental understanding while working toward an engineering goal and remaining alert for new applications. One of the best ways of introducing this line of thinking is to develop an understanding of structure-property relationships through basic crystal chemistry and crystal physics (1). For many problems of interest to ceramists and materials engineers, it is helpful to ask:

What are the atoms involved and how are they arranged?
How does this arrangement lead to certain mechanisms of electronic or atomic motion?

How do these mechanisms give rise to the observed properties?
How are these properties represented in equation form?
How does symmetry modify the coefficients appearing in these equations?
What controls the magnitudes of the coefficients? Are there useful trends and "Rules of Thumb"?
Based on these structure-property relationships, when are exceptionally outstanding properties likely to develop?
What good are they? How can engineers use these ideas?

CRYSTAL CHEMISTRY

In teaching crystal chemistry to Penn State juniors, our course objectives are as follows:

- To become familiar with the raw materials used to make engineering materials. Mineral names and formulae .
- To study the atomic structure of crystalline and noncrystalline engineering materials. Atomic models of ceramics, metals and polymers.
- To learn the systematics of crystal chemistry: bond lengths, bond strengths, atomic coordination, crystal symmetry.
- To investigate structure property relationships. The correlations with electrical, thermal, chemical, mechanical, optical and magnetic properties.
- To appreciate the engineering significance of these ideas to commercial products.

The best way of visualizing the atomic structures of ceramics and glasses is to build models. It is easy to see why MgO has a much higher melting point than PbO when looking at the models. It is easy to see why graphite is a good lubricant, why clay and water interact so readily, and why barium titanate spontaneously polarizes.

Table 1 lists the models we build in our introductory crystal chemistry course. Thirty hours of model building are accompanied by informal discussion of atomic coordination, chemical bonding, crystallographic symmetry, and structure-property relationships. Raw material specimens and ceramic products are circulated among the students to emphasize the usefulness of the materials being modeled.

The first four laboratory sessions are devoted to basic structures illustrating the five principal types of chemical bonding, and after that we do some fairly sophisticated model building. It is important to move beyond the more elementary rocksalt, diamond, and metal structures. Many of our students have seen these structures several times in introductory courses in chemistry, physics, and materials science, as well as in high school courses. They appreciate the challenge of the cordierite, spinel, kaolinite and feldspar structures, along with the more free-form glass structures.

In building the models, I use the Orbit and Minit Molecular Building Systems utilizing flexible plastic straws and connectors. The Group Sets for Lattices have a large selection of different types of connectors and straw lengths. The kits can be ordered from Cochranes of Oxford, Ltd., Leafield, Oxford, England OX8 5NT.

Table I. Crystal structures assembled in introductory crystal chemistry.

Ionic Solids:	Halite and Fluorite
Covalent Crystals:	Diamond. Zincblende. Wurtzite
Metals:	Copper (FCC). Iron (BCC), Magnesium (HCP)
Molecular Solids:	Ice and Polyethylene
Simple Oxides:	Rutile and Alumina
Silicate Classification:	0-, 1-, 2-. 3-D Silicates and Silicate Glass
Silica Polymorphs	Quartz, Cristobalite, Tridymites
Modified Silicates:	Soda-silica Glass and Soda Feldspar
Aluminosilicates:	Mullite and Cordierite
Layer Silicates:	Kaolinite. Talc and Mica
Electroceramics:	Perovskite and Ferrites
Raw Materials:	Calcite, Borax. Litharge
Non-oxide Ceramics:	Silicon Nitride, Graphite
Defects:	Edge and Screw Dislocations, Grain Boundaries

Discussions of anisotropy develop naturally from crystal models. The structures of graphite and hexagonal boron nitride (Fig. 1) are especially instructive. Thermal conductivity coefficients are about four times larger parallel to the layers than in the perpendicular direction. This structure-property relationship can be further amplified with discussions of the correlations between thermal conductivity and chemical bonding, and with bondlength.

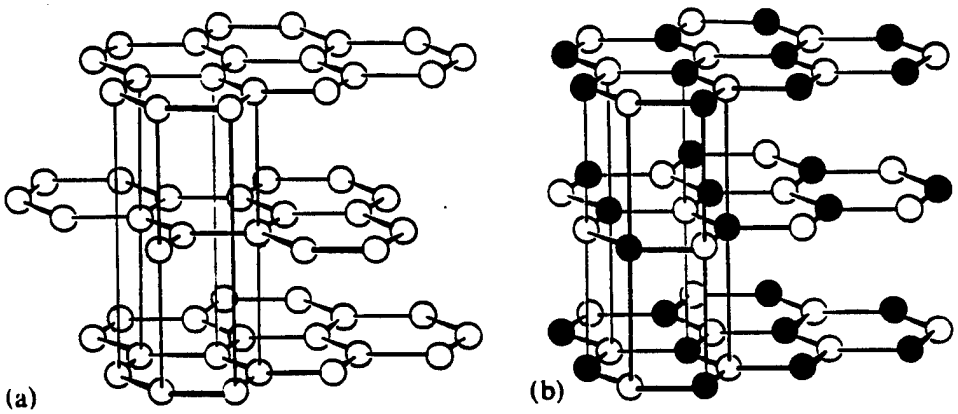

Fig. 1 Crystal structures of (a) graphite and (b) boron nitride. Both are layer structures with highly anisotropic physical properties. The stacking of the layers is slightly different in the two structures.

"Rules-of-Thumb" help put students in touch with reality since most involve properties of practical importance. They provide the physical and chemical intuition required for back of the envelope calculations. and for rapid recall at technical meetings. Table 3 lists 30 of the rules described in our introductory crystal chemistry and crystal physics. Common sense ideas like these also provide a way of facilitating discussion of more theoretical concepts.

Table 2. Empirical rules-of-thumb of importance in materials science and engineering (2).

1. Abrahams-Kurtz' relation for ferroelectric phase transitions.
2. Arrhenius' rule relating chemical reaction rate and temperature.
3. Berezin-Yvatkin's rule between ionic conductivity and lattice parameters.
4. Boyer-Beaman's relation between glass transition temperature and melting point.
5. Carnelly's rule for melting points and thermal expansion coefficient.
6. Do-Yen-Chen's equation relating critical temperature to melting and boiling points.
7. Dulong-Petit's values for high temperature specific heat.
8. Eberhart's formulae for surface tension of metals and their oxides.
9. Fine-Brown-Marcus' rules relating elastic stiffness and melting point.
10. Friedrich-Mayer's relationships for electronic conductivity of oxides.
11. Goldschmidt's rules for atomic coordination changes at high temperature and pressure.
12. Gorecki's formulae for Young's modulus, bulk modulus and shear modulus.
13. Hagg's critical radius ratio for interstitial alloys.
14. Hopper's rules for electron velocities in solids.
15. Hume-Rothery and Brewer predictions for metallic structures and solid solutions.
16. Kapellos-Maurides' rules for estimating electronegativity values.
17. Kern's rules for thermal conductivity of liquid mixtures and solutions.
18. Keyes' relation between elastic stiffness and lattice parameter.
19. Kummler's relation between dielectric constant, refractive index and molecular dipole moment.
20. Linde's and Matthiessen's rules for electrical conductivity of alloys.
21. Longinescu's relation between melting point and molecular weight for organic solids.
22. Matthias' rules for superconducting metals and alloys.
23. Mooser-Pearson's and Pamplin's rules for predicting new semiconductors.
24. Moss' and Ravindra-Srivastava's rules for refractive indices and band gaps.

Table 3. Empirical rules-of-thumb of importance in materials science and engineering (2).

1. Abrahams-Kurtz' relation for ferroelectric phase transitions.
2. Arrhenius' rule relating chemical reaction rate and temperature.
3. Berezin-Yvatkin's rule between ionic conductivity and lattice parameters.
4. Boyer-Beaman's relation between glass transition temperature and melting point.
5. Carnelly's rule for melting points and thermal expansion coefficient.
6. Do-Yen-Chen's equation relating critical temperature to melting and boiling points.
7. Dulong-Petit's values for high temperature specific heat.
8. Eberhart's formulae for surface tension of metals and their oxides.
9. Fine-Brown-Marcus' rules relating elastic stiffness and melting point.
10. Friedrich-Mayer's relationships for electronic conductivity of oxides.
11. Goldschmidt's rules for atomic coordination changes at high temperature and pressure.
12. Gorecki's formulae for Young's modulus. bulk modulus and shear modulus.
13. Hagg's critical radius ratio for interstitial alloys.
14. Hopper's rules for electron velocities in solids.
15. Hume-Rothery and Brewer predictions for metallic structures and solid solutions.
16. Kapellos-Maurides' rules for estimating electronegativity values.
17. Kern's rules for thermal conductivity of liquid mixtures and solutions.
18. Keyes' relation between elastic stiffness and lattice parameter.
19. Kummler's relation between dielectric constant. refractive index and molecular dipole moment.
20. Linde's and Matthiessen's rules for electrical conductivity of alloys.
21. Longinescu's relation between melting point and molecular weight for organic solids.
22. Matthias' rules for superconducting metals and alloys.
23. Mooser-Pearson's and Pamplin's rules for predicting new semiconductors.
24. Moss' and Ravindra-Srivastava's rules for refractive indices and band gaps.

25. Mott's formula relating Mohs, Knoop and Vickers hardness values.

26. Nernst-Thompson's rule relating solubility and dielectric constant.

27. Pauling's and Meyer's rules for ionic coordination and crystal structures.

28. Pilling-Bedworth's predictions for oxidation resistance of metals.

29. Pugh's rules predicting brittle behavior from bulk modulus/shear modulus ratio.

30. Richard's relationship between heat of fusion and melting point.

31. Shewmon's and Tamman's rules for diffusion coefficients and annealing temperatures.

32. Snoek's limits relating magnetic permeability and frequency.

33. Stoneham's rules for wetting of liquid metals and oxide surfaces.

34. Trouton's formula for latent heat of evaporization and boiling point.

35. Wagner-Hauffe's rules governing oxidation rates of metals.

36. Weidemann-Franz's law relating the thermal and electrical conductivity of metals.

37. Zachariasen's rules for oxide glass formation and structure.

CRYSTAL PHYSICS

Forty years ago, as a student at Cambridge University, I attended the lectures on crystal physics given by W. A. Wooster. This course, together with others on crystallography, X-ray diffraction, crystal optics, and crystal chemistry formed the undergraduate tripos on crystallography.

Standard crystal physics deals with the tensor properties of solids, beginning with scalar properties like specific heat, and finishing with fourth-rank tensors like elasticity. The tensor and matrix mathematics, along with Neumann's Principle relating the property coefficients to symmetry, form a common theme which ties the course together, thus providing a useful framework for dealing with anisotropy in solids.

To augment the standard topics of pyroelectricity, permittivity, piezoelectricity, and elasticity, I usually introduce a number of transport properties, magnetic effects, acoustic and optical phenomena which bring in nonlinearity, time reversal operators, continuous groups, icosahedral symmetry, and color symmetry. There is a very large literature on modern crystal physics which is not adequately treated in the standard texts like J. F. Nye's "Physical Property of Crystals" (3). These ideas are not hard to grasp when treated pictorially, and help to introduce students to research topics of current interest.

As in crystal chemistry, I like to use a lot of models in the course. To represent the directional properties, I have a number of balsa wood models showing how property coefficients vary with direction.

In developing a good understanding of symmetry, it is important to be able to visualize mirror planes, rotation axes, and inversion centers in three dimensions. Combinations of these three symmetry elements make up the 32-point groups governing the physical properties of single crystals.

Geometric models help a lot in visualizing the point groups. The cut-out drawing in Fig. 2 is a scale model of an alumina crystal, point group $\bar{3}$ m. Cut-out models of all 32 crystal classes can be found in my book, "Classic Crystals" (4) written with Steven Markgraf. Each model is a scale replica of a real crystal with the correct dimensional ratios and interplanar angles. Miller indices on each face help the students identify the symmetry directions.

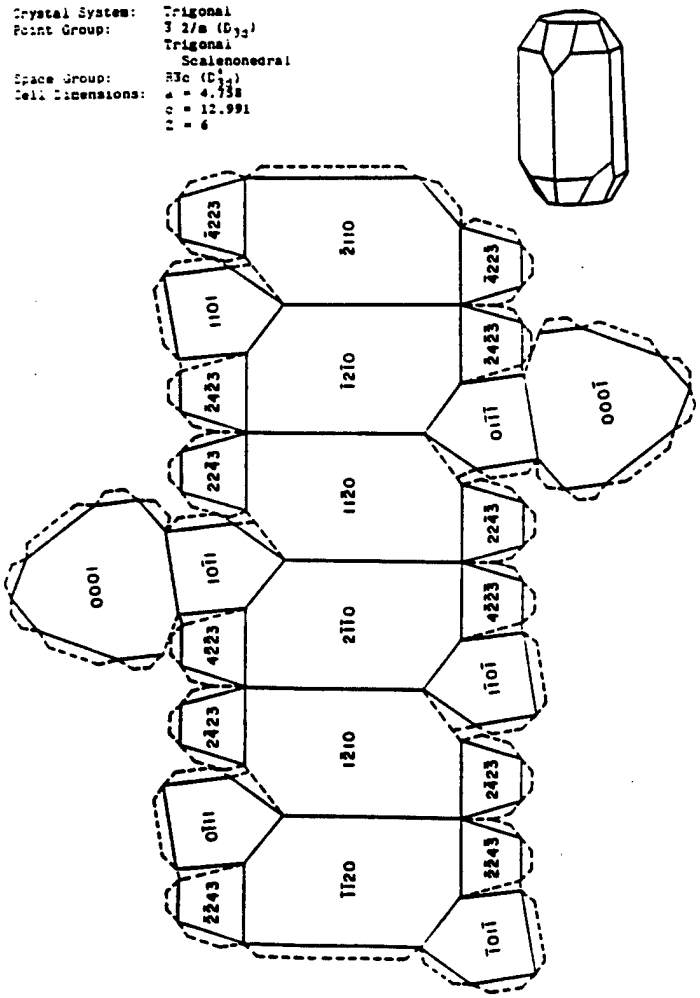

Fig. 2 Symmetry-related faces on a morphological model of sapphire. The models are constructed by folding along the dotted lines, cutting along solid lines, and applying glue to the tabs.

The concepts of crystal physics extend far beyond the geometries of single crystals. Of special interest to the study of polycrystalline solids, glasses, and liquids are the seven limiting groups, sometimes called the Curie groups. All contain ∞-fold rotation axes in which when rotated about the axis through any angle, brings the substance into a symmetry-equivalent position. Ceramic bodies with huge numbers of randomly oriented crystallites have spherical symmetry ∞∞m, while those processed by uniaxial hot-pressing generally have cylindrical texture, point group ∞/mm. Poled ferroelectric ceramics belong to conical group ∞m, magnetized ferrites to ∞/m m', optically active liquids to ∞∞, and cholestoric liquid crystals to ∞2. All homogeneous materials can be represented by a point group which governs the tensor properties and their matrix representations.

SUMMARY

Crystal chemistry and crystal physics courses are an excellent way of developing an understanding of the structure-property relationships underlying materials science and engineering. Three-dimensional models, along with hand specimens of minerals, crystals, ceramics, and finished products, help greatly in developing a real "feel" for the subject.

Crystal chemistry and crystal physics courses taught at the Pennsylvania State University are available on video-tape (5).

REFERENCES:

1. R. E. Newnham, "Structure-Property Relationships", Springer Verlag, Berlin, Germany (1975).

2. D. Fisher, "Rules of Thumb for Engineers and Scientists", Gulf Publishing Company, Houston, Texas (1991).

3. J. F. Nye, "Physical Properties of Crystals", Clarendon Press, Oxford, United Kingdom (1957).

4. R. E. Newnham and S. A. Markgraf, "Classic Crystals: A Book of Models", Materials Education Council, 106 Materials Research Laboratory, University Park, PA (1985).

5. Complete Courses in Materials Science and Engineering, Video-tape, live-audio, available from the Materials Education Council, 106 Materials Research Laboratory, University Park, PA 16802.

APPENDIX 6

Innovations in Materials Research, Vol. 1, No. 1 (1996) 11-22

NEW APPLICATIONS OF PHOTOSTRICTION

Kenji Uchino
International Center for Actuators and Transducers
Materials Research Laboratory, The Pennsylvania State University
University Park, PA 16802

ABSTRACT

Photostriction in ferroelectrics arises from a superposition of photovoltaic and inverse piezoelectric effects. (Pb,La)(Zr,Ti)O_3 ceramics doped with WO_3 exhibit large photostriction under irradiation of near-ultraviolet light, and are applicable to remote control actuators and photoacoustic devices. Using a bimorph configuration, a photo-driven relay and a micro walking device have been developed, which are designed to start moving as a result from the irradiation, having neither electric lead wires nor electric circuits. The mechanical resonance of the bimorph was also induced by an intermittent illumination of purple-color light; this verified the feasibility of the photostriction to "photophone" applications.

Keywords: *Photostriction, photovoltaic effect, piezoelectricity, bimorph, photoacoustic, photophone, mechanical resonance.*

INTRODUCTION

Photostrictive effect is a phenomenon in which strain is induced in the sample when it is illuminated. This effect is focused especially in the fields of micromechanism and optical communication. With decreasing the size of miniature robots/actuators, the weight of the electric lead wire connecting the power supply becomes significant, and remote control will definitely be required for sub-millimeter devices. A photo-driven actuator is a very promising candidate for micro-robots. On the other hand, the key components in the optical communication are a solid state laser as a light source, an optical fiber as a transfer line, and a display/ a telephone as a visual/audible interface with the human. The former two components have been developed fairly successfully, and the photo-acoustic device (i. e. an optical telephone or a "photophone") will be eagerly anticipated in the next century.

Photostrictive devices which are actuated when they receive the energy of light will be particularly suitable for use in the above-mentioned fields. In principle, the photostrictive effect arises from a superposition of a photovoltaic effect, where a large voltage is generated in a ferroelectric through the irradiation of light,[1)] and a piezoelectric effect, where the material expands or contracts under the voltage applied. It is noteworthy that this photostriction is neither the thermal dilatation nor the pyroelectrically-produced strain associated with a temperature rise due to the light illumination. Also the photovoltaic effect mentioned here generates a greater-than-band-gap voltage (several kV/cm), and is quite different from that based on the p-n junction of semiconductors (i. e. solar battery).

This paper describes the details of the fundamental photostrictive effect in (Pb,La)(Zr,Ti)O_3 ceramics first, then introduces its applications to a photo-driven relay, a micro walking machine and a photophone, which are designed to function as a result of irradiation, having neither lead wires nor electric circuits.

RELATION TO PREVIOUS WORK

Photostriction phenomenon was discovered by Dr. P. S. Brody and the author independently almost at the same time in 1981.[2] Dr. Brody has not reported much after the discovery, and most of the studies have been made by the author's group, including materials development, device disigning, control techniques and applications. Very recently, Prof. T. Fukuda et al. are investigating the photostrictive actuators from an application point of view using our PLZT ceramics.[3]

PHOTOSTRICTIVE PROPERTIES

PRINCIPLE

The main features of the "bulk" photovoltaic effect are summarized as follows:

1) This effect is observed in a uniform crystal or ceramic having noncentric symmetry, and is entirely different in nature from the p-n junction effect observed in semiconductors.

2) A steady photovoltage/current is generated under uniform illumination.

3) The magnitude of the induced voltage is greater than the band gap energy of the crystal.

Although the origin of this photovoltaic effect has not been clarified yet, the key point to understand it is the necessity of both *impurity doping* and *crystal asymmetry*. Figure 1 illustrates one of the proposed models, the electron energy band model proposed for $(Pb,La)(Zr,Ti)O_3$.[4,5] The energy band is basically generated by the hybridized orbit of p-orbit of oxygen and d-orbit of Ti/Zr. The donor impurity levels induced in accordance with La doping (or other dopants) are present slightly above the valence band. The transition from these levels with an asymmetric potential due to the crystallographic anisotropy may provide the "preferred" momentum to the electron. Electromotive force is generated when electrons excited by light move in a certain direction of the ferroelectric crystal, which may arise along the spontaneous polarization direction.

The asymmetric crystal exhibiting a photovoltaic response is also piezoelectric in principle, and therefore, a photostriction effect is expected as a coupling of the bulk photovoltaic voltage (E^{Ph}) with the piezoelectric strain constant (d).

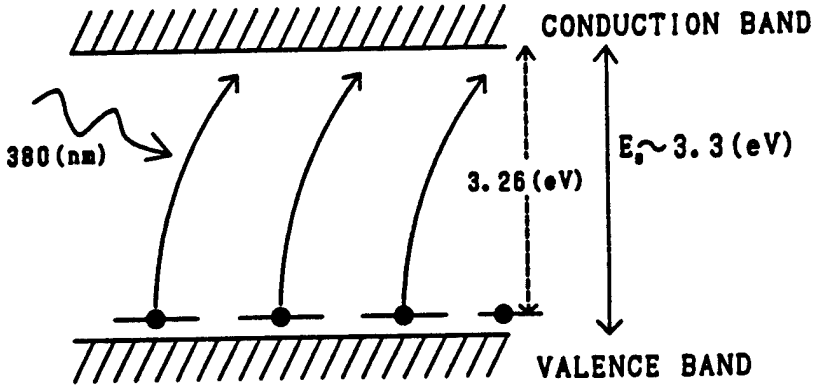

Figure 1. Energy band gap model of excited electron transition from impurity level in PLZT.

INSTRUMENTATION

The radiation from a high-pressure mercury lamp was passed through infrared-cut optical filters. The light with the wavelength peak around 370 nm, where the maximum photovoltaic effect of PLZT is obtained, was then applied to the sample. A xenon lamp was also used to measure the wavelength dependence of the photovoltaic effect. The light source was monochromated by a monochromator to 6 nm HWHM.

The photovoltaic voltage under illumination generally reaches several kV/cm, and the current is on the order of nA. The induced current was recorded as a function of the applied voltage over a range -100 V to +100 V, by means of a high-input impedance electrometer. The photovoltaic voltage and the current were determined from the intercepts of the horizontal and the vertical axes, respectively. The data are shown in Fig. 2.[5] Photostriction was directly measured by a differential transformer or an eddy current displacement sensor.

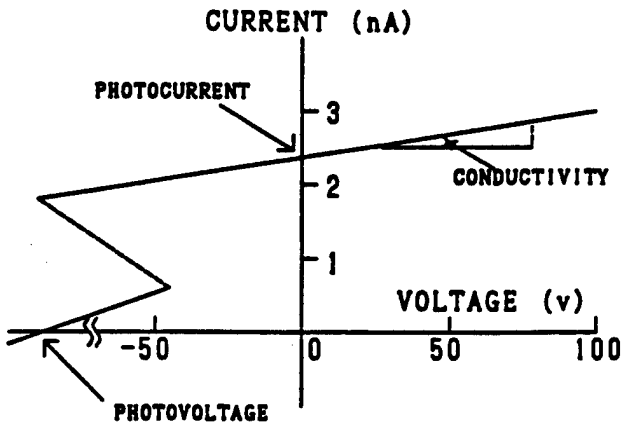

Figure 2. Photocurrent measured as a function of applied voltage under illumination.

MATERIALS RESEARCH

The figure of merit of the photostriction is evaluated by the product of the photovoltaic voltage (E^{ph}) and the piezoelectric coefficient (d). PZT based ceramics are currently focused because of their excellent piezoelectric properties, i. e. high d values. PLZT is one of such materials, which is also famous as a transparent (good sintered without pores) ceramic applicable to electrooptic devices.

PLZT (x/y/z) samples were prepared in accordance with the following composition formula:

$$Pb_{1-x}La_x(Zr_yTi_z)_{1-x/4}O_3.$$

Figures 3(a) and 3(b) illustrate the contour maps of the photovoltaic response and the piezoelectric strain constant d33 on the PLZT phase diagram.[6,7] The d33 shows the maximum around the morphotropic phase boundary (MPB) between the tetragonal and rhombohedral phases, and increases gradually with increasing the La concentration up to 9 mol %. On the contrary, the photovoltage exhibits the maximum also around the MPB, but in the tetragonal region with 3 mol % of La. The largest pruduct $d_{33} \cdot E^{ph}$ was obtained with the composition (3/52/48).

The interrelation of the photovoltaic current with the remanent polarization for the PLZT family is very intriguing (Fig. 4).[8] The average remanent polarization exhibiting the same magnitude of photocurrent differs by 1.7 times between the tetragonal and rhombohedral phases; this suggests the photo-induced electron excitation is related to the (0 0 1) axis-oriented orbit, i. e. the hybridized orbit of p-orbit of oxygen and d-orbit of Ti/Zr.

Impurity doping on PLZT also affects the photovoltaic response significantly.[5] Figure 5 shows the photovoltaic response for various dopants with the same concentration of 1 atomic % into the base PLZT (3/52/48) under an illumination intensity of 4 mW/cm^2 at 366 nm. The dashed line in Fig. 5 represents the constant power curve corresponding to the non-doped PLZT (3/52/48). Regarding the photostriction effect, it is known that as the photovoltaic voltage increases, the strain value increases, and with increasing photocurrent, there is an increase in the overall response. The photovoltaic response is enhanced by donor doping onto the B-site (Nb^{5+}, Ti^{5+}, W^{6+}). On the other hand, impurity ions substituting at the A-site and/or acceptor ions substituting at the B-site, whose ionic valences are small (1 to 4), have no significant effect on the response. Figure 6 shows the photovoltaic response plotted as a function of at.% of WO_3 doping concentration.[9] Note that the maximum power is obtained at 0.4 at.% of the dopant.

Even when the composition is fixed, the photostriction still depends on the sintering condition or the grain size.[7] Figure 7 shows the dependence of the photostrictive characteristics on the grain size. The smaller grain sample is preferrable, if it is sintered to a high density.

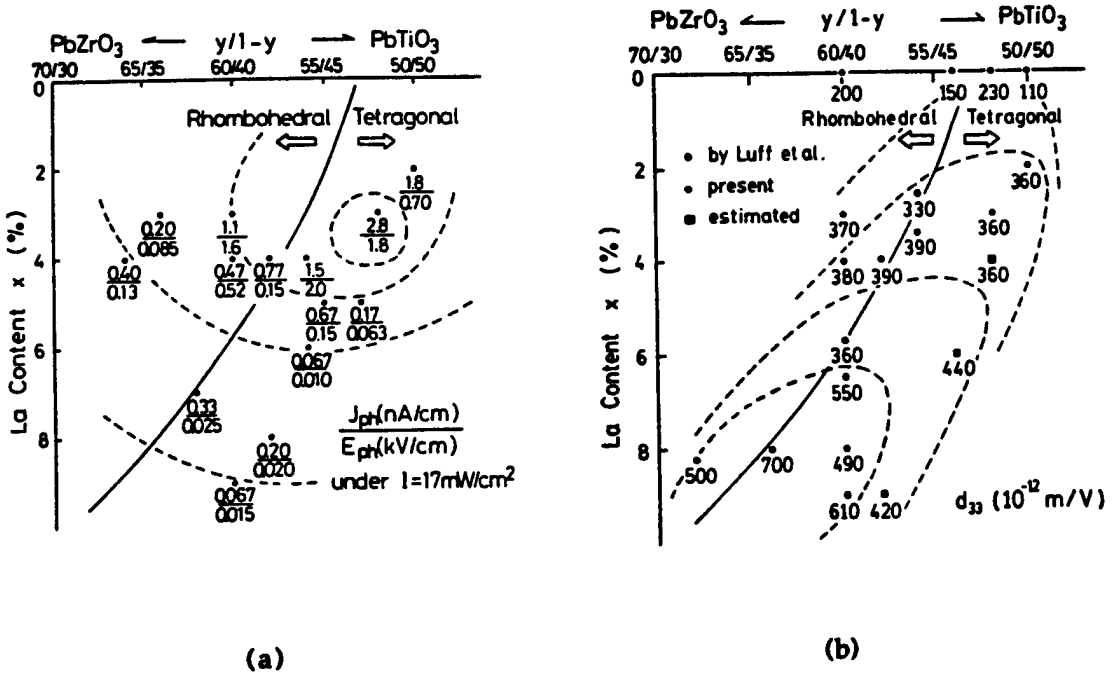

Figure 3. Photovoltaic response (a) and piezoelectric constant d33 (b) of PLZT plotted on the phase diagram near the morphotropic phase boundary between the tetragonal and rhombohedral phases.

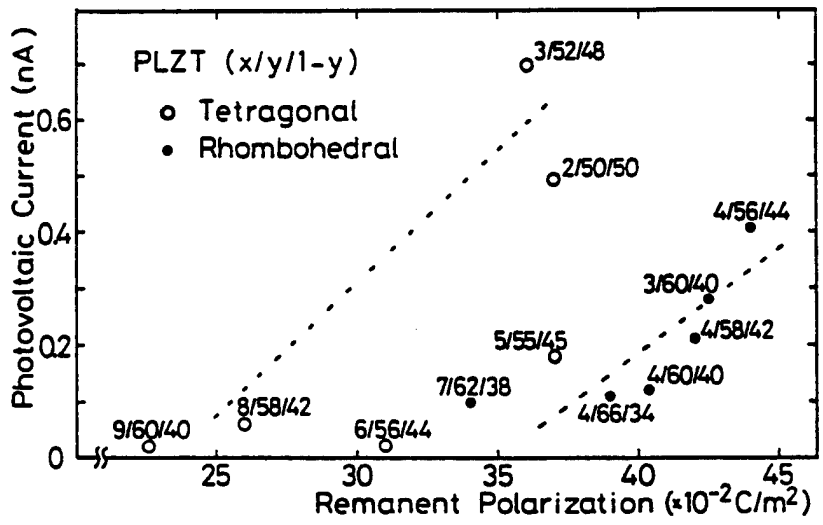

Figure 4. Interrelation of photovoltaic current with remanent polarization in PLZT family

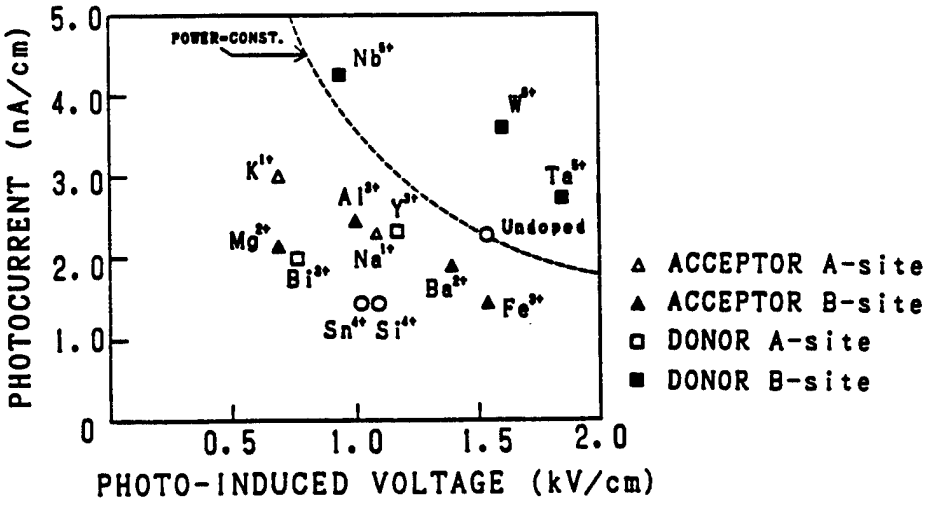

Figure 5. Photovoltaic response of PLZT for various impurity dopants (illumination intensity:4mW/cm^2).

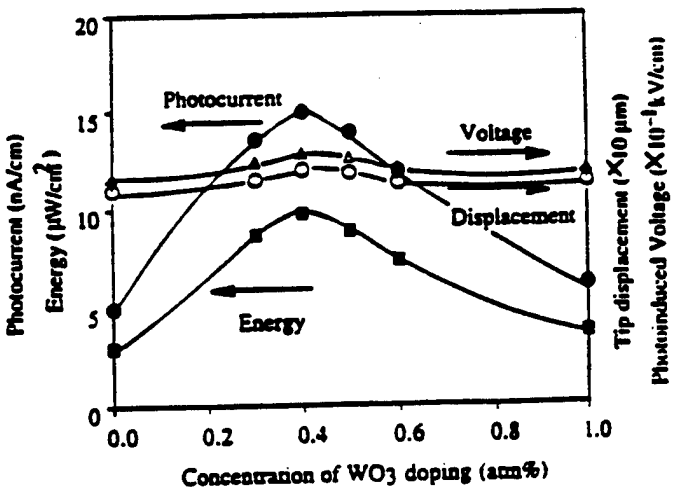

Figure 6. Photovoltaic current, voltage, power and tip displacement of a bimorph specimen as a function of dopant concentration in WO_3 doped PLZT (3/52/48).

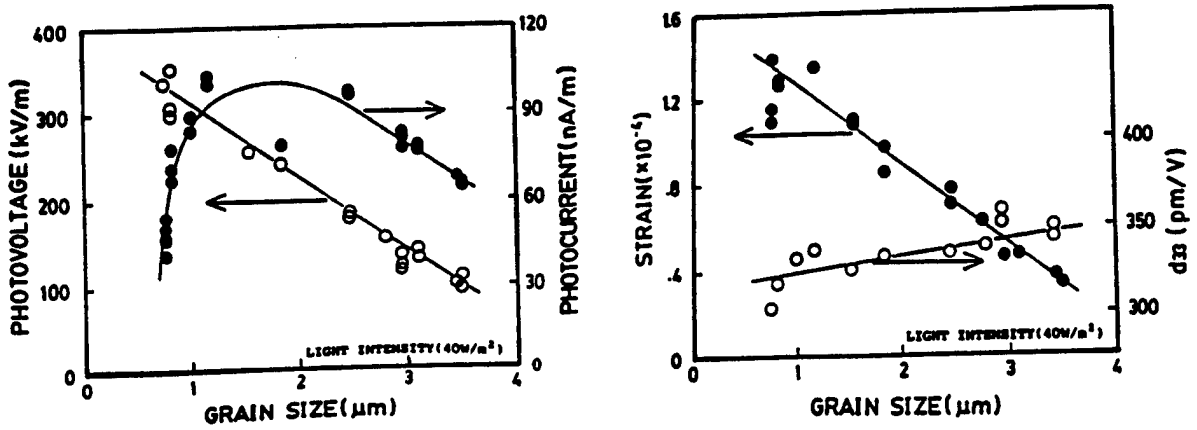

Figure 7. Grain size dependence of photostrictive characteristics in PLZT (3/52/48).

EFFECT OF LIGHT POLARIZATION DIRECTION

Effect of the light polarization direction on the photovoltaic phenomenon was investigated on the polycrystalline PLZT, using an experimental setup shown in Fig. 8(a).[10] This experiment is important when the photostriction is employed to "photophones", where the sample is illuminated with the polarized light traveling through an optical fiber. The rotation angle q was taken from the vertical spontaneous polarization direction, as shown in Fig. 8(a). Even in a polycrystalline sample, both the photovoltaic voltage and current provided the maximum at q = 0 and 180 deg and the minimum at q = 90 deg (Fig. 8(b)); this also indicates that the contributing electron orbit may be the p-d hybridized orbit mentioned above.

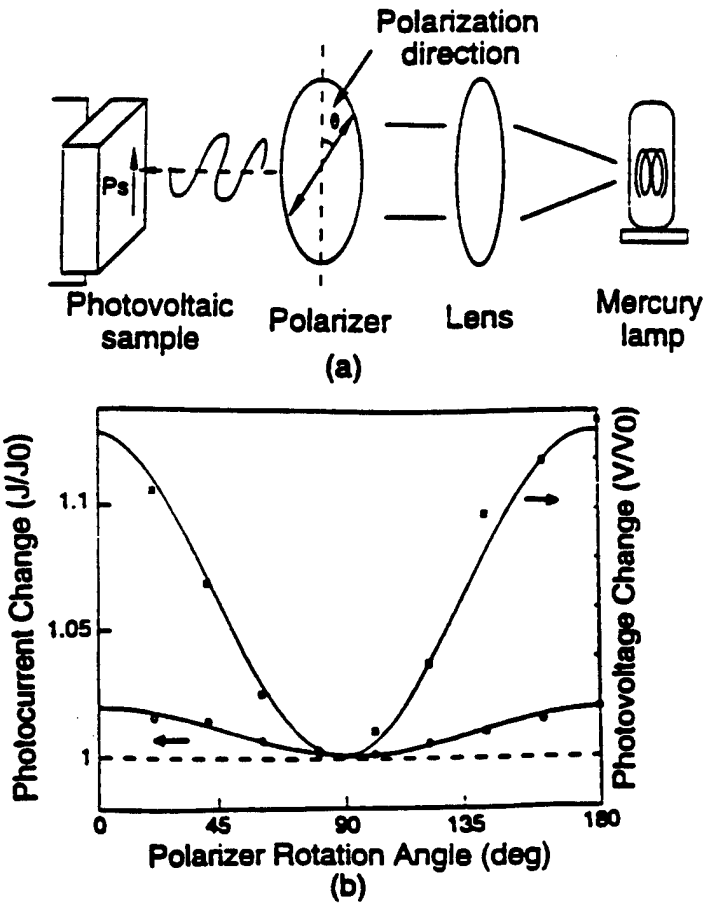

Figure 8. (a) Measuring system of the dependence of photovoltaic effect on light polarization direction, and (b) photovoltaic voltage and current as a function of the rotation angle.

DISPLACEMENT MAGNIFICATION MECHANISM

Since the maximum strain level of the photostriction is only 0.01 % (this corresponds to 1 mm displacement from a 10 mm sample), we need to consider a sophisticated magnification mechanism of the displacement. We employed a bimorph structure, which is anologous to a bimetal consisting of two metalic plates with different thermal expansion coefficients bonded together to generate a bending deformation according to a temperature change. Two PLZT plates were pasted back to back, but were placed in opposite polarization, then connected on the edges electrically, as shown in Fig. 9.[5] A purple light (366 nm) was shined to one side, which generated a photovoltaic voltage of 7 kV across the length. This caused the PLZT plate on that side to expand by nearly 0.01 % of its length, while the plate on the other (unlit) side contracted due to the piezoelectric effect through the photovoltage. Since the two plates were bonded together, the whole device bent away from the light. For this 20 mm long and 0.35 mm thick bi-plate, the displacement at the edge was 150 mm, and the response speed was a couple of seconds.

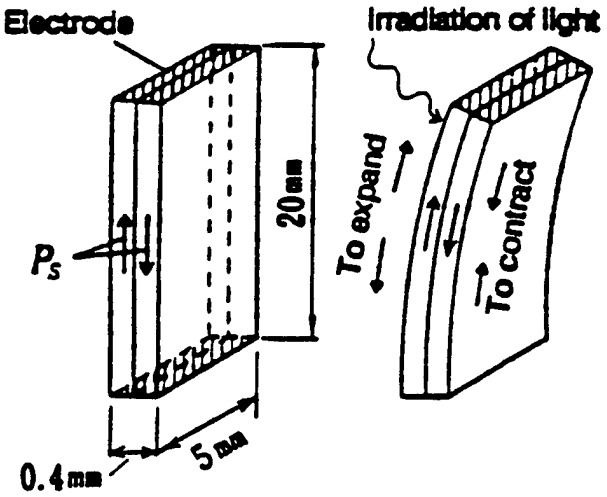

Figure 9. Structure of the photo-driven bimorph and its driving principle.

DEVICE APPLICATIONS

In this section we will introduce the applications of photostriction to a photo-driven relay, a micro walking machine and a photophone, which are designed to function as a result of irradiation, having neither lead wires nor electric circuits.

PHOTO-DRIVEN RELAY

A photo-driven relay was constructed using a PLZT photostrictive bimorph as a driver which consists of two ceramic plates bonded together with their polarization directions opposing each other (Fig. 10).[5] A dummy PLZT plate was positioned adjacent to the bimorph to cancel the photovoltaic voltage generated on the bimorph. Utilizing a dual beam method, switching was controlled by alternately irradiating the bimorph and the dummy. The time delay of the bimorph that ordinarily occurs in the off process due to a low dark conductivity could be avoided, making use of this dual beam method. Figure 11 shows the response of a photostrictive bimorph made from PLZT doped with 0.5 at% WO_3 under an illumination intensity of 10 mW/cm^2. The amount of displacement observed at a tip of the bimorph (20 mm long and 0.35 mm thick) was $\pm$150 mm. A snap action switch was used for the relay. Switching by a displacement of several tens of micron was possible with this device. The on/off response of the photo-driven relay is shown in Fig. 12. The typical delay time was 1 - 2 seconds.

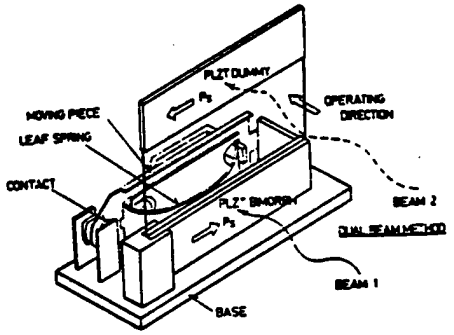

Figure 10. Structure of the photo-driven relay.

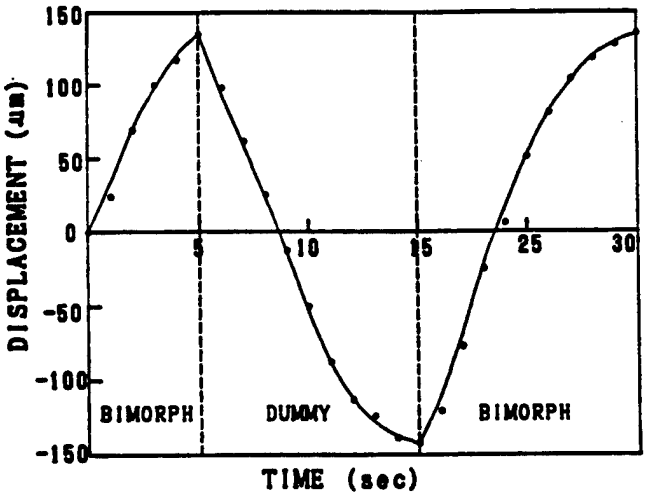

Figure 11. Tip deflection of the bimorph device made from WO_3 0.5 at.% doped PLZT under a dual beam control (illumination intensity: 10 mW/cm^2).

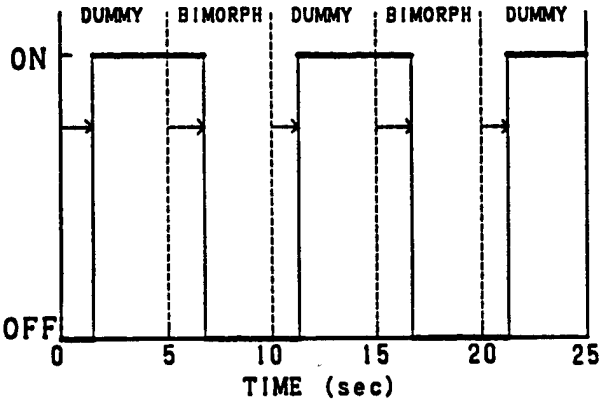

Figure 12. On/off response of the photo-driven relay.

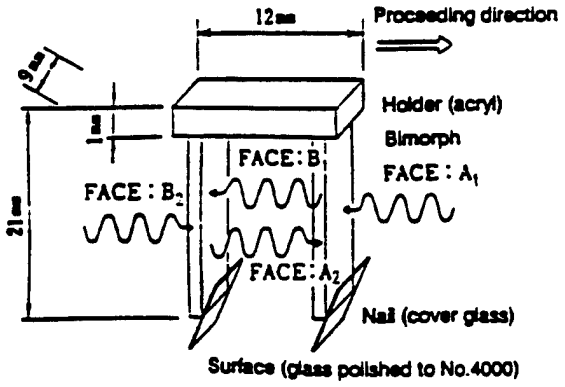

Figure 13. Structure of the photo-driven micro walking machine, and the irradiation directions.

MICRO WALKING DEVICE

A photo-driven micro walking machine has also been developed using the photostrictive bimorphs.[11] It was simple in structure, having only two ceramic legs (5mmx 20mmx 0.35mm) fixed to a plastic board (Fig. 13). When the two legs were irradiated with purple light alternately, the device moved like an inchworm. The photostrictive bimorph as a whole was caused to bend by ±150 mm as if it averted the radiation of light. The inchworm built on a trial basis exhibited rather slow walking speed (several tens mm/min) as shown in Fig. 14, since slip occurred between the contacting surface of its leg and the floor. The walking speed can be increased to approximately 1 mm/min by providing some contrivances such as the use of a foothold having microgrooves fitted to the steps of the legs.

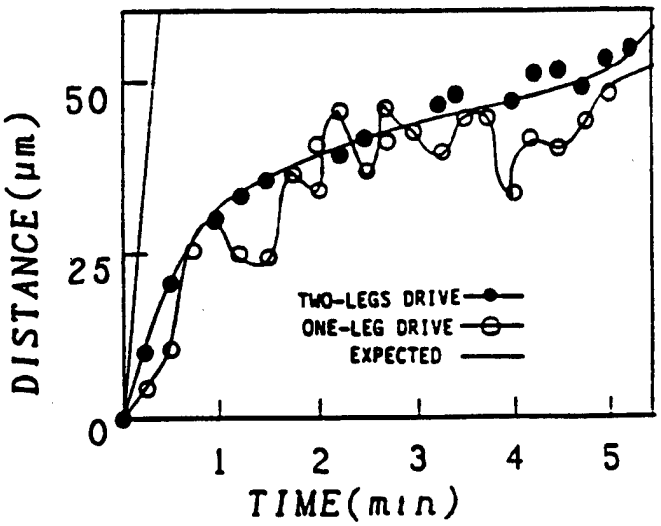

Figure 14. Position change of the photo-driven micro walking machine with time.

PHOTOPHONE

The technology to transmit voice data (i. e. a phone call) at the speed of light through lasers and fiber optics has been advancing rapidly. However, the end of the line -- interface speaker -- limits the technology, since optical phone signals must be converted from light energy to mechanical sound via electrical energy at present. The photostriction may provide new photoacoustic devices.

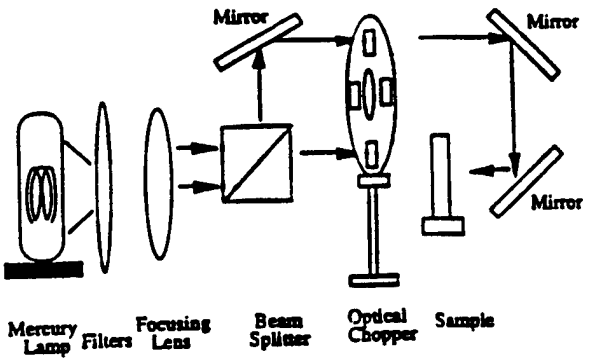

Figure 15. Experimental setup for the photo-induced mechanical resonance measurement.

Photo-mechanical resonance of a PLZT ceramic bimorph has been successfully induced using chopped near-ultraviolet irradiation, having neither electric lead wires nor electric circuits.[12] A thin cover glass was attached on the photostrictive bimorph structure to decrease the resonance frequency so as to easily observe the photo-induced resonance. Figure 15 shows the experimental setup with an optical chopper. A dual beam method was used to irradiate the two sides of the bimorph alternately; intermittently with a 180 deg phase difference. The mechanical resonance was then determined by changing the chopper frequency.

The tip displacement of the thin-plate-attached sample as a function of chopper frequency is presented in Fig. 16. Photo-induced mechanical resonance was successfully observed. The resonance frequency was about 75 Hz with the mechanical quality factor Q of about 30. The maximum tip displacement of this photostrictive sample was about 5 μm at the resonance point, smaller than the level required for audible sound. However, the achievement of photo-induced mechanical resonance in the audible frequency range suggests the promise of photostrictive PLZT bimorph-type devices as photo-acoustic components, or "photophones", for the next optical communication age.

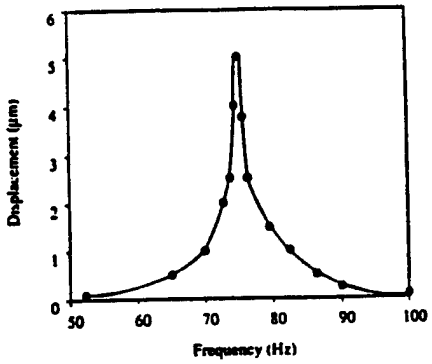

Figure 16. Photo-induced mechanical resonance behavior of the PLZT bimorph.

CONCLUSION

Photostrictive actuators can be driven only by the irradiation of light, so that they will be suitable for use in actuators, to which lead wires can hardly be connected because of their ultra-small size or of their employed conditions such as ultra-high vacuum or outer space. The photostrictive bimorphs will also be applicable to "photophones." The new principle actuators have considerable effects upon the future micro-mechatronics.

This work was partly supported by US Army Research Office through Contract No. DAAL 03-92-G-0244.

REFERENCES

1. V. M. Fridkin, *Photoferroelectrics*, Ed. by M. Cardona, P. Fulde, H. -J., Queisser, Solid State Sciences 9, Springer-Verlag, New York (1979).
2. A. M. Glass, D. von der Linde, D. H. Austin and T. J. Negran, *J. Elec. Mater.*, 4 (5), 915 (1975).
3. P. S. Brody, *Ferroelectrics*, 50, 27 (1983).

4. T. Fukuda, S. Hattori, F. Arai, H. Matsuura, T. Hiramatsu, Y. Ikeda and A. Maekawa, *Rob. Automation*, 2,618 (1993).
5. M. Tanimura and K. Uchino, *Sensors and Materials*, 1, 47 (1988).
6. K. Uchino, M. Aizawa and Late S. Nomura, *Ferroelectrics*, 64, 199 (1985).
7. T. Sada, M. Inoue and K. Uchino, *J. Ceram. Soc. Jpn.*, 5, 545 (1987).
8. K. Uchino, Y. Miyazawa and S. Nomura, *Jpn. J. Appl. Phys.*, 22(Suppl. 22-2), 102 (1983).
9. S. Y. Chu, Z. Ye and K. Uchino, *J. Adv. Performance Mater.* [in press].
10. S. Y. Chu, Z. Ye and K. Uchino, *Smart Mater. Struct.*, 3, 114 (1994).
11. K. Uchino, *J. Rob. Mech.*, 1, 124 (1989).
12. S. Y. Chu and K. Uchino, *Proc. 9th Int'l Symp. Appl. Ferroelectrics*, State College (1994)[in press].

APPENDIX 7

Jpn. J. Appl. Phys. Vol. 35 (1996) pp. L 516–L 518
Part 2, No. 4B, 15 April 1996

Acoustic Emission (AE) Measurement Technique in Piezoelectric Ceramics

Hideaki ABURATANI and Kenji UCHINO
International Center for Actuators and Transducers, Materials Research Laboratory, The Pennsylvania State University, University Park, PA 16802, USA

(Received February 29, 1996; accepted for publication March 15, 1996)

Special care must be taken in measuring the acoustic emission (AE) in piezoelectric ceramics, because a self vibration of the ceramics is caused by a power supply through a feedback system. Significantly different data from the results previously reported were obtained by eliminating the self vibration of the ceramics. The dynamic contribution of 180° and non-180° domain reorientation on the AE generation were discussed on the basis of AE data observed in lead zirconate-titanate (PZT) ceramics.

KEYWORDS: acoustic emission (AE), domain, domain reorientation, piezoelectric ceramics, PZT

1. Introduction

Acoustic Emission (AE) method is a technique to detect pulses of released elastic strain energy caused by deformation, crack growth and phase change in a solid.[1] The AE method has been used to study fundamental domain motions in ferromagnetic and ferroelectric materials, as well as mechanical and fatigue properties of materials (i.e., non-destructive evaluation). In ferroelectric and piezoelectric materials, the AE method has been used to determine phase change,[2–4] to detect domain reorientation[5–7] and to monitor crack propagation.[8,9] Nevertheless, recent research has revealed a significant problem in most of the previous AE studies. A self-vibration of the sample generated by the combination of the power supply and the piezoelectric device might conceal the true AE signal.

This paper deals with a technique for the AE measurement on the piezoelectric materials and provides an example measurement on PZT piezoelectric ceramics. The AE generation induced in the sample under bipolar or unipolar electric field drive is discussed in conjunction with the 180° and non-180° domain reorientation.

2. New Experimental Setup

Figure 1 shows the measurement system. The field induced AE and displacement were observed simultaneously. The AE signal was detected by an AE sensor (NF Corporation AE-904E) with its resonant frequency of 450 kHz. The AE signal was amplified by 40 dB through a preamplifier (NF, AE-922) and by 50 dB with a main amplifier (NF, AE-9913). The amplified signal was counted after passing through a high-pass filter (100 kHz) and a discriminator with lower and higher threshold levels of 300 mV and 600 mV. Disc specimens of piezoelectric ceramic PZT-5A (i.e., a commercially available soft PZT with high sensitivity, permittivity and time stability) with 12.7 mm in diameter and 0.3 mm in thickness were employed for this study. Gold electrodes were sputtered on both surfaces. The AE sensor was attached to the sample through copper-foil, and silicone grease. The sample was driven by a triangular wave with $-3\,\mathrm{kV/mm} \leftrightarrow +3\,\mathrm{kV/mm}$ at 0.02 Hz for bipolar driving and with $0 \rightarrow +3\,\mathrm{kV/mm}$ at 0.04 Hz for unipolar driving. A modification to the AE measurement system was the introduction of an external resistor (R) in series and a capacitor (C) in parallel to the power supply in order to eliminate the high frequency component completely.

3. Results and Discussion

Figure 2 shows the AE ringdown count at an external electric field $E = 0\,\mathrm{V/mm}$ measured without R and C, which corresponds to the conventional measuring setup. A large number of the AE count was observed even at 0 V/mm. The count at 0 V/mm was probably caused by a high frequency component of voltage/current from the power supply through a feedback circuit, resulting in a vibration of the piezoelectric sample. In order to elimi-

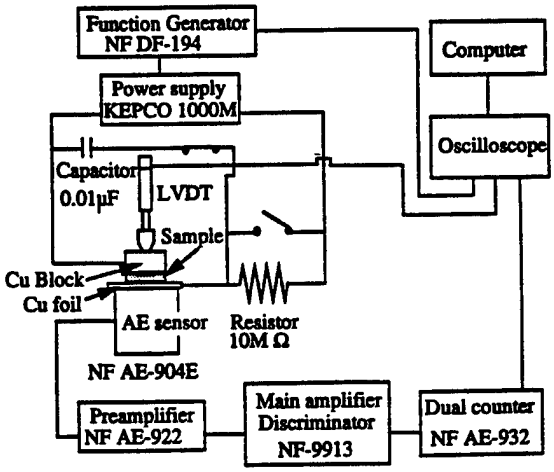

Fig. 1. A new AE measurement system.

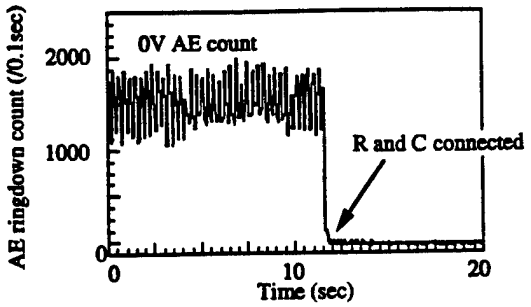

Fig. 2. AE count at 0 V/cm with and without resistor or capacitor.

nate this vibration, both a resistor (R) of 10 $M\Omega$ and a capacitor (C) of 0.01 μF were connected to the sample to increase the time constant (RC) of the system (i.e.. to suppress the high frequency component (Fig. 1)). The AE count at 0 V/mm completely vanished when R and C were connected to the sample. Figure 3 shows the change in the induced displacement when R and C were connected. A large time constant in the whole system (0.1 s) caused some distortion in the induced displacement curve; however, the displacement magnitude was maintained.

Figure 4 shows the AE count and the induced displacement as a function of time under a bipolar and an unipolar drive using the conventional setup (without R and C). The AE was continuously counted during the bipolar drive, except when displacement switching occurred. In an unipolar drive, the AE count showed the minimum at the maximum induced displacement under the standard setup. Yet, by changing the amplification from 90 dB to 85 dB, the maximum AE count was observed at the maximum displacement (Fig. 4(c)). This difference might be caused by an overload of the filter circuit at the higher amplification. The AE results similar to these data under both bipolar and unipolar driving were reported in most of the previous studies.

On the contrary, in the AE measuring system with R and C, the results were completely different. The AE was observed only after the polarization switching under a bipolar drive, while no AE was observed under an unipolar drive (Fig. 5). Considering that the non-180° domain reorientation contributes mainly to the unipolar hysteresis and that both the 180° domain and non-180° domain reorientations contribute to the bipolar switching, our results implied that the 180° domain reorientation primarily generates the AE and that the non-180° domain reorientation does not significantly affect the AE in PZT ceramics. This seems to be reasonable, because the 180° domain wall motion is usually much quicker than the non-180° domain wall, leading to a larger stress release.

Figure 6 shows the induced displacement and the AE count as a function of the magnitude of the applied field. At a lower field, a very small number of the AE were detected even after the displacement switching, and the AE count increased with the applied field. It seemed that

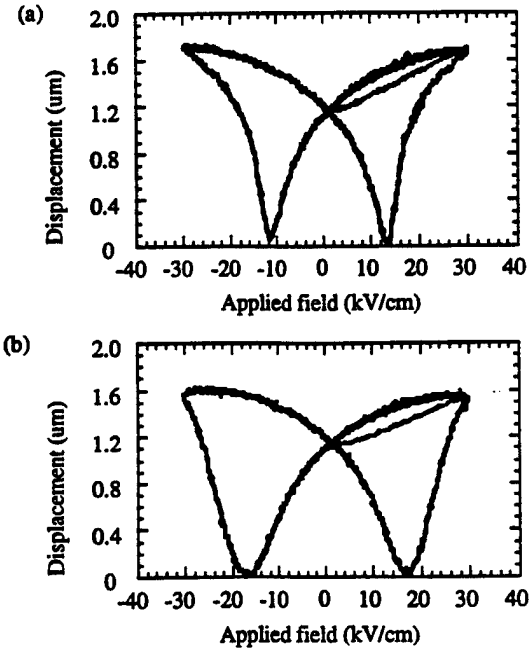

Fig. 3. Induced displacement of the PZT: (a) without R or C and (b) with R and C.

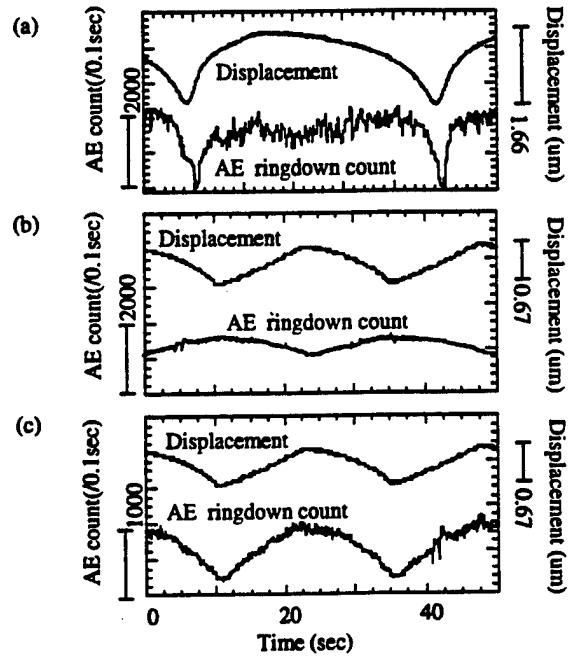

Fig. 4. AE count and induced displacement using the conventional setup: (a) under a bipolar drive, (b) under a unipolar drive and (c) under a unipolar drive at 85 dB.

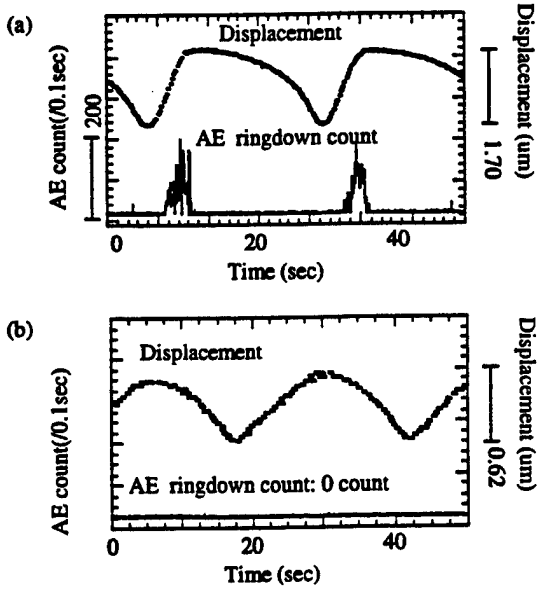

Fig. 5. AE count and induced displacement using a new setup: (a) under a bipolar drive (b) under a unipolar drive.

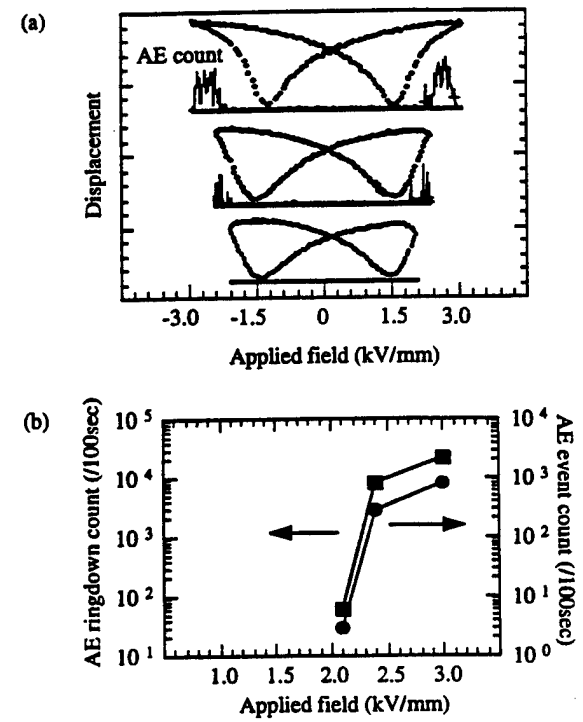

Fig. 6. (a) Induced displacement with various applied field (b) AE count as a function of applied field.

the induced-displacement switching was mainly caused by the non-180° domain reorientation; moreover, the amount of 180° domain reorientation was too small to generate AE at a lower applied field.

If the AE count in the conventional setup was really caused by the domain motion, the same count should be observed in the modified setup as long as the induced displacement was maintained. Yet, the AE was observed only after polarization switching with a bipolar drive. Thus, the AE count in the conventional setup was not caused by the domain motion, but it was just due to the vibration of the sample. This vibration was caused by the coupling of the piezoelectric response of the sample and the feedback in the power supply. Therefore, no AE was observed when the displacement switching occurred, which means the sample lost its piezoelectricity. Thus the vibration level was large enough to conceal the true AE signals.

4. Conclusion

In the AE measurement of piezoelectric ceramics, the sample vibration was observed, and it was determined that it completely concealed the true AE signal due to the domain reorientation. This vibration was caused by the combination of the piezoelectricity and high frequency component from the power supply. The vibration can be eliminated by increasing the time constant of the whole system.

The AE was observed only after the induced displacement switching under a bipolar drive. On the contrary, no AE was observed with an unipolar drive. It was suggested that the 180° domain reorientation contributes more to the AE generation than the non-180° domain reorientation in PZT ceramics.

Acknowledgement

This work was supported by the Office of Naval Research through Contract No. N00014-92-J-1510.

1) R. Halmshaw: *Non-Destructive Testing* (Edward Arnold, London, 1991) 2nd ed., Chap. 2, p. 273.
2) P. Buchman: Solid State Electronics. **15** (1972) 142.
3) I. J. Mohamad, E. F. Lambson, A. J. Miller and G. A. Saunders: Phys. Lett. A **71** (1979) 115.
4) V. A. Kalitenko, V. M. Perga and I. N. Salivonov: Sov. Phys. Solid State **22** (1980) 1067.
5) H. Iwasaki and M. Izumi: Ferroelectrics **37** (1981) 563.
6) Y. Saito and S. Hori: Jpn. J. Appl. Phys. **33** (1994) 5555.
7) M. Arai, Y. Sugawara and K. Uchino: *Proc. Ultrasonic Symp., Hawai, 1990* (IEEE) p. 1197.
8) A. Furuta and K. Uchino: J. Am. Ceram. Soc. **76** (1993) 1615.
9) H. Aburatani, S. Harada, K. Uchino, A. Furuta and Y. Fuda: Jpn. J. Appl. Phys. **33** (1994) 3091.

MATERIALS STUDIES

APPENDIX 8

Ferroelectric Letters, 1996, Vol. 21, pp. 27–33
Reprints available directly from the publisher
Photocopying permitted by license only

DIELECTRIC, PYROELECTRIC AND PIEZOELECTRIC PROPERTIES OF CALCIUM-MODIFIED LEAD MAGNESIUM TANTALATE-LEAD TITANATE CERAMICS

S.W. CHOI, J.M. JUNG AND A.S. BHALLA*
Department of Physics, Dankook University,
29 Anseodong, Cheonan, Chungnam, Korea
*Material Research Laboratory, The Pennsylvania State University
University Park, PA 16802 USA

Abstract Dielectric, pyroelectric and piezoelectric properties of relaxor ferroelectrics in solid solution, formulated $0.65(Pb_{1-x}Ca_x)(Mg_{1/3}Ta_{2/3})O_3$-$0.35PbTiO_3$, have been investigated. Complete single-phase perovskite with high density was obtained with all samples fired at 1250℃. The Curie temperature and pyroelectric peak temperature decrease almost linearly as the amount of Ca in the compositions increases. The transition temperature of the solid solutions can easily be controlled by Ca additions in the PMT-PT. Dielectric, pyroelectric and piezoelectric constants achieved maximum values for x=0.02. Compositions near 0.65PMT-0.35PT-0.12Ca have been identified to have high dielectric constants(~15000) and low dissipation factors(~0.015) near room temperature.

(Received for Publication December 20, 1995)

INTRODUCTION

Relaxor perovskite $Pb(Mg_{1/3}Ta_{2/3})O_3$-PMT was first synthesized by Soviet workers in the early 1960s[1]. Relaxor ferroelectrics are typically characterized by the display of a broad dielectric peak with frequency dispersion of a paraelectric-ferroelectric phase transition. The main feature of the dielectric properties of PMT was a broad maximum of dielectric constant well below room temperature. However, with the addition of $PbTiO_3$-PT(Curie temperature ~490℃), the compositions in PMT-PT solid solution exhibit a morphotropic phase boundary between a rhombohedral and tetragonal phases at about 35 mol% PT[2].

In a well known $Pb(Zr_xTi_{1-x})O_3$ piezoelectric material, the compositions near the morphotropic phase boundary separating rhombohedral and tetragonal phases exhibit large dielectric and piezoelectric anomalies[3]. Similar properties are also seen in other lead-based relaxor-lead titanate(PT) ferroelectric binary materials, such as $Pb(Zn_{1/3}Nb_{2/3})O_3$-$PbTiO_3$[4] and $Pb(Mg_{1/3}Nb_{2/3})O_3$-$PbTiO_3$[5]. The compositions near the 0.65PMT-0.35PT solid solution morphotropic phase boundary, where large values of dielectric constants could be expected, have a transition into the paraelectric phase around 100℃. Thus, these compositions are not suitable for room temperature switching application. Previously, the effects of Ba, Sr and La additions on the dielectric properties of the system PMT-PT were studied, and the dielectric properties of the base composition were improved through selection of additives[6,7,8].

In the present work we have studied the effects of replacing of Pb by Ca on

Communicated by Dr. George W. Taylor

the dielectric, pyroelectric, piezoelectric properties and microstructure of $0.65(Pb_{1-x}Ca_x)(Mg_{1/3}Ta_{2/3})O_3$-$0.35PbTiO_3$ composition near the morphotropic phase boundary(PMT-PT). The purpose of the investigation was to develop ceramics having higher dielectric properties near room temperature.

EXPERIMENTAL PROCEDURE

Reagent-grade oxide powders of $PbCO_3$, TiO_2, Ta_2O_5, MgO and $CaCO_3$ with purity better than 99.8 % were used as starting raw materials. The columbite precursor method by Swartz and Shrout[9] for the synthesis of the various compositions was used. The sintered samples were characterized by x-ray diffraction to insure phase purity. The grain size was determined on fracture surfaces of pellets using scanning electron microscopy(SEM). Opposite faces of the samples were coated with sputtered silver electrodes.

Dielectric properties were measured with an Impedance Analyzer(HP4192A), control unit and it's interface. The dielectric constant and dissipation factor were measured as a function of temperature at various frequencies between 0.1 and 100 kHz with a temperature rate of 4 ℃/min. The pyroelectric coefficient and spontaneous polarization were measured by the static Byer-Roundy method[10] as the samples were heated, again at a rate of 4 ℃/min, through the phase transition region. Prior to the dielectric, pyroelectric and piezoelectric measurements the specimens were poled by applying a DC field of 20 kV/㎝ at room temperature. Piezoelectric d_{33} was measured by using Berlincourt d_{33} meter. Electromechanical coupling factor k_p was measured by using resonance-antiresonance method[11].

RESULTS

Microstructure and X-ray analysis

Fig.1 shows SEM observations of the fractured surfaces of undoped and Ca-doped 0.65PMT-0.35PT, fired at 1250℃ for 4h. Clearly, this sample reveals homogeneous microstructure consisting of large grains($\sim 3\mu$m) as the Ca content increased from 0 to 2 mol%. These ceramics have densities of more than 95% of the theoretical densities. A homogeneous grain structure was obtained with 2 mol% substitution of Ca for the composition 0.65PMT-0.35PT, which gave the highest percentage of theoretical density. From these data it may be concluded that small substitutions of Ca for Pb in the base composition improve the densification and grain refinement which related to dielectric properties.

Fig.2 shows the XRD patterns of the calcined powder and fired specimens for undoped, Ca-doped 0.65PMT-0.35PT. The 0.65PMT-0.35PT-xCa(x=0~0.12) compositions calcined at 850℃ for 5h contained >10% of pyrochlore phase

while the samples sintered at 1250℃ for 4h resulted in almost complete formation of perovskite phase. Addition of Ca to the base composition apparently does not affect the pyrochlore-perovskite transformation.

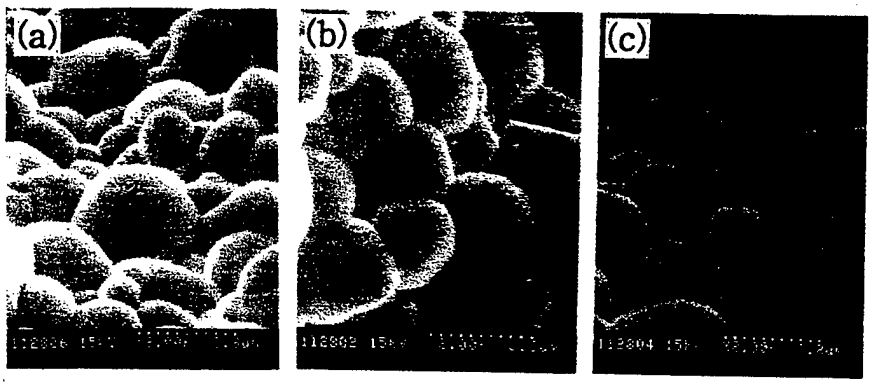

FIGURE 1. Microstructure of 0.65PMT-0.35PT-xCa ceramics sintered at 1250℃/4h. (a)x=0.0 (b)x=0.01 (c)x=0.05

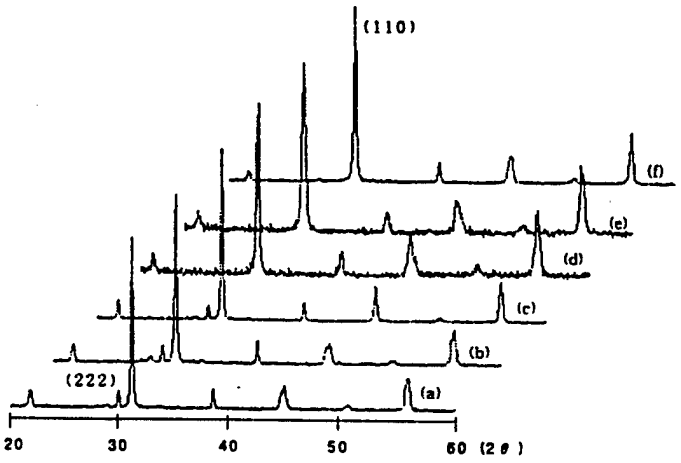

FIGURE 2. X-ray diffraction patterns for 0.65PMT-0.35PT-xCa ceramics. (a)x=0.0 (b)x=0.02 (c)x=0.12, calcined at 850℃/5h (d)x=0.0 (e)x=0.02 (f)x=0.12, sintered at 1250℃/4h

Dielectric properties

Fig.3 shows temperature dependence of dielectric constant and dissipation factor for the base composition modified with 0, 2 and 12 mol% Ca. All compositions show a broad maximum for the dielectric constant. All of the samples exhibited frequency dispersion behavior of both dielectric constant and dissipation factor, which is a characteristic of relaxor ferroelectrics. When the amount of Ca is increased to more than 2 mol%, the dielectric peak is lowered as well as broadened. It was also interesting to note that the substitution of

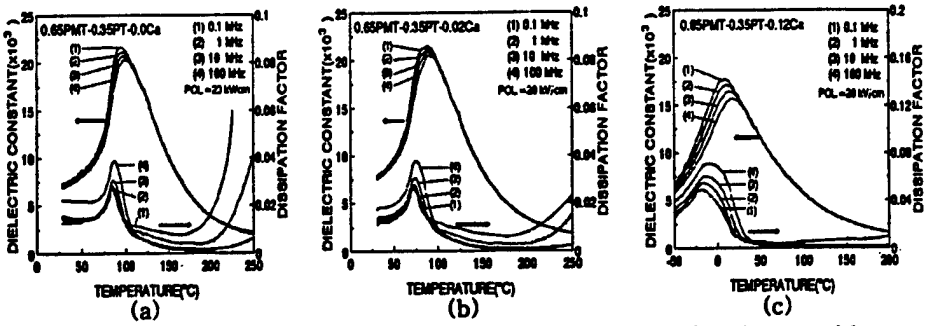

FIGURE 3. Variation of dielectric constant and dissipation factor with temperature and frequency for 0.65PMT-0.35PT-xCa ceramics. (a)x=0.0 (b)x=0.02 (c)x=0.12

Ca in the composition enhanced broadening of the dielectric peak, and highly diffuse phase transition was observed for compositions having Ca content >2 mol%. It is clear that both the diffuseness and frequency dependence of Curie temperature become prominent as the amount of Ca increases. The increase in diffuseness with the amount of Ca corresponds to decrease in dielectric constant (K_{max}). In the compositions with higher than 2 mol% Ca, the decrease in the maximum value of the dielectric constant even when no pyrochlore phase was found to be present occured mainly due to the detrimental effect of addition of Ca. Later Chen et al[12, 13] reported that the decrease in the dielectric constant is not only due to pyrochlore phase but also other factors such as lattice impurities and intergranular phases. It should be noted that we did not analysis the grain boundaries hear and further study is needed to determine the effect of intergranular phases.

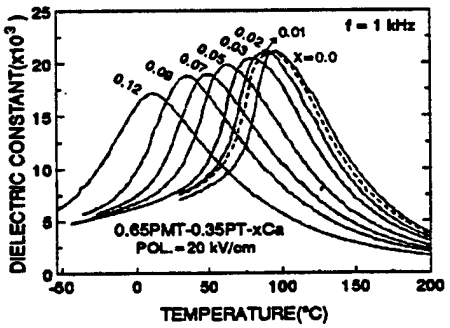

FIGURE 4. Dielectric constant as a function of temperature for 0.65PMT-0.35PT-xCa ceramics.

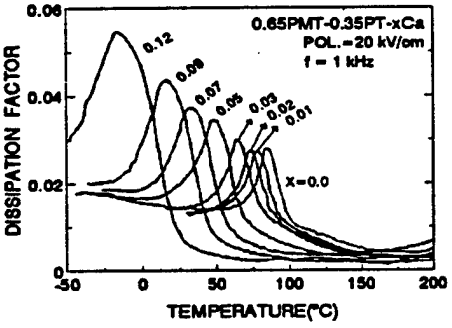

FIGURE 5. Dissipation factor as a function of temperature for 0.65PMT-0.35PT-xCa ceramics.

Fig.4 shows plots of dielectric constant vs. temperature at 1 ㎑ for compositions 0.65PMT-0.35PT system containing different amounts of Ca. The

dielectric constant slightly rises up to 2 mol% Ca and then decreases with further addition of Ca. The decrease in dielectric constant is accompanied by a lowering of the transition temperature. Small amounts of Ca act as fluxes, and Ca maintains its fluxing action up to 2 mol%.

Fig.5 shows plots of dissipation factor vs. temperature at 1 ㎑ for compositions 0.65PMT-0.35PT containing different amounts of Ca. The dissipation factor slightly decreases with additions of Ca up to 2 mol% and then increases with further additions of Ca. Further increase in Ca content appeared to be detrimental, as shown by the considerably lowered dielectric constant and increased dissipation factor. The composition 0.65PMT-0.35PT with 12 mol% Ca have been identified to have high dielectric constants(~15000) and low dissipation factors(~0.01) near room temperature. It was found that partial substitutions of Ca for Pb were quite effective in decreasing the Curie temperature. The Curie temperature decreases sharply with increasing Ca, the composition 0.65PMT-0.35PT-0.12Ca has its T_c value near room temperature. Curie temperature of the binary system vary almost linearly with amounts of Ca as can be seen in Fig.6. It is clear that the addition of Ca shift T_c downward significantly, about 8 ℃/mol%, which is lower than the value reported in study using a nonstoichiometric doping of Sr in PMT-PT system[7].

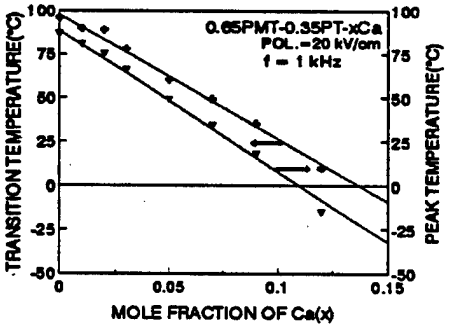

FIGURE 6. Variation of Tc and peak temperature as a function of x for 0.65PMT-0.35PT -xCa ceramics.

These two effects should be properly sorted out in order to obtain ceramics which can be utilized at room temperature.

Pyroelectric and piezoelectric properties

Fig.7 shows temperature dependence of pyroelectric coefficient for the base composition modified with Ca as a function of amount of additive from 0 to 12 mol%. Pyroelectric coefficient increases with increasing x until x~0.02 is reached. However, for x more than ~0.02, pyroelectric coefficient decreased. In most cases like in dielectric data, substitution of Ca in the composition enhanced broadening of the pyroelectric peak. The decrease in pyroelectric coefficient similar to that K vs T (Fig.4) data is accompanied by a lowering of the pyroelectric peak temperature. The pyroelectric peak temperature decreases with increase of Ca content as can be seen in Fig.6. The effects should be properly sorted out in order to obtain pyroactive ceramics, which can be utilized at room temperature. Composition 0.65PMT-0.35PT-0.09Ca has their pyroelectric peak value near room temperature. The results further indicated that it was necessary to have a nominal addition of 2 mol% Ca to obtain the

high pyroelectric coefficient(Fig.7).

Fig.8 shows the room-temperature values of piezoelectric d_{33} and electromechanical coupling factor k_p of the composition 0.65PMT-0.35PT-xCa as a function of mole fraction of Ca. The maximum piezoelectric d_{33} and electromechanical coupling factor k_p are observed at 2 mol% calcium doping. The foregoing composition is in good agreement with those exhibiting maxima in spontaneous polarization.

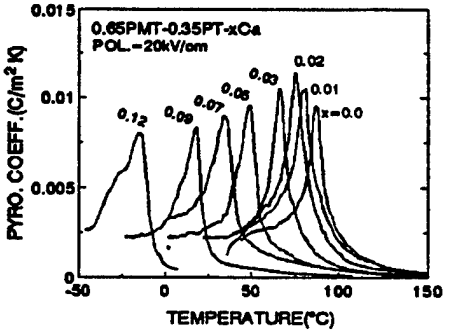

FIGURE 7. Pyroelectric coefficient as a function of temperature for 0.65PMT-0.35PT-xCa ceramics.

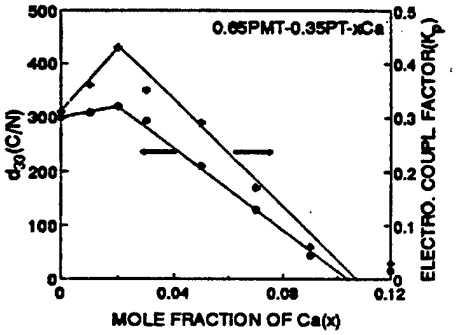

FIGURE 8. Piezo. d_{33} constant and electromechanical coupling factor k_p for 0.65PMT-0.35PT-xCa ceramics at room temperature.

CONCLUSIONS

0.65PMT-0.35PT-xCa (x=0~0.12) ceramics fired at 1250℃ showed a single-phase perovskite structure. These ceramics have densities of more than 95% of theoretical densities. The optimum amount of Ca added is about 2 mol% in this research. Further addition of Ca, however, caused a degraded dielectric, pyroelectric and piezoelectric constants even though no pyrochlore phase was found to be present. The Curie temperature and pyroelectric peak temperature decrease almost linearly as the amount of Ca in the compositions increases. Compositions near 0.65PMT-0.35PT-xCa (x=0.09~0.12) have been identified to have high dielectric, pyroelectric constants and low dissipation factors near room temperature.

ACKNOWLEDGMENT

This work was supported by the Korea Science and Engineering Foundation (KOSEF) through the Research Center for Dielectric and Advanced Matter Physics (RCDAMP) at Pusan National University.

REFERENCES

1. V.A. Bokov and I.E. Myl'nikova, Sov. Phys. Solid State, 2, 2428(1961)
2. Y.J. Kim and S.W. Choi, Ferroelectrics, 108, 241(1990)
3. B.Jaffe, R.S. Roth and S.Marzullo, J. Res. Natl. Bul. Stand., 55, 239(1955)
4. S.Nomura, T.Takahashi and Y.Yokomizo, J. Phys. Soc. Japn., 27, 262(1969)
5. S.W. Choi, T.R. Shrout, S.J. Jang and A.S. Bhalla, Ferroelectrics, 100, 29(1969)
6. S.W. Choi and J.M. Jung, Proc. ISAF'94, 806(1994)
7. J.M. Jung, Y.H. Park and S.W. Choi, Proc. ISAF'94, 810(1994)
8. Y.J. Kim, S.W. Choi and A.S. Bhalla, Ferroelectrics; to be pbulished
9. S.L. Swartz and T.R. Shrout, Mat. Res. Bull., 17, 1245(1982)
10. R.L. Byer and C.R. Roundy, Ferroelectrics, 3, 333(1972)
11. Proc. IRE, Inst. Radio Engs., 49(7), 1161(1961)
12. J. Chen and M.P. Harmer, J. Am. Ceram. Soc., 73, 68(1990)
13. J. Chen, A. Gorton, H.M. Chen and M.P. Harmer, J. Am. Ceram. Soc., 69, C303(1986)

APPENDIX 9

ELSEVIER

November 1996

Materials Letters 29 (1996) 127–129

MATERIALS LETTERS

Preparation of phase-pure perovskite lead indium niobate ceramics

Edward F. Alberta, Amar S. Bhalla *

Materials Research Laboratory, The Pennsylvania State University, University Park, PA 16802, USA

Received 14 May 1996; accepted 19 May 1996

Abstract

To date, attempts to fabricate single phase perovskite $Pb(InNb)_{1/2}O_3$ (PIN) ceramics have met with only limited success. This paper describes a processing method for synthesizing phase-pure PIN ceramics using the wolframite precursor method. Dielectric properties of these undoped ceramics seem to be superior to those reported by previous investigators and are comparable to the single crystal properties of lead indium niobate.

Keywords: Lead indium niobate; Single phase; Perovskite; Disordered; Antiferroelectric; Dielectric properties

1. Introduction

Lead indium niobate $Pb(In_{1/2}Nb_{1/2})O_3$ (PIN) is an interesting order–disorder relaxor ferroic material. In its disordered state PIN is a relaxor ferroelectric with a pseudo-cubic perovskite structure. Annealing PIN at a suitable temperature causes the material to order into an orthorhombic phase. This phase is antiferroelectric and is isostructural with lead zirconate.

Previous attempts to fabricate single-phase perovskite PIN ceramics in the past have had only limited success. Groves [1] and more recently Park and Choo [3] reported a maximum perovskite content of 95% and 98%, respectively, in their methods of preparing PIN. These two reports, however, use additives of In_2O_3 and Li_2CO_3 to aid in the formation of the perovskite phase. Park [1] showed that a calcined PIN powder could be formed but subsequent sintering steps caused the formation of small quantities of the unwanted pyrochlore phase. Both groups discount any deleterious effects of the pyrochlore phase in such small quantities either on sintering or on their ferroic properties. However, the addition of excess indium and/or lithium does seem to affect the transition temperatures of this material. There may also be possible effects of the pyrochlore phase on the order–disorder behavior of the ceramics. Hence, it is desirable to produce 100% phase-pure perovskite PIN ceramics. In this paper we report the synthesis of PIN with 100% perovskite phase both before and after the sintering process.

2. Experimental and results

Several different methods to synthesize PIN were tried in our approach. The first of which was the

* Corresponding author.

PII S0167-577X(96)00138-3

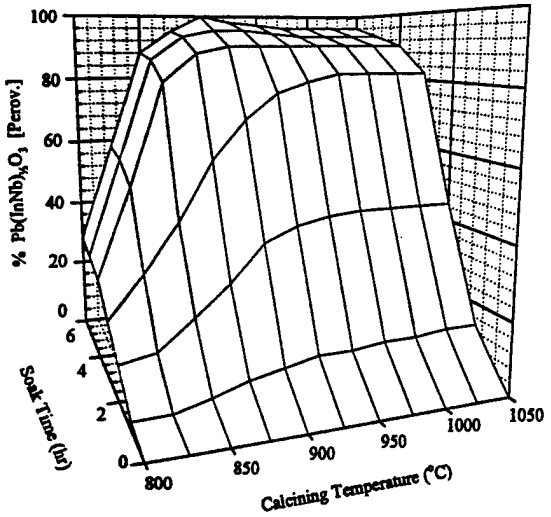

Fig. 1. Effect of calcining conditions on the production of perovskite PIN powders using 2 mol% excess In_2O_3 and 3 mol% Li_2CO_3.

conventional mixed oxide method. Stoichiometric amounts of PbO (100Y electronic grade, Hammond Lead Products), In_2O_3 (99.999%, Cerac Specialty Metals) and Nb_2O_5 (99.99%, Fansteel Metals) were milled in a Nalgene bottle with zirconia media and ball milled for 12 to 18 h in both acetone and alcohol. Following the milling operation, the powder was placed in a drying oven for 24 h at 100°C. Various calcining conditions between 700 and

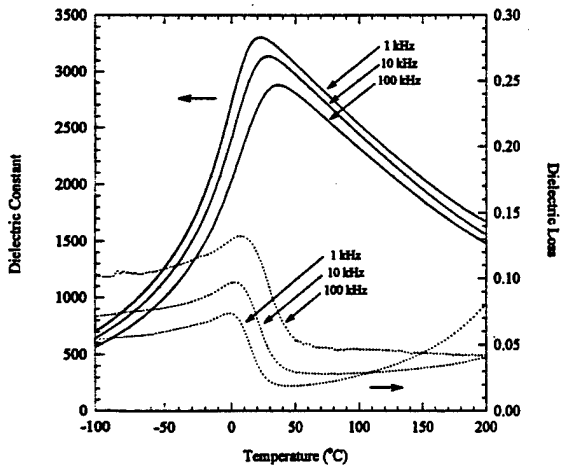

Fig. 2. Dielectric constant and loss of a 98% perovskite PIN ceramic with 2 mol% excess In_2O_3 and 3 mol% excess Li_2CO_3. (Cooling at 4°C/min.)

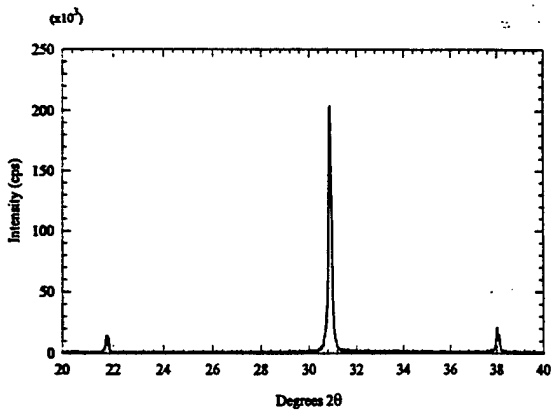

Fig. 3. X-ray diffraction pattern for an undoped phase-pure PIN ceramic.

1200°C were used. It was found that a maximum perovskite content of 80% could be attained after 4 h of calcination at 1050°C. This result is effectively the same as that of pervious reports by Kupriyanov and Fesenko [2], Stenger and Burgraaf [4] and Groves [1].

In our second approach, an indium niobate precursor with the wolframite structure was tried. Swartz and Shrout [5], using a magnesium niobate precursor, were able to synthesize phase-pure lead magnesium niobate (PMN) ceramics. Initial attempts to synthesize PIN with the wolframite method did not enhance the production of the perovskite phase to 100%. The addition of Li_2CO_3 was used, as sug-

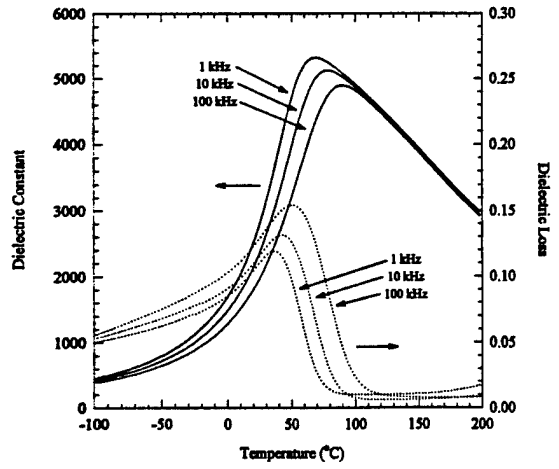

Fig. 4. Dielectric constant and loss for an undoped phase-pure PIN ceramic. (Cooling at 4°C/min.)

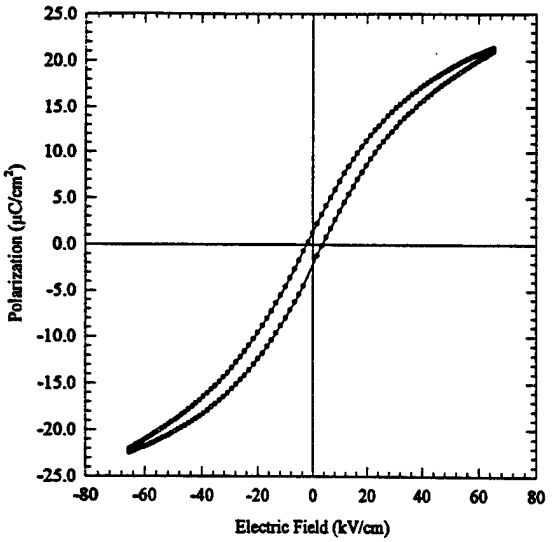

Fig. 5. Dielectric hysteresis loop for an undoped phase-pure PIN ceramic.

gested by Groves in his studies, to increase the perovskite phase content, but, only resulted in a powder containing 90% of the perovskite phase. Both Park and Choo [3] and Groves [1] also reported that excess In_2O_3 should be helpful in enhancing the perovskite phase content. The addition of 2 mol% excess indium in conjunction with control of lead and indium volatilization (requiring sealed crucibles with source powders) resulted in a single phase calcined powder. It was also found that the processing temperature, as well as soak time, had a critical effect on the perovskite content in the indium doped PIN (Fig. 1).

Sintering of these ceramics was done similarly in sealed crucibles at 1050°C for 2 h. This resulted in a ceramic with greater than 98% perovskite phase and 90% theoretical density. The behavior of the dielectric constant as a function of temperature (Fig. 2) for this sample was approximately the same as that found by Groves [1]. However, K and T_m were both lower than those quoted by Park and Choo [3].

Our third approach attempted to synthesize PIN without the previously mentioned doping. Using the wolframite precursor method and an oxygen atmosphere, consistently phase-pure calcined powders were produced. The calcining atmosphere was maintained using an oxygen furnace set at a low flow rate. Lead and indium sources were also added within the crucibles for control of lead and indium volatilization; however, in this case the crucibles were only covered and not sealed.

Using these powders we could easily avoid the formation of the pyrochlore phase and sintered the PIN ceramics into phase-pure perovskite bodies at temperatures as high as 1100°C. Fig. 3 shows an X-ray diffraction pattern of a ceramic with no detectable pyrochlore phase. The dielectric constant showed a maximum value of 5500 at 66°C which is higher than those reported by either of the groups (Fig. 4). The transition temperature was in the same temperature range as reported by Park and Choo [3].

A typical dielectric hysteresis loop of these samples is shown in Fig. 5. The maximum polarization was found to be 22 $\mu C/cm^2$ at a field of 60 kV/cm. Electrostriction measurements were also undertaken on these samples. The maximum strain was found to be approximately 0.08% under electric field (Fig. 5).

3. Conclusions

Single phase perovskite ceramics have been fabricated using the wolframite precursor method and calcining under oxygen. Dielectric properties of these undoped ceramics seem to be superior to those reported by previous investigators. Specifically, the maximum dielectric constant of 5500 is the largest found for a disordered ceramic. The transition temperature was also found to be nearly equal to that of a single crystal. At room temperature the dielectric constant was found to be 2000 with dissipation factor of 0.072. Finally, dielectric hysteresis measurements show a maximum polarization of 22 $\mu C/cm^2$ at a field of 60 kV/cm.

References

[1] P. Groves, Ferroelectrics 65 (1985) 67.
[2] M.F. Kupriyanov and E.G. Fesenko, Sov. Phys. Cryst. 10 (1965) 189.
[3] S.S. Park and W.K. Choo, Ferroelectrics 118 (1991) 117.
[4] C.G.F. Stenger and A.J. Burgraaf, Phys. Stat. Sol. 61a (1980) 275.
[5] S.L. Swartz and T.R. Shrout, Mater. Res. Bull. 17 (1982) 1245.

APPENDIX 10

The effect of ferroelastic coupling in controlling the abnormal aging behavior in lead magnesium niobate-lead titanate relaxor ferroelectrics

Q. M. Zhang, J. Zhao, T. R. Shrout, and L. E. Cross
Materials Research Laboratory, The Pennsylvania State University, University Park, Pennsylvania 16802

(Received 26 January 1996; accepted 27 December 1996)

The abnormal aging behavior, i.e., severe aging in the electric field induced piezoelectric coefficient while very weak dielectric aging, observed in the relaxor ferroelectric lead magnesium niobate-lead titanate (PMN-PT) ceramics under a dc electric bias field, can be significantly reduced by hot isostatic pressing (HIP) treatment on presintered samples. The aging can also be reduced by doping suitable amounts of either La (donor) or Mn (acceptor). We suggest that the reduction in the aging is due to the introduction of additional random fields into the material, which reduces the probability of the growth of micropolar regions into metastable and/or stable macropolar domains. The abnormal aging behavior and the effectiveness of HIP in reducing it indicate the importance of the elastic energy in controlling the aging and relaxor behavior in PMN-PT relaxor ferroelectrics.

I. INTRODUCTION

Aging or the change of the material properties with time is of great concern in many areas of application for ferroelectric ceramics. In the past decade, there were many experimental investigations devoted to the aging phenomena in the relaxor ferroelectric materials, especially in PMN-PT ($Pb(Mg_{1/3}Nb_{2/3})O_3$–$PbTiO_3$) and PLZT (lanthanum modified lead zirconate titanate) solid solution systems.[1–4] The objective of these investigations was to identify the basic mechanisms associated with aging phenomena so that they can be minimized and also to elucidate the polarization mechanism in this class of materials. From those investigations, it was found that aging in PMN-PT and PLZT exhibits quite different behaviors compared with those in normal ferroelectric ceramics such as barium titanate and lead zirconate titanate and is more complex.[5] For instance, as revealed by several recent experiments, aging of the dielectric behavior in PMN-PT depends strongly on the frequency and occurs even at temperatures where the material is in the pseudo-cubic phase (nonferroelectric phase). In addition, aging was found to be not log linear with time, but follows a time dependent curve of stretched exponential type:

$$d = d_\infty + d_1 \exp[-(t/\tau)^\nu] \qquad (1)$$

where t is the aging time, d_1 represents the part of the material constant varying with time and d_∞ is the time independent part, and τ measures the aging rate. Hence, the ratio of d_1/d_∞ in Eq. (1) is a measure of the degree (or amount) of aging in the corresponding property.[6,7] Equation (1) describes a relaxation process with a broad distribution of relaxation times and a smaller ν ($\nu \leq 1$) corresponds to a broader distribution of relaxation times.[8] As has been reported in an earlier publication, in PMN-PT, ν changes with temperature and decreases as the temperature approaches T_m, the temperature of dielectric constant maximum. In addition, the amount of aging increases as the aging temperature is lowered toward T_m.[6]

In a more recent investigation, it was found that in relaxor PMN-PT ceramics, the amount of aging increases with PT content. For specimens aged under a dc bias field, it was also shown that the direction of the defect electric field developed during the aging is opposite to that of the applied dc bias field. In addition, the piezoelectric coefficients in the field-biased state exhibited more severe aging relative to the dielectric aging under the same condition. From these observations, it was suggested that the aging in the field-biased state may be closely related to the growth of the micropolar regions into metastable (and stable) macropolar domains. Furthermore, it was proposed that the interaction of the polarization with the stress field plays a very important role in the aging process.[6]

The aim of the present study is to explore possible ways to reduce or eliminate the aging observed and to search for the possible mechanisms of the aging phenomena in the relaxor PMN-PT in the electric field-biased state. Undoubtedly, aging in the relaxor ferroelectric materials is a very complicated process which involves both a change in the defect structures and host lattice, as well as the interaction between them. Even for normal ferroelectric ceramics where the polarization mechanism is relatively well understood, many questions concerning

the aging mechanisms remain, such as what are the relevant structural changes occurring in the material in the aging process and how the domain boundaries interact with and are stabilized by the defect fields developed during the aging process. Hence, the main focus of the work will be to present experiment results in a logical manner along with the rationale behind the study, and the possible conclusions can be drawn from these experiments.

II. EXPERIMENTAL

All the specimens used in this investigation were made by the mixed oxide method following the columbite B-site precursor method as described by Swartz and Shrout.[9] Most of the specimens were sintered at a temperature of 1250 °C for 2–6 h followed by annealing in an oxygen-rich atmosphere at 900 °C for 6–24 h. Other sintering and annealing conditions were also tried to examine their effect on the aging process. In spite of some variations in the aging rate and amount of aging as these conditions varied, no significant improvement and systematic trend in the aging processes were observed. Our earlier study showed that during the aging process, there was a buildup of a defect field originated from space charges trapped at the porous regions. Hot isostatic pressing (HIP) was used to densify the specimens to minimize these regions. The density of HIP samples is at about 99.5% theoretical density compared with 95% for the conventionally sintered samples. In this study, HIP was carried out at 1100 °C under 20 MPa pressure in air. HIP samples were subsequently annealed in an oxygen-rich atmosphere at 900 °C for 6 h. Figure 1 presents the SEM data on fractured surfaces for samples (0.72PMN–0.28PT) before and after the HIP.

The aging experiments were performed in the temperatures above T_m, i.e., the phase diagram region labeled "cubic" in Fig. 2, and at compositions with PT content below the morphotropic phase boundary (MPB) (PT $< 33\%$) where the materials are in the relaxor region and exhibit typical electrostrictive behavior,[10,11] and for the specimens under a dc bias field. In this phase diagram region, the strain (S) is related to the applied electric field (E) through a quadratic relationship, $S = ME^2$ where the proportional constant M is termed as the electric field related electrostrictive coefficient. For many device applications, a dc bias field E_{bias} is applied onto the specimen to break the center of symmetry, and under this condition, the strain versus electric field follows approximately a linear relationship which can be described by an effective piezoelectric coefficient d ($d = \Delta S/\Delta E$).

Both pure PMN-PT and PMN-PT doped with La [$y \leq 1$ in $(Pb_{(1-3y/2)}La_y)(Mg_{1/3}Nb_{2/3})_{(1-x)}Ti_xO_3$)] and with

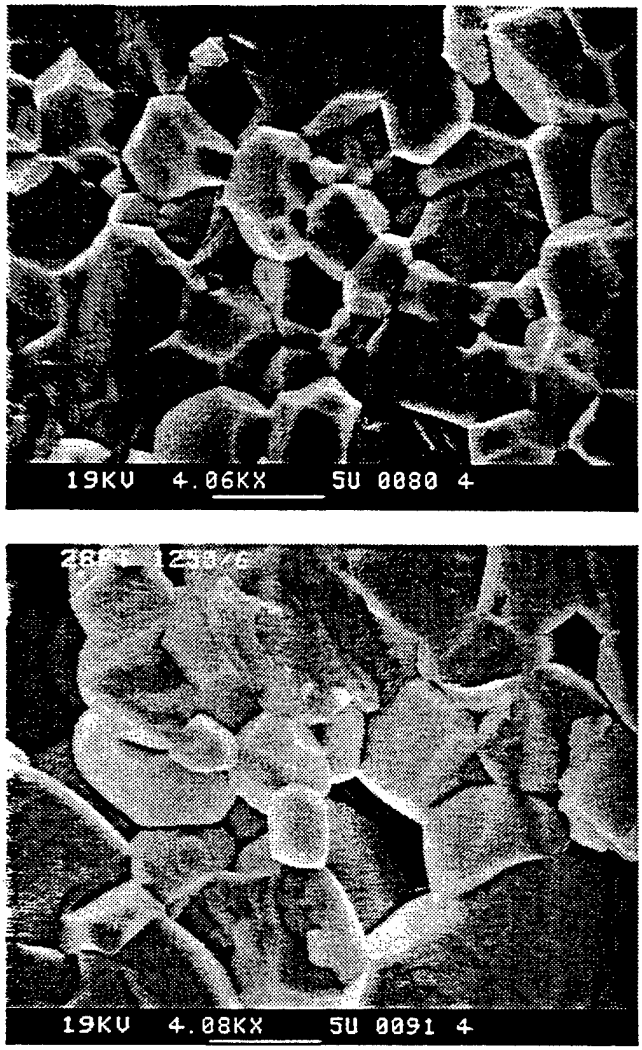

FIG. 1. SEM data on fractured surfaces of 0.72PMN–0.28PT before (lower figure) and after (upper figure) the HIP.

Mn were investigated. In a previous publication, we showed that as the composition approaches the MPB, the aging in the field-biased state becomes severe.[6] Hence, the current investigation was concentrated on the phase diagram region near the MPB.

The change of the dielectric constant, the effective piezoelectric coefficient, and the polarization level at the dc field biased state as a function of time were recorded simultaneously. This is quite different from most of the earlier aging experiments where only the dielectric aging was investigated, and hence the results provide more complete information about the aging process. The piezoelectric coefficient, either d_{33} or d_{31}, was measured by a double beam laser dilatometer.[12] The dielectric aging under a dc bias field was evaluated using a setup shown in Fig. 3 where the current passing through the small resistor R was measured and the polarization level was determined by a standard Sawyer–Tower circuit.[13] In all these experiments, the temperature was controlled

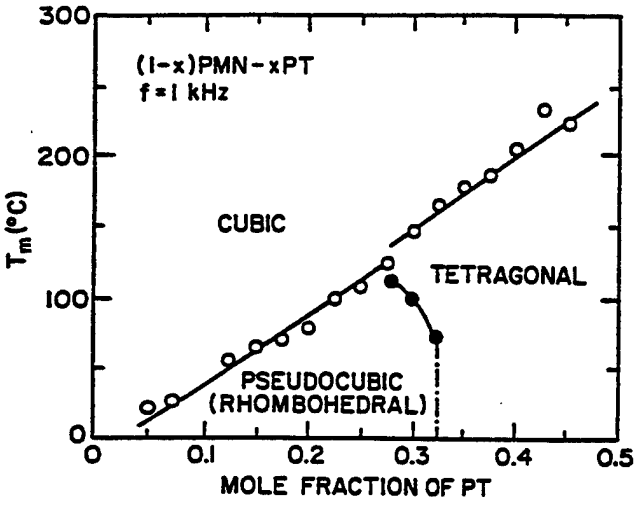

FIG. 2. Phase diagram of the PMN-PT solid solution system (from Choi *et al.*[10]).

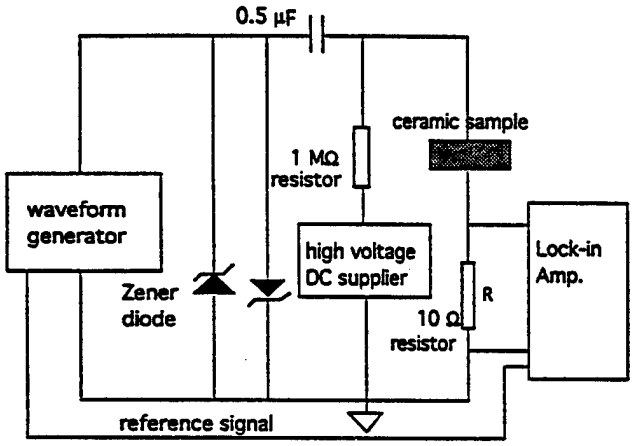

FIG. 3. Schematic drawing of the experimental setup used to measure the dielectric constant of PMN-PT under a dc bias field.

within ±0.1 °C by a LakeShore temperature controller (model 321). The sample thickness is 1 mm and the area is about 25 mm^2. In addition, the dielectric constant and the current released during the sample heating were acquired as a function of temperature for samples without dc bias fields. The capacitance measurement was made with a multifunction LCR meter (HP 4274A), and the current was measured with a pA meter (HP 4140B). For these experiments, the temperature change was provided by a Delta temperature chamber controlled by a HP computer. To probe the change in the structure due to the HIP process, x-ray powder diffraction measurement was also carried out using a Scintag diffractometer (Cu K_α source).

Although the aging rate and the amount of aging vary with frequency and dc bias field level, which are interesting and deserve detailed investigation, they are not the theme of the paper and the general trends reported here will not change markedly with these variables as revealed by the experimental observations. The data on the aging behavior reported here are at a fixed frequency of 1 kHz with a dc bias field level of 5 kV/cm.

III. RESULTS AND DISCUSSION

A. Effect of HIP

Shown in Fig. 4 are the aging data for HIP samples of the composition 0.68PMN–0.32PT doped with 1 mole % La which has T_m at a temperature near 129 °C. Compared with the aging data for conventionally sintered samples of the same composition as shown in Fig. 5, it is obvious that HIP significantly reduces and nearly eliminates aging in both the dielectric constant and the effective piezoelectric coefficient. To make a quantitative comparison, Eq. (1) is used to fit the data in

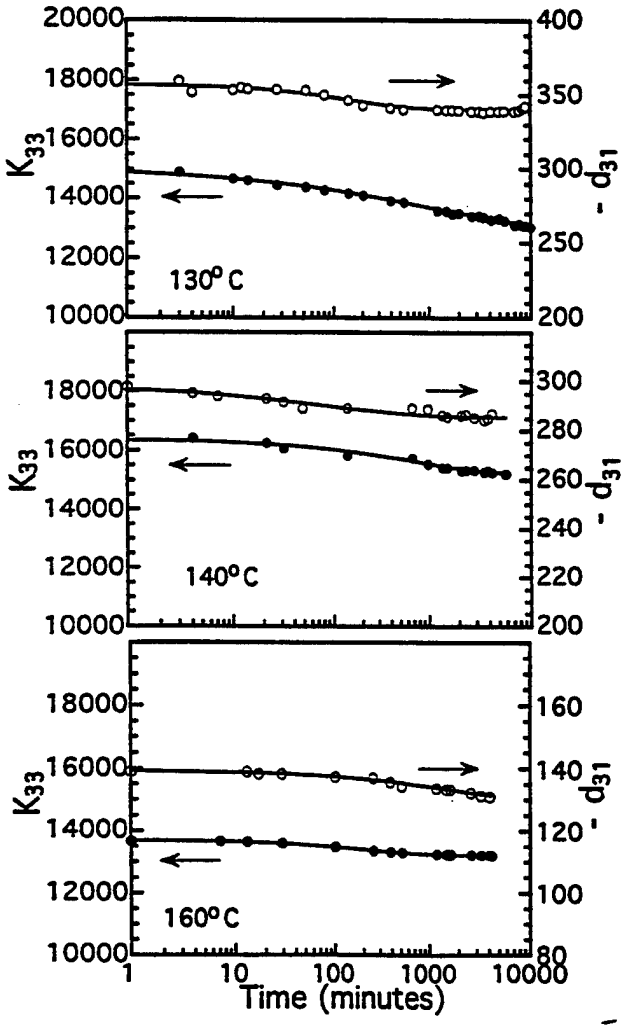

FIG. 4. Aging data for HIP samples of composition 0.68PMN–0.32PT doped with 1 mole % La. The solid lines are the fitting using Eq. (1), and solid circles and open circles are the experimental data points. The experimental temperatures are indicated in the figure and the bias field is 5 kV/cm.

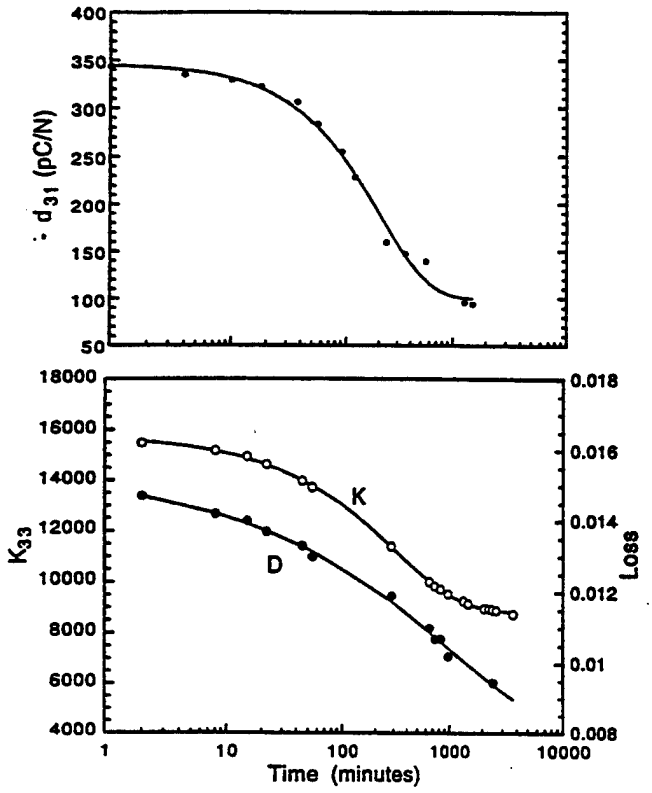

FIG. 5. The aging data for regularly sintered samples of composition 0.68PMN–0.32PT doped with 1 mole% La. The solid lines are the fitting using Eq. (1), and solid circles and open circles are the experimental data points. The bias field is 5 kV/cm and the temperature is 140 °C. The data here are for the comparison with those in Fig. 4 and, clearly, HIP nearly eliminates the aging in the samples.

Figs. 4 and 5 and the results are listed in Table I. Aging experiments were also carried out on other PMN-PT compositions, and similar results were obtained.

The results demonstrate that the HIP treatment on presintered ceramic specimens is a very effective means in reducing or eliminating the observed aging in relaxor PMN-PT. To shed some light on the possible mechanisms behind this improvement on the aging properties in HIP specimens, it is instructive to consider first what might happen in the aging process of relaxor PMN-PT under a dc electric field.

TABLE I. Comparison of the amount of aging in d_{31} and K_{33} (Figs. 4 and 5) for 0.68PMN–0.32PT doped with 1% La for HIP and non-HIP samples.[a]

	d_{31}; d_1/d_∞		K_{33}; K_1/K_∞	
Temp.	HIP	Non-HIP	HIP	Non-HIP
130 °C	0.049		0.12	
140 °C	0.046	2.5	0.08	0.8
160 °C	0.06		0.04	

[a]For dielectric constant, Eq. (1) is written as $K = K_\infty + K_1 \exp[-(t/\tau)^v]$.
For the piezoelectric coefficients, Eq. (1) is in the form of $d = d_\infty + d_1 \exp[-(t/\tau)^v]$.

From the current understanding on the relaxor ferroelectrics, the polarization mechanism in the material is from the micropolar clusters and their dynamic nature and the induced ferroelectric transition in the nonpolar microregions.[14,15] The response of these micropolar and nonpolar regions to external fields yields the observed large dielectric constant and electrostrictive strain. The inability of the micropolar regions to grow in size as the temperature is lowered is due to the existence of local random fields that lower the local symmetry compared with the global symmetry and prevent the development of normal long-range order.[16] The existence of such randomness or random field is crucial for the material to exhibit relaxor behavior. When a dc bias field is applied to the material, it will tend to overcome the local random fields and induce a macroscopic polarization (coalescing of the micropolar regions). Now the question is whether this process is fully reversible, that is, as one reduces this external ordering field, whether the original state will be fully recovered. Clearly, it will depend on the magnitude of the energy barriers in breaking up a large polarization region into microregions, which are functions of temperature and related to the microstructures, and also depend on the temperature where the aging experiment is performed. For a material with strong local random fields, this process will be nearly fully recovered and no aging or very small aging in the material properties will be expected. This could be the situation for the PMN-PT at low PT content where the material shows very little aging. As the composition approaches the MPB, earlier experimental results from dielectric constant measurements and transmission electron microscopy (TEM) studies already showed that the material becomes more normal-ferroelectric-like, i.e., a reduction in the dielectric dispersion, a sharpening in the dielectric constant peak, and the disappearing of "random" structural inhomogeneity on the nanometer scale.[10,17] Therefore, it is expected that under a dc bias field there is an increased probability to form large size polar domains which may not be switchable thermally and will not follow the change of external fields. The slow increase of the population of large metastable (and/or stable) polar domains with time should be one of the causes for the observed aging here.

In aged samples, by reversing the direction of dc bias field, the induced piezoelectric constant can be recovered in a large part (more than 90%). This is consistent with the fact that the large polar regions formed during the aging are broken up by a reverse electric field which causes the polarization switching in the material.

As we have shown in an earlier publication and the data in Fig. 4, in the dc field-biased state, the aging in the piezoelectric coefficient is more severe compared with

the dielectric aging under the same dc bias. In some cases, the dielectric constant shows very little aging while a severe aging is observed in the piezoelectric coefficient as shown in Fig. 6 which was taken from 0.72PMN–0.28PT at 140 °C (T_m = 138 °C). We do not have the explanation on why in some specimens, although the dielectric aging is relatively weak compared with the aging in the piezoelectric coefficient, it is still substantial (the data in Fig. 5), while for other specimens, the dielectric aging is very little (the data in Fig. 6).

From the thermodynamics consideration, for an electrostrictive material biased under an external field, the effective piezoelectric coefficient d_{ij} has the relationship:

$$d_{33} = 2Q_{11}K\epsilon_0 P \quad (\text{or } d_{31} = 2Q_{12}K\epsilon_0 P), \quad (2)$$

where Q_{ij} is the charge-related electrostrictive coefficient, P is the polarization level at the dc biased state, K is the dielectric constant, and ϵ_0 is the vacuum dielectric permittivity.[18] Equation (2) suggests that there should be reduction in either P or Q_{ij}, or both in the aged sample if K does not change very much during the aging. Our experimental results indicate that P is indeed reduced in the aging process. However, for all the specimens measured, the reduction in P is too small to account for the reduction in d_{ij}. Hence, it is Q_{ij} that bears the main responsibility for the aging in d_{33} and d_{31}. In other words, the polarization slowly loses its ferroelastic component in the aging process. In terms of the polar region reorientation processes which are responsible for the large polarization and strain in PMN-PT, the results imply that the energy barriers for the polarization switching processes which generate strain response in the material are much higher than those for the pure ferroelectric polarization switching processes, which generate only the dielectric response. It should be pointed out that while the former processes must be originated from the non-180° polarization reorientation or switching processes and the change of polarization level in the nonpolar regions, the latter can involve both the pure 180° polarization change and some collective non-180° polarization reorientation processes which do not generate net strain response in the material such as the processes proposed by Arlt and the process involving two simultaneous 90° polarization switchings, which is equivalent to a net 180° polarization switch in the material.[19] As the specimen ages, the total polarization regions participating in non-180° polar reorientations and the reversible polarization changes which contribute to the strain response diminish while the total polarization regions participating in 180° polar reorientations (including the collective non-180° reorientations which do not generate strain response in the material) may not change or even increase as reflected by the small dielectric aging observed. Hence, in this abnormal aging process most of the polarization regions in the material are not pinned, but instead, are converted from the non-180° motions to the 180° motions.

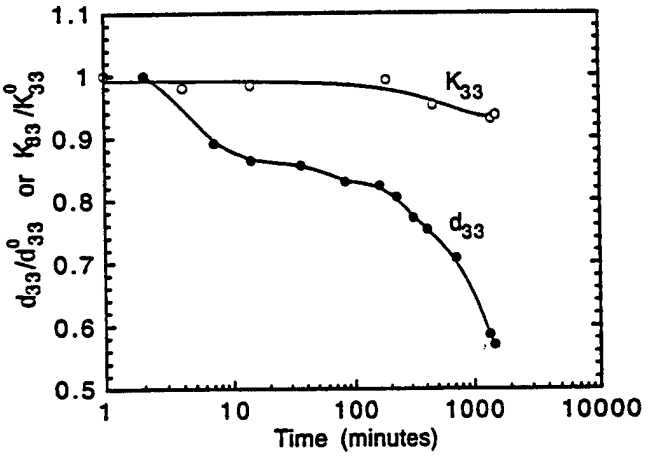

FIG. 6. The abnormal aging behavior where the piezoelectric coefficient exhibits severe aging while the dielectric aging is very weak. The data are taken from regularly sintered samples of composition 0.72PMN–0.28PT. The experimental temperature is 140 °C and the bias field is 5 kV/cm. The solid lines are drawn as a guide to the eyes, and open and solid circles are the data points.

From a previous study, it was found that during aging, there is a buildup of an internal defect field whose direction is against that of the applied dc field. We believe that this field is the result of drifting space charge deposited at the pore regions as schematically shown in Fig. 7. For a ceramic specimen sintered using a conventional method which has about 95% theoretical density, there are porous regions inside grains and in the grain boundaries as shown in Fig. 1 which serve as the sites to trap the space charges as they drift under an external dc field. HIP, which densifies the specimen to 99.5% theoretical density, reduces these regions and the defect field associated with them significantly as observed experimentally. The defect field schematically shown in Fig. 7 can also provide some explanation to the large decrease in the piezoelectric coefficient and small change in the dielectric constant in the aging process if we assume that this defect field does not pin the polarization except reversing the field direction locally. However, the data from the Mn-doped specimens presented below seem to indicate that this effect cannot be the major source for the observed abnormal aging behavior.

Therefore, the results indicate that the interaction of the polar regions with the stress field, i.e., the ferroelastic coupling, plays a major role here in producing the abnormal aging and in determining the response behavior in relaxor PMN-PT. Hence, this effect may be effective in breaking the local symmetry and generating the relaxor response.

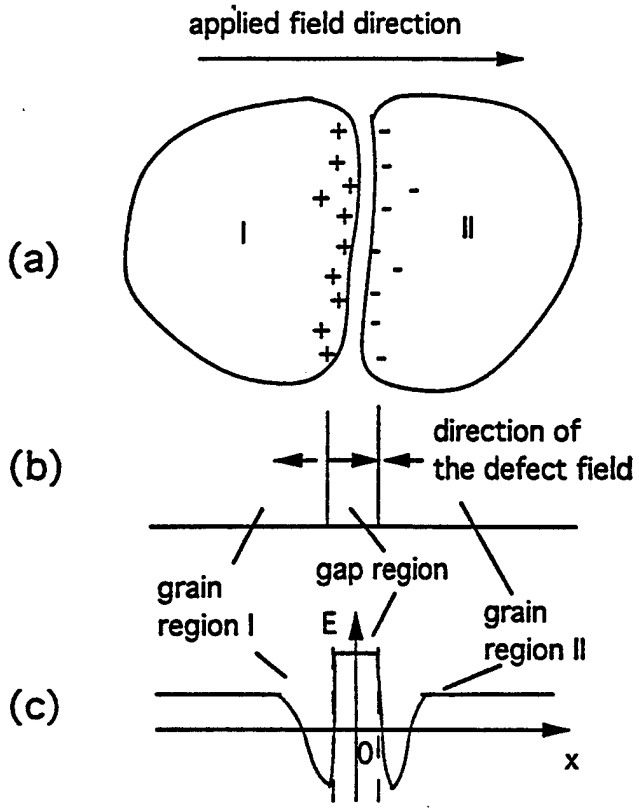

FIG. 7. Schematic drawing of the space charge distribution and the resulting defect electric field near the gap or grain boundary region for PMN-PT under dc bias field. (a) shows the space charge distribution, (b) shows the directions of the defect field in the gap region and inside the grains, and (c) shows the spatial distribution of the total electric field inside the sample.

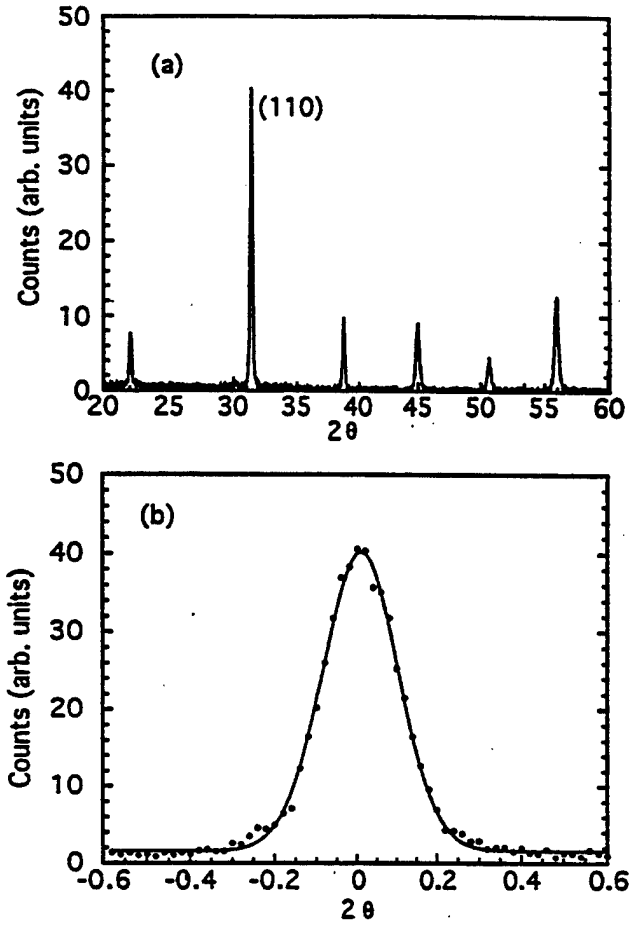

FIG. 8. (a, b) X-ray powder diffraction data of HIP samples of composition 0.7PMN–0.3PT doped with 1 mole% La (top figure) and the fitting of the (110) diffraction peak with a Gaussian line shape (bottom figure). In the bottom figure, the solid curve is the fitting of a Gaussian line shape from which FWHM is calculated and solid circles are the data points.

Based on the discussion above, the possibility of random stresses introduced in the HIP and subsequent O_2 annealing process in the specimens was examined. A series of x-ray diffraction measurements were carried out on HIP and conventionally sintered samples. Shown in Fig. 8 are the x-ray powder diffraction data taken from 0.7PMN–0.3PT with 1% La HIP sample (annealed in O_2 atmosphere). Listed in Table II are the peak width measured in full width at half maximum (FWHM) for HIP and regularly sintered samples of this composition. Apparently, the peak width of the samples treated with HIP and O_2 annealing is approximately 10% wider than that of the conventionally sintered samples. Similar results were also observed for other composition samples. The broadening of the x-ray diffraction peak width in the HIP samples is interpreted as the evidence for a nonuniform microstrain distribution.[20] From the data in Table II, it can be estimated that the nonuniform strain distribution introduced by HIP is at about 0.05% strain level in the sample (measured in FWHM). The significant reduction of the aging in HIP samples may be in part due to this inhomogeneous strain pattern and stress field which should be in the μm and sub-μm spatial scales and through the ferroelastic coupling, prevent the formation of large size metastable (and/or stable) polar clusters.

TABLE II. The x-ray peak width (measured in full width at half maximum in degrees for θ) for HIP and conventionally sintered samples.

Diffraction peak	100	110	111	200	210	211
HIP sample	0.1087	0.1136	0.110	0.176	0.183	0.180
Regular sample	0.0963	0.1055	0.105	0.162	0.166	0.163

B. Effect of doping

From the analysis and data presented thus far, it seems that to reduce the aging in the field-biased state, a material should be moved into a state that is more relaxor-like. In the relaxor PMN-PT system, it has been shown that La doping will move the material into a more relaxor state as indicated by a broadening of the

dielectric constant peak and a lowering of T_m.[21] Hence, by doping with a suitable amount of La, one would expect to achieve a reduction of the aging in the material. The experimental results performed here confirm this and are consistent with those from the earlier investigations.[4] However, the reduction is not as significant as the HIP treatment.

On the other hand, the experimental results here show that a small amount of Mn doping also results in a reduction in the aging. Shown in Fig. 9 are the aging data taken from the specimens of La-modified 0.71PMN–0.29PT with and without Mn doping (0.05 wt.%). The two samples show very different aging characteristics, and the piezoelectric coefficient of the Mn-doped samples exhibit smaller aging. For comparison, the dielectric constant as a function of temperature of the two samples was also measured and presented in Fig. 10. A reduction in the maximum dielectric constant and broadening of the peak width are observed for the Mn-doped sample, suggesting that the Mn-doped sample is more relaxor-like compared with the non-Mn-doped sample. In addition, the low frequency dielectric loss at high temperature region, which is likely associated with the space charge conduction, is reduced significantly.

There are additional changes observed in Mn-doped samples:

(i) The direction of the defect field established during aging becomes parallel to the external dc bias field. After these aged specimens were cooled down to room temperature under no external dc bias field, the remanent d_{33} value was measured using a Berlincourt

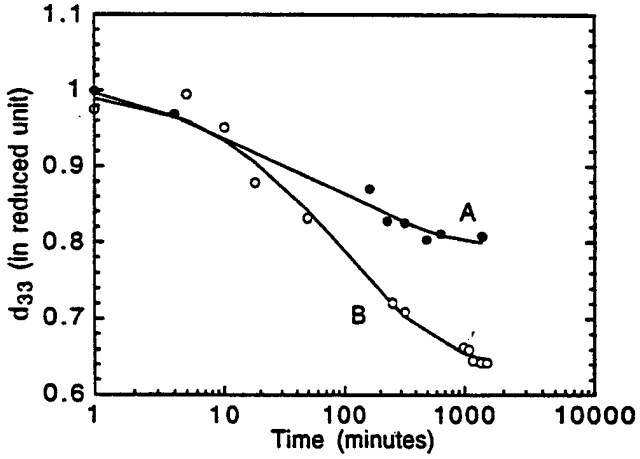

FIG. 9. Aging data illustrating the reduction of the aging in the piezoelectric coefficient in the dc electric field biased state. The curve A is from the Mn-doped sample (0.05 wt.%) and the curve B is from the sample without Mn doping (0.71PMN–0.29PT with 0.5% La). Open and solid circles are the data points, and solid lines are drawn to guide the eye.

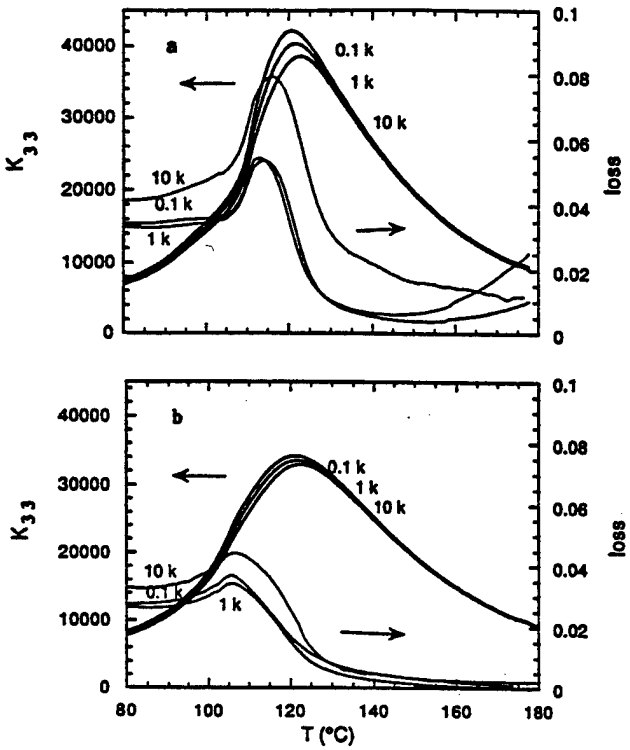

FIG. 10. Dielectric constant and dielectric loss as a function of temperature for conventionally sintered samples: (a) 0.71PMN–0.29PT with 0.5% La, and (b) 0.05 wt.% Mn doped 0.71PMN–0.29PT with 0.5% La.

d_{33} meter. For Mn-doped specimens, the d_{33} was found to be positive while for nondoped specimens, the d_{33} was negative.

(ii) Shown in Fig. 11 are the experimental results of charge release during the sample heating for aged samples. In these experiments, the aged samples were cooled down to room temperature without a dc bias field, and the current released as the samples were heated up in a constant temperature rate was measured. For non-Mn-doped samples (curves *a* and *b*), the charge released from trapped space charges was observed at a temperature near and above their T_m. These charges were compensated by the local polar regions at low temperatures ($<T_m$). The release of these charges as a result of the vanishing of local polarization at temperatures above T_m gives rise to the irregular current curve observed. On the other hand, for Mn-doped samples (curve *c*), as a result of the stabilization of polar regions by the defect field associated with Mn which has the same direction as that of the applied dc bias field, a well-defined pyroelectric peak was observed.[3]

These results indicate that Mn doping significantly reduces the mobile space charges in the host lattice. In addition, it is also likely that Mn defects in the host lattice trap oxygen vacancies, which are believed to be quite mobile in perovskite structure, to form a

$Mn^{2+}-V_O^{\cdot\cdot}$ (and/or $Mn^{3+}-V_O^{\cdot\cdot}$) complex, producing defect dipoles.[22,23] As a result, the defect field due to the accumulation of the drifting space charge in the porous regions observed in the non-Mn-doped samples is eliminated. It may be the combined effects of the reduced space charges and the irregularities introduced by the random distribution of the $Mn^{2+}-V_O^{\cdot\cdot}$ (and/or $Mn^{3+}-V_O^{\cdot\cdot}$) complex in the lattice which reduce the aging in the material.

For both La-doped and Mn-doped samples, HIP followed by O_2 annealing significantly reduces or nearly eliminates the aging in both the piezoelectric coefficient and dielectric constant in the field-biased state.

IV. SUMMARY

This paper shows that the abnormal aging behavior, i.e., severe aging in the piezoelectric coefficient and weak dielectric aging, observed in relaxor PMN-PT in the electric field biased state can be nearly eliminated by HIP treatment on presintered ceramic samples. The aging can also be reduced by doping suitable amounts of either La (donor) or Mn (acceptor).

The results suggest that the aging observed in relaxor PMN-PT is due to the growth of the metastable and/or stable polar regions under the bias field (or defect field). Hence, by moving the material deeper into the relaxor state (by introducing extra randomness in the material by doping and HIP), the aging can be reduced or nearly eliminated. The abnormal aging behavior reveals that the growth of the micropolar regions does not have a significant effect on the 180° polarization reorientation process, which is pure ferroelectric in nature. In other words, for PMN-PT the energy barriers for the pure non-180° polarization reorientation processes which generate both the polarization and strain responses in the material are much higher than those of the 180° polarization reorientation process and the collective non-180° processes which do not change the macroscopic strain state in the material. Therefore, by HIP treatment, which introduces random stress fields into the sample, one can effectively reduce or nearly eliminate the aging in PMN-PT in the field-biased state. These results also indicate the importance of the elastic energy in controlling the relaxor behavior in PMN-PT in comparison with the electric energy.

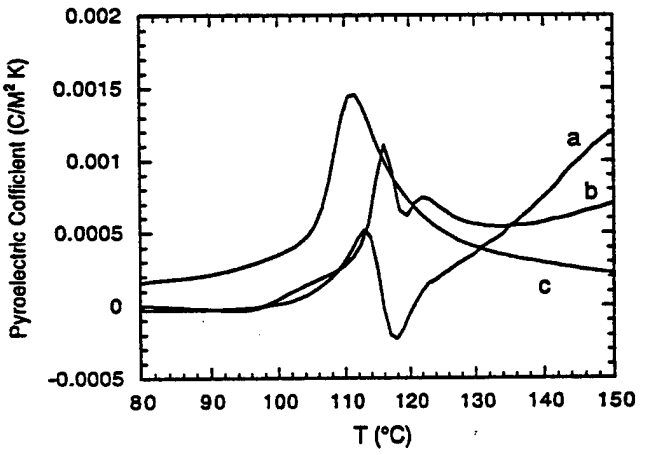

FIG. 11. Comparison of the charge release data for Mn doped and undoped samples. All the samples were aged at 140 °C for more than one day under a 5 kV/cm dc bias field. The data were taken during heating (heating rate is 2 °C/min) after the dc bias field was removed and the samples were subsequently cooled down to room temperature. Curve *a* is 0.735PMN–0.265PT, curve *b* is 0.71PMN–0.29PT with 0.5 mole% La, and curve *c* is from the sample in *b* doped with 0.05 wt.% MnO.

ACKNOWLEDGMENTS

The authors wish to thank Professor S.J. Jang for many stimulating discussions. This work was supported in part by a contract from Tektronix, Inc. and in part by the Office of Naval Research.

REFERENCES

1. W.A. Schulze, J.V. Biggers, and L.E. Cross, J. Am. Ceram. Soc. **61**, 46 (1978).
2. G. Borchhardt, J. von Cieminski, and G. Schmidt, Phys. Status Solidi (a) **59**, 749 (1980).
3. W. Pan, E. Furman, G.O. Dayton, and L.E. Cross, J. Mater. Sci. Lett. **5**, 647 (1986).
4. T.R. Shrout, W. Huebner, C.A. Randall, and A.D. Hilton, Ferroelectrics **93**, 361 (1989).
5. W.A. Schulze and K. Ogino, Ferroelectrics **87**, 361 (1988).
6. Q.M. Zhang, J. Zhao, and L.E. Cross, J. Appl. Phys. **79**, 3181 (1996).
7. T. Nomura, N. Kawano, J. Yamamatsu, T. Arashi, Y. Nakano, and A. Sato, Jpn. J. Appl. Phys. **34**, 5389 (1995).
8. K.L. Ngai, A.K. Rajagopal, and C.Y. Huang, J. Appl. Phys. **55**, 1714 (1984).
9. S.L. Swartz and T.R. Shrout, Mater. Res. Bull. **17**, 1245 (1982).
10. S.W. Choi, T.R. Shrout, S.J. Jang, and A.S. Bhalla, Ferroelectrics **100**, 29 (1989).
11. S.J. Jang, Ph.D. Thesis, The Pennsylvania State University (1979).
12. Q.M. Zhang, S.J. Jang, and L.E. Cross, J. Appl. Phys. **65**, 2807 (1989).
13. J.K. Sinha, J. Sci. Instrum. **42**, 696 (1965).
14. L.E. Cross, Ferroelectrics **76**, 241 (1987).
15. G.A. Smolenskii, J. Phys. Soc. Jpn. **28**, 26 (1970).
16. D. Viehland, S. Jang, L.E. Cross, and M. Wuttig, Philos. Mag. B **64**, 335 (1991).
17. A.D. Hilton, C.R. Randall, D.J. Barber, and T.R. Shrout, Ferroelectrics **93**, 379 (1989).
18. A.F. Devonshire, Philos. Mag. **3**, 85 (1954).
19. G. Arlt, private communications.
20. B.D. Cullity, *Elements of x-ray diffraction* (Addison-Wesley Publishing Company, Inc., Reading, MA, 1977).
21. N. Kim, M.S. Thesis, The Pennsylvania State University (1990).
22. P.V. Lambeck and G.H. Jonker, Ferroelectrics **22**, 729 (1978).
23. D.M. Smyth, Prog. Solid State Chem. **15**, 145 (1984).

APPENDIX 11

Ferroelectrics, 1996, Vol. 188, pp. 109–124
Reprints available directly from the publisher
Photocopying permitted by license only

THE PIEZOELECTRIC, ELASTIC AND DIELECTRIC CONSTANTS FOR CERAMICS IN THE SOLID SOLUTION: $(x)\ PbZrO_3 - (1 - x - z)\ Pb(Zn_{1/3}Nb_{2/3})O_3 - (z)\ PbTiO_3$

EDWARD F. ALBERTA and AMAR S. BHALLA
The Pennsylvania State University, Materials Research Laboratory, University Park, Pennsylvania 16802, USA

and

T. TAKENAKA
Faculty of Science and Technology, Science University of Tokyo, Noda, Chiba-ken 278, Japan

(Received June 7, 1995; in final form January 8, 1996)

In earlier work the existence of a morphotropic phase boundary separating an antiferroelectric and a ferroelectric phase has been found in the solid solution system $(x)\ PbZrO_3 - (1 - x - z)\ Pb(Zn_{1/3}Nb_{2/3})O_3 - (z)\ PbTiO_3$ [PZNT (x/z)]. This paper further explores the electrical field dependence of various material properties near this boundary. Some of those properties measured are the piezoelectric coefficients (d_{31}, k_{31} and k_p), the dielectric constant (ε_{33}), and the elastic constant (s^E_{11}). In addition, the pyroelectric effect and hysteresis behavior are also examined.

Keywords: Relaxor ferroelectrics, PZN-PT-PZ, field dependent properties.

INTRODUCTION

Material systems capable of altering their physical properties in response to environmental changes are becoming increasingly attractive. Applications of these very smart systems are indeed numerous. A few of these are: mechanical vibration control, acoustic damping, aerodynamic flow control, micro-positioning, chemical detection, and temperature control. Piezoelectric sensor/actuator materials seem to be promising candidates for use in many of these applications.[1]

Control over the piezoelectric response is the key to the operation of such a device. Previous work by Kumar[2] has shown that the elastic properties of a multilayer piezoelectric transducer can be altered in response to an applied stress. This was accomplished by sensing the stress applied to the device and subsequently altering the applied driving voltage. Another of smart piezoelectric devices is the tunable transducer. This type of transducer exploits the non linearity in the piezoelectric response that is found in some materials. Previous work by Taylor[3] has shown that the morphotropic phase boundary composition $0.9Pb(Mg_{1/3}Nb_{2/3})O_3 - 0.1PbTiO_3$ [PMN:PT] displays this form of nonlinear piezoelectric response. By applying a small dc bias to the material, d_{33} can be seen to increase from 0 pC/N at zero field to a maximum of 1500 pC/N at 3.7 kV/cm.

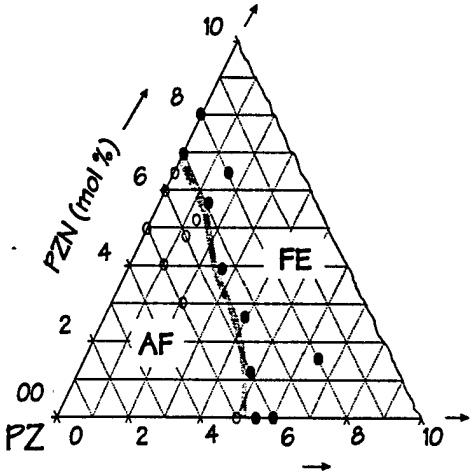

FIGURE 1 Ternary phase diagram of the PZN-PZ-PT system showing the room temperature antiferroelectric-ferroelectric morphotropic phase boundary.

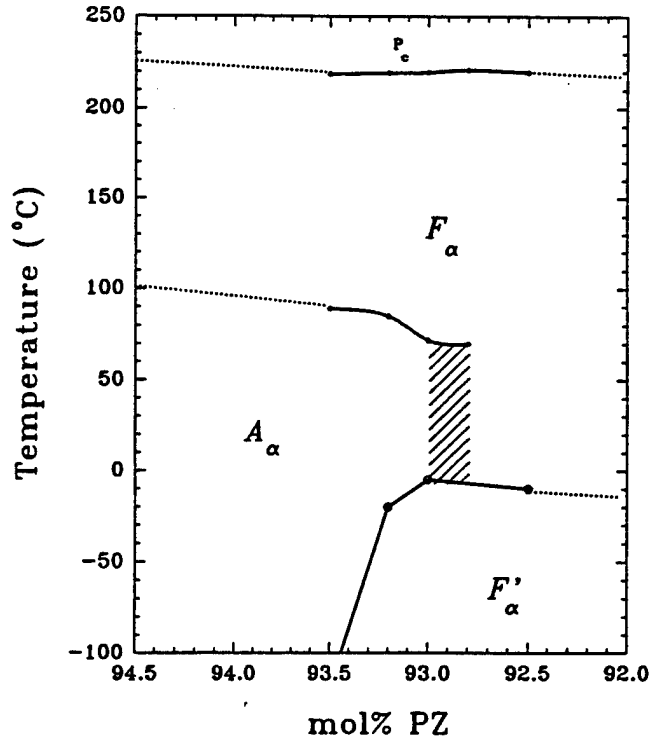

FIGURE 2 Binary phase diagram of the PZN-PZ system showing the antiferroelectric-antiferroelectric morphotropic phase boundary.

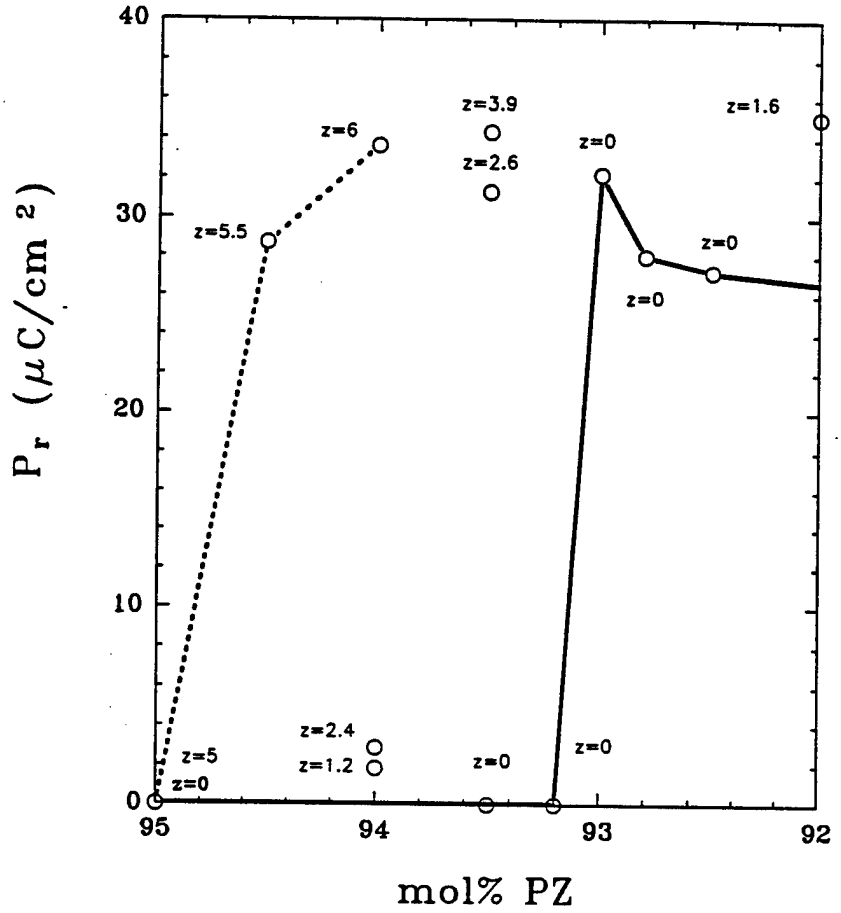

FIGURE 3 Summary of remanent polarization data as a function of composition measured at room temperature. Solid line indicates the data for PZZN. Dashed line indicates the data for PZT. Subscripts indicate the cocentration of PT (i.e. z = mol% PT).

The PZNT system, due to similarities with PMN:PT, was thought to possibly exhibit analogous behavior. Takenaka[4] first explored this system near the room temperature orthorhombic to rhombohedral morphotropic phase boundary. Remanent polarizations of approximately 30 $\mu C/cm^2$ and piezoelectric coupling factors of k_{15} ~ 58%, k_{33} ~ 30% and k_{31} ~ 10% were found. The system was also thought to be promising for pyroelectric applications due to relatively large values of the pyroelectric coefficient and low dielectric constant in compositions with this rhombohedral phase transition near room temperature.

This paper reports the electric field dependence of various material parameters. Among these are the real and imaginary parts of the dielectric constant (ε_{33}), elastic compliance (s_{11}^E), and the piezoelectric coefficient d_{31}. Also, hysteresis and pyroelectric properties are addressed.

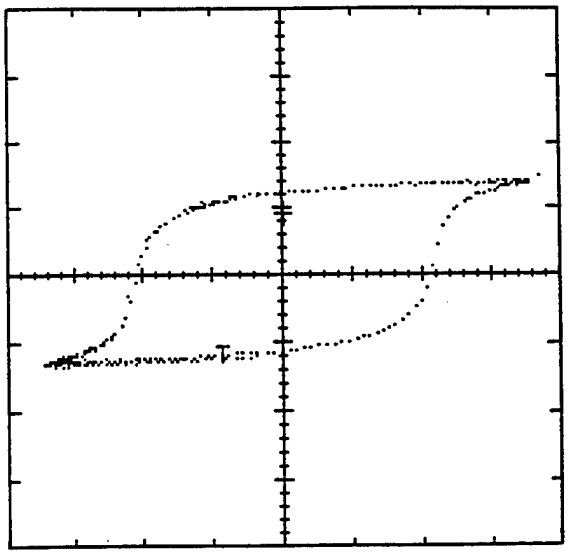

FIGURE 4 Ferroelectric hysteresis loop for PZZN (92.5) measured at a frequency of 0.10 Hz at 25°C. E_c = 15.55 kV/cm and P_r = 27.2 μC/cm^2.

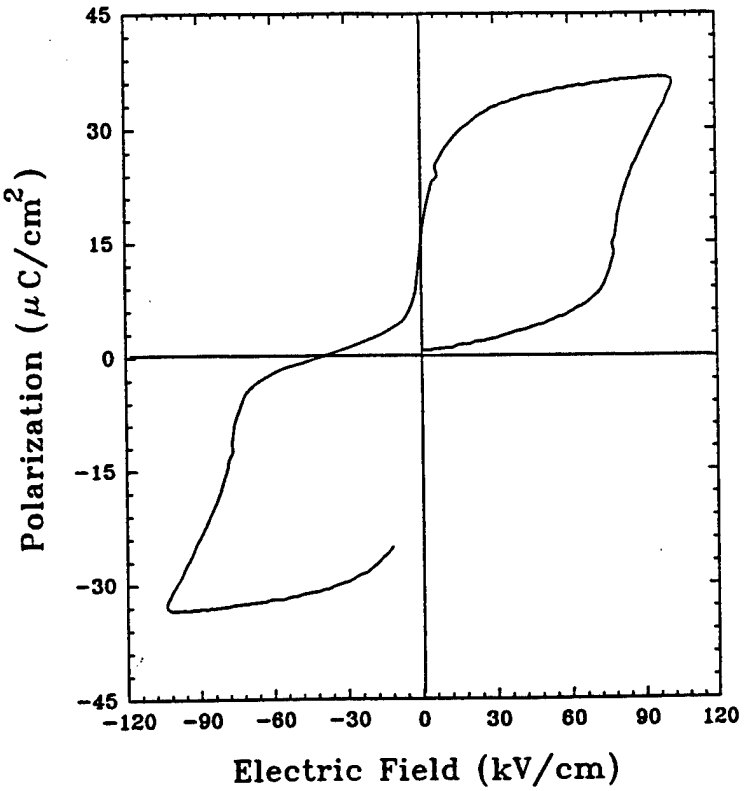

FIGURE 5 Antiferroelectric hysteresis loop for PZNT (95/5) measured at a frequency of 0.10 Hz at 25°C.

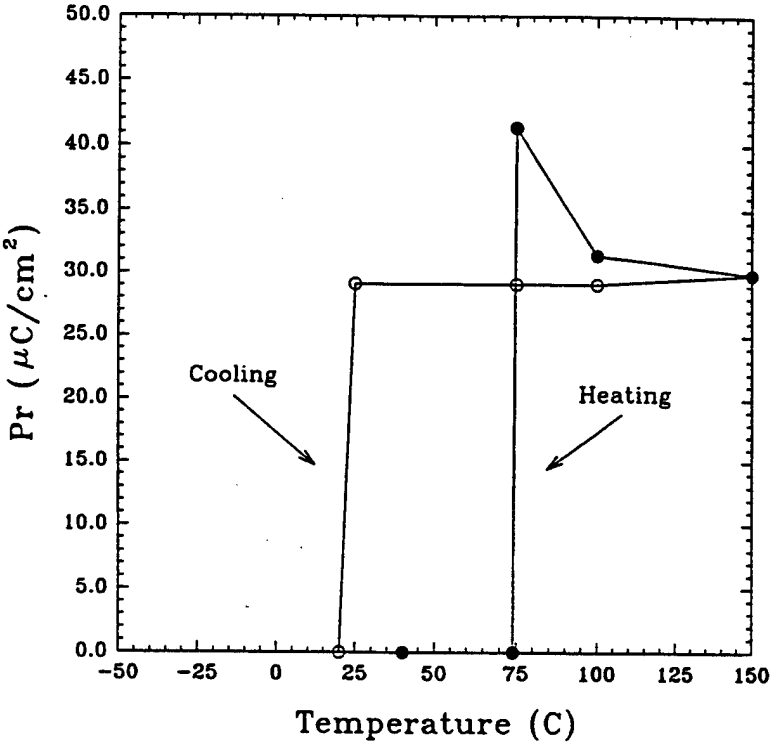

FIGURE 6 Remanent polarization, P_r, and coercive field, E_c, as a function of temperature for PZZN (93.5).

EXPERIMENTAL PROCEDURES

Ceramic samples of various PZNT (x/z) compositions near the room temperature morpotropic phase boundary were prepared. Those samples ocntaining 0 mol% PT (i.e. $y = 0$) were referred to as PZZN (x). For all experiments the samples were polished to a 1 μm finish using diamond paste.

The polarization versus electric field hysteresis loops were generated at 10 Hz using a modified Sawyer-Tower circuit. During the experiment the samples were immersed in a silicone oil bath. The bath temperature was controlled by a nitrogen fed furnace. Data was acquired using an automated measurement system controlled by a desk top computer.

The temperature dependence of the dielectric constant was measured at various frequencies in a temperature range from −100°C to 250°C using a computer controlled measurement system. This system consisted of a multifrequency LCR meter (HP4274A, Hewlett Packard Co.), desktop computer (HP 9816) and a nitrogen fed furnace. Various electrical bias voltages were then applied to the sample by an external power supply.

For piezoelectric measurements, the samples were prepared as thin disks with typical dimensions of 20 × 0.2 mm or as long thin bars with typical dimensions of 20 × 2 × 0.2 mm. All resonance measurements were made using an HP 4192A Impedance Analyzer. The calculations of the compliance, s_{11}^E, piezoelectric coeffi-

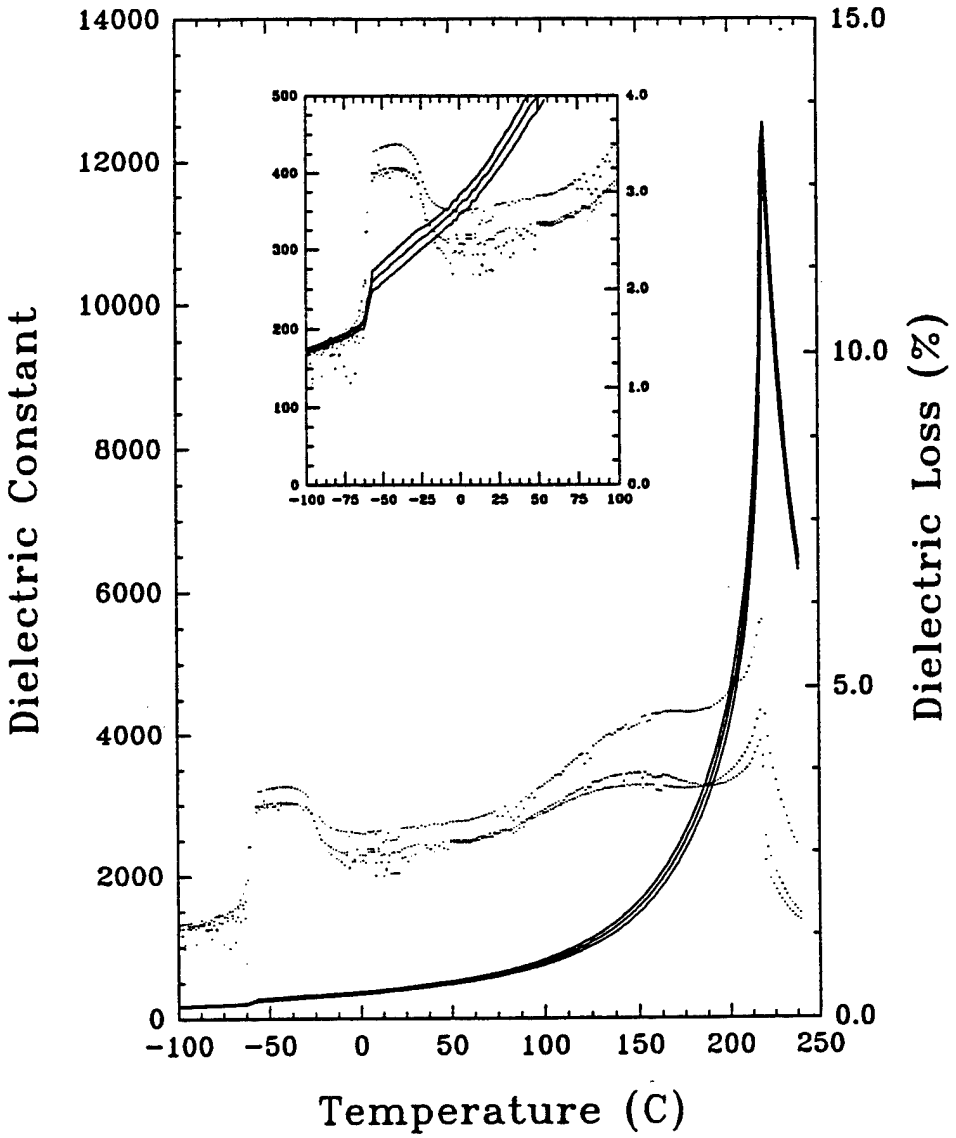

FIGURE 7 Frequency dependence of the dielectric constant and dielectric loss during cooling at 4°C/min for PZZN (93.5).

cient, d_{31}, dielectric constant, ε_{33}, and coupling coefficient, k_{31}, were made using the appropriate admittance equation of either a bar or disk resonator. For the bar shaped resonators, the imaginary values of these parameters were found by assuming the s_{11}^E, d_{31} and ε_{33} to be complex values as follows:

$$Y = j\frac{\omega l w}{t}\left(\varepsilon_{33}^T - \frac{d_{31}^2}{s_{11}^E}\right) + j\frac{2wd_{31}^2}{s_{11}^E t\sqrt{\rho s_{11}^E}}\tan\left(\frac{\omega l\sqrt{\rho s_{11}^E}}{2}\right) \quad (1)$$

where w = width, ρ = density, t = thickness, ω = frequency and l = length.

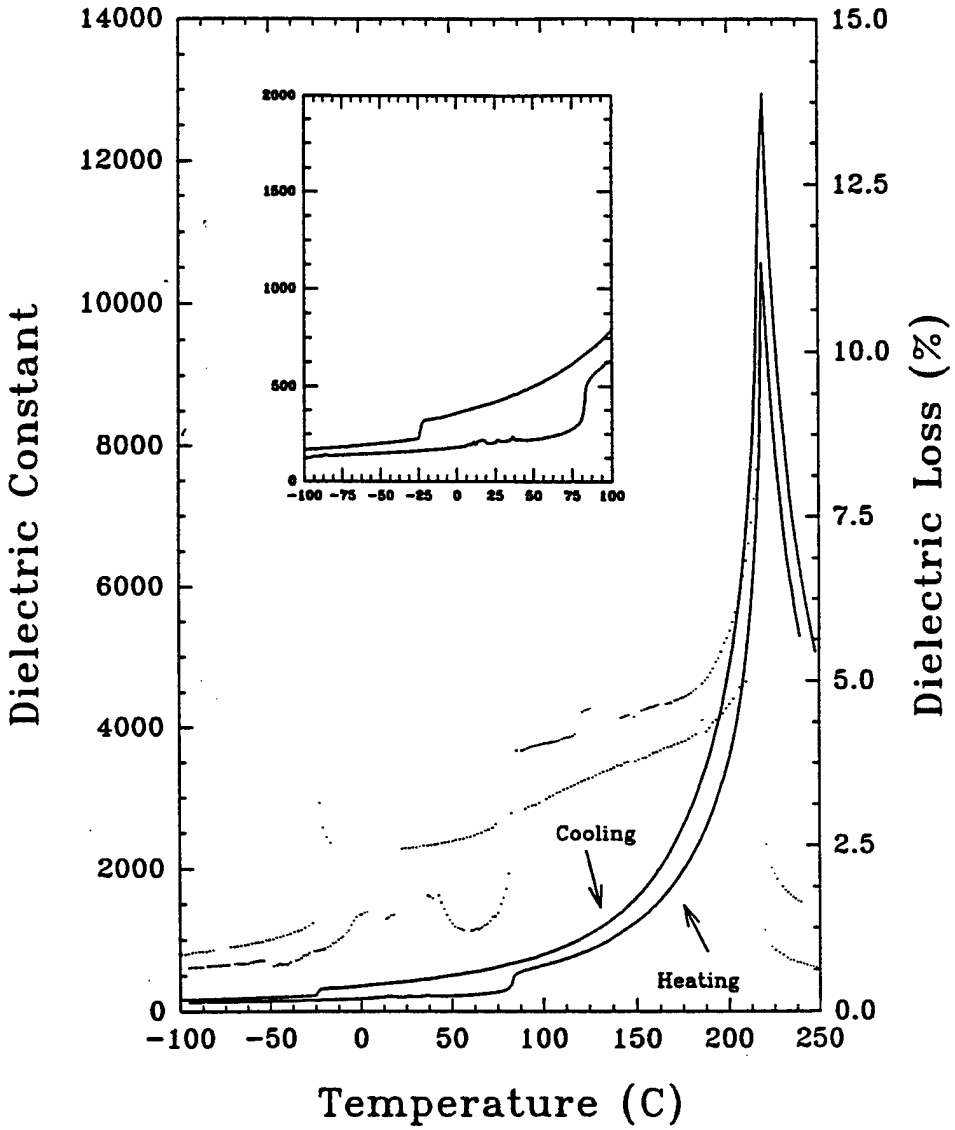

FIGURE 8 Dielectric constant and dielectric loss for PZZN (92.5) as a function of temperature (data taken at ±4°C/min with no applied bias).

and

$$s_{11}^{E} = s_{11}^{E'} + js_{11}^{E''} \tag{2}$$

$$d_{11} = d_{11}' + jd_{11}'' \tag{3}$$

$$\varepsilon_{11}^{T} = \varepsilon_{11}^{T'} + j\varepsilon_{11}^{T''} \tag{4}$$

The complex admittance equation is then solved by the method described by Smits[5] and latter by Damjanovic.[6] This method involves an iterative calculation using an initial guess of the elastic constant and three values of the admittance near resonance.

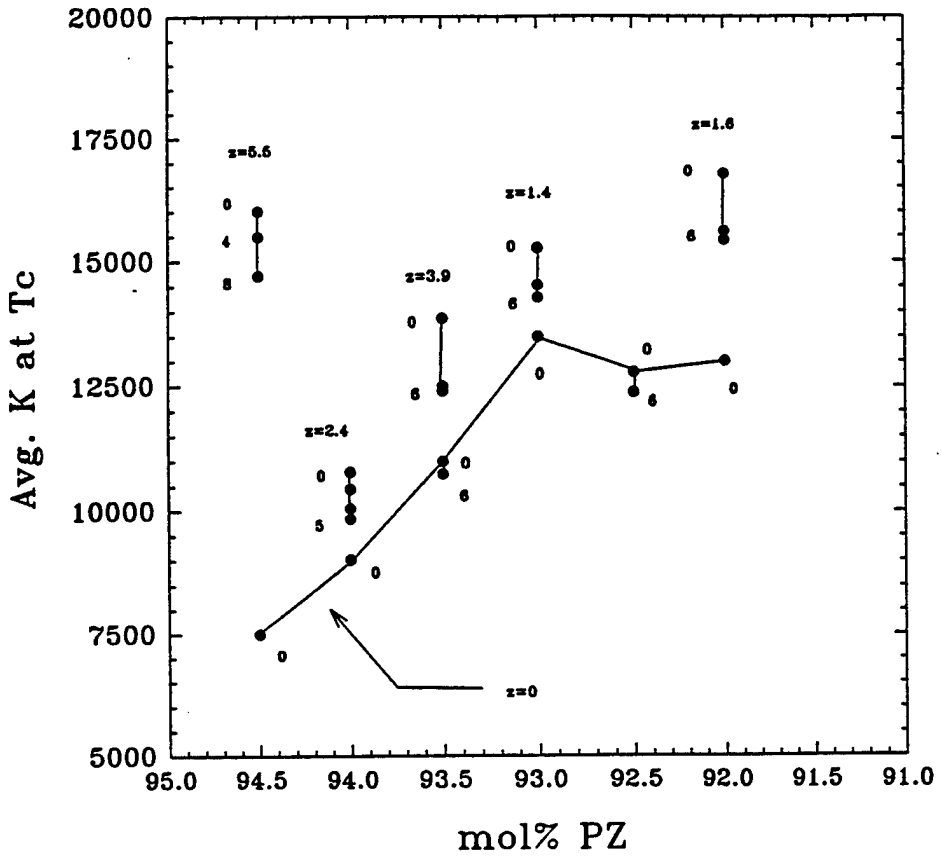

FIGURE 9 Maximum average dielectric constant at the Curie point measured at a frequency of 1 kHz. Superscripts indicate the applied bias in kV/cm. (z indicates the concentration of PT in mol%.)

The pyroelectric data was obtained using the Byer-Roundy method. The pyroelectric coefficient, p_3, and spontaneous polarization, P_s, for the ceramic specimens were measured using an HP-4140B picoammeter controlled by an HP-9121 computer. Temperature was regulated by a Delta Design 2300 furnace with a working temperature range of −175°C to 250°C. Samples were poled in the sample holder at 100°C and poled during cooling to the starting temperature. The samples were then heated at +4°C/min as the data was taken.

RESULTS AND DISCUSSION

(a) Hysteresis Measurements

Hysteresis data was taken for six PZZN compositions. These were x = 92.5, 92.8, 93.0, 93.2, 93.5 and 95.0 mol% PZ. Initially, the hysteresis loops were made using samples with no prior heat treatment. The results showed the antiferroelectric to ferroelectric phase transition (A_α to F_α) to be located between the compositions PZZN (93.0) and PZZN (93.2) (Figure 3). The ferroelectric compositions showed coercive

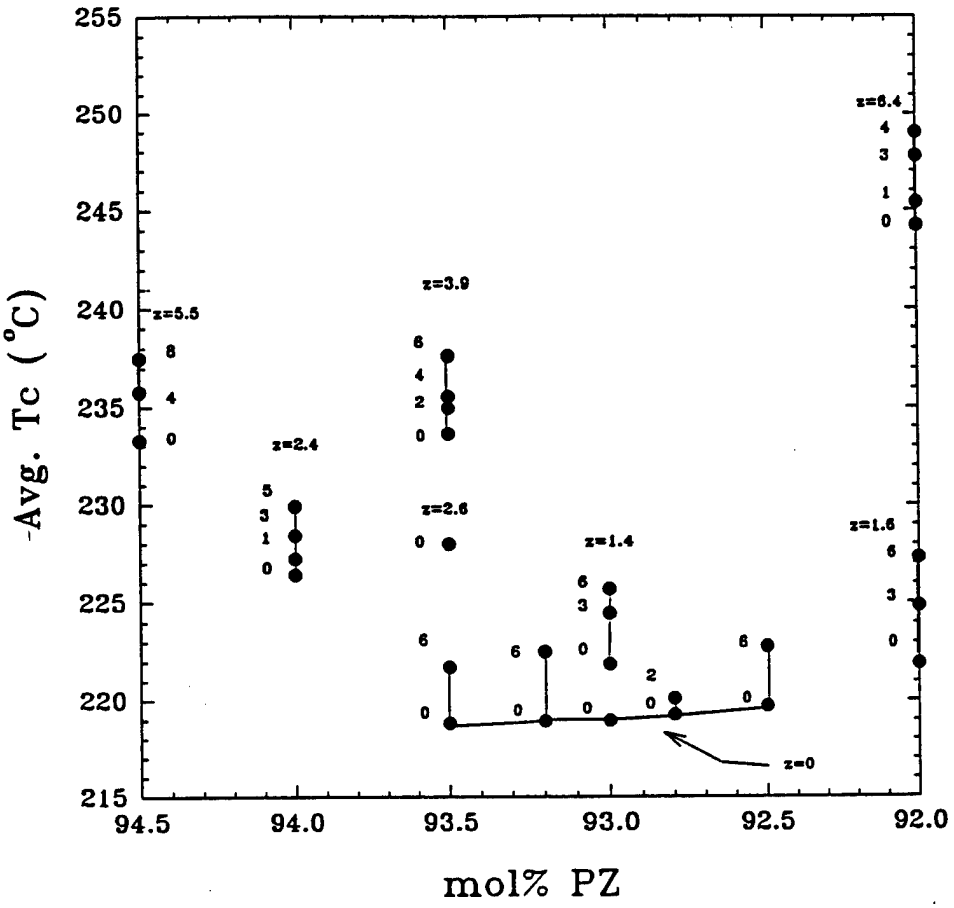

FIGURE 10 Average Curie point measured at 1 kHz. Superscripts indicate the applied bias in kV/cm. (z indicates the concentration of PT in mol%.)

fields between 15 kV/cm and 16 kV/cm. The remanent polarization in both PZZN (92.8) and PZZN (92.5) was approximately 28 $\mu C/cm^2$ and decreased slightly with increasing concentration of PZ. For PZZN (93.0) the remanent polarization was found to be 32.2 $\mu C/cm^2$. This was slightly higher than that would have been predicted based on the previously mentioned values and is probably due to the morphotropic phase boundary and its increased number of domain states. With further increases in concentration of PZ above 93.0% (i.e., PZZN (93.2), PZZN (93.5), etc.) the remanent polarization falls to 0.00 $\mu C/cm^2$.

The room temperature antiferroelectric phase compositions, PZZN (93.2), PZZN (93.5) and PZZN (95.0) showed no hysteresis initially. Typical antiferroelectric behavior was found for PZNT (95/5). The antiferroelectric hysteresis loop for this composition is shown in Figure 5.

Next, the samples were poled at 100°C for 15 minutes and then cooled, with the field still applied, to room temperature. Following this treatment, all three showed ferroelectric hysteresis loops comparable to those of the ferroelectric samples studied. This implies that the F_a phase is metastable at room temperature in these composi-

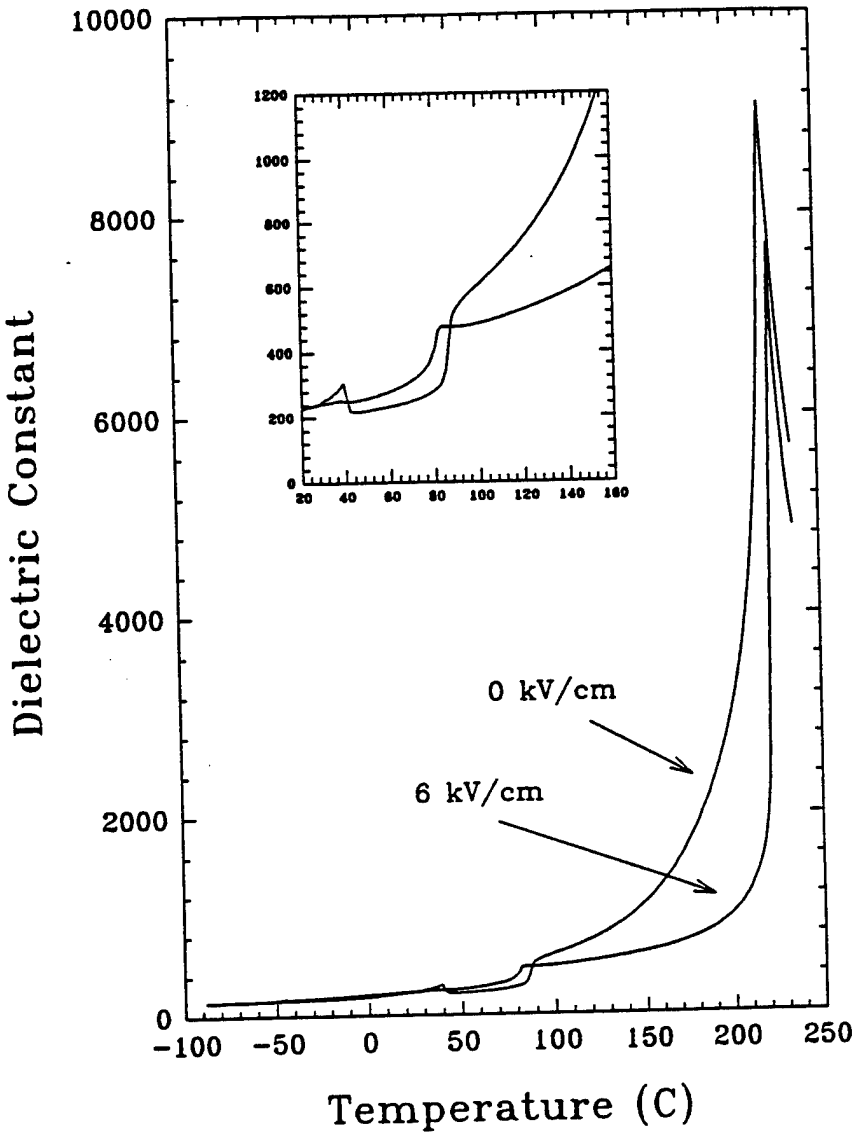

FIGURE 11 The effect of electric bias on the dielectric constant and dielectric loss for PZZN (93.2) (data taken on heating at +4°C/min).

tions. The coercive field for this induced phase was found to be between 15 kV/cm and 16 kV/cm. The induced remanent polarization decreased with increasing concentration of PZ to a low of 6.13 $\mu C/cm^2$ in PZZN (95.0).

The temperature dependence of P_r for PZZN (93.5) is shown in Figure 6. This confirms that the F_α phase is stable during cooling to 20°C. During heating, however, the F_α phase is not stable until 75°C. After combining the heating and cooling data, a thermal hysteresis of 55°C is observed.

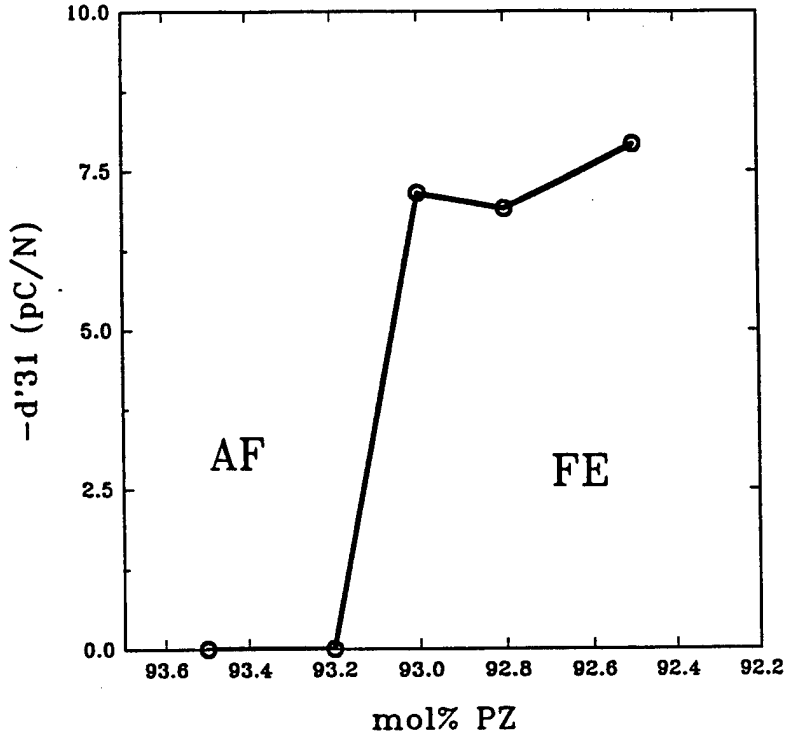

FIGURE 12 Variation in d'_{31} as a function of composition for PZZN ceramics measured at room temperature. The antiferroelectric-ferroelectric phase boundary is located between $x = 93.0$ and 93.2 mol% PZ.

(b) Dielectric Measurements

Due to the large concentration of PZ in the compositions studied, the relaxor nature of the PZN component was suppressed. To illustrate this the frequency dependence of PZZN (93.5) from the dielectric data taken during cooling at −4°C/min is used. Figure 7 shows the dielectric constant and loss measured at frequencies of 1 kHz, 10 kHz and 100 kHz. This shows very little frequency dispersion, and the phase transitions are typically affected by less than 0.2°C. From these data, it has been determined the PZNT ceramics with $y < 8.0\%$ PZN do not show any relaxor behavior.

The thermal hysteresis found in these compositions can be as much as 120°C in the lower temperature phase transitions. However, at the Curie point the hysteresis is limited to ~2°C. Figure 8 shows the thermal hysteresis for heating and cooling rates of ±4°C/min in PZZN (92.5).

Figure 9 shows the average maximum dielectric constant at the Curie temperature (T_c) from heating and cooling cycles as a function of mol% PZ. Maximum dielectric constant decreases as the concentration of PZN is decreased. Also, as expected, increasing the concentration of PT increases the maximum dielectric constant at T_c. The variation in T_c with mol% PZ can be seen in Figure 10. This, for example shows an increase of 10°C between PZNT (93.5/2.6) and PZNT (93.5/3.9) which is an increase in PT of 1.3 mol%.

Figures 9 and 10 also show the influence of electric bias. The average dielectric

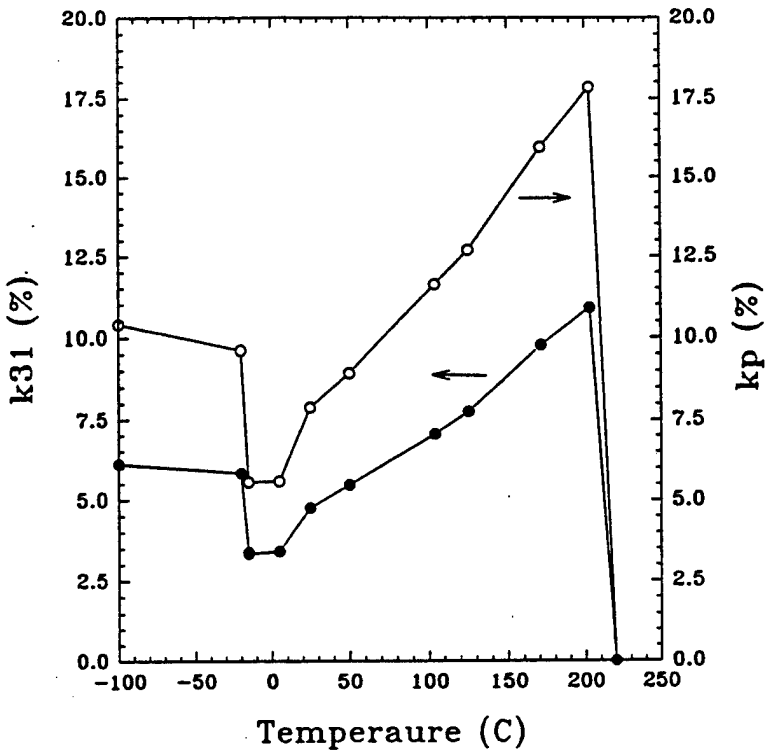

FIGURE 13 Temperature dependence of the piezoelectric coupling coefficients (k_{31} and k_p) for a PZZN (93.0) ceramic measured with no applied electrical bias.

constant at T_c for PZNT (93.5/2.6) can be seen to decrease with bias. The bias field also causes a shift in T_c which can be seen in Figure 10. This shows the increase in T_c for various compositions in the PZNT system as the bias field is increased. The effect of bias on the dielectric constant and loss in PZZN (93.2) for the whole temperature range studied is shown in Figure 11.

(c) Piezoelectric Measurements

The electric bias dependence of real part of d_{31} after poling at room temperature is shown in Figure 12. This shows that the piezoelectric effect is linear as a function of bias. The room temperature antiferroelectric to ferroelectric phase boundary can be located between PZZN (93.2) and PZZN (93.0) by plotting $-d'_{31}$ versus composition. Using a Berlincourt meter, the value of d_{33} was found to be between 55 and 60 pC/N in all the ferroelectric samples. The temperature dependence of k_{31} and k_p was found for a morphotropic phase boundary composition. The composition used was PZZN (93.0) and the measurements were conducted using an incremental cooling run with no applied bias.

The results for the PZZN compositions showed little if any dependence on electric bias. The real part of $-d_{31}$ was found to be 6–7 pC/N and the imaginary part to be 0.35 to 0.45 pC/N. The coupling coefficient, k_{31}, was found to be 5–8% at room

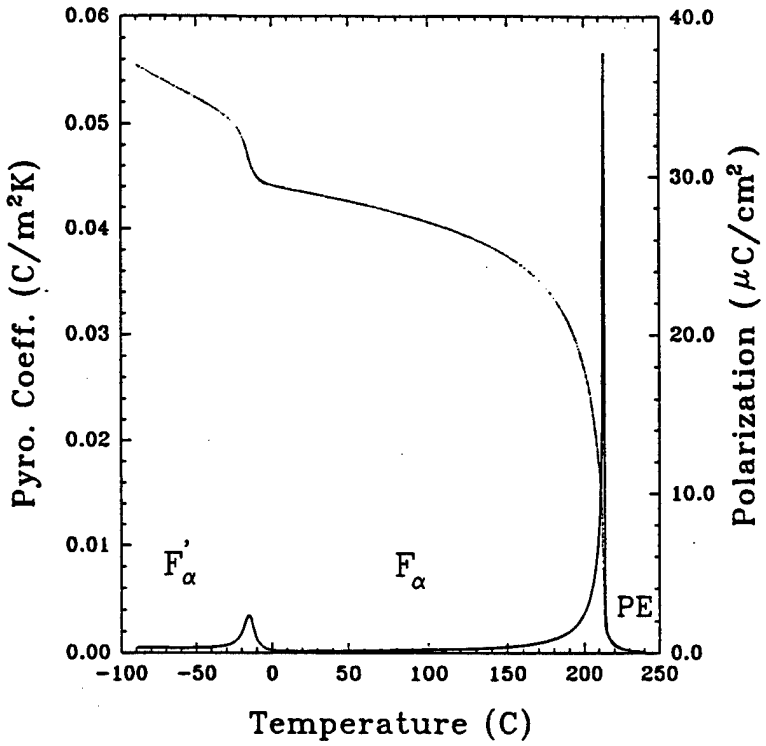

FIGURE 14 Pyroelectric coefficient and spontaneous polarization for a PZZN (92.5) ceramic measured while heating at +4°C/min. Sample poled during cooling from 100°C.

TABLE I

Hysteresis data for various PZZN and PZNT compositions measured at room temperature and at a frequency of 0.10 Hz

Composition:	After poling at 25 C:			After poling at 100 C:		
PZ / PZN / PT	Ps	Pr	Ec	Ps	Pr	Ec
95.0 / 5.0 / 0.0	AFE	AFE	AFE	6.7	15.4	6.13
93.5 / 6.5 / 0.0	AFE	AFE	AFE	30.7	29.1	16.36
93.0 / 7.0 / 0.0	36.0	32.2	15.25	36.0	32.2	15.25
92.8 / 7.2 / 0.0	33.6	28.0	15.90	33.6	28.0	15.90
92.5 / 7.5 / 0.0	27.2	27.2	15.55	27.2	27.2	15.55
94.5 / 0.0 / 5.5	31.9	28.7	12.15	---	---	---
93.5 / 2.6 / 3.9	37.7	34.3	11.78	---	---	---
92.0 / 1.6 / 6.4	26.8	25.0	9.20	---	---	---
92.0 / 6.4 / 1.6	40.2	35.1	15.05	---	---	---

TABLE II

Summary of the complex piezoelectric and elastic coefficients for selected PZNT compositions. Measurements were made at room temperature with no applied bias after poling at 25°C.

Composition: PZ / PZN / PT	d33 (pC/N)	-d'31 (pC/N)	-d"31 (pC/N)	s'11 (x10-12 m2/N)	s"11 (x10-12 m2/N)	k31 (%)	kp (%)	loss tangents (%)		
								Dielectric	Mechanical	Piezoelectric
95.0 / 5.0 / 0.0	0.0	0.00	0.00	---	---	0.00	0.00	---	---	---
93.5 / 6.5 / 0.0	0.0	0.00	0.00	---	---	0.00	0.00	---	---	---
93.5 / 6.5 / 0.0 (1)	52.0	5.20	0.26	7.30	0.014	4.00	---	1.90	1.92	5.01
93.2 / 6.8 / 0.0	0.0	0.00	0.00	---	---	0.00	0.00	---	---	---
93.0 / 7.0 / 0.0	60.0	7.20	---	7.95	---	4.77	7.88	---	---	---
92.8 / 7.2 / 0.0	58.0	6.10	0.26	7.60	0.025	4.24	---	1.95	3.25	4.22
92.5 / 7.5 / 0.0	57.0	7.08	---	7.91	---	4.49	7.49	---	---	---
92.0 / 6.4 / 1.6	55.0	4.25	0.35	7.22	0.027	3.54	---	5.34	3.77	8.32
92.0 / 1.6 / 6.4	59.0	9.95	0.22	8.49	0.014	6.97	---	---	---	---
93.5 / 3.9 / 2.6	60.0	16.03	---	7.86	---	3.80	6.15	---	---	---

Note 1: Measurements made after poling at 100 °C.

temperature. From the compositions studied, PZNT (93.5/2.6) was found to have the optimum properties. For this composition, the values of d'_{31}, k_{31} and k_p were found to be 16.0 pC/N, 4% and 6%, respectively. Again, these values were nearly bias independent.

(d) Pyroelectric Measurements

PZZN (92.5) showed the largest pyroelectric coefficient and remanent polarization of the compositions studied. Figure 14 shows the variation in these parameters as a function of temperature. At room temperature, the spontaneous polarization was found to be 28.9 $\mu C/cm^2$ and agrees with the data from hysteresis measurements. The F'_a to F_a transitions in this composition was found at $-15°C$ and the F_a to Paraelectric transition is located at 215.09°C.

CONCLUSIONS

Various compositions in the PZ-PZN-PT ternary system have been studied to determine their weak field piezoelectric and dielectric response at room temperature. Some of the conclusions that have been made are as follows:

Hysteresis results indicate that the location of the AF-FE boundary is between $x = 93.0\%$ and $x = 93.2\%$ PZ. Large values of P_r (~30 $\mu C/cm^2$) and low values of E_c (~10 kV/cm) for $x < 92.8\%$ PZ have been obtained. Also, with decreasing PZ concentrations hysteresis loops become increasingly square in nature.

Room temperature dielectric constants near 250 have been measured and can be altered with suitable compositional adjustments. Large hysteresis in heating and cooling cycles has been displayed, especially in the low to high temperature rhombohedral phase transition. Curie temperatures near 225°C have been found to decrease with both increasing bias field and increasing concentrations of PT.

Piezoelectric coefficient d'_{31} at 25°C was found to be between -5 pC/N and -10 pC/N and linear with electrical bias fields up to 20 kV/cm. The real elastic coefficient s'^E_{11} was found to be between 7 and 9×10^{-10} m^2/N and constant for electric bias fields of up to 20 kV/cm. The piezoelectric coupling coefficient k_{31} was found to be between 2% and 8%.

The PZNT phase diagram has been refined to show the AF-FE boundary at room temperature. In addition, after poling at elevated temperatures, the ferroelectric phase has been shown to be stable when cooled to room temperature. Finally, the composition PZZN (92.5) has been shown to have strong pyroelectric properties.

REFERENCES

1. R. E. Newnham and G. R. Ruschau, "Smart Electroceramics," *J. Am. Ceram. Soc.*, 74, 463–80 (1991).
2. S. Kumar, "Smart Materials for Acoustic Vibration Control," Ph.D. Thesis, The Pennsylvania State University, 1991.
3. D. J. Taylor, "Electric and Elastic Coefficients of PMN-Based Ceramics Under DC Bias for Smart Sensor Applications," Ph.D. Thesis, The Pennsylvania State University, 1992.

4. T. Takenaka, A. S. Bhalla and L. E. Cross, "Dielectric Piezoelectric and Pyroelectric Properties of Lead Zirconate-Lead Zinc Niobate Ceramics," *J. Am. Ceram. Soc.*, **72**, 1016–23 (1989).
5. J. Smits, "Iterative Method for Accurate Determination of the Real and Imaginary Parts of the Materials Coefficients of Piezoelectric Ceramics," *IEEE Transactions on Sonics and Ultrasonics*, **SU-23**, 393 (1976).
6. D. Damjanovic, "Highly Anisotropic Electromechanical Properties in Modified Lead Titanate Ceramics," Ph.D. Thesis, The Pennsylvania State University, 1987.
7. D. J. Taylor, D. Damjanovic and A. S. Bhalla, "Pyroelectric and Dielectric Properties of PMN-Based Ceramics Under DC Bias," *Ferroelectrics*, **118**, 143 (1990).

APPENDIX 12

Polarization Responses in Lead Magnesium Niobate Based Relaxor Ferroelectrics

Q. M. Zhang and J. Zhao

Materials Research Laboratory and Department of Electrical Engineering

The Pennsylvania State University, University Park, PA 16802

Abstract:

We demonstrate that by making use of the change of the electrostrictive coefficients Q_{ij}, especially the volumetric coefficient, with temperature and bias field, one can gain direct experimental information on the nature of the polarization in lead magnesium niobate based relaxor ferrelectrics. We show that the polarization response at temperatures near the dielectric constant maximum is mainly through the polar-vector reorientation of the nano-polar regions, as suggested by the polar glass model. As the temperature is lowered to near and below the freezing transition, the polarization response is through the phase switching and intrinsic contributions rather than the domain wall motions as in normal ferroelectrics.

PACS No: 77.65.-j, 77.84.-s, 77.80.Bh

Sub. Appl. Phys. Lett.

The relaxor ferroelectric materials have attracted a great deal of attention in the past several decades due to their technologic importance and peculiar phase transition behavior.[1-2] One classical system is $Pb(Mg_{1/3}Nb_{2/3})O_3$ (PMN) and its solid solution with $PbTiO_3$ ((1-x)PMN-xPT, x<0.3). The materials are characterized by a broad dielectric maximum with a strong frequency dispersion at temperatures just below the dielectric maximum (T_m). Moreover, at the zero field cooled state, the materials remain in the cubic phase macroscopically even at temperatures near zero Kelvin while microscopically, the lattice is split into polar regions with the coherence length on the order of 10 nm. It has been observed that these nano-polar regions persist to temperatures far above T_m. Many models have been proposed for this class of materials. Among them, the superparaelectric model, the polar glass model, and the random field model are the ones which have received the most attention.[2-5] More recently, based on model calculation, it was suggested that the polarization mechanism at temperatures near T_m in PMN is through the domain wall type motion rather than the polar region reorientation as suggested by the polar glass model.[6] Although each of these models has merit, there exists no direct experimental result related to the basic polarization mechanisms in relaxor ferroelectrics and on the nature of the nano-polar regions, which are crucial to the understanding of relaxor behavior and to attest different models.

Mesoscopically, the morphology of PMN based relaxors, without external poling fields, consists of nano-polar regions embedded in a non-polar matrix.[2,7,8] The polarization responses of the material, hence, can be from different mechanisms: the polar-vector reorientation of the polar regions, as suggested by the superparaelectric model and dipole glass model, the expanding and shrinking of these regions (breathing mode of the polar regions), and the induced phase transformation between the cubic (paraelectric) and rhombohedral (ferroelectric) phases. In addition, there will be contributions from the change of polarization in the cubic and rhombohedral phases which are usually termed as intrinsic contributions to the polarization. One of the unique features related to PMN-based relaxor materials is that these polarization mechanisms are also ferroelastic. Moreover, they can be grouped into those generating a

volume strain and those with zero volume strain. It is this volumetric technique, introduced recently, that will be used to probe the nature of the polarization and its dynamics in PMN based relaxors.[9]

Because of symmetry, the polar vectors of nano-polar regions are distributed randomly in all possible directions. Hence, the breathing mode motions of polar regions with opposite polar directions will resemble the 180° type domain wall motion in regular ferroelectric, while those with polar directions other than 180° will resemble non-180° type wall motions. In this letter, the polar region motions of these types are termed as quasi-domain wall motions for the sake of simplicity. As for uncompensated breathing mode motions of polar regions, because they are related to the phase transformation they will be included in the category of phase switching. Apparently, neither the polar vector reorientation nor the quasi-domain wall motion generates volume strain. On the other hand, the polarization changes from the phase switching and intrinsic contribution are associated with a volume strain.

PMN and 0.9PMN-0.1PT, both exhibiting typical relaxor behavior, were chosen for this investigation. The dielectric maximum T_m is ~10 °C for PMN and 38 °C for 0.9PMN-0.1PT (at 1 kHz). The use of two compositions instead of one is to ensure the reliability of the results. Ceramic samples were prepared as described in Ref. 10. The typical sample size is about 0.5x0.5x0.5 cm^3. The strains S_1 and S_3, where S_1 and S_3 are the transverse and longitudinal strains, respectively, were measured by both the strain gauge method and the laser dilatometer method. In the strain gauge method, measurements on S_1 and S_3 were carried out simultaneously by attaching two strain gauges onto two faces with one parallel and the other perpendicular to the applied electric field direction, respectively. The signal output from the strain gauge amplifier was detected by both a lock-in amplifier and a digital oscilloscope. In the laser dilatometer method, S_1 and S_3 were acquired separately and the results are consistent with those obtained using the strain gauge technique.[11] The polarization P_3 was obtained by a Sawyer-Tower circuit where again, the output signal was measured by both a lock-in amplifier and a digital oscilloscope, concomitantly with the strain measurement. In the field range

reported, the difference between the data obtained from the lock-in amplifier and those from the digital oscilloscope is within the data scatter which is about ±5%. The amplitude of applied AC voltage is about 200 V/cm with a frequency of 10 Hz. Experiments were carried out during both cooling and heating cycles and except for the data of 0.9PMN-0.1PT at below 15 °C, which is related to the approaching of the freezing transition of the material, there is no significant difference between the data in the two temperature directions.

Presented in figure 1 are the variation of the electrostrictive coefficient Q_{11} and Q_{12} for PMN and 0.9PMN-0.1PT as a function of temperature, where Q_{11} and Q_{12} are defined as:

$$S_3 = Q_{11} P_3^2 \quad \text{and} \quad S_1 = Q_{12} P_3^2 \qquad (1)$$

For PMN, in the experimental temperature range (from -45 °C to 125 °C), the measured Q_{ij} does not show marked changes with the applied field amplitude, while for 0.9PMN-0.1PT, the data at temperatures above 10 °C only depend weakly on the field amplitude and below that temperature, the data exhibit a strong dependence on the field amplitude. The change in the field amplitude dependent behavior in 0.9PMN-0.1PT is related to the freezing temperature T_f below which the polarization hysteresis loop exhibits a substantial remnant polarization and the polarization-field relationship is strongly hysteretic. For 0.9PMN-0.1PT, T_f is at about 10 °C while for PMN, it lies about -70 °C, below the experimental temperature.[3,4,12] By combining Q_{11} and Q_{12}, the volumetric electrostrictive coefficient Q_h ($Q_h = Q_{11} + 2\,Q_{12}$) can be obtained as presented also in figure 1.

One of the salient features of figure 1 is that the electrostrictive coefficient Q_{ij} varies with temperature for both PMN and 0.9PMN-0.1PT. Furthermore, compared with Q_{11} and Q_{12}, the relative change of Q_h with temperature is quite substantial. For 0.9PMN-0.1PT, it increases from 0.002 m^4/C^2 at -10 °C to about 0.013 m^4/C^2 at 120 °C. And for PMN, it increases from 0.004 m^4/C^2 at -45 °C to about 0.023 m^4/C^2 at 120 °C. Considering the fact that there is a 48 °C difference in T_m between the two compositions, we shift the temperature scale for PMN upwards by 48 °C and overlap it with that of 0.9PMN-0.1PT. As shown in figure 2, the results from the two systems are consistent with each other. As we have pointed out, Q_h

measures the volume strain, the data presented in figure 2 reveal that compared with the polarization mechanisms at higher temperatures, the polarization response at low temperatures (near and below T_m) involves very little volumetric strain. In another words, the polarization response is from either the quasi-domain wall type motion or polar-vector reorientation or both.

Another interesting feature from figures 1 and 2 is that at high temperatures, the increase of Q_h is due to both the increase of Q_{11} and decrease of $|Q_{12}|$ with temperature. From the available lattice constant data on the cubic and rhombohedral phases of PMN, it can be shown that for the phase transformation from the cubic to the rhombohedral,[12-14] both Q_{11} and Q_{12} in single crystals are positive where Q_{11} is measured along the [111] direction of the cubic unit cell along which the spontaneous polarization lies and Q_{12} is related to the strain in the plane perpendicular to the spontaneous polarization direction. Averaging over all the directions yields a near zero Q_{12} for a PMN ceramic sample,[15] which is consistent with the experimental data in which at 120 °C, $Q_{11}/|Q_{12}|$ of PMN is above 7. On the other hand, for the polar vector reorientation or the quasi-non-180° domain wall motion process, Q_{12} should be equal to $-Q_{11}/2$, as observed at temperatures near T_m.[7] The decrease of $|Q_{12}|$ with temperature in the ceramic samples and a large ratio of $Q_{11}/|Q_{12}|$ at high temperatures are clear indications that at high temperatures, the contribution to the polarization response from the phase switching becomes increasingly important. It should be pointed out that the experimental temperature here is still far below the temperature where the nano-polar regions disappear, which for PMN is above 300 °C, and at that temperature, the polarization response should be from the intrinsic.[2]

Hence, in PMN and 0.9PMN-0.1PT, the experimental results establish that in the experimental temperature range there exist at least two types of polarization processes: phase switching which involves volume strain (P_v) and quasi-domain type motion or polar vector reorientation (P_d) which does not involve volume strain. It is apparent that the measured Q_h^m is related to Q_h^{Tr}, which is from P_v, through:

$$Q_h^m = Q_h^{Tr} \frac{P_v^2}{(P_v + P_d)^2} \qquad (2)$$

where we assume that the total polarization is P_v+P_d. Apparently, from the data in figure 2, $Q_h^{Tr}>0.023$ m^4/C^2, which indicates that at near and below T_m, more than 90% of the polarization response is from either the quasi-domain wall type or polarization reorientation which does not involve volume strain. While at higher temperatures, there is a substantial increase in P_v with respect to P_d, resulting in a large Q_h^m.

In order to determine whether the quasi-domain wall type motion or the polar vector reorientation is responsible for the polarization response at temperatures near T_m, we note that there is a fundamental difference between the polarization due to the quasi-domain wall motions and the polarization due to the polar vector reorientation. That is, for the quasi-domain wall type motions of the nano-polar regions, under an external poling field, the system becomes no-longer isotropic and part of the polar region motions will be converted from the quasi-domain wall type to the phase switching which will produce volume change, because the expanding of one polar region may not be compensated by the contracting of another region. While for polar vector reorientation, there will still be no volume strain under external bias fields.

The influence of the DC electrical bias field on Q_h was investigated and the data presented in figure 3 show that for 0.9PMN-0.1PT at temperatures above 20 °C, Q_h does not exhibit significant changes with DC bias electrical fields. The results presented here, hence, support the notion that at the temperatures near T_m the polarization response from the nano-polar region is through the polar vector reorientation. On the other hand, at temperatures near and below T_f, a large increase of Q_h was observed for a bias field of higher than 800 V/cm, indicating that the major contribution to the polarization response is due to the phase switching and intrinsic contributions, rather than the domain wall motions or the polar vector reorientation. This is quite different from the behavior at temperatures near T_m. The experimental data, therefore, also establish a direct evidence of a polarization freezing process, i.e., as the system goes

through the freezing transition, the polarization response of the nano-polar regions evolves from the polar-vector reorientation to the breathing mode type motion.

The authors wish to thank Volkmar Mueller for the assistance during this experiment and Professor L. E. Cross for stimulating discussions. We appreciate the financial support by the Office of Naval Research.

References:

1. G. A. Smolensky and A. I. Agranoskaya, Sov. Phys. Solid State 1, 1429 (1959).

2. L. Eric Cross, Ferro. 76, 241 (1987).

3. V. Westphal, W. Kleeman, and M. D. Glinchuk, Phys. Rev. Lett. 68, 847 (1992).

4. D. Viehland, S. J. Jang, L. E. Cross, and M. Wuttig, J. Appl. Phys. 68, 2916 (1990).

5. E. V. Colla, E. Yu. Koroleva, N. M. Okuneva, and S. B. Vakhrushev, Phys. Rev. Lett. 74, 1681 (1995).

6. A. E. Glazounov, A. K. Tagantsev, and A. J. Bell, Phys. Rev. B53, 11281 (1996).

7. Q. M. Zhang, H. Wang, N. Kim, and L. E. Cross, J. Appl. Phys. 75, 454 (1994).

8. J. Chen, H. M. Chan, and M. P. Harmer, J. Am. Ceram. Soc. 72, 593 (1989).

9. P. Bonneau, P. Garnier, G. Calvarin, E. Husson, J. R. Gavarri, A. W. Hewat, and A. Morell, J. Solid State Chem. 91, 350 (1991).

10. S. L. Swartz and T. R. Shrout, Mat. Res. Bull. 17, 1245 (1982).

11. Q. M. Zhang, S. J. Jang, and L. E. Cross, J. Appl. Phys. 65, 2807 (1989).

12. G. Calvarin, E. Husson, and Z. G. Ye, Ferro. 165, 349 (1995).

13. P. Bonneau, P. Garnier, E. Husson, and A. Morell, Mat. Res. Bull, 24, 201 (1989).

14. N. de Mathan, E. Husson, G. Calvarin, and A. Morell, Mat. Res. Bull, 26, 1167 (1991).

15. A. F. Devonshire, Phila. Mag. 42, 1065 (1951).

Figure captions:

Figure 1. The electrostrictive coefficients Q_{ij} as a function of temperature measrured at 10 Hz. (a) Q_{11} and Q_{12} for 0.9PMN-0.1PT; (b) The volumetric electrostrictive coefficients Q_h (= $Q_{11}+2Q_{12}$) for 0.9PMN-0.1PT; (c) Q_{11} and Q_{12} for PMN; (b) Q_h for PMN.

Figure 2. By shifting the temperatures of PMN up 48 °C (to account for the difference in T_m between PMN and 0.9PMN-0.1PT), the data of PMN (open circles) overlap with those of 0.9PMN-0.1PT (crosses). Data show that as temperature increases, Q_{11} increases while Q_{12} decreases.

Figure 3. The effect of DC bias field on the volumetric electrostrictive coefficient Q_h for 0.9PMN-0.1PT. Open circles are Q_h measured without bias field, pluses are under 800 V/cm, and crosses are under 3 kV/cm DC bias field. The large increase of Q_h with DC bias field at low temperatures indicates the polarization response is through the phase switching and intrinsic processes.

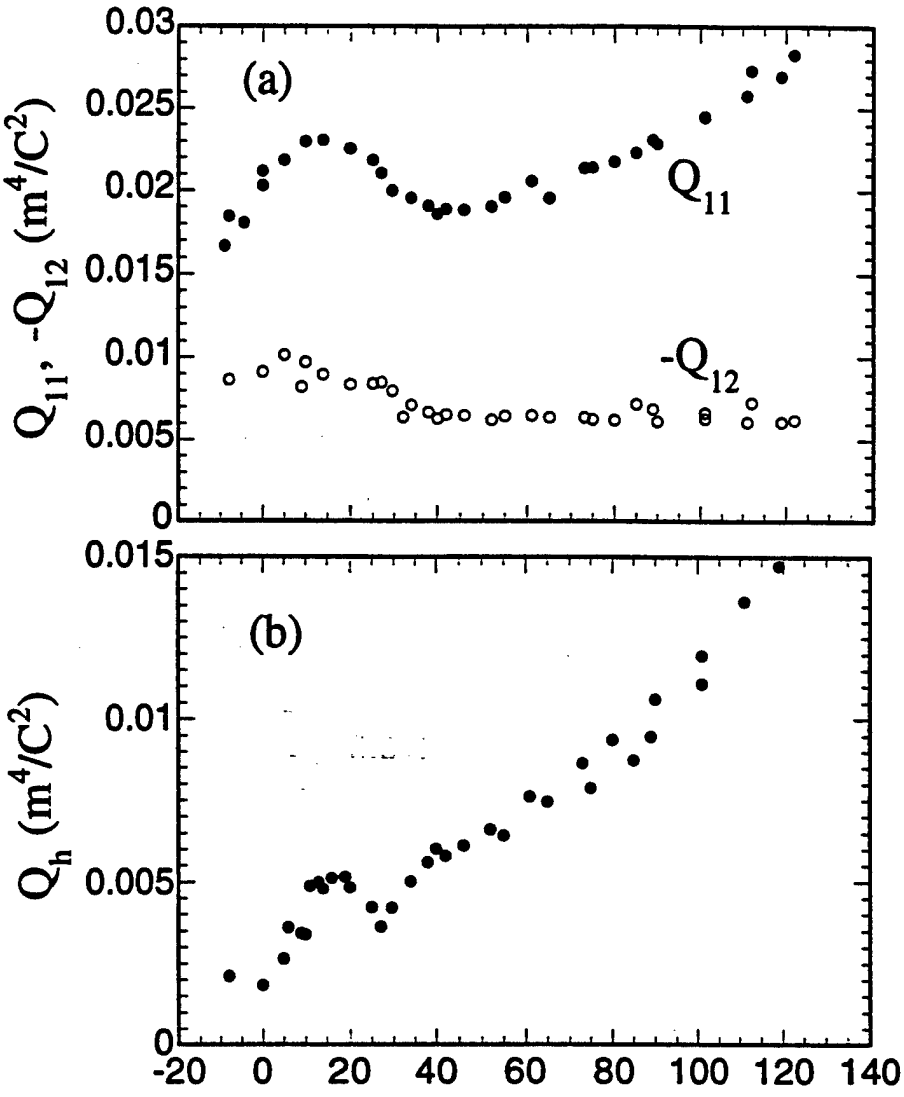
(a)
Q_{11}
$-Q_{12}$
Q_{11}, $-Q_{12}$ (m^4/C^2)
0.03
0.025
0.02
0.015
0.01
0.005
0
(b)
Q_h (m^4/C^2)
0.015
0.01
0.005
0
-20
0
20
40
60
80
100
120
140

F. 1

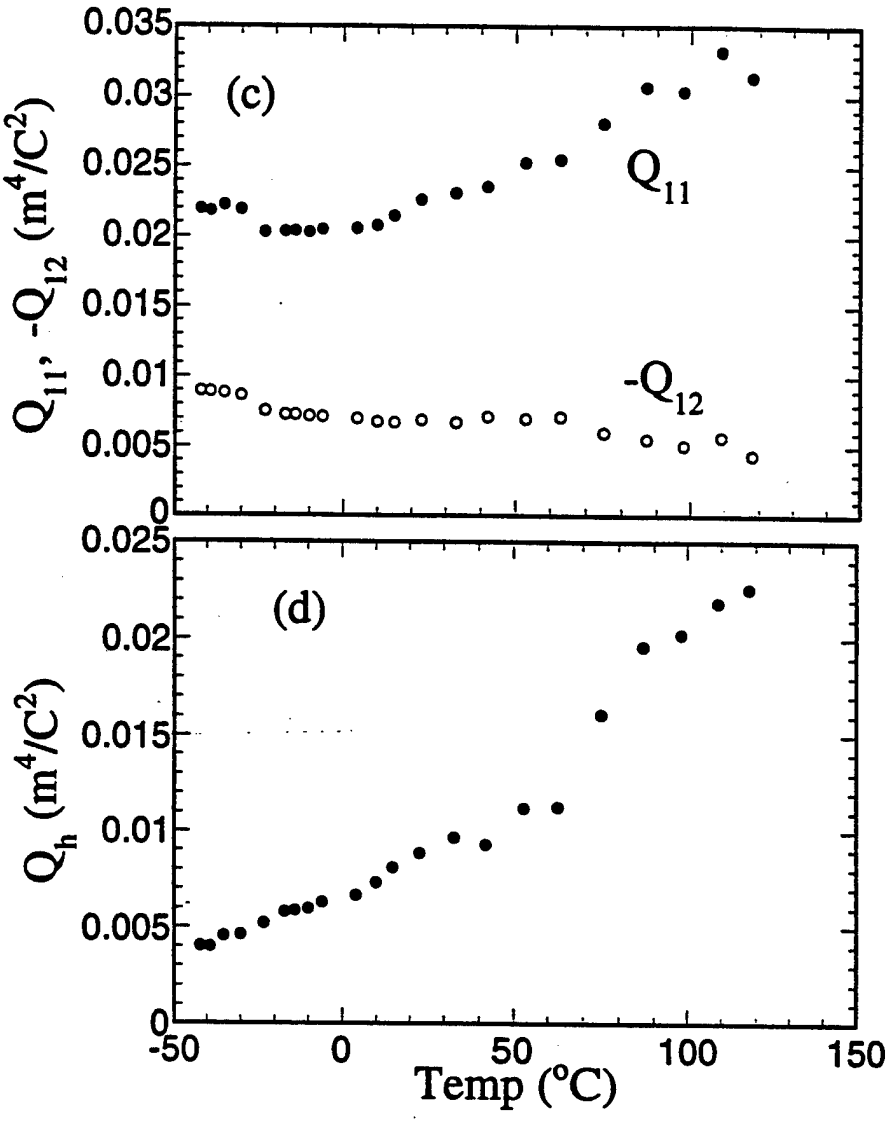
(c)
Q_{11}
$-Q_{12}$
Q_{11}, $-Q_{12}$ (m^4/C^2)
0.035
0.03
0.025
0.02
0.015
0.01
0.005
0
(d)
Q_h (m^4/C^2)
0.025
0.02
0.015
0.01
0.005
0
-50
0
50
100
150
Temp (°C)

F. 1

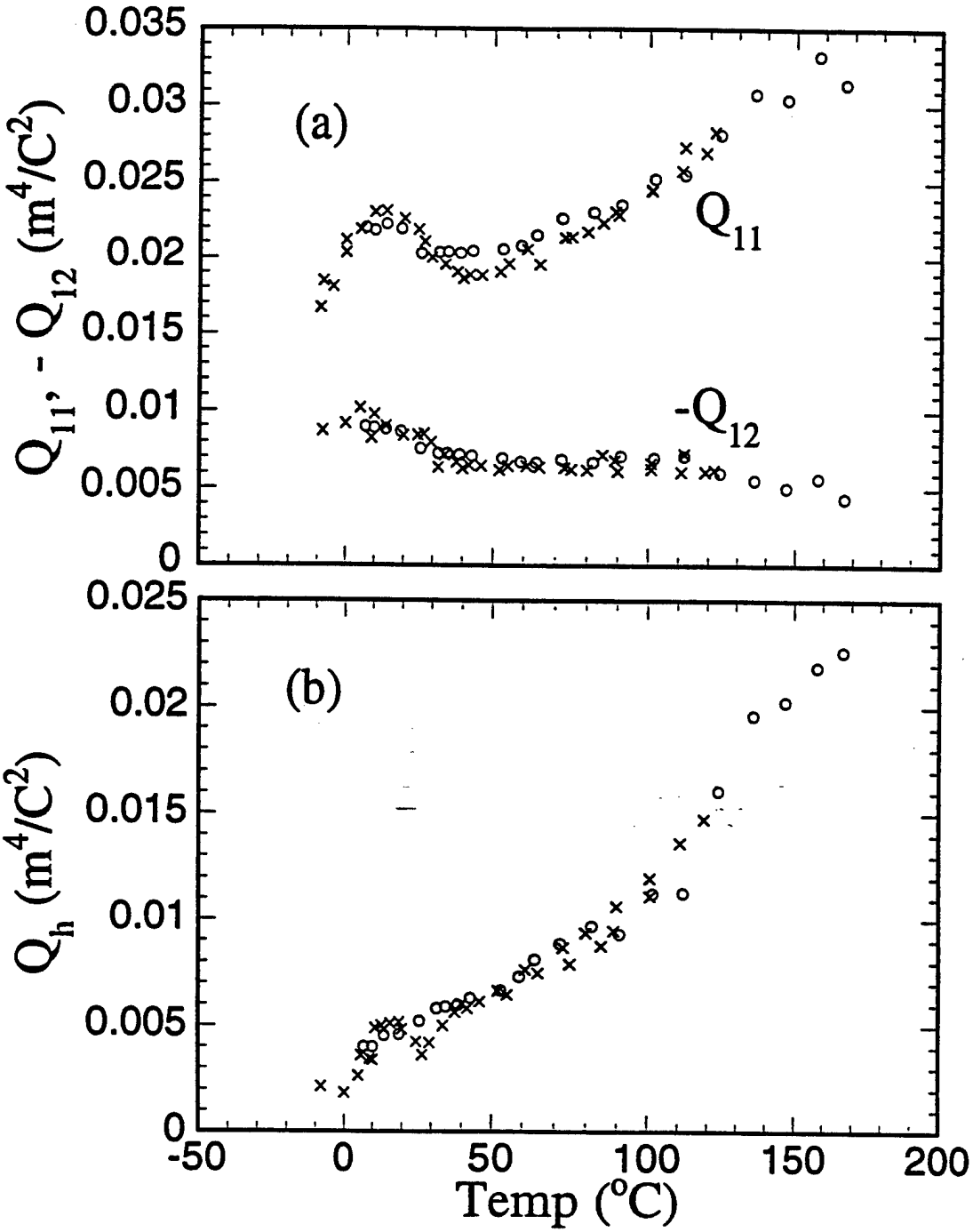
(a)
Q_{11}
$-Q_{12}$
Q_{11} - Q_{12} (m^4/C^2)
0.035
0.03
0.025
0.02
0.015
0.01
0.005
0
(b)
Q_h (m^4/C^2)
0.025
0.02
0.015
0.01
0.005
0
-50
0
50
100
150
200
Temp (°C)

F. 2

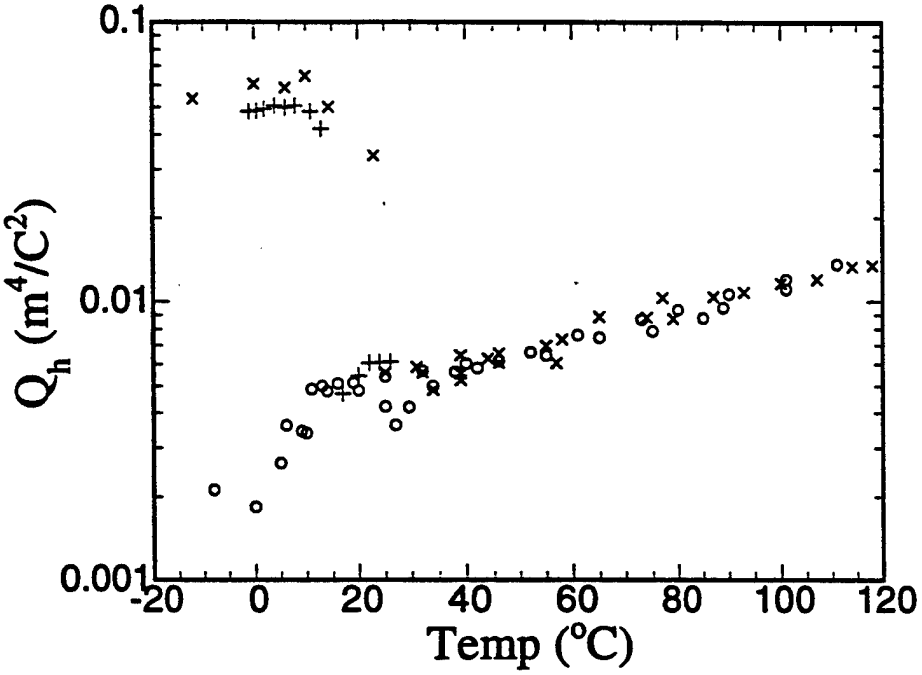
0.1
0.01
0.001
Q_h (m^4/C^2)
-20
0
20
40
60
80
100
120
Temp (°C)

APPENDIX 13

Sub. to
Phys. Rev. Lett.

Nonlinearity and Scaling Behavior in Donor Doped Lead Zirconate Titanate Piezoceramic

Volkmar Mueller and Q. M. Zhang

Materials Research Laboratory, The Pennsylvania State University,

University Park, PA 16802

Abstracts: Two different effective thresholds for the onset of nonlinearity of dielectric and piezoelectric coefficients in donor doped lead zirconate titanate (PZT) piezoceramics at electric ac-fields $E_{c1}\approx 100$V/cm and $E_{c2}\approx 1$V/cm are found. Both are characterized by non-analytic scaling behavior $x=x_0+A[E-E_c)/E_c]^{\varphi}$ above the respective threshold. The values of the effective exponent φ are apparently independent of the particular ceramic system which indicates a universal behavior of soft PZT. We suggest that the nonlinearity is dominated by the dynamics of the domain wall in a randomly pinned medium.

PACS No.: 77.84.-s, 77.84.Dy, 77.80.Dj, 68.35.Rh

Lead zirconate titanate $Pb(Zr_xTi_{1-x})O_3$ (PZT) piezoceramic represents an important example of ferroelectric materials which are used for technical devices converting electrical into mechanical energy, such as piezoelectric actuators, transducer, resonators and motors. In these applications, the piezoceramic is often subjected to high electric fields where its polarization-field and strain-field dependence is strongly nonlinear.[1] The dielectric properties of PZT are substantially influenced by the motion of domain walls which separate homogeneous regions with different orientation of the spontaneous polarization (domains).[2] Most of the domain walls in piezoceramics are additionally ferroelastic (non-180° walls) and contribute therefore also considerably to the piezocoefficient. In PZT ceramics which were doped with donor dopants such as La or Nb (soft PZT) to achieve an exceptional high domain wall mobility, experimental results indicate that a threshold for the onset of nonlinearity exists at $E_c \approx 100V/cm$.[3,4] It is believed, that the onset of irreversible domain wall motion above threshold leads to the significant nonlinearity. However, the mechanisms causing the domain wall related nonlinearity are poorly understood.

For small amplitudes $E<E_c$ of the ac-field, oscillations of domain walls which are pinned at the grain boundary and at randomly distributed defects within the grain are excited. The walls oscillating within their pinning potential with amplitudes much smaller than the lattice constant contribute in these materials considerably to the linear (zero field) susceptibility $\chi_{lin}=\partial P/\partial E$.[3] At low frequencies, an additional frequency dependent contribution to χ_{lin} arises in weak fields $E<<E_c$ due to fluctuations of parts of the wall between different metastable configurations.[5] Above E_c, the walls are depinned and start

to move freely. It was assumed that depinned walls move in an anharmonic potential so that the restoring force F_r acting on a wall depends nonlinearly on the distance Δx from its equilibrium position.[6]

In this paper, we present the results of a comprehensive study of the nonlinear dielectric and electromechanical response of several donor doped (soft) PZT piezoceramics. In order to investigate the influence of different symmetry conditions on the experimental result, the experiments were carried out in sinusoidal ac-fields which were applied both parallel and perpendicular to the poling direction of the ceramic. Piezoelectric properties were studied in addition to the dielectric measurements because this provides information about whether it is the ferroelastic or the non-ferroelastic walls which are depinned. We find that in soft PZT ceramics, in addition to the threshold reported earlier, there exists another threshold at much weaker field level. Above both effective thresholds, a non-analytic scaling behavior of the nonlinear coefficient $\chi_{nl}=P_{nl}/E$

$$\chi_{nl} = A[(E - E_c)/E_c]^{\varphi} \qquad (1)$$

is observed. The corresponding effective exponents φ are found to be independent of the particular ceramic system which indicates a universal behavior of soft PZT associated with the depinning of ferroelectric domain walls.

Theoretical models treat the threshold of collective interface motion in media with quenched random pinning disorder as a dynamical critical phenomenon with all features of conventional critical phenomena such as scaling laws and critical exponents near

threshold.[7] The subject is of great interest because it is common to a class of very different physical systems including incommensurate charge density wave systems[8], flux line lattices in type-II superconductors[9], Mott-Anderson insulators[10]and two-fluid interfaces in a random medium.[11] Though our data do not probe the critical region of a probable depinning transition in PZT-piezoceramic, the effective exponent determined experimentally in weak fields is surprisingly consistent with the theoretical mean field result.[7]

A series of donor doped PZT corresponding to different dopant level and type was chosen for this study. Presented here are the results from Motorola 3203HD, Tokin N-21 and Morgan-Matroc PZT-5H [12], which show very different Curie temperatures and weak signal dielectric and piezoelectric response. Results from other soft PZT's are consistent with those presented. The measurements were performed at room temperature. Samples were cut from the bulk material and sputtered with gold electrodes on the major faces. The 3203HD and N-21 ceramics were poled for 1 minute at a field E=20kV/cm and a temperature T=373K; PZT-5H was poled by the manufacturer. The field induced strain S(E) was measured by a glass fiber sensor (MTI 2000) under stress free (nonresonant) conditions at a frequency f=100Hz. Simultaneously, the polarization P(E) was determined using a Sawyer-Tower circuit.[2] Both the S(t) and the P(t) signal were analyzed in their first harmonic components $S^{(1f)}$ and $P^{(1f)}$ using digital lock-in amplifiers DSR-830 (Stanford Instruments). We note that all higher-order odd harmonics can basically contribute to the fundamental harmonic. However, we find that in the field range measured $S^{(1f)}$ and $P^{(1f)}$ are nearly the same as the maximum value P_{max} and S_{max} of

polarization and strain, respectively. If the ac-field is applied parallel to the poling direction of the ceramic ($E=E_3$), effective dielectric and piezoelectric coefficients $\chi_{33}=P_3^{(1f)}/E_3$ and $d_{33}=S_3^{(1f)}/E_3$ were obtained whereas an ac-field perpendicular to this direction ($E=E_1$) probes $\chi_{11}=P_1^{(1f)}/E_1$ and $d_{15}=S_5^{(1f)}/E_1$. Special attention was paid to detect the influence of dielectric heating and field induced changes of the domain structure in large fields. Therefore, a digital oscilloscope was used to compare the results obtained in the continous wave and tone burst mode where 5 periods of the ac-voltage were followed by a 3 second zero voltage dwelling time. In this paper, we report data obtained only in the field range where P_{max} and S_{max} do not depend on the mode chosen in the experiment. Particularly, we deal here with fields well below the depoling field of the ceramic. At weak fields, only the permittivity was measured using a General Radio 1616 precision capacitance bridge with an DSR-830 lock-in amplifier as an indicator.

Figure 1 presents the dependence of the effective piezoelectric and dielectric coefficients on the amplitude E of the ac-field for Motorola 3203HD. The field dependence is obvious for both directions of the field but more pronounced for $E=E_1$. From symmetry considerations it follows that the Taylor-expansions of two coefficients $z(E_1)$ and $y(E_3)$ are different:

$$z(E_3) = z_0 + z_{nl} = z_0 + \frac{z_1}{2}E_3 + \frac{z_2}{4}E_3^2 + \ldots$$
$$y(E_1) = y_0 + y_{nl} = y_0 + \frac{y_2}{4}E_1^2 + \ldots \qquad (2)$$

Here z stands for χ_{33} and d_{33} and y represents χ_{11} and d_{15}, respectively, and higher order terms are neglected.

Figure 2 shows that both the nonlinear dielectric and piezoelectric coefficients yield an excellent power law form as given in Eq.(1) which supports the hypothesis of a finite threshold for domain wall motion in soft PZT suggested earlier.[3,4] The threshold field E_{c1}=100±50 V/cm, however, can only be estimated approximately because this value depends crucially on the choice of the linear coefficient in the scaling procedure which is at fields close above E_{c1} much larger than the corresponding nonlinear terms. We also note that at least the dielectric coefficients exhibit a weak dependence on the ac-field even for $E<E_{c1}$ which will be discussed later. Due to this difficulty, we can not determine whether E_{c1} depends on the direction of the external field. The effective exponent φ was determined to be φ=1.0±0.1 for fields parallel and φ=1.2±0.1 for fields perpendicular to the poling direction of the ceramic. The former exponent seems to be consistent with Eq.(2) provided that the contribution of terms higher than linear in E can be neglected in the field range under consideration. The latter exponent is much smaller than φ=2 as expected from Eq.(2). Note that the addition of a reasonable number of higher order terms to the Taylor expansion in Eq.(2) will not lead to the experimentally observed scaling behavior. We have also measured the response of the system at lower frequencies to ensure that the exponents do not depend on frequency.

It should be pointed out that the ceramic systems under investigation differ significantly with respect to their linear dielectric and piezoelectric coefficients and to their Curie temperature which indicates the crucial role played by concentration and type of the

donor dopants added.[2] However, for a given direction of the field, the scaling of data obtained on different ceramics yields the same value of the scaling exponent which moreover does not depend on whether it is the dielectric or piezoelectric data that are analyzed. This indicates a universal behavior in the soft PZT piezoceramics investigated.

In small fields $E<E_{c1}$, we find a weak but significant ac-field dependence of the permittivity in both directions of the external field. The resolution of the strain measurement, however, is not sufficient to allow us to determine whether the piezoelectric coefficient exhibits a similar behavior. In what follows, we will therefore limit the discussion on the dielectric behavior in small fields.

Generally, the influence of the ac-field amplitude on the PZT-ceramic is twofold. First, it leads to a reversible increase of the permittivity as we have discussed for strong fields in the preceding paragraphs. Second, it changes the sample properties irreversibly which may be connected with a deaging, i.e. a partial turning back of the aging process which sets in after the poling of the ceramic. Since reversible and irreversible effects have in weak fields the same order of magnitude, we can not neglect the deaging of the sample and consider here the difference

$$\Delta\chi = \chi(E_m) - \chi(E_0) \qquad (3)$$

which we find to be independent of the particular aging state of the ceramic. Here, $\chi(E_m)$ is the susceptibility measured for a given field value E_m and $\chi(E_0)$ is the susceptibility determined *immediately after* the measurement at E_m is completed using a sufficiently small field $E_0 \leq 0.5$V/cm for which no ac-field dependence can be observed. The resulting function $\Delta\chi$ (E_{ac}) shown in Figure 3 increases for all material systems under investigation

and for both directions of the external field monotonically with E_{ac}. Despite the fact that $\Delta\chi << \chi_{lin}$, the weak field curves are similar to the ac-field dependence observed in large fields. Particularly, the weak field data can also be scaled according to Eq.(1) which is shown in Figure 4. Note that we analyze here only the ac-field dependent part $\Delta\chi$ of the susceptibility and avoid thus the ambiguity due to the unknown field independent part χ_{lin}. Therefore, the nonlinear fits provide much more precise information about the threshold E_{c2} which we find to depend on the particular ceramic system. For the materials under investigation, the threshold values are in the range $0.4V/cm < E_{c2} < 2V/cm$ and seem to be associated with the linear susceptibility of the ceramic.[13] The effective scaling exponent φ, on the other hand, shows no significant dependence on the material and hence, on the dopants type and concentration. We find, for both directions of the external field, the value $\varphi = 1.5 \pm 0.1$. As in the large field region, this result can not be attributed to the simple Taylor-expansion given in Eq.(2).

Now we discuss the observed nonlinearity of PZT piezoceramics in terms of the motion of domain walls driven by an external electric field. It was suggested that the anharmonic potential energy $U(\Delta x)$ of the wall displaced by a distance Δx from the equilibrium position may be the reason for the nonlinear domain wall response.[6] Nevertheless, any nonlinearity attributed to the potential energy of the wall has to meet the symmetry conditions and is therefore qualitatively inconsistent with the experimentally observed non-analytical scaling behavior of the PZT piezoceramics. On the other hand, the energy dissipation of the moving walls is treated up to now by a friction force depending linearly on the wall velocity.[6,14,15] This assumption seems to be oversimplified for the

description of the dynamics of a ferroelectric domain wall which represents a system with many degrees of freedom moving through a pinning medium with quenched disorder. Theoretical models developed in the context of charge density wave systems which treat the depinning transition of an elastic interface as a dynamical critical phenomenon predict a scaling behavior similar to Eq.(1) between force and velocity above the onset of interface motion[7,16]. It should be pointed out that experimental data obtained for a technical piezoceramic represent an average over all grains, 180°- and several types of non-180° domain walls with different orientations to the external field. This seems to be one reason that we cannot scale our data obtained in weak fields closer to the effective threshold E_c. We are aware, therefore, that our experiments may not probe the critical region of a probable depinning transition in soft PZT. Therefore, the effective exponents describing the non-analytic scaling behavior of the piezoceramics should not be mistaken with critical exponents of the theoretic models mentioned above. Thus it is surprising that the value of the effective exponent $\varphi=1.5\pm0.1$ found experimentally in weak fields agrees well with the theoretical mean-field exponent $\varphi=3/2$.[7] Moreover, an effective exponent $\varphi=1.45\pm0.03$ was determined recently for (non-ferroelastic) 180° domain walls in the improper ferroelectric lock-in phase of a purified incommensurate single crystal.[17] Apparently, the dynamics of domain walls leads to a similar non-analytic scaling in very different ferroelectric systems for which there seems to be no explanation at present.

The authors are grateful to Jayanth Banavar for stimulating discussions and acknowledge financial support from the Office of Naval Research.

References

[1] L.E. Cross, " Ferroelectric Ceramics: Tailoring Properties for Specific Applications" in "Ferroelectric Ceramics", edited by N. Setter and E.L. Colla (Birkhaeuser Verlag, Basel 1993)

[2] M. E. Lines and A.M. Glass, "Principles and Applications of Ferroelectrics and Related Materials", (Clarendon Press, Oxford, 1977)

[3] Q.M. Zhang, W. Y. Pan, S.J. Jang and L.E. Cross, J. Appl. Phys. **64**, 6445 (1988).

[4] Y. Saito, Jpn. J. Appl. Phys. **34**, 5313 (1995).

[5] T. Nattermann, Y. Shapir and I. Vilfan, Phys. Rev. B **42**, 8577 (1990).

[6] S. Li, W. Cao and L.E. Cross, J. Appl. Phys. **69**, 7219 (1991), see also S. Li, W. Cao, R.E. Newnham and L.E. Cross, Ferroelectrics 139, 25 (1993).

[7] D. S. Fisher, Physical Review B **31**, 1396 (1985).

[8] S. Bhattacharya, M. J. Higgins and J.P. Stokes, Phys. Rev. Lett. **63**, 1503 (1989).

[9] S. Bhattacharya and M. J. Higgins, Phys. Rev. Lett. **70**, 2617 (1993).

[10] F. Ladieu, M. Sanquer, J.P. Bouchad, Phys. Rev. B **53**, 973 (1996).

[11] J. Stokes, A.P. Kushnick, and M.O. Robbins, Phys. Rev. Lett. **60**, 1386 (1988).

[12] We studied PZT 3203HD from Motorola Inc, NM, USA, PZT N-21 from Tokin Inc., Japan and PZT-5H from Morgan-Matroc Inc, OH. USA. All are PZT-ceramics with different level of donor doping. Typical sample dimensions were 5·5·3mm.

[13] V. Mueller and Q. M. Zhang, to be published.

[14] J. Fousek and B. Brezina, J. Phys. Soc. Jpn. 19, 830 (1964).

[15] G. Arlt and N. A. Pertsev, J. Appl. Phys.**70** , 2283 (1991).

[16] P.B. Littlewood, in "Charge Density Waves in Solids", edited by L.P. Gorkov and G. Gruner (Elsevier, Amsterdam, 1989)

[17] T. Hauke, V. Mueller, H. Beige and J. Fousek, J. Appl. Phys. **79**, 7958 (1996).

Captions

FIG. 1. AC-field dependence of normalized dielectric and piezoelectric coefficients $\varepsilon_r=\varepsilon/\varepsilon_{cr}$ and $d_r=d/d_{cr}$ obtained on Motorola 3203HD. ε_{cr} and d_{cr} are the values of the corresponding coefficient determined at threshold E_{c1}=100V/cm.

FIG. 2. Scaling plot of $\xi=\chi_{nl}/A$ (see Eq.(1)) versus reduced field for the piezoceramics investigated. The quantity was evaluated above threshold E_{c1}=100V/cm from both dielectric and piezoelectric data obtained perpendicular to the poling direction. The quoted exponent refers to the straight line shown in the figure.

FIG. 3. AC-field dependence of the reversible exzess part $\Delta\chi$ of the suszeptibility (see text for details) around weak field threshold E_{c2}. The data were evaluated from the dielectric coefficients ε_{33} obtained on Motorola 3203HD and ε_{11} obtained on PZT-5H, respectively. The lines represent least square fits of the experimental data above threshold according to Eq.(1).

FIG. 4. Scaling plot of $\Delta\chi$ versus reduced field above weak field threshold E_{c2}. The quantities were evaluated from the coefficients ε_{33} obtained on Motorola 3203HD and ε_{11} obtained on PZT-5H and Tokin N-21, respectively. The lines represent least square fits of the linear part of the curves.

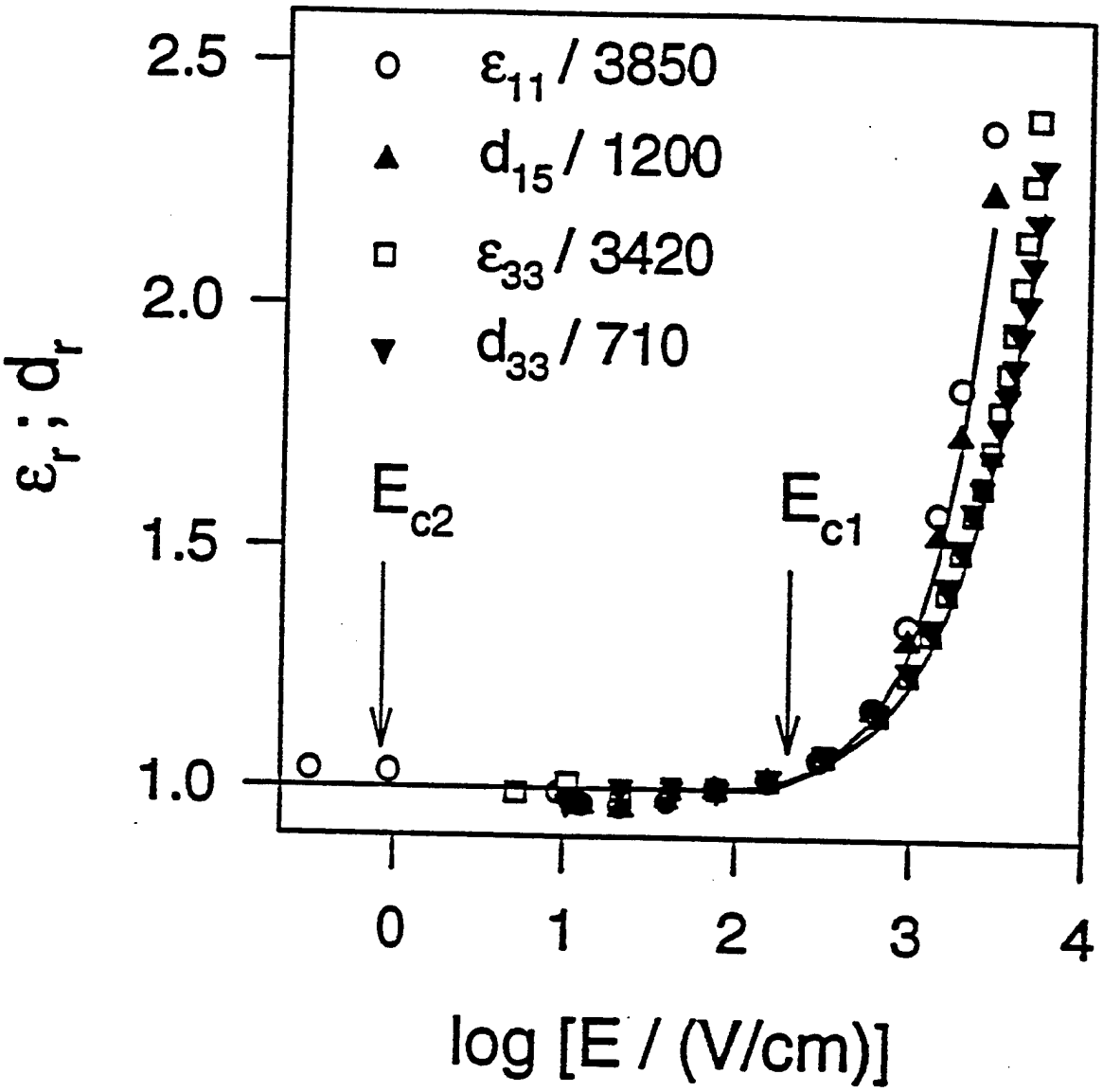
2.5
2.0
1.5
1.0
ε_r ; d_r
ε_{11} / 3850
d_{15} / 1200
ε_{33} / 3420
d_{33} / 710
E_{c2}
E_{c1}
0
1
2
3
4
log [E / (V/cm)]

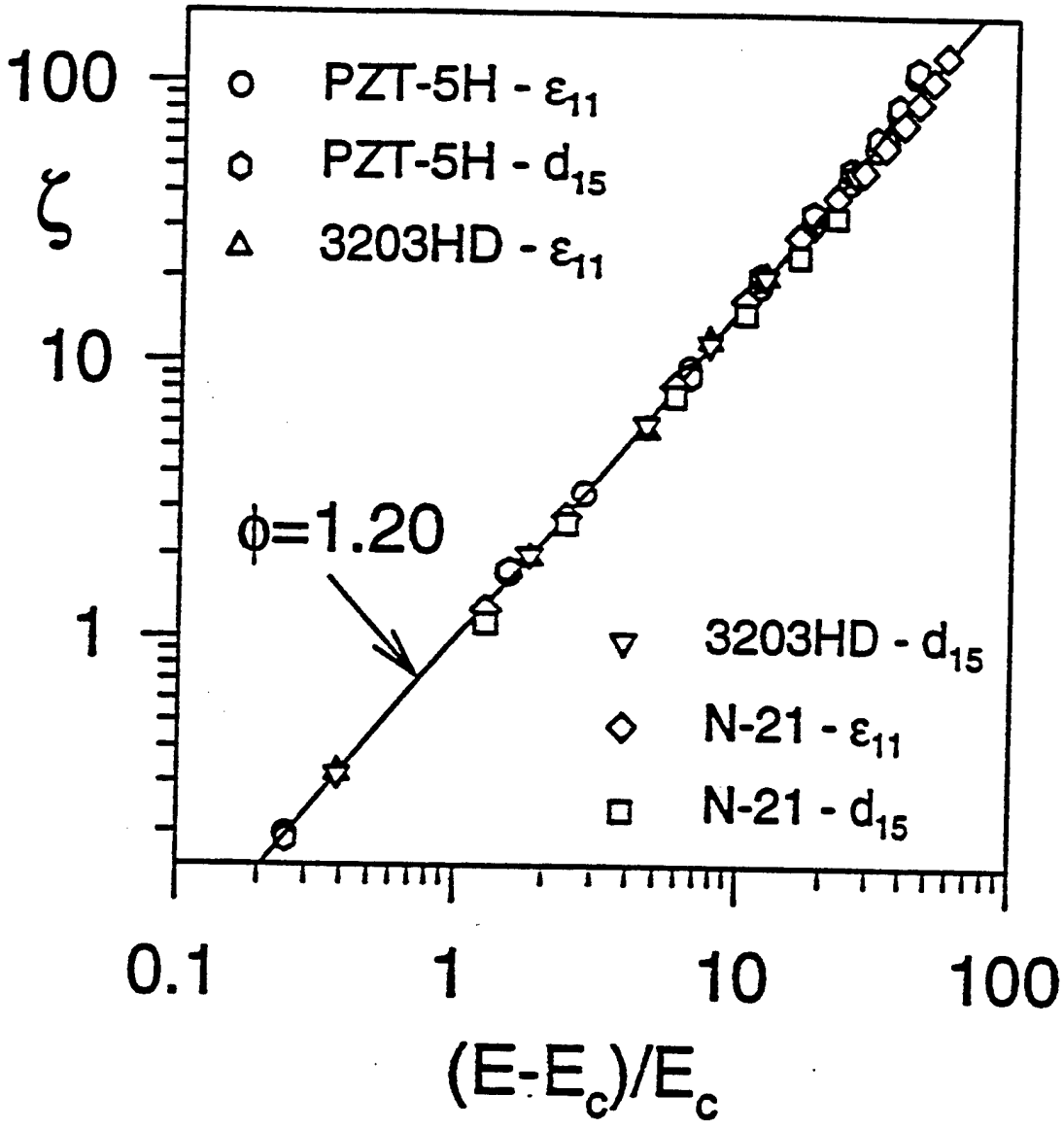
100
10
1
ζ
PZT-5H - ε11
PZT-5H - d15
3203HD - ε11
ϕ=1.20
3203HD - d15
N-21 - ε11
N-21 - d15
0.1
1
10
100
(E-Ec)/Ec

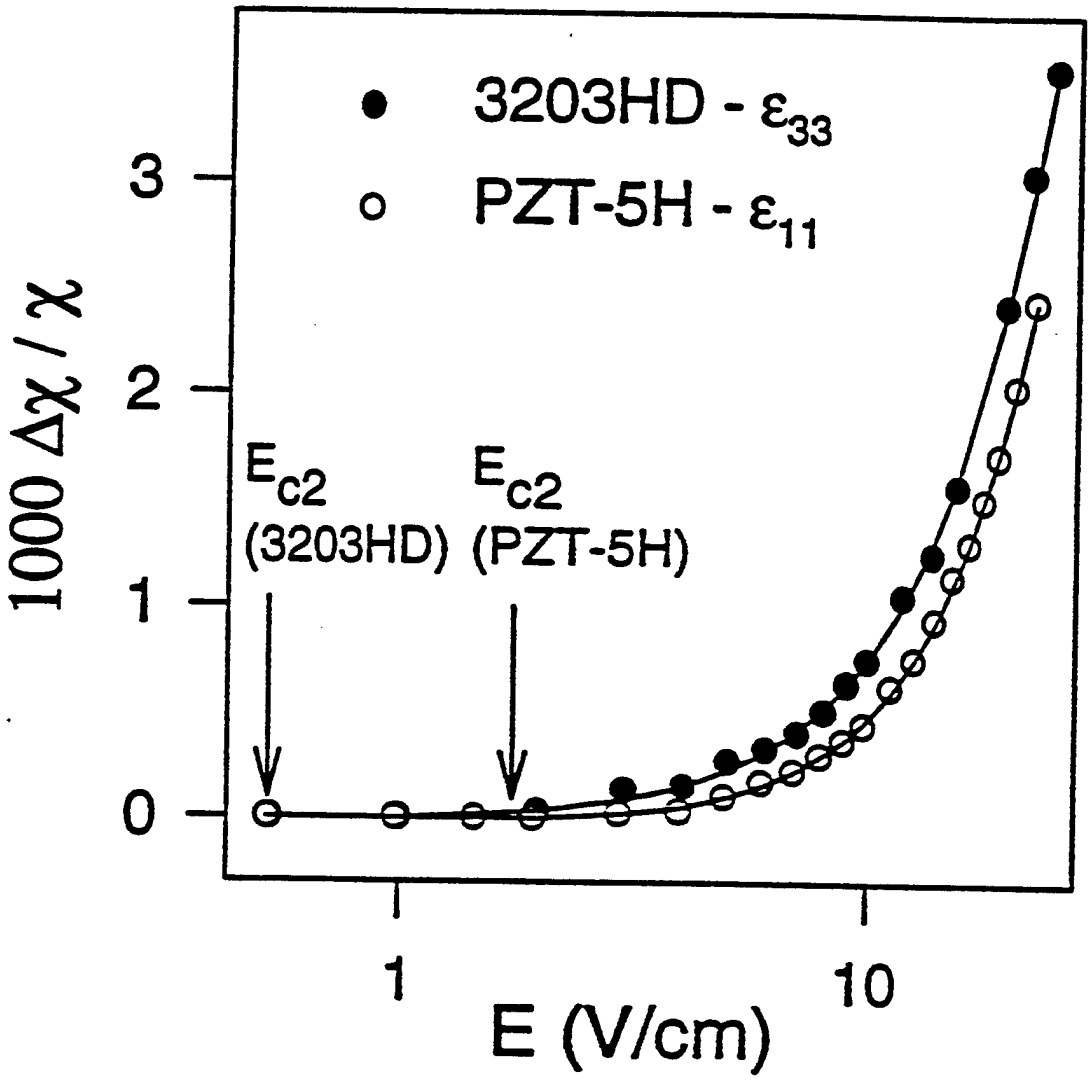
3203HD - ε_{33}
PZT-5H - ε_{11}
E_{c2} (3203HD)
E_{c2} (PZT-5H)
1000 $\Delta\chi / \chi$
0
1
2
3
1
10
E (V/cm)

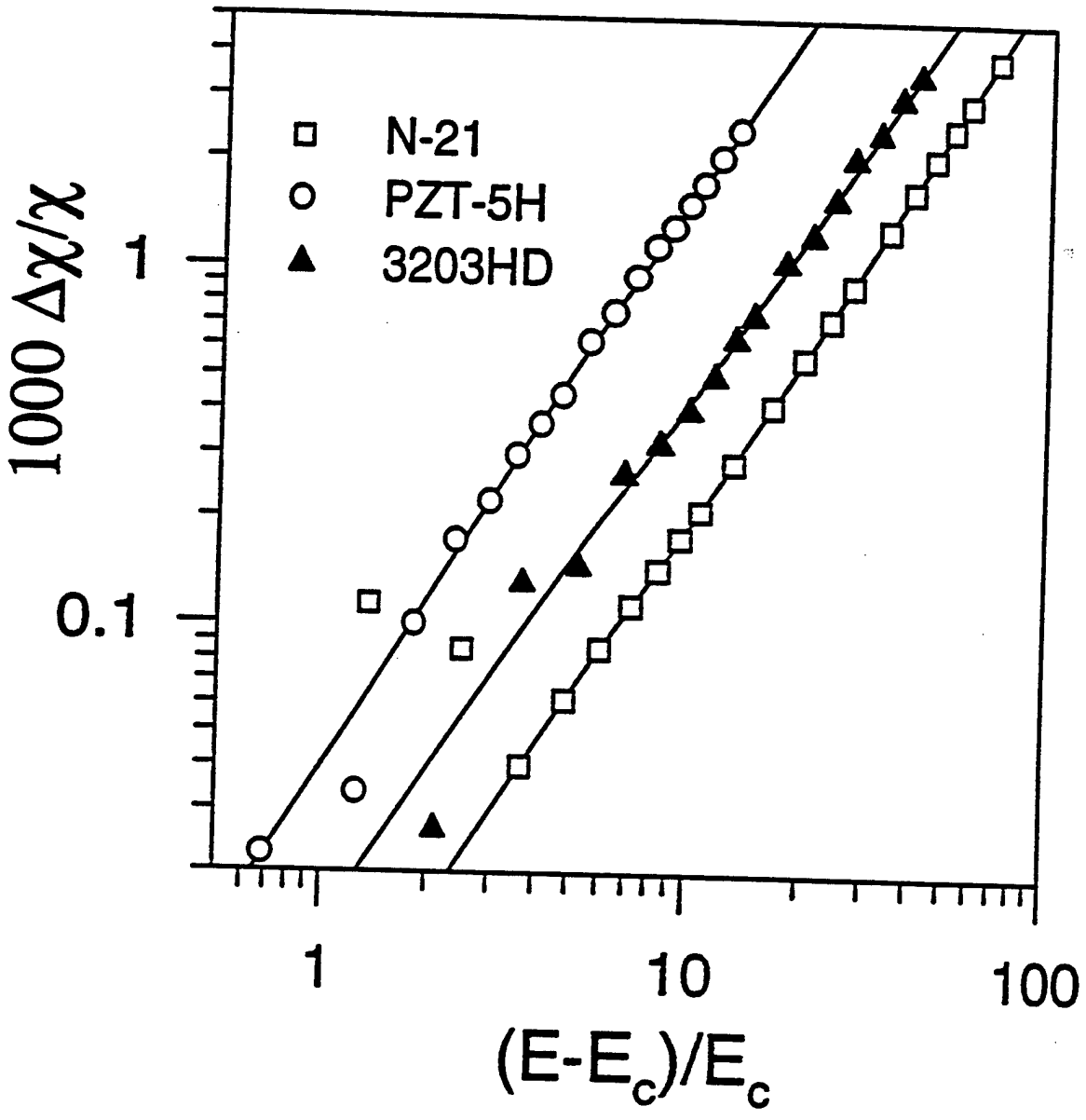
N-21
PZT-5H
3203HD
1000 Δχ/χ
1
0.1
1
10
100
(E-E_c)/E_c

APPENDIX 14

Change of the weak-field properties of $Pb(ZrTi)O_3$ piezoceramics with compressive uniaxial stresses and its links to the effect of dopants on the stability of the polarizations in the materials

Q. M. Zhang, Jianzhong Zhao, K. Uchino, and Jiehui Zheng
Materials Research Laboratory, The Pennsylvania State University, University Park, Pennsylvania 16802

(Received 7 March 1996; accepted 11 June 1996)

The properties of several $Pb(ZrTi)O_3$ (PZT) piezoceramics under compressive uniaxial stresses were characterized. It was observed that uniaxial stresses have a marked effect on the soft PZT materials, including reducing the piezoelectric coefficients and depoling the samples at relatively low stress levels. The effect of the uniaxial stresses on the properties of hard PZT's is more complicated because the domain structure of the materials can be changed substantially without depoling the samples. Therefore, under a compressive stress along the poling direction, the piezoelectric and electromechanical coupling factor can be increased markedly due to both the increased non-180° domain boundary motions and the deaging effect. In addition, the experimental results support the notion that the difference between a hard PZT and a soft PZT lies in the types of defects introduced by dopants. Immobile defects create frustrations in the lattice and result in a soft behavior, and mobile defects stabilize the polarization and produce a hard behavior.

I. INTRODUCTION

In many transducer and actuator applications, the piezoelectric ceramics are subjected to high mechanical stress field. A prior knowledge of how the material properties change under different load conditions is crucial for proper design of a device and for suitable selection of materials for a specific application. In addition, for almost all the ferroelectric films grown on foreign substrates, the thermal strain mismatch between the film and substrate will result in a residual stress which will affect the behavior of these films. Hence, the knowledge and understanding of the change of the related material properties of piezoelectric ceramics under different load conditions will be beneficial for these applications.

In general, a piezoelectric ceramic derived from ferroelectric materials has a complicated domain structure in its grains.[1,2] The properties of the material are derived from both the intrinsic contribution, which is the response from a single domain, and extrinsic contributions, which are from domain boundary motions (and sometimes also from phase boundary motions).[1–3] Utilizing the phenomenological theory, the change of material properties under different load conditions can be understood for a single domain, single crystal ferroelectric material (intrinsic contribution).[4] However, for most of the piezoelectric ceramics, it was found that the extrinsic contributions play a very important, and quite often, a major role in determining the properties of a material.[2,3,5] As has been demonstrated earlier, by carefully measuring the change of the response behavior of a piezoceramic material with external conditions, one can also gain quantitative information on the distributions of the polarization vector in a material, changes in the domain structures, and the relevant energies required to change the domain structures.[6]

For a piezoelectric ceramic material for transducer, actuator, and sensor applications, under small signal conditions, the relevant parameters are defined by the constitutive equations[7]:

$$D_i = \epsilon_{ij}^T E_j + d_{im}^d T_m \tag{1a}$$

$$S_k = d_{jk}^c E_j + s_{km}^E T_m \tag{1b}$$

where D_i is the electric displacement, S_k is the strain component, E_j is the applied electric field, and T_m is the stress component ($i, j = 1–3$, and $m, k = 1–6$). The proportional coefficients ϵ_{ij}^T, d_{im}^d, d_{jk}^c, and s_{km}^E are the dielectric constant, the piezoelectric coefficients of the direct and converse effects, and the elastic compliance, respectively. For a single crystal material, from the Maxwell relation, it can be shown that the piezoelectric coefficient in the direct effect d_{im}^d is equal to that in the converse effect d_{jk}^c.[4] For a ceramic sample, the results of a recent experiment also indicate that at the small signal level, $d_{ij}^c = d_{ij}^d$ holds to a good degree.[8]

For most of the ceramic transducer materials, the proportional coefficients in Eq. (1) will change with the driving field amplitude and with the mechanical load and electric load conditions. It is our intention to systematically characterize all these changes for the

piezoelectric ceramics currently used in the transducer, actuator, and sensor areas. Some of the results related to the polarization and electric field induced strains with the driving field amplitude at the stress-free condition have been published earlier.[9,10] The effort here was to develop a technique that would allow us to characterize all the proportional coefficients in Eq. (1) under a uniaxial stress with well-defined mechanical and electric boundary conditions. In addition, the dependence of these coefficients on the uniaxial stress at small signal level for several widely used piezoceramic ceramics, i.e., lead zirconate titanate (PZT) ceramics, is reported.

Many experimental investigations have been conducted in the last forty years on the dependence of the properties of a piezoceramic material on the mechanical stresses.[11-17] However, for the uniaxial stress effect, these experiments suffered the problem that the mechanical boundary condition was not well defined. For example, in order to determine d_{ij}^c, the electric field induced strain should be measured under a constant stress with a weak ac electric field; i.e., the second term on the right-hand side of Eq. (1b) should be constant. Similarly, the dielectric constant ϵ_{ij}^T should also be measured at a constant stress level.

II. EXPERIMENTAL

The experimental setup developed in the investigation is schematically drawn in Fig. 1. The mechanical stress was provided by a Universal Test Machine (UTM, series 1101 from ATS). A unique feature of the setup is that in the experimental system, a multilayer ceramic actuator and a feedback control loop were introduced. The function of this additional unit to the commercial UTM is to maintain a high mechanical stiffness for dc stresses while providing a very high compliance for dynamic (ac) stresses when d_{ij}^c and ϵ_{ij}^T are measured. The basic principle of the feedback loop here is if during the experiment there is a stress change, for example, due to the change in the sample dimension as an ac electric field is applied to the test sample, an error signal proportional to that stress change will be generated. This signal is amplified and used to drive the multilayer actuator to eliminate the stress change. As a result, the stress level during the measurement of ϵ_{33}^T and d_{ij}^c can be maintained at a constant level. Although there are hydraulic systems available commercially that can be used as the stress control system, they are usually operated at low frequency range. The control unit here can provide a much broader frequency range, especially to high frequencies (kHz range). The multilayer actuator was also used to drive the test samples in the measurement of d_{ij}^d and s_{ij}^E. The results allow direct calculation of the electromechanical coupling factors of these materials under uniaxial stress conditions.

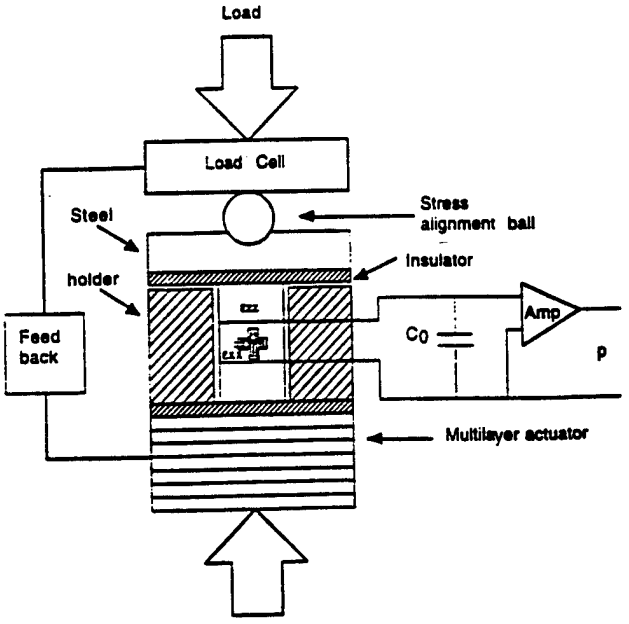

FIG. 1. Schematic drawing of the experimental setup for characterizing the influence of uniaxial stresses on the properties of ferroelectric materials. The dc load is provided by a UTM.

The dimensions of the test sample were 4.8 · 4.8 · 5 mm^3. In order to satisfy the requirement that the length of the sample should be at least three times longer than the lateral dimension to ensure a uniaxial stress, three ceramic samples were stacked together to form a test sample assembly of dimensions 4.8 · 4.8 · 15 mm^3.[18] To further reduce the end clamping effect in the lateral directions, the data were taken from the sample at the middle when all three sections were subjected to the same driving conditions.

The dielectric constant was measured using a multifrequency LCR meter (HP model 4192A). The d_{33}^d and d_{31}^d were determined from the charge output of a sample when it was subjected to an ac stress signal. The strain response of the samples was measured by a strain gauge (KYOWA KFR-02-120-C1-11). To improve the signal-to-noise ratio, the voltage signal from the strain gauge amplifier was measured by a Lock-in amplifier.

For the dielectric constant and d_{ij}^d measurement, it was found that the results did not crucially depend on the alignment of the sample. However, for d_{ij}^c and s_{ij}^E measurements, large error may result even for a very small misalignment of the sample (the stress was not uniformly applied to the test sample) or if the sample was not prepared properly so that the two faces that were subjected to the stress were not exactly parallel to each other. A special sample holder was designed to ensure a proper alignment of the test samples.

All the results reported here were acquired at room temperature and a frequency of 10 Hz. It is expected that upon changing the stress level, there is a finite

time period for the material to reach a new equilibrium state. It was found that most of the changes of the data occurred at the first 5 min after the change of the dc stress level. We also examined several samples under longer waiting time periods and found that there are not marked changes in the weak signal properties between the data taken after 10 min and after one day. This is consistent with the earlier experimental observations that the aging of the weak signal material properties in the stresses state is small (or takes a very long time).[13] Hence, in the experiment, all the data were taken 10 min after the change of the stress level. The results reported were taken from the first stress cycle. the error for the dielectric constant and piezoelectric coefficient is within ±4%. For the elastic compliance, the error is within ±6%. The error range was determined by repeating the measurement on test samples cut from the same large sample.

The PZT ceramic samples selected for the study are PZT-5H, PZT-5A, PZT-4, and PZT-8 purchased from Morgan Matroc, Inc.[19] PZT-5H and PZT-5A are donor doped (La in PZT-5H and Nb in PZT-5A). PZT-4 and PZT-8 are acceptor doped (Cr in PZT-4 and Fe and Mn in PZT-8). PZT-5H and PZT-5A are soft type PZT which have high piezoelectric, dielectric coefficients, and elastic compliance, while PZT-4 and PZT-8 are hard type PZT which have relatively low piezoelectric, dielectric coefficients, and elastic compliance. For the convenience of the presentation, the relevant parameters for these materials at stress-free conditions are listed in Table I. Apparently, the responses of the materials evolve from soft to hard following the sequence of PZT-5H, PZT-5A, PZT-4, and PZT-8.

III. EXPERIMENTAL RESULTS

Shown in Fig. 2 are the stress dependence of d_{33}^{c} and d_{33}^{d} for PZT-5H. Apparently, within the data scatters, d_{33}^{c} and d_{33}^{d} are the same in the stress range the measurement was made. In fact, for all the samples investigated, the piezoelectric coefficients, both d_{33} and d_{31}, determined from the converse effect and direct effect are the same within the data scatter. To our knowledge, this is the first direct comparison of the piezoelectric coefficients from the two effects measured simultaneously on a same sample. The results here indicate that for ceramic samples the weak signal piezoelectric coefficients determined from the direct and converse piezoelectric effects are approximately the same even when the samples are subjected to uniaxial stresses. Hence, in the following discussion, we will not make a distinction between the piezoelectric coefficients determined from the direct and converse effects.

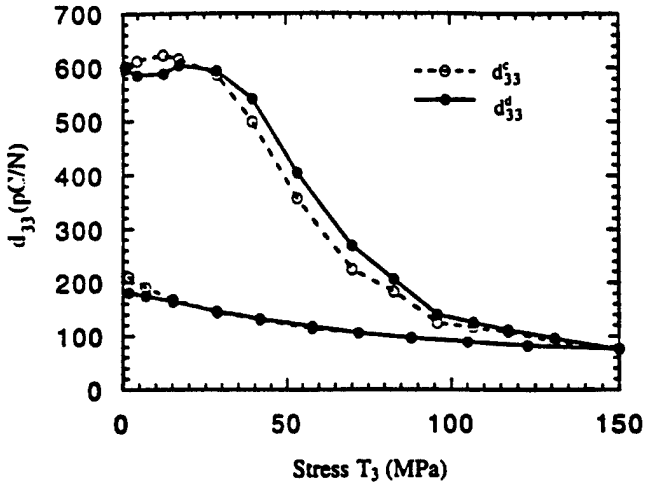

FIG. 2. The dependence of the weak signal piezoelectric coefficients d_{33}^{c} (the direct piezoelectric effect) and d_{33}^{d} (the converse piezoelectric effect) of PZT-5H on the compressive uniaxial stress T_3. Within the data scatter, the two are nearly the same in the experimental stress range.

TABLE I. The properties of PZT piezoceramics under stress-free condition.

Material	PZT-5H	PZT-5A	PZT-4	PZT-8
d_{33}	593	374	296	225
d_{31}	−274	−171	−123	−97
ϵ_{33}	3400	1700	1300	1000
s_{33}	20.7	18.8	15.5	13.9
s_{13}	−8.45	−7.22	−5.31	−4.6
s_{11}	16.5	16.4	12.3	11.1
k_{33}	0.75	0.7	0.7	0.64
k_{31}	0.39	0.34	0.33	0.3

d: pC/N, s: 10^{-12} m^2/N.

Shown in Fig. 3 are the dependence of d_{33}, d_{31}, ϵ_{33}, s_{33}, and s_{13} on the compressive stress parallel to the polar axis (T_3). At the stress level below about 30 MPa, d_{33} and d_{31} stay approximately at constant values. At higher stresses, the piezoelectric activity drops quite rapidly. For instance, as T_3 increases from 30 MPa to 60 MPa, the piezoelectric activity drops more than half. At 150 MPa, there is very small piezoelectric activity left. Upon releasing of the uniaxial stress, there is a weak increase of d_{ij}; however, the value of d_{ij} at zero stress now becomes much smaller than the initial value, indicating that there is a substantial depoling of the sample under the compressive stress. Clearly, PZT-5H is not suitable for high stress applications. In contrast, the dielectric constant does not show as much variation, and as the stress increases from zero to about 40 MPa, the dielectric constant shows a slight increase, and beyond that, the dielectric constant drops. The effect of the compressive stress on the elastic compliance is always monotonical; i.e., increasing the stress stiffens the sample. For this material in the stress range studied, the ratios of d_{31}/d_{33} and s_{13}/s_{33} do not change with stress.

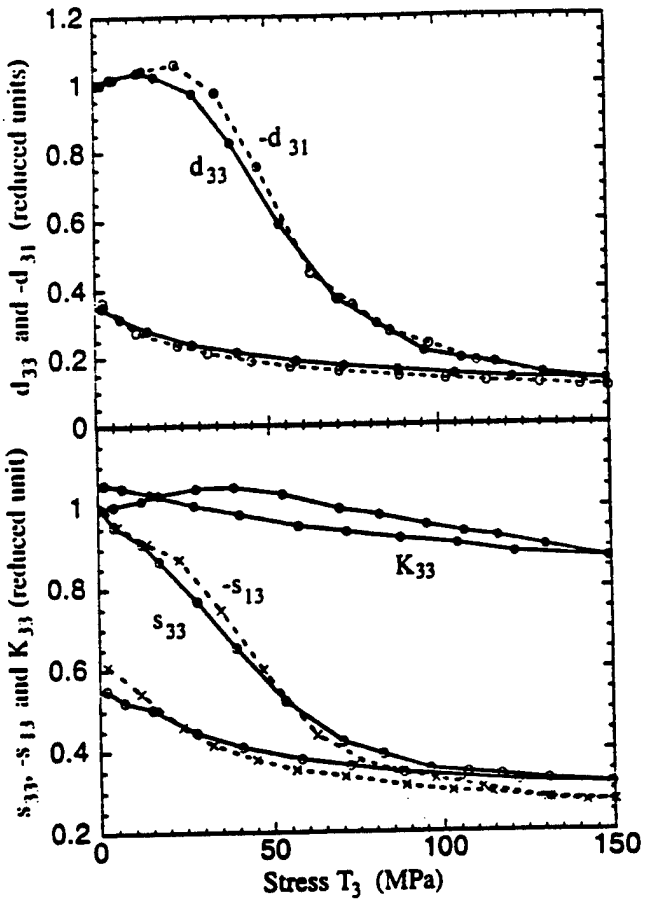

FIG. 3. The dependence of the weak signal piezoelectric coefficients (d_{33} and d_{31}), dielectric constant K_{33}, and elastic compliance (s_{33} and s_{13}) of PZT-5H on the compressive uniaxial stress T_3.

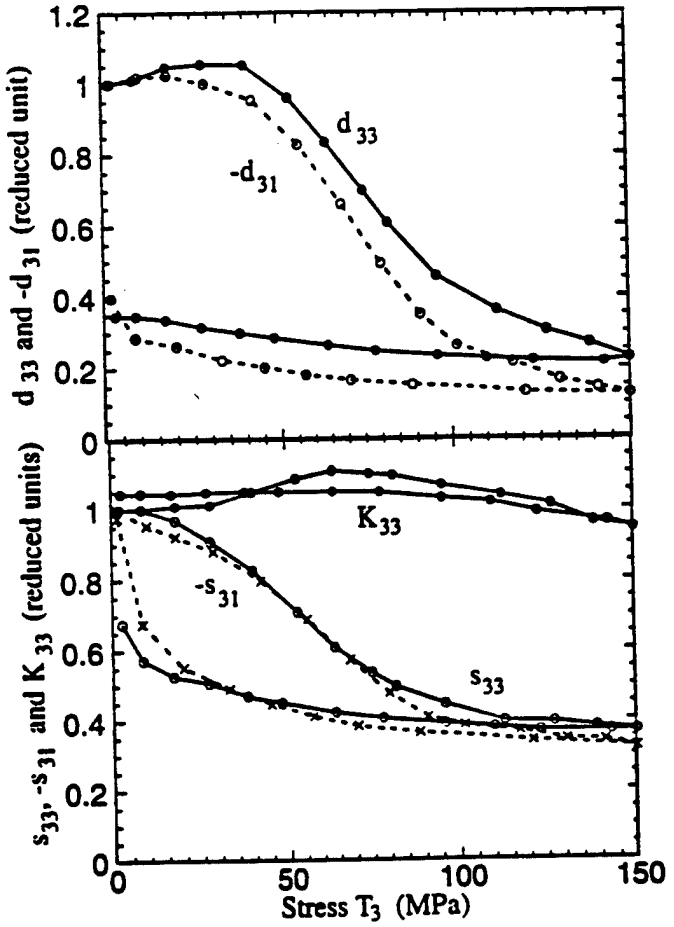

FIG. 4. The dependence of the weak signal piezoelectric coefficients (d_{33} and d_{31}), dielectric constant K_{33}, and elastic compliance (s_{33} and s_{13}) of PZT-5A on the compressive uniaxial stress T_3.

Figure 4 presents the data for PZT-5A of the influence of the compressive stress T_3 on d_{33}, d_{31}, ϵ_{33}, s_{33}, and s_{31}. As expected, the effect of stress on PZT-5A is less than that on PZT-5H. The piezoelectric coefficients stay at approximately constant values for T_3 below about 50 MPa as the stress is increased from the initial state. Under high stress load, the sample was also partially depoled as indicated by a much reduced d_{ij} value as T_3 is reduced from 150 MPa to zero. The elastic stiffening of the sample under stress was also observed and the increase of the dielectric constant with stress was more pronounced for PZT-5A. For this material, the ratio of $|d_{31}/d_{33}|$ exhibits some decrease with stress while the ratio of $|s_{13}/s_{33}|$ does not change with stress.

For PZT-4, as the data presented in Fig. 5, the effect of T_3 on the piezoelectric response is quite interesting. Both d_{33} and d_{31} exhibit a marked increase with T_3: d_{33} reaches a peak value at about 60 MPa while d_{31} does so at about 90 MPa. Upon reducing the stress to zero, both d_{33} and d_{31} exhibit higher values. This is also quite different from those observed in the soft PZT materials. The results imply that there is no significant depoling in the sample under a compressive stress at the 150 MPa level. In addition, the change of the domain configuration due to T_3 provides an enhanced piezoelectric response. In this stress region, the elastic compliance decreases while the dielectric constant increases with T_3. In addition, at high stress levels, there is a large increase in the ratios of $|d_{31}/d_{33}|$ and $|s_{13}/s_{33}|$.

For PZT-8, an even harder material, increasing the compressive stress T_3 up to 150 MPa does not cause the piezoelectric coefficients to subside as observed in other PZT ceramics. Instead, a slow increase of the piezoelectric coefficients with T_3 was observed. At 150 MPa, d_{31} is about 55% higher and d_{33} is about 45% higher than the initial values, respectively. The dielectric constant also exhibits a similar increase. While in the same stress range, the elastic compliance s_{33} and s_{13} stay nearly constant. The data are presented in Fig. 6.

The influence of the compressive stress T_1 on the properties of these piezoceramics was also characterized. Shown in Fig. 7 are the experimental results. The highest stress level employed in the experiment was 150 MPa. For all the samples tested, the dielectric constant ϵ_{33} does

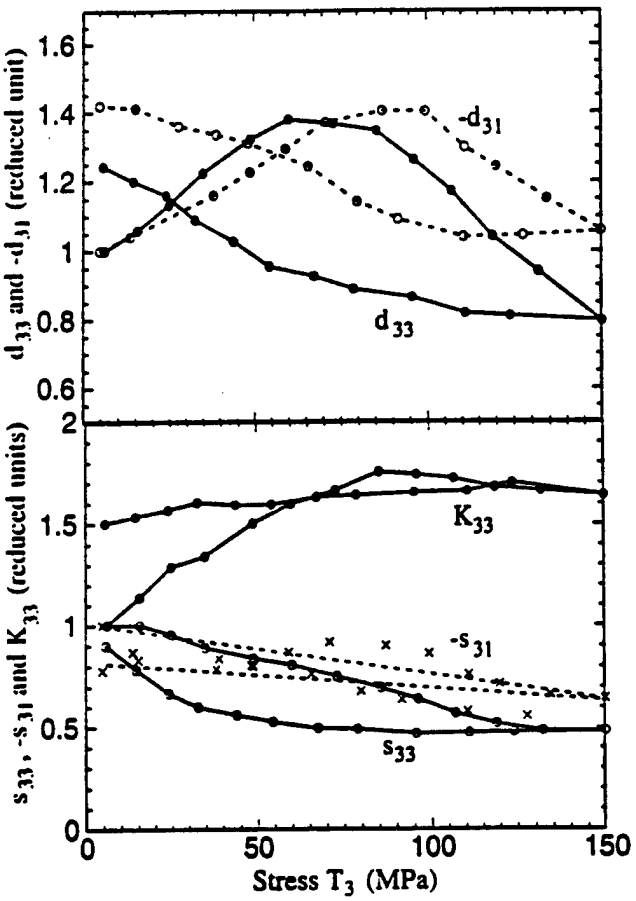

FIG. 5. The dependence of the weak signal piezoelectric coefficients (d_{33} and d_{31}), dielectric constant K_{33}, and elastic compliance (s_{33} and s_{13}) of PZT-4 on the compressive uniaxial stress T_3.

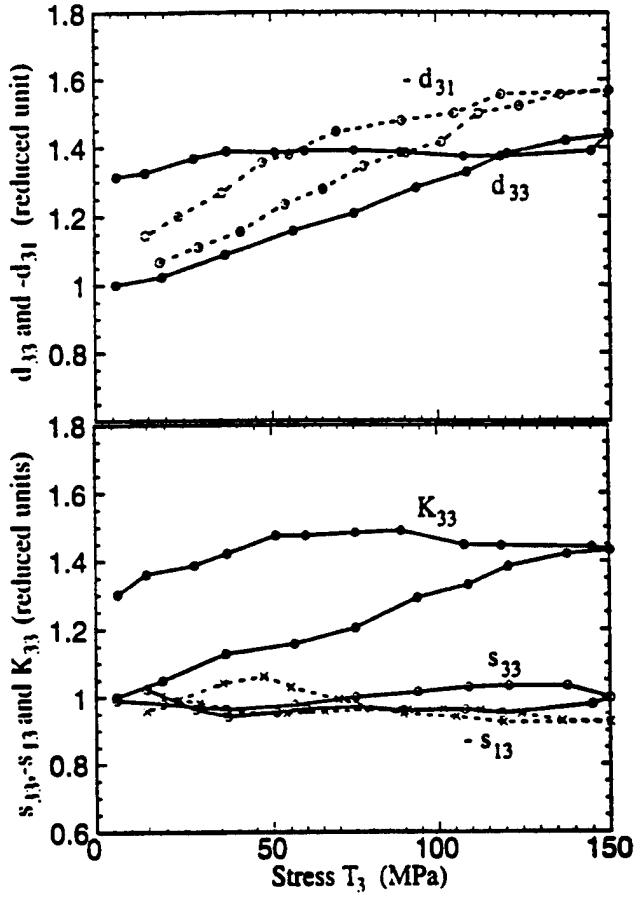

FIG. 6. The dependence of the weak signal piezoelectric coefficients (d_{33} and d_{31}), dielectric constant K_{33}, and elastic compliance (s_{33} and s_{13}) of PZT-8 on the compressive uniaxial stress T_3.

not show marked change with stress and exhibits very little hysteresis upon the stress cycle. In contrast, the piezoelectric coefficient d_{31}, which is the piezoelectric response parallel to the direction of the compressive stress, shows a steady decrease with T_1. For PZT-5H, -5A, and -4, the reduction is quite substantial. At 150 MPa, d_{31} for PZT-5H is only a little over 10% of the initial stress-free value. For PZT-5A and -4, the response behavior to the stress is very similar and the value at 150 MPa is at about 20% of the initial value. In contrast, the effect of T_1 on PZT-8 is less severe and d_{31} at 150 MPa is about 60% of the initial value and upon the stress cycle, the material does not show much hysteresis. Hence, when using piezoceramic at d_{31} mode under high loads, PZT-8 is a better choice than the others. The elastic compliance s_{11} also becomes smaller as T_1 increases.

From the data acquired, the electromechanical coupling factors k_{33} and k_{31} with the stresses T_3 and T_1 can be evaluated. Presented in Figs. 8 and 9 are the results for k_{33} and k_{31}, respectively. For both PZT-5H and -5A, there is a small increase in k_{33} with T_3 before the samples become partially depoled. However, for PZT-4 and -8, even though their initial k_{33} is lower than those of PZT-5A and -5H, with increased T_3, their k_{33} can reach about 0.8, a marked increase from the stress-free value. On the other hand, k_{31} always decreases with T_1. For PZT-8, the effect of T_1 is not as significant as in other examples.

IV. DISCUSSION

The results presented indicate that mechanical stresses can induce substantial changes in the properties of the PZT piezoceramics. When utilizing these materials against mechanical load, d_{33} mode is preferable to d_{31} mode. As seen in the previous section, for PZT-5H, d_{33} does not change with T_3 if the stress is below 30 MPa, while d_{31} in the same stress range is reduced by 50%. On the other hand, if the d_{31} mode has to be used under load, PZT-8 is a better choice than the others. Although PZT-4 is also a hard material, the dependence of its piezoelectric properties on T_1 is quite similar to that of the soft material PZT-5A.

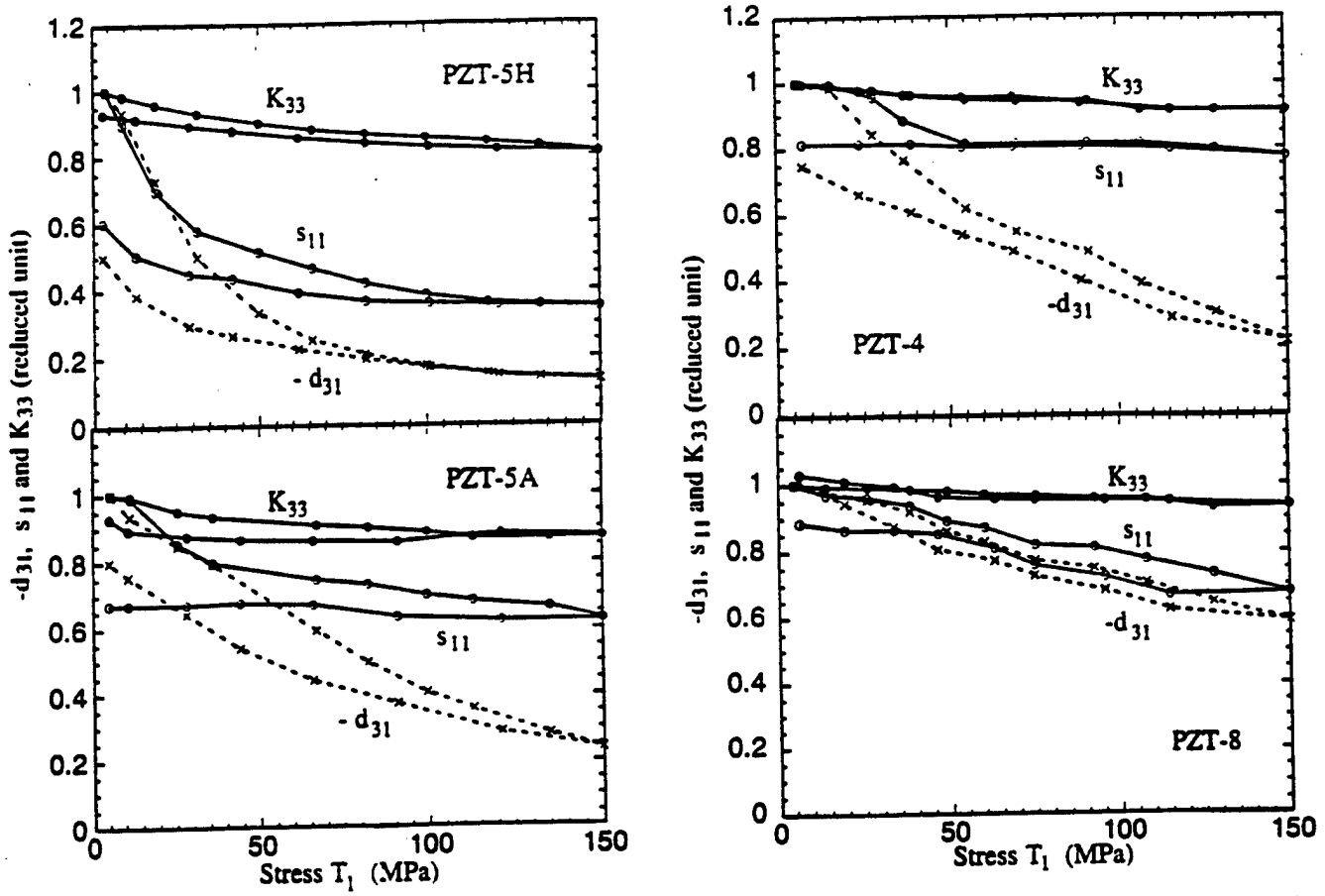

FIG. 7. The dependence of the weak signal piezoelectric coefficient d_{31}, dielectric constant K_{33}, and elastic compliance s_{11} on the compressive uniaxial stress T_1 for PZT-5H, PZT-5A, PZT-4, and PZT-8.

For PZT materials studied here, one interesting question is what role the dopants play in producing the hard and soft materials.[1] The results here provide some insight on the mechanisms of the dopants in producing different response behaviors in PZT ceramics.

In the PZT piezoceramics investigated here, there are two types of boundaries that can contribute to the response behaviors of the material, i.e., the domain boundaries and the phase boundaries (between the tetragonal phase and rhombohedral phase). The appearance of domain structures in a ferroelectric ceramic material is common, and can reduce the electric energy and release stresses at the grain boundaries.[1,4,5] Depending on whether the polarization vectors in the neighboring regions are in anti-parallel configuration or otherwise, 180° wall and non-180° walls can exist. The 180° wall movement produces only the dielectric response while non-180° wall movement produces the dielectric, piezoelectric, and elastic responses. In poled PZT ceramics, it has been shown that the density of 180° domain walls is relatively low compared with non-180° domain walls.[20,21] When a PZT piezoceramic is subjected to an external field, its domain structure will change. In the literature, the change of the domain configurations is often described by the movements of the domain and phase boundaries. Since it does not affect the discussion, we will not differentiate the phase boundary motions from the domain boundary motions here.

In PZT piezoceramics, it has also long been recognized that changing the type of dopants and doping level can change the domain boundary activities markedly. For a donor-doped material, the response is soft type, i.e., increased dielectric and piezoelectric responses, while in an acceptor-doped material, the response of the domain structure is significantly reduced. It is widely believed that in donor-doped PZT's, lead vacancies are created which form defect dipoles with the dopants and are not mobile. On the other hand, for acceptor-doped PZT's, oxygen vacancies are created to form mobile defect dipoles.[1] Although there have been many discussions concerning the functions of the dopants in PZT piezoceramics, the link between the defects formed due to the doping and the "hard" or "soft" PZT behavior is still not very clear. We believe that it is the difference in the mobility (translational and/or orientational) of the defects in the host lattice that makes the responses in the soft and hard materials different. In this scenario, in PZT's with mobile defect dipoles, the dipoles will

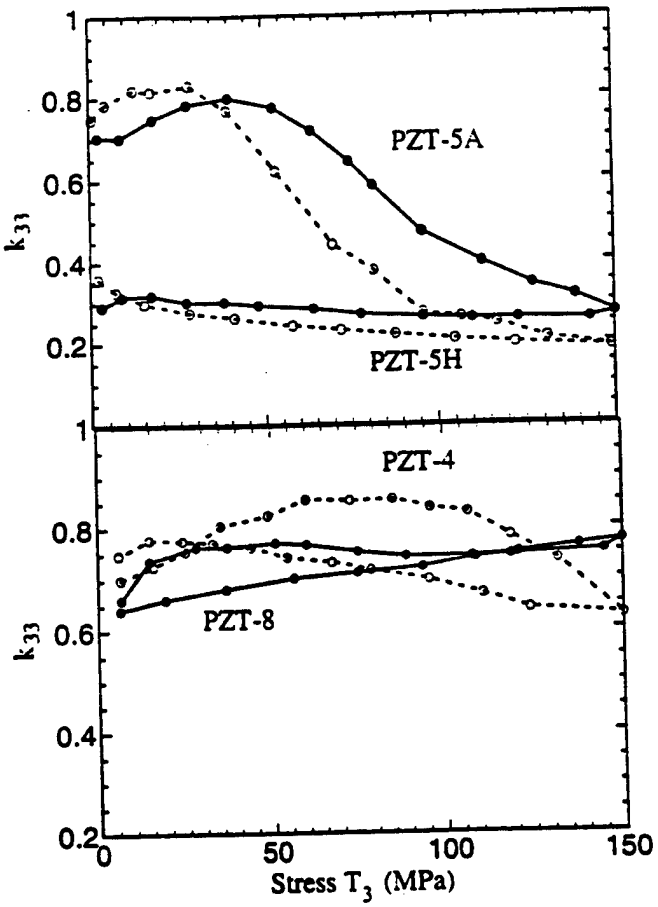

FIG. 8. The dependence of the longitudinal electromechanical coupling factor k_{33} on the compressive uniaxial stress T_3 for the four PZT piezoceramics investigated.

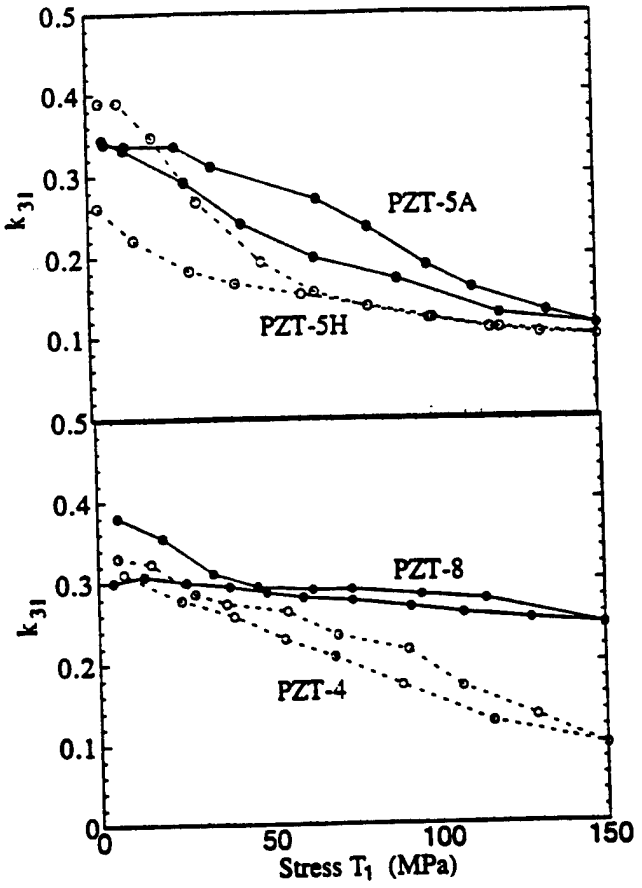

FIG. 9. The dependence of the transverse electromechanical coupling factor k_{31} on the compressive uniaxial stress T_1.

gradually align with the polarization in the surrounding host lattice and, therefore, act as a local field stabilizing the polarization (and the domain wall structures). As a result, the domain structure becomes very stable which results in weak dielectric, piezoelectric, and elastic responses. It is this slow alignment of the mobile dipoles with the polarizations in the surrounding lattices that causes a long aging time in hard PZT materials. Hence, by raising the temperature, aging time can be reduced as observed.[22] On the other hand, the immobile defect dipoles in the PZT lattice will act as frozen in random fields which introduces frustrations to the domain structures since some of the defect dipoles will not align with the preferred polarization direction in a poled material. As a consequence, the domain structure is not very stable against external applied fields (mechanical stress and electric field) and the material exhibits a soft behavior. A schematic drawing of the two situations is presented in Figs. 10(a) and 10(b).

In a piezoceramic material, there is a distribution of polarization about the poling direction. As a compressive T_3 stress is applied to a sample, some polarizations will move away from the poling direction, as schematically drawn in Fig. 10(c). As a consequence, there will be changes in the domain structures. If the poling level of the sample is not changed significantly, this change in the domain structure may induce increases in the piezoelectric and dielectric responses of the material, as observed in soft PZT's which show some increases in d_{33}, d_{31}, and ϵ_{33} at low stress level and hard PZT's where this increase in d_{33}, d_{31}, and ϵ_{33} extends to a higher stress region. The phenomenon could be analogous to that observed in $Pb(Zn_{1/3}Nb_{2/3})O_3$ single crystals where larger piezoelectric constants are obtained when the crystal is poled along an axis different from the direction of the spontaneous polarization compared with that poled along the direction of the spontaneous polarization.[23] The large drop in the piezoelectric coefficients of the soft PZT's at high stress level is due to the stress depoling effect. For hard PZT's the depoling stress level is higher than 150 MPa. Further study to higher stress level will be carried out to locate the depoling stress fields for hard PZT materials.

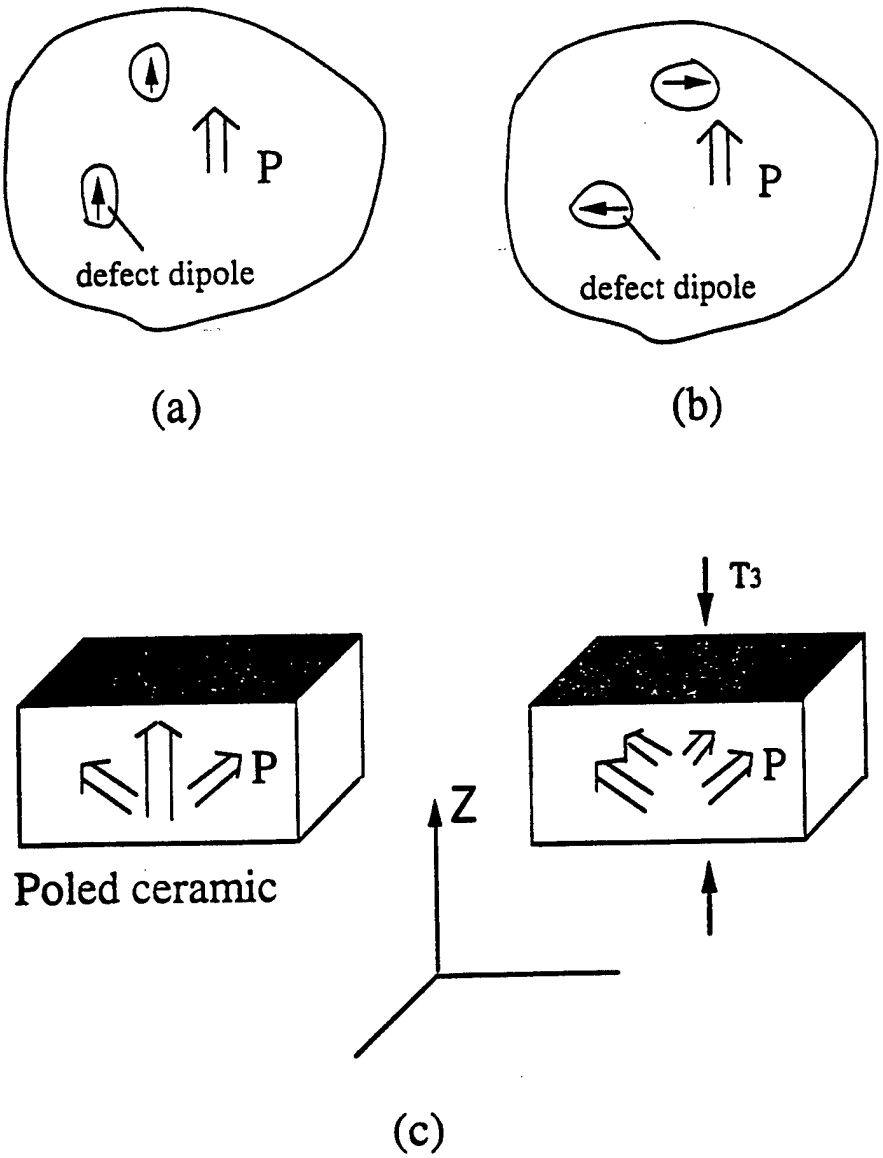

FIG. 10. (a) Schematic drawing of a hard PZT material where the defect dipoles align with the polarization in the host lattice and stabilize the polarization. The mobile defects slowly align with the surrounding host lattice during the sample aging. (b) Schematic drawing of a soft PZT material where the defect dipoles do not align with the polarization in the host lattice and introduce frustrations which lead to the "soft" behavior of the material. (c) Schematic drawing of the effect of the compressive stress T_3 on the polarization vector distribution in a poled ceramic sample. T_3 will move the polarization directions to the plane perpendicular to it.

As we have pointed out, the behaviors of hard PZT's are due to the stabilization of the domain structure by the defect dipoles which align with the polarizations of the host lattice during the aging process. Therefore, the change in the domain structure due to the stress T_3 will incur the misalignment of the polarization with the defect dipoles in some regions since the defects cannot follow this change in a short time period. Hence, in these regions, the function of defect dipoles becomes quite similar to those in a soft PZT material, i.e., introducing frustrations in the new domain structure and raising the piezoelectric and dielectric constants in the material. This is another source to increase the dielectric and piezoelectric constants in a hard PZT material which can be termed as deaging effect. The degree of this contribution will depend on how much the stress can perturb the domain structure in the material before the depoling occurs. With a long time aging, it is expected that these dipoles will gradually align with the new domain structures, and the PZT's under stress field will return to hard behavior. However, as has been shown in an early study, even for a sample aged after a long time under stress field, there is still a large increase in the piezoelectric and dielectric constants.[13] This result indicates that the increased non-180° domain boundary motions in the hard PZT's can

contribute markedly to the piezoelectric and dielectric constants.

One interesting feature revealed by this study is that for the PZT ceramics, even in the stress region where the piezoelectric and dielectric constants exhibit increases with the stress T_3, the elastic compliance always decreases. Only for PZT-8, the elastic compliances stay nearly constant with the stress. In the soft PZT's the result indicates that the change in the domain configuration due to the compressive T_3 stress will always reduce the small signal compliance, while in the hard PZT's, the combined effect of the change in the domain configuration and the deaging results in a much smaller change in the elastic compliance with stress compared with the soft PZT's.

The reduction of d_{31} and s_{11} with the compressive stress T_1 is understandable. The effect of the stress is to move the polarization vectors away from the direction of the stress field which will apparently reduce the non-180° degree domain wall motions in that direction. Here, the deaging effect is not sufficient to bring the d_{31} up in the hard PZT's.

Since the change in the domain structure plays a very important role in the response behaviors of the PZT's to external stresses, x-ray diffraction measurement, which characterizes the non-180° changes of the polarization vectors in the materials, will be carried out in the future.

V. SUMMARY AND CONCLUSIONS

A new and unique apparatus was developed which allows one to measure all the proportional coefficients in the constitutive equations under uniaxial stresses for a piezoceramic material with well-defined mechanical boundary conditions. Making use of this device, the properties of several PZT piezoceramics under uniaxial stresses were characterized. It was observed that uniaxial compressive stresses have a marked effect on the soft PZT materials, including reducing the piezoelectric coefficients and depoling the samples at relatively low stress levels. The effect of the uniaxial stresses on the properties of hard PZT's is more complicated because the domain structure of the materials can be changed substantially without depoling the samples. Therefore, under a compressive T_3 stress, the piezoelectric and electromechanical coupling factor can be increased substantially due to both the increased non-180° domain boundary motions and the deaging effect. Hence, the application of compressive stress T_3 can be a useful technique to enhance the piezoelectric responses in hard PZT's. In addition, the experimental results support the notion that the difference between a hard PZT and a soft PZT lies in the types of defects introduced by dopants. Immobile defects create frustrations in the lattice and result in a soft behavior, and mobile defects stabilize the polarization and produce a hard behavior.

For the applications of the PZT materials under external stresses, the results indicate that the d_{33} mode is preferred over the d_{31} mode. For d_{31} mode operation under external stresses, PZT-8 seems to be a better choice than the others.

ACKNOWLEDGMENTS

The authors wish to thank Professor L. E. Cross and Professor T. Shrout for stimulating discussions. Financial support of this work by the Office of Naval Research through Grant Nos. N00014-94-1-1140 and N0014-92-J-1510 is greatly appreciated.

REFERENCES

1. B. Jaffe, W. R. Cook, and H. Jaffe, *Piezoelectric Ceramics* (Academic Press, London and New York, 1971).
2. G. Arlt, J. Mater. Sci. **25**, 2655 (1990).
3. X. L. Zhang, Z. X. Chen, L. E. Cross, and W. A. Schulze, J. Mater. Sci. **18**, 968 (1983).
4. A. F. Devonshire, Philos. Mag. **3**, 85 (1954).
5. Q. M. Zhang, H. Wang, N. Kim, and L. E. Cross, J. Appl. Phys. **75**, 454 (1994).
6. M. E. Lines and A. M. Glass, *Principles and Applications of Ferroelectrics and Related Materials* (Clarendon Press, Oxford, 1977).
7. IEEE Standard on Piezoelectricity, ANSI/IEEE, Std. 176 (1988).
8. H. Wang, Q. M. Zhang, and L. E. Cross, Jpn. J. Appl. Phys. **32**, L1281 (1993).
9. Q. M. Zhang, W. Y. Pan, S. J. Jang, and L. E. Cross, J. Appl. Phys. **64**, 6445 (1989).
10. Q. M. Zhang, H. Wang, and J. Zhao, J. Intel. Mater. Syst. Struct. **6**, 84 (1995).
11. D. Berlincourt and H. Krueger, J. Appl. Phys. **30**, 1804 (1959).
12. H. Krueger and D. Berlincourt, J. Acoust. Soc. Am. **33**, 1339 (1961).
13. R. Y. Nishi, J. Acoust. Soc. Am. **40**, 486 (1966).
14. H. Krueger, J. Acoust. Soc. Am. **42**, 636 (1967).
15. Y. Nakajima, T. Hayashi, I. Hayashi, and K. Uchino, Jpn. J. Appl. Phys. **34**, 235 (1985).
16. K. Uchino, *Piezoelectric & Electrostrictive Actuators* (Morikita Pub., Tokyo, 1986).
17. Hengchu Cao and A. G. Evans, J. Am. Ceram. Soc. **76**, 890 (1993).
18. H. Wang, Q. M. Zhang, L. E. Cross, and A. O. Sykes, J. Appl. Phys. **74**, 3394 (1993).
19. PZT-5H, PZT-5A, PZT-4, and PZT-8 are the trademarks of Morgan Matroc, Inc. (Bedford, OH) for its PZT piezoceramics.
20. R. Gerson, J. Appl. Phys. **31**, 188–194 (1960).
21. D. Berlincourt, SC-4443(RR), Sandia Corp. Tech. Rept. (1960).
22. W. A. Schulze and K. Ogino, Ferro. **87**, 361 (1988).
23. J. Kawata, K. Uchino, and S. Nomura, Jpn. J. Appl. Phys. **21**, 1298 (1982).

APPENDIX 15

journal

J. Am. Ceram. Soc., 79 [12] 3297-304 (1996)

Effect of Compositional Variations in the Lead Lanthanum Zirconate Stannate Titanate System on Electrical Properties

Kelley Markowski, Seung-Eek Park,* Shoko Yoshikawa,* and L. Eric Cross*

Materials Research Laboratory, Pennsylvania State University, University Park, Pennsylvania 16802

The purpose of this work was to evaluate the effect of compositional modifications on the electrical properties of lead lanthanum zirconate stannate titanate (PLZST) ceramics, as well as to examine their electrically induced phase-change behavior. Variations in the Ti:Sn ratio were evaluated. Increased Ti^{4+} content produced the following: decreased switching field, related to an increased antiferroelectric–ferroelectric (AFE–FE) transition temperature; constant hysteresis (ΔE) correlated with a constant temperature of the maximum dielectric constant (T_{max}); a sharper dielectric-constant maximum peak; and increased room-temperature dielectric constant (K). Variations in the Zr:Sn ratio also were evaluated. Increased Zr^{4+} content produced the following: increased hysteresis with increased T_{max}, decreased maximum dielectric constant, and decreased switching field with increased AFE–FE transition temperature (T_{AFE-FE}). From these results, with respect to compositional modifications, the AFE–FE switching field (E_{AFE-FE}) and ΔE were observed to be dependent strongly on T_{AFE-FE} and T_{max}, respectively. Negligible change existed in the strain achievable at the switching field, which remained constant for all compositions at ~0.16%. The significance of this research was the ability demonstrated to tailor the properties of phase-change materials through compositional modifications.

I. Introduction

THE transition from the antiferroelectric (AFE) to the ferroelectric (FE) phase in the PZST (lead zirconate stannate titanate) family of ceramics can occur with the application of an electric field. This field-induced transition is accompanied by a volume expansion. This expansion is due to the larger volume of the FE phase, as compared to the AFE phase. The result is that, on switching, large strains can be achieved. The magnitude of the strains produced can be 3–4 times larger than that of conventional piezoelectrics. These high-strain and associated high-polarization phenomena have been investigated for applications including charge-storage capacitors[1,2] and high-strain transducers and actuators.[3–5] These phase-change materials also have been investigated for their shape-memory effects and superelasticity.[6] The intrinsic contribution to the strain based on crystallographic data is 0.5%.[7] Previous studies have reported strains as high as 0.8%.[8,9] This is likely due to extrinsic factors such as intermediate phases, which are not easily reproducible. Strains of 0.2% were readily achieved for these compositions at the AFE–FE switching field, which is reasonable, considering that these samples were polycrystalline. Strain has been demonstrated to continue to increase with increasing electric field, even after AFE–FE switching occurs.[5,10] However, the phenomenology of this behavior is not fully understood. For application of this material, lower switching fields coupled with high strain values are preferred. Large hysteresis is an undesirable characteristic where high-frequency driving is required. The driving frequency is dependent on the actual geometry of a device and the ability of that device to dissipate generated heat. Figure 1 shows typical AFE polarization and strain behavior and defines the terminology used in this discussion to characterize the phase-change behavior.

In this study, compositional variations in the PLZST family of ceramics will be discussed. These variations include changes in the Ti:Sn ratio and variations along the antiferroelectric-tetragonal/ferroelectric-rhombohedral (AFE_{Tet}/FE_{Rhom}) morphotropic phase boundary (MPB). Attempts have been made to study the maximum strain attainable and to reduce the field necessary to observe AFE–FE switching and minimize the amount of hysteresis. The influence of composition on hysteretic properties, dielectric properties, and strain, along with the interdependence of each, also will be discussed.

II. Experimental Procedure

(1) Sample Preparation

The compositions discussed in this paper were prepared according to the formulas presented, respective to each section in the PLZST system, in Tables I and II. Polycrystalline ceramic materials investigated in this study were prepared by solid-state reaction, using the appropriate amounts of reagent-grade raw materials: lead carbonate ($2PbCO_3 \cdot Pb(OH)_2$, Hammond Lead Products, Hammond, IN), lanthanum oxide (La_2O_3, Alfa Products Co., Danvers, MA), zirconium dioxide (ZrO_2, Harshaw Chemical Co., Cleveland, OH), titanium dioxide (TiO_2, Whitaker, Clark and Daniels Co., Plainfield, NJ), and tin oxide (SnO_2, Alfa Products, Ward Hills, MA). The chemical purity of each was >99%. The processing flowchart used to prepare the samples is shown in Fig. 2. The sintering process was conducted in a lead-rich environment to minimize lead volatilization. After sintering, the samples experienced ~2% weight loss. The samples were pale yellow after sintering and remained this color throughout processing. To enhance densification and increase the electric-breakdown strength further, the sintered specimens were hot isostatically pressed (HIPed) for 2 h at 1200°C in an air atmosphere under a pressure of 20 MPa. After hot isostatic pressing (HIPing), the samples were 98% dense with no significant weight loss, and the average grain size, observed using scanning electron microscopy (SEM), was 4–5 μm. Disk samples (with a diameter of 11 mm and a thickness of 0.3 mm) were then prepared by polishing with silicon carbide and alumina polishing powders to achieve flat and parallel surfaces onto which gold was sputtered.

(2) Characterization Techniques

(A) Phase and Microstructure: Calcined and sintered powders were examined by X-ray diffractometry (XRD) to

W. A. Schulze—contributing editor

Manuscript No. 192365. Received August 24, 1995; approved May 20, 1996.
Supported by NCCOSC Contract No. 66001-93-C-6016 through Alliant Tech Systems, Aura Ceramics, and an ARPA contract through AFOSR, Boeing SSRC Consortium.
*Member, American Ceramic Society.

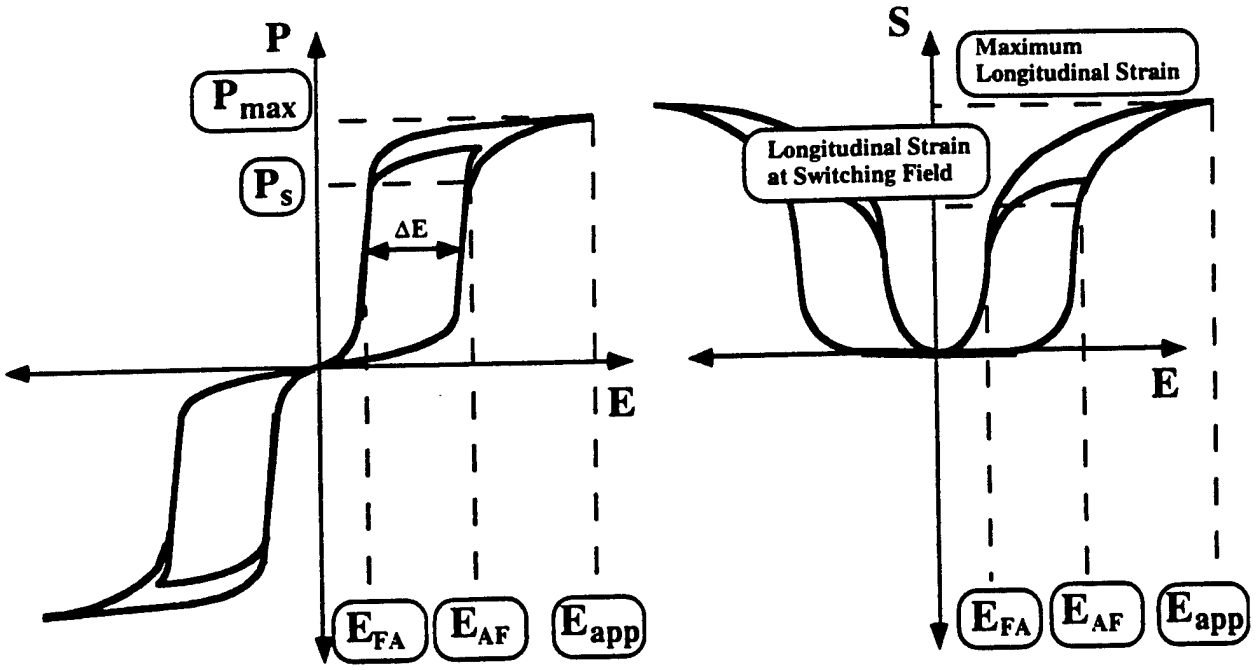

Fig. 1. Typical polarization and strain behavior of AFE–FE phase-change materials (E_{AF} is the electric field at which AFE–FE switching occurs: E_{FA} the electric field at which FE–AFE switching occurs; E_{app} the maximum applied field; P_{max} the maximum polarization; and ΔE the hysteresis. $E_{AF} - E_{FA}$).

ensure phase purity and to identify the crystal structure. Typically, the samples showed a tetragonal structure within the detection limit of XRD (<2%).

(B) Dielectric Properties: Multifrequency meters (Models 4274A and 4275A LCR, Hewlett-Packard, Palo Alto, CA) were used in conjunction with a computer-controlled temperature chamber (Model MK 2300, Delta Design, San Diego, CA) to measure capacitance as a function of temperature and frequency. Capacitance was converted to dielectric permittivity using the sample geometry and the permittivity of air. Measurements were taken from 100 Hz to 100 kHz at temperatures of −150°–250°C.

(C) Polarization and Strain: High-field measurements included polarization and strain hysteresis using a computer-controlled modified Sawyer tower system with an input/output card (National Instrument Co., Baltimore, MD) and a linear variable displacement transducer (LVDT) sensor driven by a lock-in amplifier (Model SR830, Stanford Research Systems, Sunnyvale, CA). The voltage was supplied using a high-voltage dc amplifier (Model 609C-6, Trek, Medina, NY). Through the LVDT sensor, the strain of the samples can be measured with the application of an applied field. Electric fields as high as ~100 kV/cm were applied using an amplified sine waveform at 0.2 Hz. During testing, the samples were submerged in Fluorinert (FC-40, 3M Corp., St. Paul, MN), an insulating liquid, to prevent arcing.

Table I. Compositions with Varying Ti:Sn Ratios of A-Composition PLZST Ceramics

Designation	Composition	Ti:Sn ratio
A-1	$(Pb_{0.98}La_{0.02})(Zr_{0.66}Ti_{0.11}Sn_{0.23})_{0.995}O_3$	11:23
A-2	$(Pb_{0.98}La_{0.02})(Zr_{0.66}Ti_{0.10}Sn_{0.24})_{0.995}O_3$	10:24
A-3	$(Pb_{0.98}La_{0.02})(Zr_{0.66}Ti_{0.09}Sn_{0.25})_{0.995}O_3$	9:25
A-4	$(Pb_{0.98}La_{0.02})(Zr_{0.66}Ti_{0.08}Sn_{0.26})_{0.995}O_3$	8:26
A-5	$(Pb_{0.98}La_{0.02})(Zr_{0.66}Ti_{0.07}Sn_{0.27})_{0.995}O_3$	7:27

Table II. Compositions Along the AFE–FE MPB of B-Composition PLZST Ceramics

Designation	Composition	Zr:Ti:Sn ratio
B-1	$(Pb_{0.98}La_{0.02})(Zr_{0.55}Ti_{0.12}Sn_{0.33})_{0.995}O_3$	55:12:33
B-2	$(Pb_{0.98}La_{0.02})(Zr_{0.60}Ti_{0.10}Sn_{0.30})_{0.995}O_3$	60:10:30
B-3	$(Pb_{0.98}La_{0.02})(Zr_{0.65}Ti_{0.10}Sn_{0.25})_{0.995}O_3$	65:10:25
B-4	$(Pb_{0.98}La_{0.02})(Zr_{0.70}Ti_{0.10}Sn_{0.20})_{0.995}O_3$	70:10:20
B-5	$(Pb_{0.98}La_{0.02})(Zr_{0.75}Ti_{0.10}Sn_{0.15})_{0.995}O_3$	75:10:15
B-6	$(Pb_{0.98}La_{0.02})(Zr_{0.80}Ti_{0.10}Sn_{0.10})_{0.995}O_3$	80:10:10

III. Results and Discussion

(1) Effects of Varying the Ti:Sn Ratio

Stoichiometrically different PLZST compositions were previously examined[1] and will be summarized here. Compositions with varying Ti:Sn ratios, i.e., moving compositionally perpendicular to the AFE_{Tet}–FE_{Rhom} MPB, were evalulated. These compositions are given in Table I and shown on the PLZST phase diagram[2] in Fig. 3.

The polarization and strain behavior for these compositions is summarized in Table III and shown in Fig. 4. The dielectric properties shown in Table III represent samples before exposure to an electric field (virgin samples). At the switching field, the longitudinal strain was 0.16%–0.18% for all compositions. This strain is reasonable for polycrystalline samples, considering X-ray investigations have shown 0.5% to be the maximum strain attainable for single crystals.[7] The maximum longitudinal strain, S_3 (%), is a function of the maximum field applied and typically was 0.4%–0.5%.

The switching field increased as the compositions moved further from the MPB, i.e., deeper into the AFE region with increased Sn^{4+} content. This can be attributed to a material with a more stable, room-temperature AFE phase existing deep within the AFE region that requires a higher field to switch to its FE phase. The polarization curves demonstrate this AFE stabilization; i.e., the polarization curve for composition A-1 exhibits only slight AFE characteristics, resembling a pinched single hysteresis, with a low switching field, whereas composition A-5 shows strong AFE behavior and distinct double-hysteresis behavior, with a high switching field. However, the switching field increased as the compositions moved farther from the MPB. Note that, although the maximum strain for composition A-3 appears very high, this sample was exposed to a significantly higher maximum field than the others. This ability to withstand the application of a high electric field may be

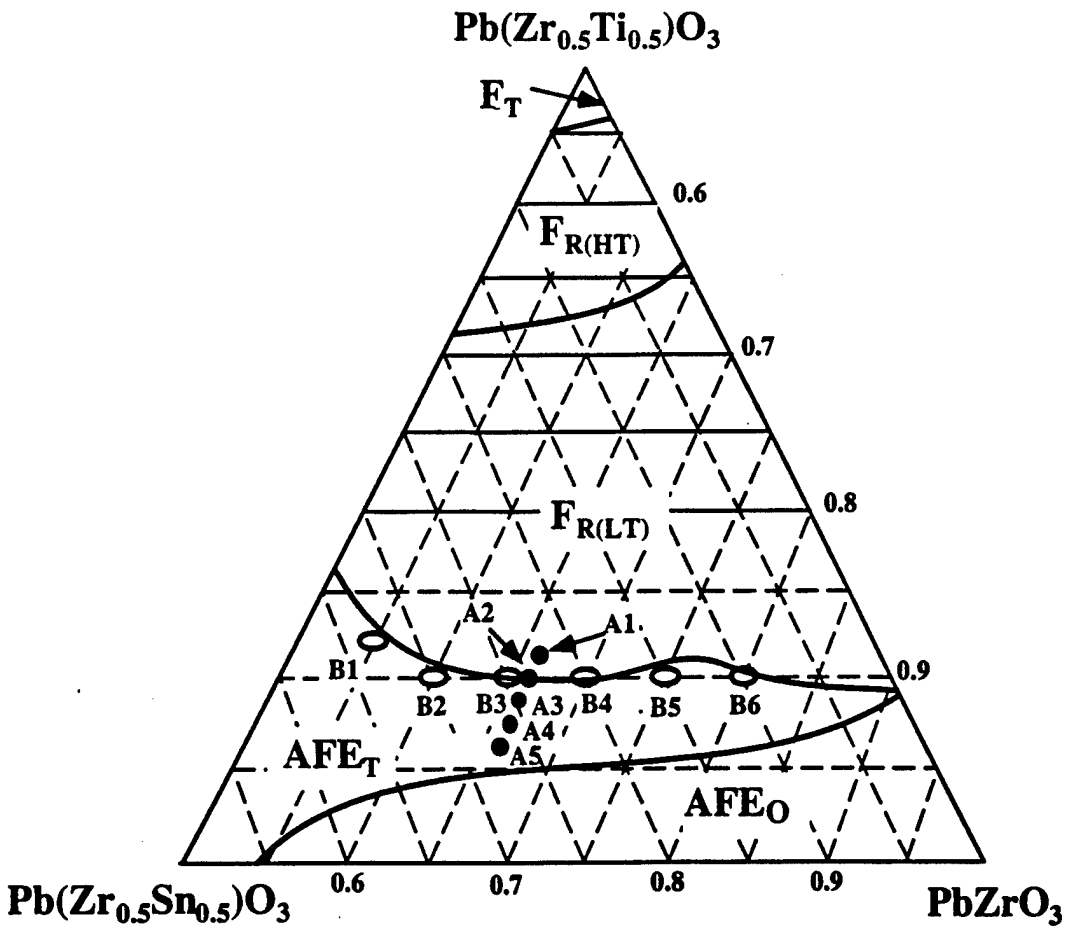

Fig. 3. PLZST phase diagram showing (●) A and (○) B compositions.

Table III. Dielectric and Field-Induced Properties of A-Composition PLZST Ceramics (Virgin Samples)

	Dielectric properties at 1 kHz			Electric-field-induced polarization and strain						
				At switching field				At maximum applied field		
Composition	K_{RT}	tan δ (%)	K_{max}	E_{AF} (kV/cm)	P_s (μC/cm²)	S_3 (%)	ΔE	E_{APP} (kV/cm)	P_{max} (μC/cm²)	S_3 (%)
A-1	860	0.72	2800	26	27	0.16	25	80	35	0.38
A-2	730	0.51	2500	37	32	0.18	25	111	38	0.42
A-3	620	0.30	2100	51	32	0.18	25	153	40	0.53
A-4	560	0.18	1700	71	32	0.16	25	133	41	0.48
A-5	500	0.18	1400	94	32	0.17	25	120	40	0.37

this indicated a stabilization of the FE phase. An increase of tan δ with increased Zr^{4+} content, which was abrupt for compositions B-5 and B-6 (Table IV), can be ascribed to this shift of transition temperature. As mentioned previously, the decrease in switching field can be associated with this shift of T_{FE-AFE}. With the exception of composition B-1, for reasons previously discussed, T_{max} increased as the Zr^{4+} content increased. This increase in K_{max} is caused by the increased ionic and dipolar contributions to K produced by the addition of Zr^{4+} ions. This increase in K was accompanied by an increase of the AFE–PE transition temperature (T_{max}). Figure 10, which shows the dependence of hysteresis with respect to T_{max}, demonstrates that the amount of hysteresis is dependent on T_{max}. This observation can be compared with those of the A compositions, which did not show a change in either hysteresis or T_{max}. To evaluate this behavior further, the dielectric and polarization data, with respect to temperature change, were obtained for composition B-6, which was FE at room temperature.

The K values of composition B-6, for the poled and virgin states, are shown in Fig. 11. Interestingly, at ~80°C, an abrupt increase exists in the K value for the poled sample. This increase corresponds to T_{FE-AFE}. Typically, for this family of materials, stable AFE compositions have a higher K after being exposed to an electric field, whereas the converse is true for FE compositions. Interestingly, at the 80°C transition, the virgin (cooling) and field-exposed (heating) curves intersect. Below 80°C (FE phase), the virgin state has a higher K value, whereas above 80°C (AFE phase), the field-exposed state has a higher K value. The polarization data has been obtained at temperatures of 25°–150°C and is shown in Fig. 12. These results clearly support the 80°C transition from FE to AFE in Fig. 11. Below 80°C, the sample (composition B-6) is FE with a large hysteresis. As the temperature increases above 80°C, the sample becomes AFE and exhibits a higher switching field and decreased hysteresis. From the polarization data, a correlation between T_{FE-AFE} and the switching field, as well as one between T_{max} and the amount of hysteresis, is confirmed. The decrease of hysteresis and increase of switching field with increased temperature are obvious. The variation of the switching field associated with the change in the T_{FE-AFE} transition is the factor influencing the stability of the AFE or FE state.

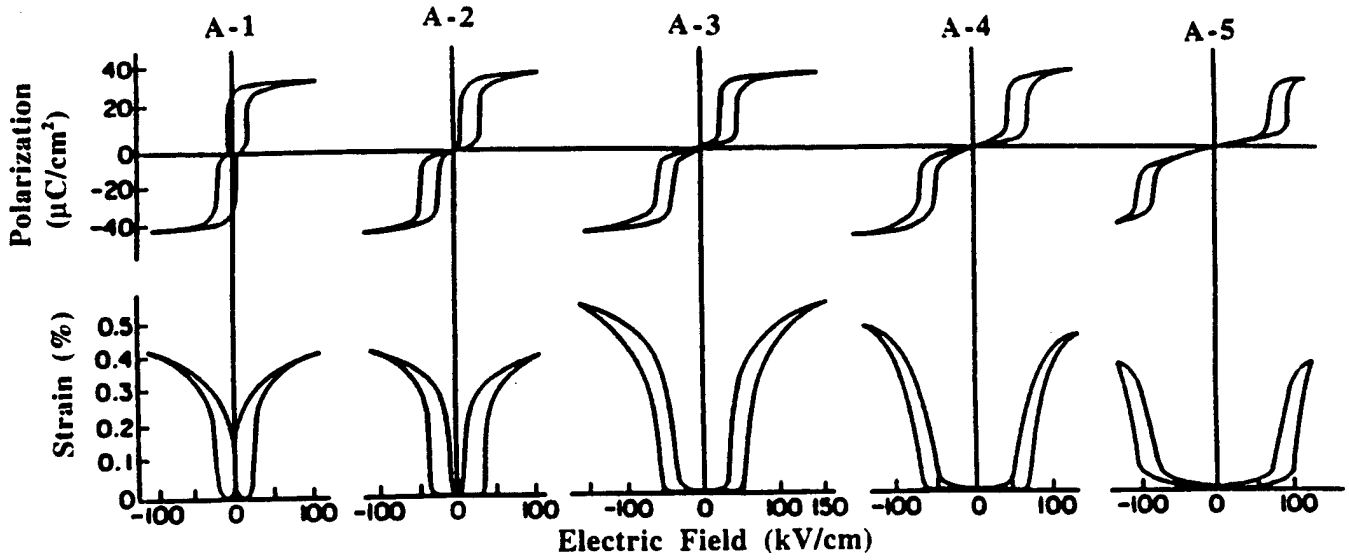

Fig. 4. Polarization and strain behavior of A compositions.

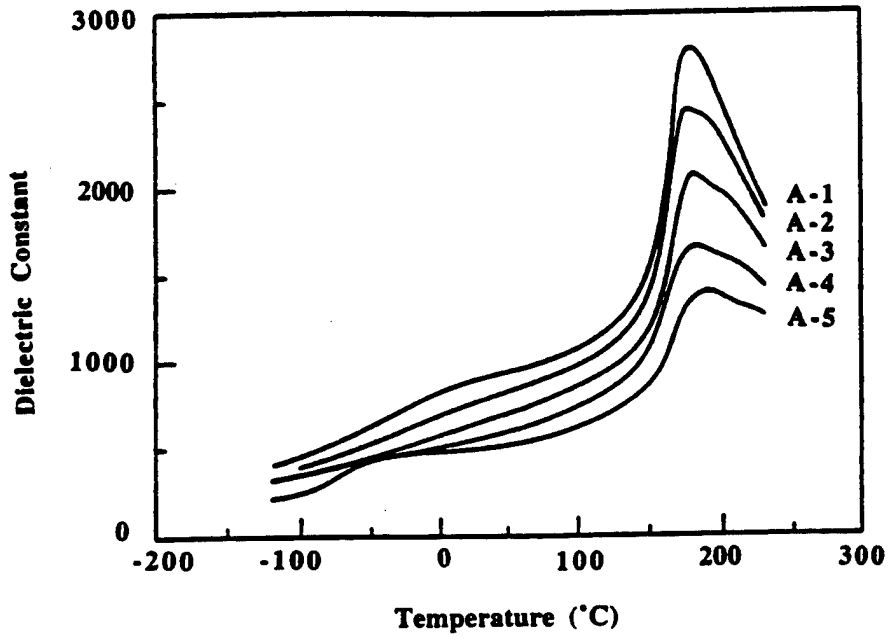

Fig. 5. Dielectric behavior of A compositions.

Table IV. Dielectric and Field-Induced Properties of B-Composition PLZST Ceramics (Virgin Samples)

	Dielectric properties at 1 kHz			Electric-field-induced polarization and strain						
				At switching field				At maximum applied field		
Composition	K_{RT}	tan δ (%)	K_{max}	E_{AF} (kV/cm)	P_S (μC/cm²)	S_3 (%)	ΔE	E_{APP} (kV/cm)	P_{max} (μC/cm²)	S_3 (%)
B-1	910	0.56	1910	26	31	0.12	18	55	34	0.27
B-2	710	0.32	1760	44	27	0.13	19	68	35	0.27
B-3	769	0.54	2210	39	33	0.16	26	64	36	0.30
B-4	840	0.95	3300	27	20	0.15	25	82	38	0.35
B-5	700	1.45	3600	28	20	0.17	30	75	42	0.40
B-6	720	2.12	5200	FE			25	50	38	0.08*

*This strain represents positive contribution only; the total strain of FE hysteresis is ~0.30%.

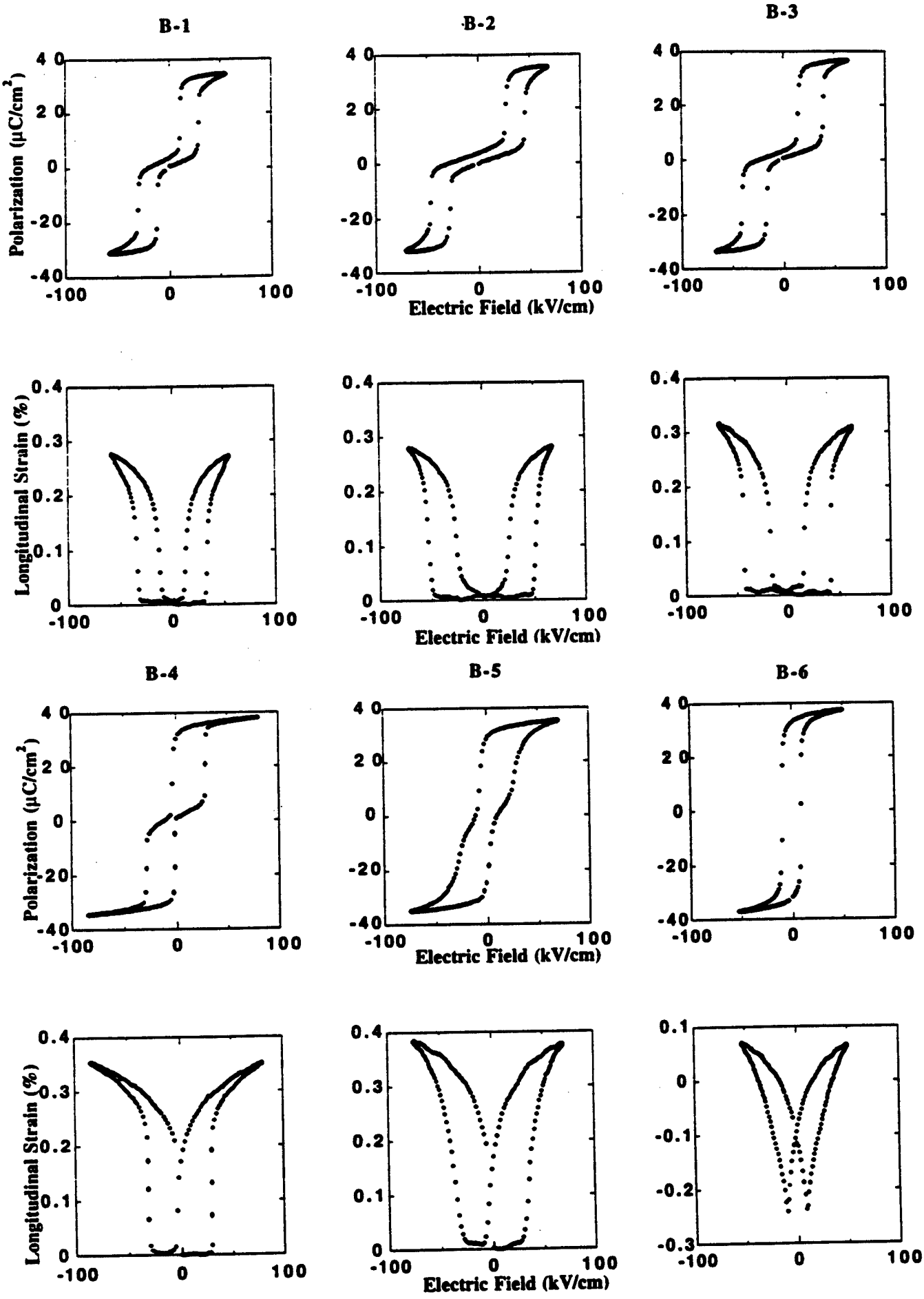

Fig. 6. Electrically induced strain and polarization of B compositions.

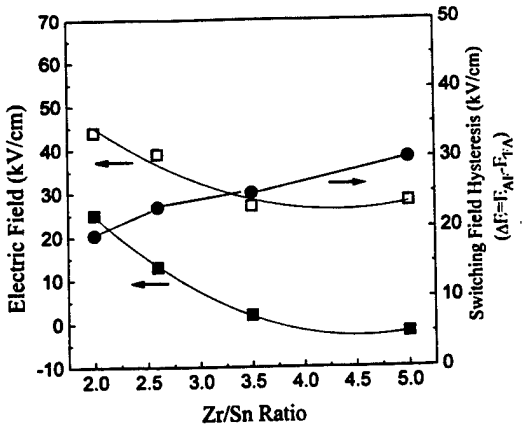

Fig. 7. Compositional dependence of switching field and hysteresis for B compositions ((□) E_{AF} and (■) E_{FA}).

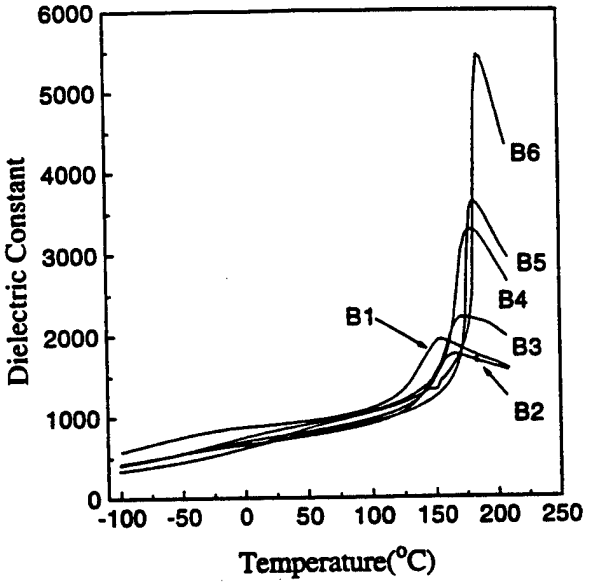

Fig. 8. Dielectric constant versus temperature for B compositions (at 1 kHz).

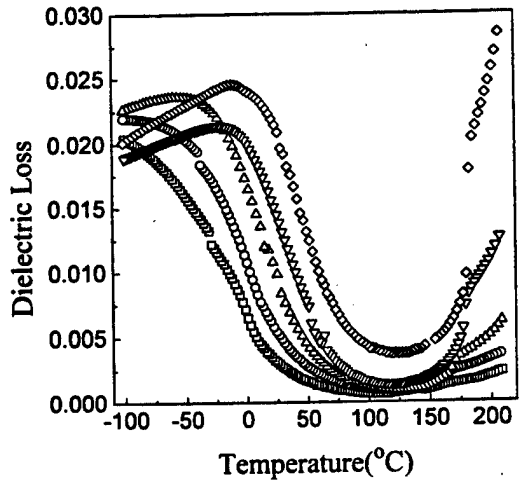

Fig. 9. Dielectric loss versus temperature for B compositions (at 1 kHz) (composition (□) B-2, (○) B-3, (△) B-4, (▽) B-5, and (◇) B-6).

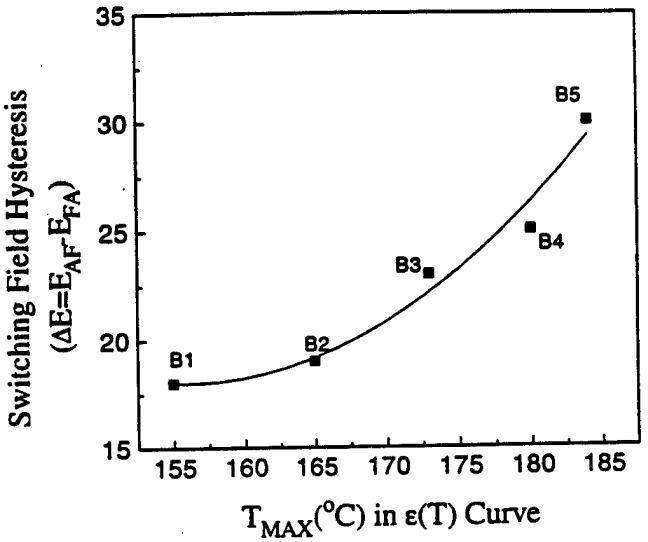

Fig. 10. Dependence of hysteresis on T_{max} for B compositions.

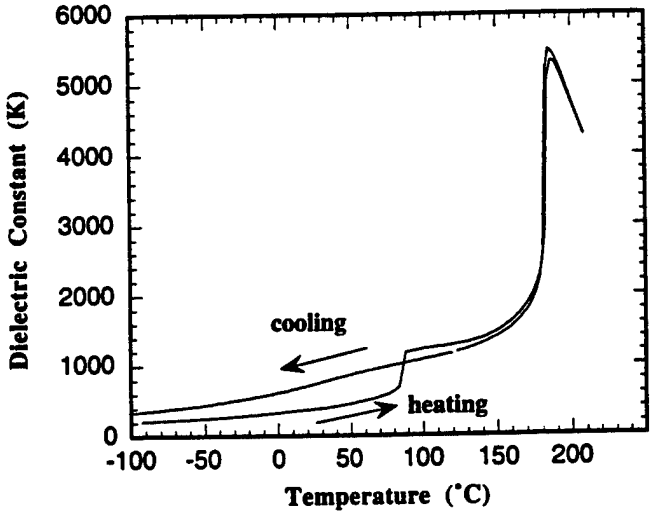

Fig. 11. Dielectric properties for poled (heating) and virgin (cooling) samples of composition B-6.

IV. Conclusions

Compositional modifications, with respect to varying Ti:Sn and Zr:Sn ratios, produced a change in phase stability. However, with these variations, increasing T_{FE-AFE} to lower the switching field always accompanied an increase in T_{max}, which can be associated with increasing hysteresis. The best-case scenario produced constant T_{max} and constant hysteresis. Therefore, to decrease the switching field and hysteresis, A-site modifications are necessary—that is, decreasing T_{max} while controlling the stability of the AFE or FE state.

On increasing the Sn^{4+} content perpendicular to the MPB, the following conclusions were made: T_{FE-AFE} decreased; the switching field increased; the dielectric maxima peak became more diffuse; and the room-temperature dielectric constant decreased. Regardless of the Ti:Sn ratio, 0.2% strain was realized at the switching field. Strain continued to increase with increasing field after phase switching; the temperature of the dielectric maximum remained the same, and the hysteresis remained at 25 kV/cm.

Increasing the Zr^{4+} content along the MPB resulted in the following: the hysteresis increased, the switching field